MODELLING THE CONFORMATIONAL CHANGE DYNAMICS OF pH-SENSITIVE CATIONIC HYDROGELS: A CASE OF GENIPIN CROSSLINKED CHITOSAN HYDROGELS

Nsidibe-Obong Ekpe Moses

Supervised by

Dr Katarina Novakovic

Dr Vladimir Zivkovic

Dr Francis Franklin

Thesis Submitted in Partial Fulfilment of the Requirements of the degree of Doctor of Philosophy

School of Engineering

Faculty of Science, Agriculture and Engineering

Newcastle University

May 2023

DECLARATION

I hereby declare that this thesis entitled ‘Modelling the conformational change dynamics of pH-sensitive cationic hydrogels: a case of genipin crosslinked chitosan hydrogels’ has been written by me and it is the record of my own research work. It has not been presented in any previous application for higher degree. All sources of information are specifically acknowledged using references.

Nsidibe-Obong Ekpe Moses.
May 2023.

DEDICATION

This work is dedicated firstly to the Almighty God for empowering me to complete this task amidst the storms that surrounded this phase of my life. Also, to my children, Andinwam Moses and Andikan Moses for the understanding they showed when I needed to be away from them to study.

ACKNOWLEGEMENTS

This study is made possible by the contributions of a good number of persons. My first heartfelt gratitude goes to my supervisors, Dr Katarina Novakovic, Dr Vladimir Zivkovic, and Dr Francis Franklin for offering constructive criticisms, guidance, and counsel at various stages of this work to a successful completion.

I am very grateful to members of my research group, particularly Dr Djurdja Vukajlovic and Dr Ana Stanojevic for their support with laboratory experience and providing experimental swelling/deswelling data for genipin crosslinked chitosan hydrogels.

More importantly, a big thank you to Tertiary Education Trust Fund (TETFund) and Federal University of Petroleum Resources Effurun, Nigeria for the sponsorship and financial support given to me to undertake this study.

I sincerely appreciate all my friends: Dr Kelechi Emerole, Dr Obaidullah Mohiuddin, Dr Ekaete Etuk, Mr. Ayodele Ebifemi, Pst. Ekwere Isaiah, and Mr Kenneth Ojimadu for talking me through the stormy period of my life during this PhD.

Finally, I appreciate my parents, Mr. and Mrs. Ekpe Moses and all my siblings, Emem, Iniobong, Mfonobong, Precious and Ubong for their understanding and encouragement as I strived to cross the finishing line.

ABSTRACT

pH responsive hydrogels are increasingly gaining grounds in medical and pharmaceutical fields, because of their ability to respond to pH variations in the body or disease site. Design and optimization of these systems for controlled drug delivery, tissue engineering and other applications require insight into the dynamics of volume variation of these materials. The conformational change dynamics of these materials when they are in contact with environments with different pH depends on the nature of the functional group attached to the backbone of the hydrogel. For hydrogels with negative fixed charged group at the backbone (that is, anionic hydrogels) their response to pH variation in the surrounding medium has been previously reported and was used to initially validate the developed anionic model before moving on to chitosan-based hydrogels. However, for cationic hydrogels (those having positive fixed charge group at their backbone) most studies have been empirical due to the complexity associated with numerical modelling of their reversible swelling-shrinking dynamics. The deformation of hydrogel in aqueous environment is a multiphysics problem that involves the interactions of chemical, electrical and mechanical fields. To describe the conformational change dynamics of the hydrogel, the numerical model should capture adequately these interacting fields. Therefore, in this study numerical modelling of the dynamic volume variation behaviour of cationic hydrogels; particularly genipin crosslinked chitosan hydrogel was approached systematically.

A multifield numerical model was first developed using COMSOL Multiphysics software to simulate the equilibrium swelling behaviour of anionic hydrogels. The performance capacity of the model was evaluated using experimental data for poly (2-hydroxyethyl methacrylate), PHEMA hydrogel. Further, the simulation platform developed for anionic hydrogels was adapted to cationic hydrogels. However, obtaining a dynamic simulation was difficult owing to numerical issues such as stability and stiffness. Although steady-state solutions were obtained, each time the pH of the surrounding medium changed from acidic to alkaline, it was required to manually change the boundary conditions especially during shrinking of the hydrogel. To circumvent this challenge, a systematic approach that combines thermodynamics modelling with chemo-mechanical modelling was adopted. The simulation results agreed with experimental data during validation. Thus, it is concluded that the model can predict the time-evolution of the volume of cationic hydrogels.

LIST OF PUBLICATIONS

Nsidibe-Obong E. Moses, Vladimir Zivkovic, Francis Franklin, Katarina Novakovic**.** Multiphysics Modelling of the Dynamic Response of pH-Sensitive Cationic Hydrogels. In: Scientific Meeting: Supercomputer modelling of advanced materials. June 2022, Royal Society, London.

Nsidibe-Obong E. Moses, Vladimir Zivkovic, Francis Franklin, Katarina Novakovic**.** Numerical Modelling and Simulation of Volume Variation of pH Sensitive Anionic Hydrogels. In: Chemical Engineering Day UK 2021. Bradford, UK.

Nsidibe-Obong E. Moses, Vladimir Zivkovic, Francis Franklin, Katarina Novakovic**.** Modelling the Swelling Dynamics of pH-Sensitive Genipin Crosslinked Chitosan Hydrogels. In: School of Engineering Postgraduate Student Research Conference. 2021, Newcastle, UK. **First Place Oral Presentation Award**.

Nsidibe-Obong E. Moses, Vladimir Zivkovic, Francis Franklin, Katarina Novakovic**.** Multiphysics Simulation of the Swelling Kinetics of pH-Responsive Anionic Hydrogels. In: COMSOL Multiphysics Conference 2020 Europe.

Nsidibe-Obong E. Moses, Vladimir Zivkovic, Francis Franklin, Katarina Novakovic**.** Multiphysics Modelling and Simulation of the Dynamics of pH-Sensitive Anionic Hydrogels in Controlled Drug Release. In: School of Engineering Postgraduate Student Research Conference. 2020, Newcastle, UK. **First Place Oral Presentation Award**

Nsidibe-Obong E. Moses, Vladimir Zivkovic, Katarina Novakovic**.** Multiphysics Model for Simulation of the Dynamics of pH-sensitive Chitosan-Genipin Hydrogels. In: School of Engineering Postgraduate Student Research Conference. 2019, Newcastle, UK. **Third Place Poster Presentation Award.**

TABLE OF CONTENTS

CHAPTER TWO: LITERATURE REVIEW

CHAPTER THREE: METHODOLOGY

CHAPTER EIGHT: RESULTS AND DISCUSSION:

Optimum Equilibrium Swelling of Genipin Crosslinked Chitosan Hydrogel

LIST OF TABLES

LIST OF FIGURES

LIST OF APPENDICES

ABBREVIATIONS

AA	Acrylic Acid
AAm	acrylamide
BEM	Boundary Element Method
BVP	Boundary Value Problem
CFD	Computational Fluid Dynamics
COD	Coefficient of Determination
DEAEMA	diethylaminoethyl methacrylate
DMAEMA	dimethylaminoethyl methacrylate
FDM	Finite Difference Method
FEA	Finite Element Analysis
FEM	Finite Element Method
FVM	Finite Volume Method
LB	Lower Boundary
LCST	Low Critical Solution Temperature
MAA	methacrylic acid
MEMS	Micro-Electro-Mechanical Systems
NP	Nernst Planck
PAA	poly (acrylic acid)
PHEMA	poly (2-hydroxyethyl methacrylate)
PK1	First Piola-Kirchoff
PK2	Second Piola-Kirchoff
PMAA	poly(methacrylic acid)
PNP	Poisson Nernst Planck
PPAA	poly(acrylamide-co-acrylamidoglycolic acid)
UB	Upper Boundary
UCST	Upper Critical Solution Temperature

SYMBOLS

c_{gel}	Concentrations inside the hydrogel (mol/m^3)
c_{sol}	Concentrations inside the surrounding medium (mol/m^3)
D_k	Effective diffusivity (m^2/s)
E	Elastic strain tensor
F	Faraday constant (C/mol)
$\mathbf{F}_{\alpha}$	Deformation gradient of the constituents φ^{α}
G	Shear Modulus (Pa)
H	Local hydration state of the hydrogel
I	Identity tensor
I	Ionic strength of the medium (mM)
J	Determinant of the deformation gradient tensor.
$\boldsymbol{J}_{\alpha}$	Jacobian of deformation gradient
K	Bulk Modulus (Pa)
k	Boltzmann's constant
K_a	Dissociation constant (mM)
K^D	Donnan coefficient of the mobile ions
$\overline{M_c}$	Average molecular weight between the crosslinks (g/mol)
M_t	Amount of water uptake at time, t.
M_{∞}	Maximum amount of water uptake by the polymer gel
m_{SR}	Mass swell ratio
N_A	Avogadro's constant
N_c	Average number of segments in the chain network
n	Diffusion index
P	First Piola-Kirchoff stress tensors (Pa)
pK_a	Acid dissociation constant for anionic hydrogel
pK_b	Acid dissociation constant for cationic hydrogel
$P_{osmotic}$	Osmotic pressure (N/m^2)
R	Universal gas constant
T	Absolute temperature (K)
V_{SR}	Volume swelling ratio
V_0	Volume before swelling (m^3)

V_s	Molar volume of the solvent
$\bar{V_r}$	Molar volume of the polymer monomer
$\mathbf{X}_\alpha$	Reference position of the particles of a fluid-saturated porous solid
$\mathbf{X}_{\boldsymbol{F}}$	Reference position of the fluid phase
$\mathbf{X}_{\boldsymbol{S}}$	Reference position of the solid phase
ΔG_{total}	Change in total free energy (J)
ΔG_{mix}	Change in free energy of mixing (J)
$\Delta G_{elastic}$	Change in elastic free energy (J)
ΔG_{ion}	Change in free energy of the ions (J)
π_{mix}	Osmotic pressure due to the mixing process (Pa)
χ	Polymer-solvent interaction parameter
ϕ	Polymer volume fraction of the hydrogel
ϕ_0	Polymer volume fraction of the hydrogel in the relaxed
$\pi_{elastic}$	Osmotic pressure due to elastic free energy (Pa)
ϑ_0	Polymer volume fraction of the hydrogel in the relaxed state
ϑ_e	Polymer volume fraction of the ionic hydrogel at equilibrium state,
ε	Relative dielectric constant of the medium
τ_1	Collective diffusion coefficient of the polymer gel (m/s^2)
α	Degree of dissociation
$\alpha_{12}(pH)$	pH-induced deformation coefficient
φ	Electric potential (V)
ϑ	Specific volume of the polymer (m^3/kg)
v_0	Number density of effective network strands (m^{-3})
μ	Chemical potentials (J)
μ_k	Mobility of the diffusive species ($m^2s^{-1}\ V^{-1}$)
k_r	Kinetic rate constant of swelling
σ	Stress tensor (Pa)
φ^α	Constituents of a fluid-saturated porous solid

SUBSCRIPTS

k	k^{th}-species ion
f	fluid
s	solvent

p	polymer
g	gel

CHAPTER 1

INTRODUCTION

1.1 Background and Motivation

Controlled drug delivery systems such as Nexplanon®-a hormonal implant (demonstrated in Figure 1.1) for contraception [1], transdermal patches (shown in Figure 1.2) for drug release through the skin and into the bloodstream [2, 3], liposomes as drug carriers [3, 4] have helped to maintain drug concentrations within the desired therapeutic range in the human body, thereby reducing the need for frequent drug administrations, leading to increased patient compliance and convenience [5]. Polymers have been used extensively in the pharmaceutical industries as binders in tablets, as film coatings to disguise the unpleasant taste of drugs and for controlled drug release applications [6, 7]. Among various kinds of polymeric materials that have been used to encapsulate drugs or used as drug release rate-controlling barriers, hydrogels have received considerable research interest [8–17]. Hydrogels are also pursued in wound healing, tissue engineering, gene delivery, ocular drug delivery, transdermal drug delivery and subcutaneous drug delivery in the form of implants [1, 17–19].

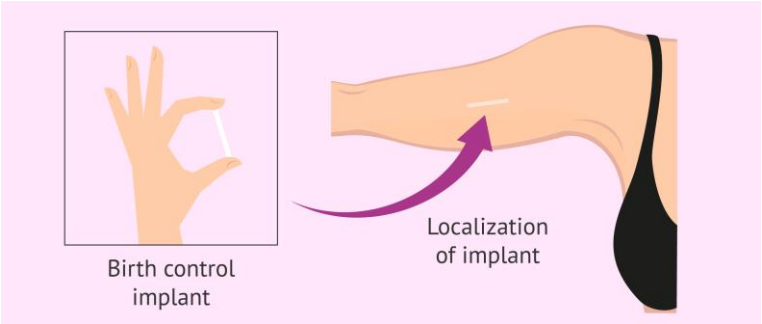

Figure 1.1: A flexible rod placed on the inside of the arm as a birth control implant [20].

Figure 1.2: Transdermal patch used for delivering a specific steady dose of drug into the skin [21].

Hydrogels are three-dimensional, frequently chemically or physically crosslinked hydrophilic polymeric materials, primarily composed of water. The volume variation behaviour of hydrogels in response to stimuli makes them considered as responsive materials [22]. When volume changes in reversible manner (as shown in Figure 1.3) in response to external stimuli, hydrogels are considered smart (intelligent) materials [23–25]. In contact with different environments (e.g., solutions that have different pH; different temperature, ionic strength, etc.), smart hydrogels are capable of swelling, thereby retaining large volume of liquid in their swollen state. Hydrogel's ability to absorb water comes from the hydrophilic functional groups located at the backbone of the polymer network, while their inability to dissolve in water is due to the crosslinks between the polymer chains [14]. Based on the nature of bonds between polymeric chains, hydrogels are categorised into chemical or physical gels. The chemical hydrogels have permanent covalently bonded crosslinked networks while physical hydrogels have networks with transient junctions that are held together by molecular entanglements or physical interactions such as ionic interactions, hydrogen bonds, or hydrophobic interactions [14].

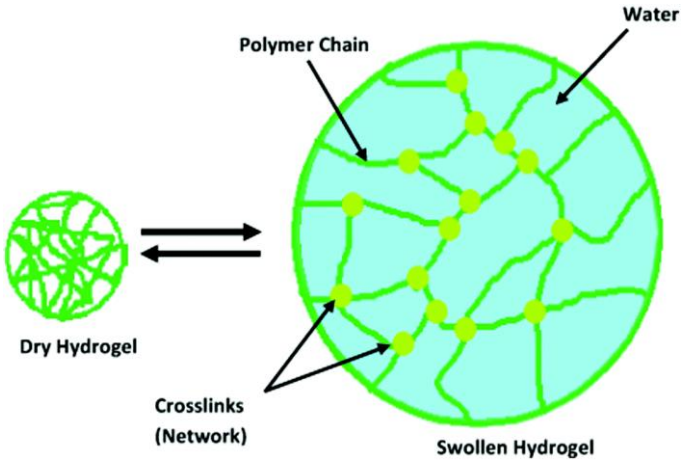

Figure 1.3: Crosslinked hydrogel undergoing reversible volume change [26]

Although hydrogels are generally prepared using hydrophilic monomers, hydrophobic monomers are sometimes used in hydrogel synthesis to tune the properties for specific applications [14]. For example, the mechanical stability of the hydrogel can be controlled by adjusting the concentration of the hydrophobic monomer used. This in turns impacts on the degradability and durability of the hydrogel [14]. Generally, hydrogels can be prepared from either synthetic polymers or natural polymers. Gels whose polymers have natural origins are called natural hydrogels, examples are gelatin and collagen. Hydrogels synthesized using

synthetic polymers such as polyamides and polyethene glycol are known as synthetic hydrogels [27]. Various natural and synthetic polymers have been studied in hydrogel-related research [28].

The hydrogel of interest in this study is chitosan-based. Chitosan is a natural cationic copolymer formed by the partial deacetylation of insoluble naturally available chitin [29–32], obtained from exoskeletons of crustaceans, fungi, and insects [28], crabs and lobsters, pens of squids, wings of insects and even nails of humans [33]. It is the second most abundant organic compound in nature after cellulose [34]. The shellfish (e.g., lobsters, shrimp, crab, etc.,) industry produces a lot of waste shell—an important source of chitin. Utilization of chitin via chitosan is therefore seen as a solution to the potential environmental problem of waste shell [33–35].

Chitosan is weakly soluble in acidic medium (specifically when the pH of the medium is less than the pK_a of the chitosan), a feature used in the preparation of chitosan-based hydrogels [36]. To stabilize them, chitosan solution is usually cross-linked by different methods aimed at tailoring their properties (porosity, mechanical strength, responsiveness) and creating a stable network for a period suitable for the application [36, 37]. Adding a suitable cross-linker does not only change the hydrogel's structure but improves its mechanical properties [36]. The need for naturally occurring cross-linking agents is on the increase in recent time, due to their inherent biocompatibility and reduced cytotoxicity [38]. One such natural cross-linker that has attracted increased research interest in recent years is genipin [36–39]. Genipin is obtained from a compound traditionally used in Chinese medicine, geniposide, which may be isolated from the fruits of Gardenia jasminoides Ellis [37, 39].

Several studies have been done to elucidate the behaviour of chitosan-based hydrogel cross-linked with genipin. For example, Damida and co-workers [36] studied the reaction kinetics of chitosan/genipin at different thermal conditions and with different cross-linker concentrations. Matcham and Novakovic [38] in their work showed how temperature and pH affect sol-gel transition in genipin crossed-linked chitosan hydrogels. The effect of cross-linker concentration on the rheological properties of chitosan-genipin hydrogels at body temperature and physiological pH was evaluated [37]. Although, much research works around chitosan cross-linked with genipin details the experimental and theoretical studies concerning

hydrogels, the dynamic responsiveness in relation to hydrogel composition remains poorly understood. For example, Jahren and co-workers at University of Cambridge have done a lot of experimental work on genipin crosslinked chitosan hydrogels with a recent work on modelling their equilibrium swelling behaviour from a thermodynamics standpoint. This thesis, on one hand, builds and improves on their work. In addition, Novakovic's group at Newcastle University has done lots of experimental work on genipin crosslinked chitosan hydrogels with nothing on mathematical modelling prior to this study. This thesis on the other hand, uses data from this group for model validation.

Moreover, designing these materials for the desired applications require mathematical models which can complement experimental studies. That is, models which can offer insights that cannot even be observed experimentally. For example, how the concentration of ions builds up or deplete within the hydrogel. How ions in solution and not just pH influence swelling or shrinking. Multifield-based numerical models describing the volume variation behaviour of swellable hydrogels with different degree and type of crosslinking while readily available in the literature for some hydrogels [40–43], particularly anionic hydrogels, are very few for studying the equilibrium swelling behaviour of cationic, specifically genipin cross-linked with chitosan hydrogels. These fast-responding hydrogels made from naturally available raw materials are sparking lots of research interest in recent times. For that reason, having numerical models to simulate the stimuli-responsive, dynamic behaviour of these hydrogels would be a significant contribution that would enhance understanding and accelerate their development for broad range of applications.

1.2 Aim and Objectives

This study is aimed at developing a numerical model that can predict dynamic volume variation behaviour of genipin crosslinked chitosan hydrogels, in response to changes in pH of their environment.

The objectives to achieve this aim are:

i. develop and validate a finite element model in COMSOL multiphysics software, for predicting the volume variation of pH responsive anionic hydrogels.
ii. adapt the framework developed in (i) above to simulate and predict steady state volume variation of pH-sensitive cationic hydrogels.

iii. develop a numerical model to simulate and predict the dynamic volume variation behaviour of pH responsive genipin crosslinked chitosan hydrogels owing to the difficulty associated with obtaining transient response using the framework in (ii).

iv. evaluate the performance of the model developed in (iii) by comparing model swelling (prediction) data with experimental swelling data for genipin crosslinked chitosan hydrogels.

v. determine the optimum parameters for equilibrium swelling of genipin crosslinked chitosan hydrogels.

1.3 Significance and Application

The model developed in this study for cationic hydrogels is easy to use and can allow for the concentration of the crosslinking reagent to be tuned during dynamic studies to predict the effect of concentration variation on the volume variation behaviour of pH responsive cationic (genipin crosslinked chitosan) hydrogels. If the initial and final swell volumes of the crosslinked hydrogels are known, the chemo-mechanical model can be employed to predict the time-evolution of the volume of the hydrogel from its initial state to its final swollen state. In addition, the model developed in this study could be adapted to model the volume variation behaviour of other cationic hydrogels and be further deployed to model pH-sensitive swelling-controlled drug delivery devices by including the drug molecule among the non-ionic diffusing species.

1.4 Scope of Study and Contribution to Knowledge

Since the nature of the fixed charge group at the backbone of the polymer network varies for different cationic hydrogels, the chemo-mechanical together with thermodynamics model developed in this study, is for predicting the conformational change dynamics of cationic genipin crosslinked chitosan hydrogels. However, the model can be adapted to simulate the conformational change dynamics of other cationic hydrogels.

A multiphysics numerical model that couples Poisson Nernst Planck and mechanical equations was first developed and solved using COMSOL Multiphysics software to simulate the equilibrium swelling behaviour of anionic hydrogels. The performance capacity of the model was evaluated using experimental data for poly (2-hydroxyethyl methacrylate), PHEMA hydrogel. Switching from modelling anionic to modelling cationic hydrogels, the simulation platform developed for anionic hydrogels was adapted to cationic hydrogels. However,

obtaining a dynamic simulation of the model for cationic (genipin crosslinked chitosan) hydrogels was difficult owing to numerical issues such as stability and stiffness. Although steady-state solutions were obtained, each time the pH of the surrounding medium changed from acidic to alkaline, it was required to manually change the boundary conditions especially during shrinking of the hydrogel.

To circumvent this challenge, a systematic approach that combines thermodynamics modelling with chemo-mechanical modelling was adopted. The thermodynamics model developed using statistical mechanics approach was used to determine the equilibrium swelling ratio, and by extension the final volume of the swollen hydrogel. With the values of initial and final volumes of the hydrogel, the chemo-mechanical model derived from first principle was used to determine or predict the time-dependent volume of the hydrogel from its initial state to its final swollen state. In essence, the modelling strategy provided in this study for modelling the dynamic response of pH-sensitive cationic hydrogels contributes to knowledge, as it helps to overcome the computational difficulties associated with applying the traditional approach used for modelling anionic hydrogels. A challenge that has restricted studies in cationic hydrogels to mainly experimentation.

Furthermore, the model developed in this work offers the advantage of allowing for the concentration of the crosslinking reagent (a very important parameter that controls the mechanical property and swelling capability of the crosslinked hydrogel) to be tuned during dynamic studies to predict the effect of concentration variation on the volume variation behaviour of pH responsive cationic (genipin crosslinked chitosan) hydrogels. In addition, by incorporating pharmaceutical compounds, or combining cationic hydrogels with DNA through conjugation (to release the DNA) or varying the concentration of the crosslinking reagent to create scaffolds of new tissues, the model can be adapted to simulate applications such as targeted drug delivery, gene delivery, and tissue engineering respectively.

1.5 Thesis Outline

This thesis is divided into nine chapters. The first chapter provides the background and motivation for this research, while the second chapter deals with the review of related literature. The review covers stimuli responsive hydrogels, their types, and the theory behind their swelling. In addition, a review on the approaches employed for mathematical modelling and simulation of the response behaviour of pH-sensitive hydrogels was made.

Chapter 3 focuses on the modelling methodology employed in this research to simulate the pH responsive behaviour of ionic hydrogels. This was described in four separate sections covering multiphysics modelling of pH-sensitive anionic and cationic hydrogels, modelling equilibrium swelling of pH-sensitive hydrogels from a thermodynamics standpoint, modelling the dynamic swelling of pH responsive genipin crosslinked chitosan hydrogels, and optimization model for equilibrium swelling of pH responsive genipin crosslinked chitosan hydrogels.

Chapter 4 presents the analysis and discussion of the results of the multiphysics simulation for equilibrium swelling of the case-studied pH-responsive anionic hydrogel. Comparison between model predictions and equilibrium swelling data for the case-studied anionic hydrogel is detailed in this chapter.

The simulation framework deployed to model equilibrium swelling of anionic hydrogel was adapted to model equilibrium swelling of cationic genipin crosslinked chitosan hydrogel, and the results of the simulation are analysed and discussed in Chapter 5.

In Chapter 6, the simulation result for the thermodynamic model developed from statistical mechanics approach (for equilibrium swelling of genipin crosslinked chitosan hydrogel) is analysed and discussed extensively. Comparison was made between model predictions and experimentally obtained values for equilibrium swell ratio.

Chapter 7 highlights the achievement of this research in simulating the dynamic volume variation behaviour of pH-sensitive genipin crosslinked chitosan hydrogels. The simulation results of the dynamic model for studying the time-dependent volume variation behaviour of cationic, genipin crosslinked chitosan hydrogels were validated in this chapter using experimental (dynamic) swelling data.

Chapter 8 focuses on statistical optimization of equilibrium swelling of pH-sensitive genipin crosslinked chitosan hydrogels to determine the optimum conditions for equilibrium swelling to be achieved in a typical drug delivery scenario.

Chapter 9 concludes on the main outcomes of this research and highlights the suggestions for further studies.

CHAPTER TWO

LITERATURE REVIEW

2.1 Stimuli-Responsive Hydrogels

Stimuli-responsive hydrogels are three-dimensional hydrophilic polymer-based materials capable of showing significant changes in their properties on exposure to external stimuli [44]. These stimuli could be physical, such as: pressure [45], temperature [46, 47], sound [48, 49], light [50, 51], electric [52] and magnetic field [53, 54] or chemical, such as: pH [55–59], solvent composition, ionic strength [60], and molecular species [15, 40].

Temperature-sensitive hydrogels show distinctive changes in their mechanical properties in response to changes in the temperature of the surroundings [61–64]. Thermo-responsive hydrogels are finding applications in biomedical fields especially in drug delivery systems used for transdermal drug delivery, oral drug delivery and in cancer therapy [44, 61–63, 65]. Temperature sensitive hydrogels can exhibit Low Critical Solution Temperature (LCST) or Upper Critical Solution Temperature (UCST). LCST is the critical temperature below which the hydrogel is miscible in all proportions, while UCST is the critical temperature above which the hydrogel is miscible in all proportions [66].

The swelling and shrinking of temperature-responsive hydrogels that corresponds with their critical solution temperature has been the mechanism behind their utilization in technologies such as drug delivery and membrane separation [67, 68]. Some common temperature-sensitive synthetic polymers employed in the fabrication of drug delivery systems include poly(organophosphazenes), polyoxazoline, poly(N-isopropylacrylamide) (pNIPAAm), while some thermo-responsive natural polymers are starch, cellulose, chitosan, gelatin/collagen [44]. The difference between natural and synthetic polymers are illustrated in Figure 2.1.

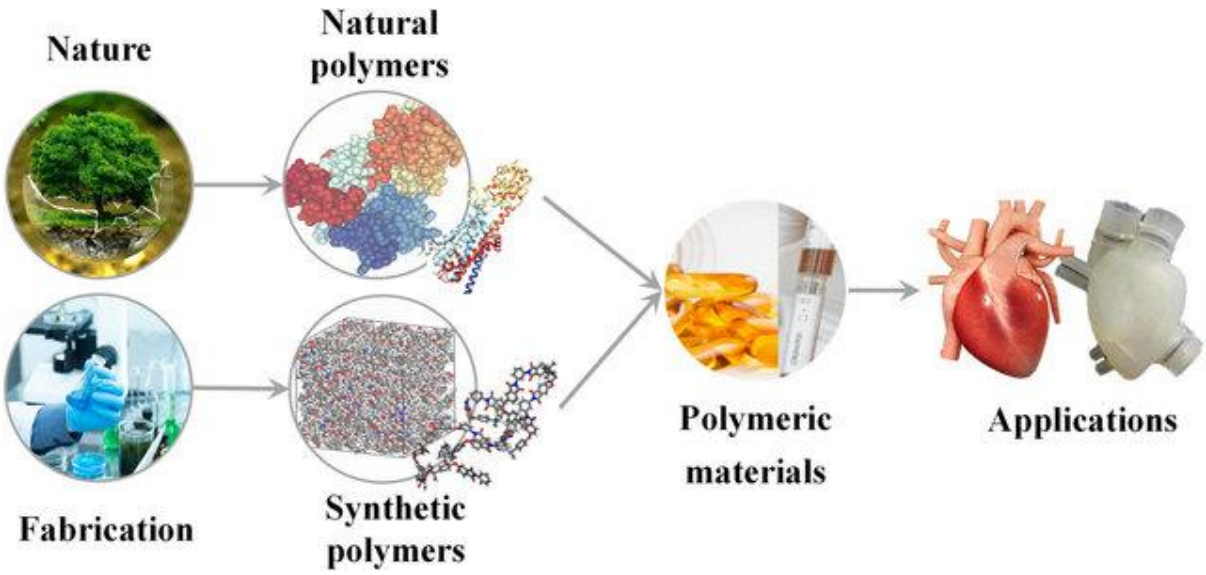

Figure 2.1: Natural (i.e., naturally occurring) vs synthetic (man-made) polymers and their applications. Adapted from [69].

pH-responsive hydrogels swell or shrink in response to changes in pH of the surrounding medium [70–72] and continues to draw interest in the development of various drug delivery systems [8, 67, 68, 72, 73]. These hydrogels play a major role in biomedical applications [74–78] particularly in drug delivery systems [79–81] because, significant pH changes occur in various parts of the human body such as the blood vessels [82], female genital tract [83], the gastrointestinal tract [84], also in disease sites such as tumour [85], and inflammation [86].

Materials used to induce pH-responsive behaviour in hydrogels can be synthetic or natural by origin. Among synthetic materials, the most common monomers employed in the development of pH-responsive hydrogels are acrylic acid (AA), acrylamide (AAm), methacrylic acid (MAA), dimethylaminoethyl methacrylate (DMAEMA), diethylaminoethyl methacrylate (DEAEMA) and ethylene glycol [87–89]. Natural polymers such as gelatin, albumin, chitosan, and alginate have been reported to demonstrate pH-responsive behaviour [88]. The major advantages of natural pH-responsive polymers, over their synthetic counterparts are biocompatibility, and majority of them have the ability to degrade overtime within the human body system, making them vey suitable for constructing devices that can be implanted in the human body or as vehicles for controlled drug delivery [71, 88].

pH-sensitive hydrogels (whether from natural or synthetic polymers) respond reversibly to changes in the pH of the external environment. Their characteristic volume-variation behaviour makes them find applications in various areas like environmental remediation [15], control of

microfluidic flow, artificial muscles and biomaterials, Micro-Electro-Mechanical Systems (MEMS)/Bio-MEMS and controlled drug delivery systems [15, 90]. Advances in the utilization of these pH-responsive hydrogels have made accurate experimental analysis of their volume-variation behaviour for systems with complex geometry a challenging task [15]. Therefore, the need and interest in mathematical modelling and simulation has been increasing over the years with a potential to become a major tool for understanding the dynamics of swelling/shrinking and predicting the performance of stimuli-responsive hydrogels.

2.2 Conformational Change of pH Responsive Hydrogels

The ability of pH responsive hydrogels to swell or shrink in response to pH changes in the surrounding medium, is a function of the ionisable pendant groups in the polymer network chain [91]. The nature of the ionisable pendant group determines if the hydrogel is anionic or cationic or zwitterionic [92–95], depending on their ability to donate or accept protons in response to pH changes in the surrounding medium [91, 96, 97]. The volume-variation behaviour of pH-responsive hydrogels strongly depends on the dissociation constant of the pendant group.

The pendant groups for anionic hydrogels ionize in solutions at a pH greater than their acid dissociation constant, pK_a. Thus, the large osmotic pressure created on the surface of the hydrogel by the cloud of ions causes the anionic pH-sensitive hydrogels to swell at $pH > pK_a$. Conversely, the pendant groups for cationic hydrogels ionize at a pH less than their base dissociation constant, pK_b. Hence, cationic pH-responsive hydrogels (e.g., gels containing –NH_2 groups) swell at $pH < pK_b$, where K_b is the dissociation constant of the basic (amine or amino) group at the polymer backbone. These behaviours are depicted in Figure 2.2.

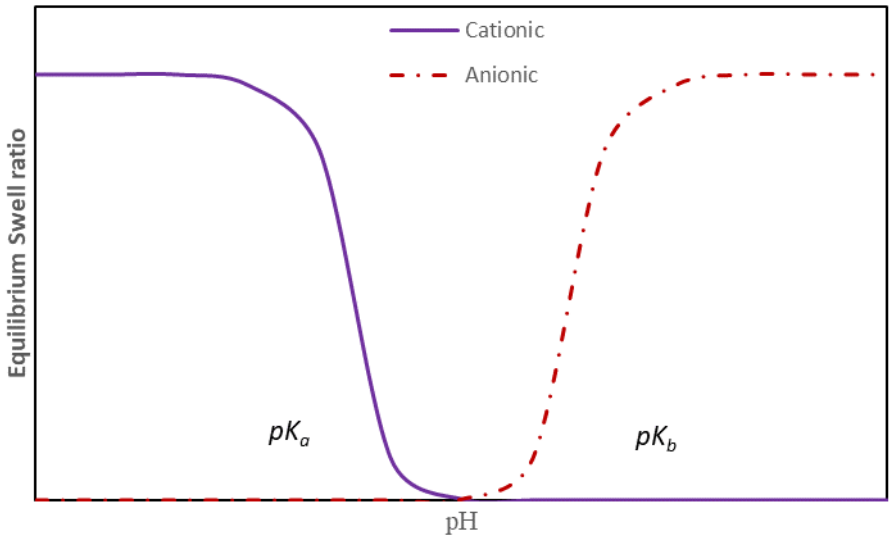

Figure 2.2: pH dependent equilibrium swelling behaviour of anionic and cationic hydrogels. Adapted from [98].

2.3 Anionic Hydrogels: poly (2-hydroxyethyl methacrylate)

As mentioned in Section 2.2, anionic hydrogels have negatively charged ions as ionizable pendant group at the backbone of the polymer network (see Figure 2.3). These hydrogels often contain weakly acid groups such as sulfonic, $–SO_3H$, or carboxylic, -COOH acid groups at the backbone of the network.

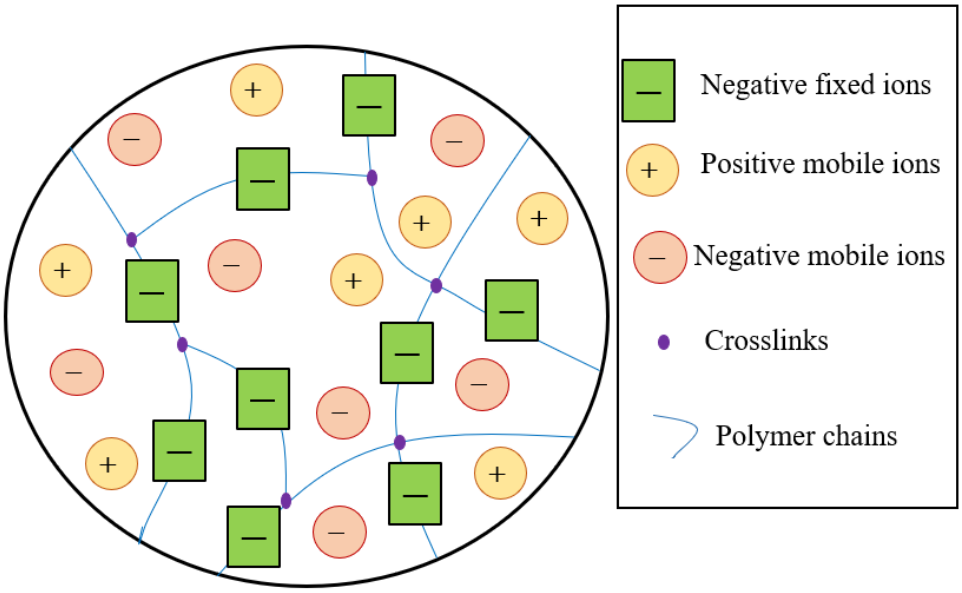

Figure 2.3: Illustrative representation of anionic hydrogel. Adapted from [99]

Due to the ability of anionic hydrogels to swell when their pK_a is lower than the pH of their surroundings, they have found applications in areas where the materials made from them are expected to swell in alkaline environment. To protect against drug release in the stomach where the pH is low, and to prevent the release of unpleasant-tasting drugs into the pH environment of the mouth [70], anionic hydrogels are employed as suitable excipients for oral delivery of therapeutics [100, 101].

Examples of anionic pH responsive hydrogels are poly (acrylic acid) (PAA), poly (methacrylic acid) (PMAA), pectin/poly (acrylamide-co-acrylamidoglycolic acid) (PPAA), poly (2-hydroxyethyl methacrylate) (PHEMA), etc.

Equilibrium swelling data for PHEMA hydrogels was used in this work for simulation studies involving anionic hydrogels because, PHEMA is a widely used material that has found applications in scaffolds for tissue engineering, artificial skin, contact lenses, and controlled drug delivery devices [102–104].

2.3.1 *PHEMA hydrogels*

Poly (2-hydroxyethyl methacrylate) hydrogels are receiving increasing attention from the research community owing to their excellent biocompatibility, similar physical properties to living tissue [105], and suitability for medical and biomedical applications [106]. Witcherle and Lim [107] were the first to study about the hydrogels of PHEMA in the development of contact lenses. PHEMA hydrogels have shown great potential in bone tissue regeneration, wound healing, and cancer therapy [108]. Although there are different approaches for PHEMA synthesis Figure 2.4 illustrates the free radical crosslinking polymerization of PHEMA.

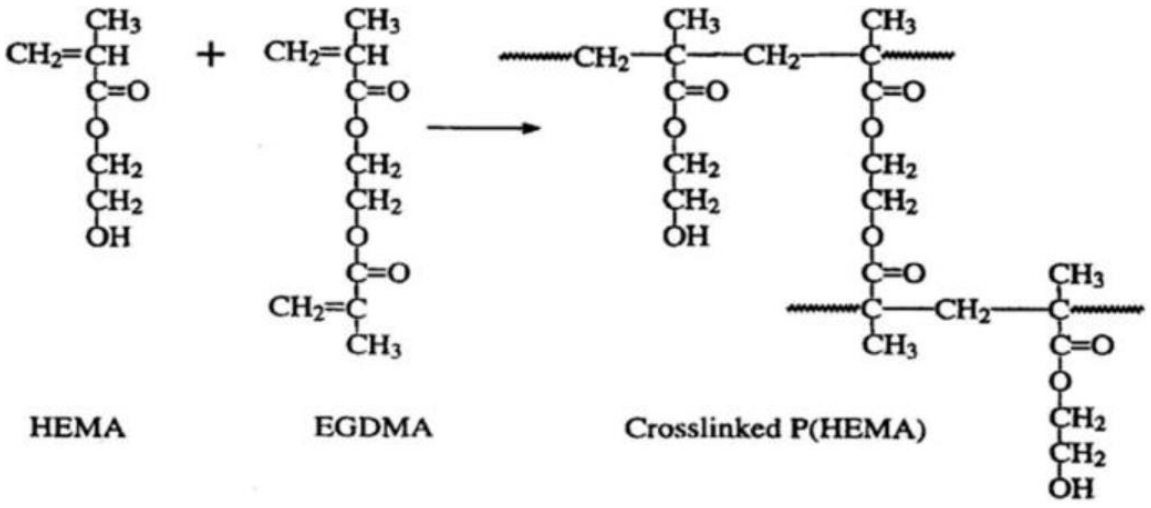

Figure 2.4: PHEMA hydrogel network synthesised from the copolymerization of HEMA with crosslinking agent Ethylene glycol dimethylacrylate (EGDMA). Reprinted from [108]

The swelling behaviour of PHEMA hydrogels have been studied both experimentally [109–111] and computationally [15]. However, this work builds on the computational approach available in the literature for anionic hydrogels and adapts it to model and simulate cationic hydrogels.

2.4 Cationic Hydrogel: Chitosan-based Hydrogels

Cationic hydrogels usually have fixed positively charged basic group as ionizable pendant group at the backbone of the polymer network (see Figure 2.5). They usually have amine, $–NH_2$ group bound to the polymer network. The reversible swelling-shrinking property in response to changes in external pH conditions makes cationic hydrogels attractive materials for a wide range of applications such as targeted drug delivery, gene delivery, and tissue engineering [112].

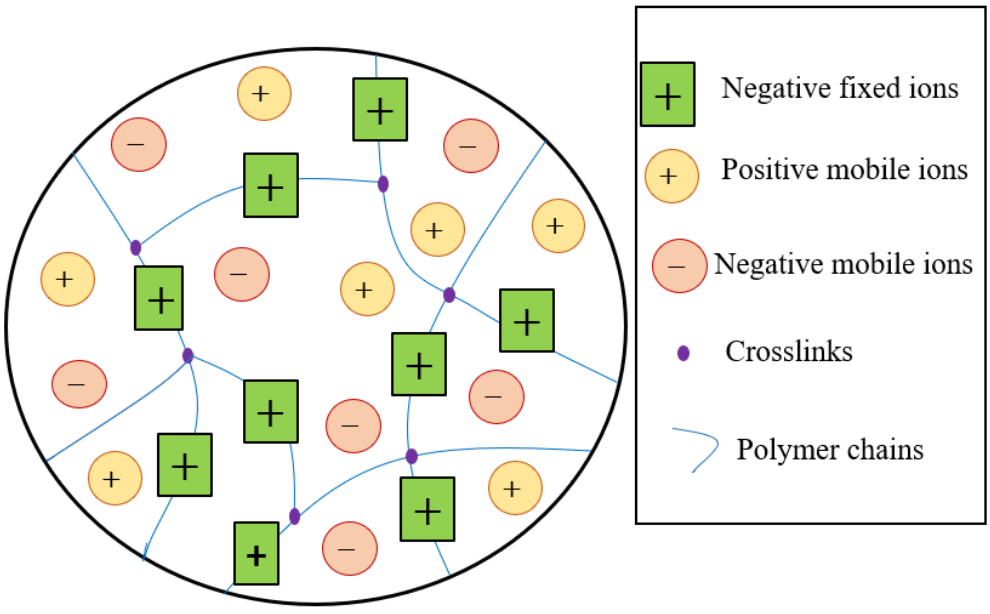

Figure 2.5: Diagrammatic representation of cationic hydrogel. Adapted from [99]

As the pH of the environment becomes less than the pK_b of the hydrogel, the amine group changes from $-NH_2$ to NH_3^+ due to protonation, resulting in electrostatic repulsion leading to swelling of the hydrogel. The extent to which the cationic hydrogel swells (i.e., swelling ratio) depends largely on the pK_b of the fixed charge, crosslinking ratio, concentration of the

monomer, pH, and ionic strength of the surrounding medium [113, 114]. The ability of pH responsive cationic hydrogels to swell at pH lower than the pH of normal body tissue have made them find applications in targeted drug delivery technology and used as carriers for anticancer drugs [115–119].

Some examples of cationic hydrogels are based on poly(lysine), poly(amido-amine), poly (*N*,*N*-dialkylaminoethyl methacrylate), chitosan, etc. For the purposes of biocompatibility, biodegradability, and non-toxicity, chitosan-based hydrogels are of interest to this study. Chitosan a natural copolymer of β −(1–4)-linked 2-acetamido-2-deoxy-D-glucopyranose and 2-amino-2-deoxy-D-glucopyranose, is formed by the partial deacetylation of insoluble naturally available chitin. Chitin is obtained from exoskeletons of crustaceans, fungi, and insects [28], crabs and lobsters, pens of squids, wings of insects and even nails of humans [33].

Chitosan-based hydrogels swell in acidic medium when $pH < pK_b$. So, to stabilize them, chitosan solution is usually cross-linked using different techniques aimed at enhancing their mechanical properties and creating a stable network for a period suitable for the application [36, 37].

For biodegradable polymers such as chitosan to last long enough when in use as drug delivery device, their general properties must be regulated for the desired application by crosslinking chitosan with other reagents. Some crosslinking agents that have been used to modulate the general properties of chitosan are ethylene glycol, glutaraldehyde, tripolyphosphate, diisocyanate and diglycidyl ether [39]. Since synthetic crosslinking agents are cytotoxic and can affect biocompatibility of chitosan in drug delivery applications [120, 121], it is important to use crosslinking agents that have low cytotoxicity and that forms stable and biocompatible crosslinked compounds [39]. Therefore, the naturally occurring crosslinking reagent of interest to this study is genipin. Genipin is obtained from a compound traditionally used in Chinese medicine, geniposide, which may be isolated from the fruits of Gardenia jasminoides Ellis [37], [39]. The structure of genipin crosslinked chitosan hydrogel is shown is Figure 2.6.

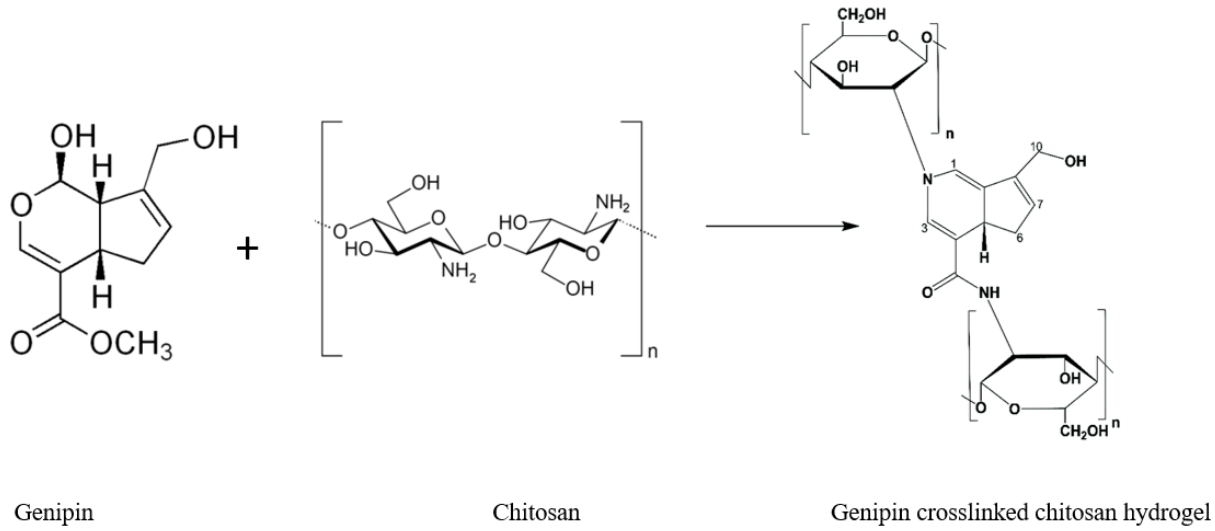

Figure 2.6: Genipin crosslinked with chitosan hydrogel. Adapted from [122].

Studies have demonstrated that crosslinking genipin with chitosan improves the water resistance, swelling and mechanical properties of the final product [39, 123–126]. For example, Vukajlović, Bretcanu, and Novakovic [127] developed two composite materials, genipin crosslinked chitosan hydrogel with the addition of Bioglass 45S5 (BG) powder, and BG scaffolds coated with the genipin cross-linked chitosan hydrogel with a potential for low load-bearing applications, and as an alternative to commonly used collagen and hydroxyapatite. Nwosu, Hurst, and Novakovic [128] studied the influence of composition of genipin-crosslinked chitosan-polyvinylpyrrolidone hydrogels on their response to pH change in their surroundings with potential application in wound dressing and drug delivery. Chung, Birch, and Novakovic [129] used genipin-crosslinked chitosan-polyvinylpyrrolidone hydrogels in their studies to culture non-differentiated adult mesenchymal stem cells for cell viability. Vo *et al.* [130] in their *in vitro* biocompatibility and biodegradability studies, showed the potential of chitosan-genipin hydrogels for vaccine delivery applications. Hurst and Novakovic [131] in their work, showed the suitability of techniques such as scanning electron microscopy, environmental scanning electron microscopy, and *in situ* Confocal Laser Scanning Microscopy (CLSM) for characterizing the network structure of genipin-crosslinked chitosan–poly(vinyl pyrrolidone) hydrogels. Where CLSM was used to track morphological changes as a function of time during swelling of the crosslinked hydrogel.

However, the swelling ratio and kinetics of swelling are dependent on the concentration of genipin used for crosslinking with chitosan. Although several experimental works on the

swelling dynamics of chitosan-genipin hydrogels are available in the literature [132–134], only a few computational-based studies have attempted to model the equilibrium swelling of genipin-crosslinked chitosan hydrogels [135]. To understand the dynamics of their conformational changes with the potential of application in controlled drug delivery technology, food packaging, and wound dressing, mathematical models with the capability of simulating and predicting their responsive dynamic behaviour are undoubtedly important.

2.5 Mechanical Properties of Hydrogels

The mechanical properties of hydrogels are properties which reflect the response or deformation of the gel under applied load or stress. These properties can be tuned or controlled to suit the desired application. Important mechanical properties considered during simulation of the anionic (PHEMA) and cationic (genipin-crosslinked chitosan) hydrogels are elastic modulus, shear modulus, and Poisson's ratio.

The elastic or Young's modulus is a measure of the stiffness of the hydrogel under stress (this implies that a stiffer hydrogel has a higher elastic modulus). It represents the linear relationship of a stress-strain curve as shown in Figure 2.7.

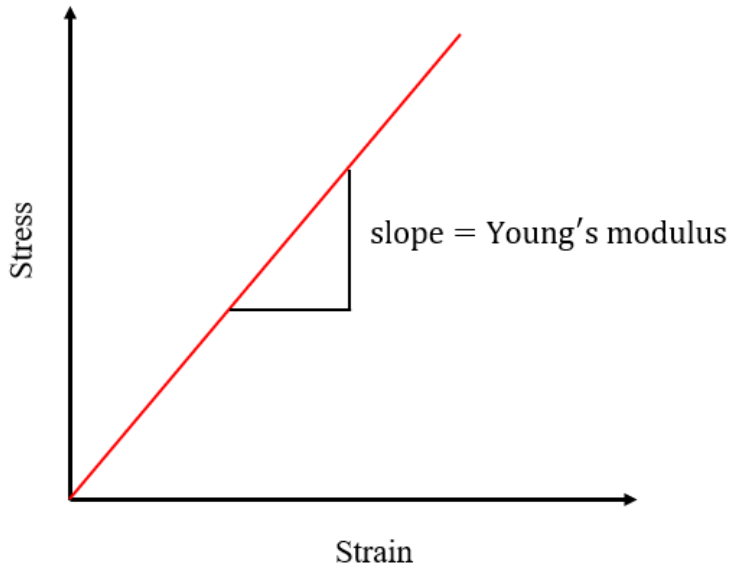

Figure 2.7: Stress-strain curve for determination of elastic modulus

Although some polymer-based materials have non-linear stress-strain behaviours, of which the modulus of elasticity cannot be determined from such plot. The hydrogels whose volume

transition behaviours are modelled in this study are assumed to undergo small deformations, hence are modelled as elastic materials. For pH responsive anionic hydrogels, the elastic modulus has been observed experimentally to vary with pH value of the surrounding medium. For $pH \leq 5$ elastic modulus is 0.29 Mpa, for $pH \geq 7.5$ elastic modulus is 0.21Mpa, and for the range $5.5 < pH < 7.5$, the elastic modulus varies linearly from 0.29 to 0.21Mpa [15].

Shear modulus (also known as the modulus of rigidity) is defined as the ratio of shear stress to shear strain, and it is a measure of the hydrogel's response to shear deformation as shown in Figure 2.8.

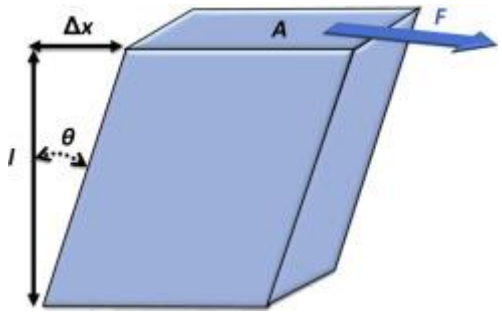

Figure 2.8: Illustration of shear modulus as a function of force, F, area, A, displacement, Δx, initial length, l, and angle of displacement, θ [136]

Poisson's ratio is a measure of the ratio of the transverse contraction (or extension) of the hydrogel to the longitudinal extension (or compression) strain in the direction of the applied force. It is the ratio of the lateral strain to longitudinal strain. Its value for most rubber-like materials is in the range of 0 to 0.5.

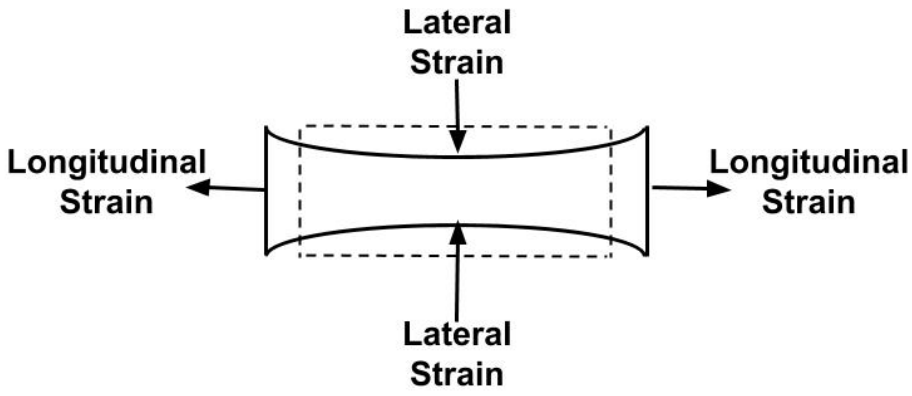

Figure 2.9: Measurement of Poisson's ratio

Poisson's Ratio of 0 means there is no lateral contraction (i.e., no reduction in the diameter of the hydrogel) during material elongation. A value of 0.5 indicates that the volume of the hydrogel will remain constant during material elongation process. The value of Poisson ratio used in this study was obtained from the work of Li [15]. Poisson's ratio, ν is related to Young's modulus E, shear modulus, G by the relation:

$$E = 2G(1 + \nu) \tag{2.1}$$

2.6 Swelling Theories for pH-Sensitive Hydrogels

When a pH-sensitive hydrogel is in contact with an aqueous medium, the pendant group at the backbone of the hydrogel undergoes protonation/ionization as the pH of the surrounding medium varies, resulting in a build-up of charge within the hydrogel. This charge build-up causes electrostatic repulsion which alters the osmotic balance between the hydrogel and the external medium causing moisture in the surrounding medium to penetrate the hydrogel thereby resulting in swelling of the hydrogel. This osmotic pressure, $P_{osmotic}$, is represented mathematically as:

$$P_{osmotic} = RT \sum \left(\left(c_{gel} - c_{sol} \right) \right) \tag{2.2}$$

where c_{gel} and c_{sol} are the concentrations inside the hydrogel and within the surrounding medium respectively. R and T are the universal gas constant and the absolute temperature respectively.

The swelling behaviour of hydrogels has been modelled over the years on microscale (scale at which the phases involved are distinguishable) or macroscale (scale at which the phases involved are indistinguishable) based on some theories known as the statistical theory, the porous media theory, the discrete element theory, the multiphase mixture theory [15, 40].

2.6.1 *Statistical theory*

Statistical theory – a macroscale approach, is based on the original work of Flory [137, 138]. This theory uses change in Gibbs free energy, ΔG, to describe the conditions in the hydrogel and in the surrounding medium [139]. The total free energy of the hydrogel-surrounding system

is the sum of the free energies due to mixing ΔG_m, elastic deformation of the hydrogel, ΔG_{el}, and concentration difference between ions inside and those outside the hydrogel ΔG_{ion}.

The equilibrium state of the swollen hydrogel is defined at the minimum of the total free energy of the hydrogel-surrounding system. At equilibrium, the chemical potentials, μ, of the fluid in surrounding medium and that in the hydrogel are identical, therefore:

$$\Delta\mu = \left(\frac{\partial \Delta G}{\partial n}\right)_{p,T} = \underbrace{\left(\frac{\partial\, \Delta G_m}{\partial n}\right)_{p,T}}_{mixing\ potential} + \underbrace{\left(\frac{\partial\, \Delta G_{el}}{\partial n}\right)_{p,T}}_{elastic\ potential} + \underbrace{\left(\frac{\partial\, \Delta G_{ion}}{\partial n}\right)_{p,T}}_{ionic\ potential} = 0 \qquad (2.3)$$

Statistical theory has been employed to model the swelling of *n*-isopropyl acrylamide hydrogels in water and aqueous solutions of ethanol and acetone [140]. Although the theory can be utilized to model equilibrium swelling, it cannot be employed for studies involving dynamic response or swelling kinetics of pH-sensitive hydrogels.

2.6.2 *Multiphase mixture theory*

For the multiphase mixture theory, the hydrogel is considered a three-phase system comprising the polymer or solid phase, s, fluid or water phase, w, and the ionic phase (constituting the cations, $+$, and the anions, $-$). This theory assumes that the gradient of chemical or electrochemical potentials balanced by frictional forces between the phases, drives the volume variation of hydrogels [43].

The system of equations describing the multiphase mixture theory are:

momentum balance equation: $\nabla.\sigma = 0$ (2.4)

system continuity equation (at steady state): $\nabla.\left(\rho^i v^i\right) = 0$ (2.5)

continuity equation of the fixed charge group: $\nabla.\left(\vartheta^w c_f v^s\right) = 0$ (2.6)

condition of electroneutrality : $\sum z_i c_i + z_f c_f = 0$ (2.7)

where $i = s, w, +, -$, v^i is the velocity of component i, and ρ^i its mass density. The stress is given within the hydrogel is given as:

$$\sigma = \boldsymbol{PI} + \lambda_s tr(E)\boldsymbol{I} + 2\mu_s \boldsymbol{E} \qquad (2.8)$$

where $\boldsymbol{P}$ is the first Piola-Kirchoff stress tensors, $\boldsymbol{I}$ and is the identity tensor and $\boldsymbol{E}$ the elastic strain tensor of the solid/polymer phase. Also, λ and μ are Lamé's coefficient of the hydrogel material.

Although the model developed from the multiphase mixture theory can describe both the equilibrium and swelling dynamics of hydrogel, its inability to capture variation of the elastic properties of the hydrogel during swelling or shrinking limits its general applicability [15].

2.6.3 *Theory of porous media*

The theory of porous media (a macroscale continuum theory) is primarily an extension of the theory of mixtures by the concept of volume fractions [141]. This theory assumes that the porous solid (i.e., hydrogel) is a control volume in which the pores are filled with fluid, and that the pores are statistically distributed [142].

Within the framework of the theory of porous media, a fluid-saturated porous solid is considered an immiscible mixture of the constituents φ^{α} with particles X_{α}. At time $t = t_0$, these particles move from different reference positions $\mathbf{X}_{\alpha}$. Thus, the motion of each constituent is described with an independent motion equation:

$$\mathbf{x} = \boldsymbol{\chi_{\alpha}}(\mathbf{X}_{\boldsymbol{\alpha}}, t) \tag{2.9}$$

where **x** is an element of the porous solid at time *t* (in the current configuration). During deformation of the hydrogel, where the fluid phase exits the control volume of the solid, the reference position of the fluid phase, $\mathbf{X}_F$ can be considered an element of the reference configuration. Eq. (2.9) written in terms of solid and fluid particle is:

$$\mathbf{x} \begin{matrix} = \boldsymbol{\chi_S}(\mathbf{X_S}, t) \\ = \boldsymbol{\chi_F}(\mathbf{X_F}, t) \end{matrix} \Big\} \tag{2.10}$$

An illustrative diagram of the motion of a fluid and a solid particle is shown in Figure 2.10.

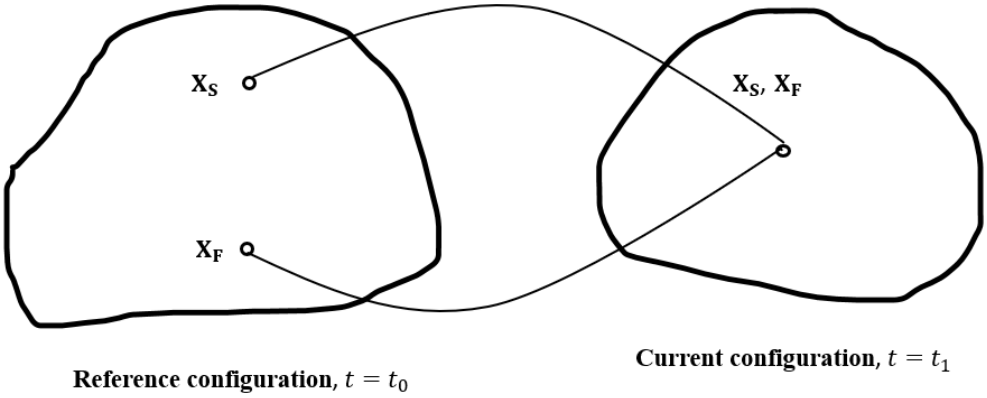

Figure 2.10: Schematic of the motion of a fluid and a solid particle in a fluid-saturated porous material. Adapted from [142].

The mechanical deformation suffered by the hydrogel as the constituents moves from the original position to a new position is mathematically defined as:

$$\mathbf{F}_{\boldsymbol{\alpha}} = \frac{\partial \mathbf{x}}{\partial \mathbf{X}_{\boldsymbol{\alpha}}} = \frac{\partial \boldsymbol{\chi}_{\boldsymbol{\alpha}}(\mathbf{X}_{\boldsymbol{\alpha}}, t)}{\partial \mathbf{X}_{\boldsymbol{\alpha}}} \tag{2.11}$$

where $\mathbf{F}_{\boldsymbol{\alpha}}$ is deformation gradient of the constituents φ^{α}. The volume ratio is defined as:

$$\boldsymbol{J}_{\boldsymbol{\alpha}} = \det(\mathbf{F}_{\boldsymbol{\alpha}}) = \frac{dV}{dV_0} \tag{2.12}$$

The mathematical complexities involve in determining the change in volume of hydrogel when coupling of the chemical, mechanical, and electrical fields is required, limits the general use of the theory of porous media for studies involving swelling of pH responsive hydrogels.

2.6.4 *Discrete element theory*

The discrete element theory considers the hydrogel as a continuum and splits it into discrete particles of certain amount of mass, interacting with each other mechanically [139, 143, 144]. Newton's equation of motion is employed to model the mechanical behaviour of the distributed system, while the chemical behaviour of the system is described using the diffusion equation for mobile ions. Wallmersperger *et al.* [139] employed the discrete element method to develop a model that describes the swelling behaviour of a polymer gel fibre in a bathing solution. Although this theory is suited for problems where the swelling behaviour of hydrogel alone is of interest, it does not capture explicitly the interaction between the hydrogel and the surrounding medium.

2.6.5 *Coupled multi-field formulation*

The coupled multi-field formulation gives insight into how the degree of swelling or shrinking of the pH responsive hydrogel is affected by the interactions between chemical, electrical and mechanical fields [40, 41].

The multifield formulation describes the chemical field using the migration-diffusion equation for the different species inside the hydrogel and in the surrounding medium. The electric field is described by the Poisson equation, while the mechanical field which embodies the deformation of the hydrogel is formulated by conducting momentum balance around the hydrogel. Detailed information and equations describing the multifield formulation approach are provided in Section 2.7.3.

The multi-field modelling strategy has been employed by various authors [15, 40, 139] to model the swelling behaviour of hydrogels, because it is comprehensive and enables full dynamic and equilibrium simulations of the volume variation behaviour of hydrogels. The comprehensive nature of this modelling approach justifies the choice of this approach as the foundation for this study. Therefore, the model for predicting the swelling behaviour of pH-sensitive anionic hydrogel was developed using the multifield approach detailed in Section 2.7.3. In addition, the framework used for modelling anionic hydrogels was adapted to model, simulate, and predict the swelling or volume variation behaviour of pH-responsive cationic hydrogels.

2.7 Mathematical Modelling of pH-Responsive Hydrogels

Having discussed in the preceding section, the various theories behind the swelling of pH-sensitive hydrogels. This section provides a review of the existing mathematical models formulated to describe the volume variation behaviour of pH-responsive hydrogels based on the theories described in Section 2.6. The volume variation behaviour of hydrogels is modelled in the literature using either statistical mechanics approach, or an empirical modelling approach, or from a first principle modelling approach that incorporates the various interacting fields.

2.7.1 *Statistical mechanics of equilibrium swelling*

This approach to modelling equilibrium swelling of stimuli-responsive hydrogels is based on the original work of Flory [137, 138] for non-ionic polymer gels. The thermodynamic theory by Flory states that, a polymer gel immersed in a fluid and allowed to reach thermodynamic equilibrium with the surrounding fluid is acted upon by two opposing forces, the force due to mixing and elasticity of the chains. The equilibrium state of the neutral or non-ionic polymer gel can be described in terms of Gibbs free energy.

$$\Delta G_{total} = \Delta G_{mix} + \Delta G_{elastic} \tag{2.13}$$

where ΔG_{total} is the change in total free energy of the polymer gel, ΔG_{mix} is the change in free energy due to mixing of the polymer chains with the fluid molecules, and $\Delta G_{elastic}$ is the change due to the elastic retractive forces within the polymer gel.

Differentiating Eq. (2.13) with respect to the number of solvent molecules entering the polymer gel, n_s, at constant temperature and pressure, gives the chemical potential of (or the osmotic pressure due to) the solvent entering the polymer gel:

$$\Delta\mu_{total} = \left(\frac{\partial \Delta G_{total}}{\partial n_s}\right)_{T,P} = \Delta\mu_{mix} + \Delta\mu_{elastic} \tag{2.14}$$

At equilibrium, the chemical potential of the solvent inside the polymer gel, μ_{in} must be equal the chemical potential of the solvent in the surrounding medium, μ_{out}. Therefore, Eq. (2.14) becomes:

$$\Delta\mu_{mix} + \Delta\mu_{elastic} = 0 \tag{2.15}$$

For ionic hydrogels, Eq. (2.15) can be extended to include change in osmotic pressure due to ionic interactions within the hydrogel, $\Delta\mu_{ions}$ [145]:

$$\Delta\mu_{mix} + \Delta\mu_{elastic} + \Delta\mu_{ionic} = 0 \tag{2.16}$$

From the Flory-Huggins polymer solution theory [138], the change in chemical potential due to mixing process is given as:

$$\Delta\mu_{mix} = -\frac{N_A kT}{V_s}[\mathrm{In}(1-\phi) + \phi + \chi\phi^2] \tag{2.17}$$

where χ is the polymer-solvent interaction parameter, N_A is Avogadro's constant, ϕ is the polymer volume fraction of the hydrogel, k is the Boltzmann's constant, and V_s is the molar volume of the solvent.

The change in chemical potential due to elasticity is based on rubber elasticity theory derived from the Gaussian chain model [146].

$$\Delta\mu_{elastic} = -\frac{N_A}{V_s}\left(\frac{\partial \Delta G_{elastic}}{\partial n_s}\right)_{n_p} \tag{2.18}$$

where the change in Gibb's free energy due to elastic retractive forces of the polymer chains is given as:

$$\Delta G_{elastic} = -\frac{RT}{V_s} N_c{}^{-1}(\phi^{1/3}\phi_0{}^{2/3} - \frac{\phi}{2}) \tag{2.19}$$

where ϕ_0 is the polymer volume fraction of the hydrogel in the relaxed or at as-prepared state. N_c is the average number of segments in the polymer chain network. In the case of highly crosslinked hydrogels, it is most appropriate to use expression that assumes the non-Gaussian chain statistics in determining osmotic pressure due to elastic forces, $\mu_{elastic}$ [146].

Moreover, several statistical mechanics models have been proposed for crosslinked polymer networks following from the original derivation of elastic free energy, $\Delta G_{elastic}$, by Flory-Rehner. These models include the affine network model proposed for describing the rubber elasticity of polymer networks by Kuhn [147], the phantom network model that takes into consideration the fluctuation around the crosslinking point in the network [148], and the percolate network model employed to determine the concentrations of the crosslinks and network strands in the polymer [149]. More detailed information about these models can be found elsewhere [150–154].

The change in chemical potential due to ionic interactions in the hydrogel, $\Delta\mu_{ionic}$, is given as [15]:

$$\Delta\mu_{ions} = \frac{fRT}{\overline{V_r}}\phi \tag{2.20}$$

where f is the charge density of the hydrogel, (i.e., the fraction of segments bearing the ionic groups). $\overline{V_r}$ is the molar volume of the polymer monomer.

Expressions that describe the contribution of ionic interactions to the change in chemical potential have been developed by Katchalsky *et al*. [155], Ricka *et al*. [156], and Brannon-Peppas [157]. The swelling or shrinking of anionic and cationic hydrogels depend strongly on the ionic strength, and the nature of the ions present in the surrounding medium. To capture the influence of these parameters, Peppas *et al*. [114] have derived expressions for estimating the polymer volume fraction of anionic and cationic hydrogels.

Anionic hydrogel:

$$\frac{V_s}{4I}\left(\frac{\phi^2}{\vartheta}\right)\left(\frac{K_a}{10^{-pH}-K_a}\right)^2 = [\mathrm{In}(1-\phi)+\phi+\chi\phi^2] + \left(\frac{V_s}{\vartheta\overline{M_c}}\right)\left(1-\frac{2\overline{M_c}}{\overline{M_n}}\right)\phi_0\left[\left(\frac{\phi}{\phi_0}\right)^{1/3}-\left(\frac{\phi}{2\phi_0}\right)\right] \quad (2.21)$$

Cationic hydrogel:

$$\frac{V_s}{4I}\left(\frac{\phi^2}{\vartheta}\right)\left(\frac{K_b}{10^{pH-14}-K_a}\right)^2 = [\mathrm{In}(1-\phi)+\phi+\chi\phi^2] + \left(\frac{V_s}{\vartheta\overline{M_c}}\right)\left(1-\frac{2\overline{M_c}}{\overline{M_n}}\right)\phi_0\left[\left(\frac{\phi}{\phi_0}\right)^{1/3}-\left(\frac{\phi}{2\phi_0}\right)\right] \quad (2.22)$$

Caykara *et al*. [158] derived the following equation to predict the equilibrium swelling behaviour of hydrogels with monoprotic acid moieties.

$$\left[\frac{K_a}{10^{-pH}+K_a}\right]^2\frac{V_s{f_i}^2}{4I\overline{V_r}^2}-\phi^{-2}In(1-\phi)-\phi^{-1}=\chi+\frac{(1-2/\Omega)}{\overline{M_c}}V_s\rho{\phi_0}^{2/3}\phi^{-5/3} \quad (2.23)$$

where $\overline{M_c}$ is the average molecular weight between the crosslinks, $\overline{M_n}$ is the molecular weight of the polymer chains prepared under identical conditions, ϑ is the specific volume of the polymer, K_a and K_b are the dissociation constants for the anionic and cationic hydrogels respectively, f_i is the molar fraction of the ionic unit in the hydrogel system, ρ is the density of the polymeric material, $\overline{V_r}$ is the molar volume of the polymer monomer, *pH* and I are the pH and ionic strength of the surrounding medium, and Ω is the functionality at the crosslinking site.

Since the model Equations (2.21), (2.22), and (2.23) captures the dependence of the swelling ratio on the nature of ions present in the solvent and the ionic strength of the surrounding media,

it can be used to predict the equilibrium volume variation behaviour of both anionic and cationic hydrogels. However, the major drawback of these models is the inability to predict time-dependent volume variation behaviour of hydrogels. Moreover, most of the parameters of these models (for example, $\overline{M_c}$, f_i, $\overline{M_n}$, Ω, $\overline{V_r}$) are difficult to ascertain as they require lots of trial and error to estimate them using experimental data.

Furthermore, this thermodynamic approach was employed by Jahren *et al*. [135] to model the equilibrium swelling behaviour of pH-sensitive genipin crosslinked chitosan hydrogel. For the first time, a model that captures the effect of change in concentration of the crosslinking reagent (and all ionizable groups present in the polymer) on the equilibrium swelling of the hydrogel was developed and validated against experimental equilibrium swelling data for pH-sensitive chitosan crosslinked with genipin, glutaraldehyde and polygenipin hydrogels [135]. Unfortunately, the discrepancy between the model prediction and the experimentally determined swelling ratio was consistently large by a factor of 30. This large error could be attributed to the choice of equations used to describe the contributions of the competing potentials. For example, the following equations were used for:

i. *Mixing potential*

$$\Delta\mu_{mix} = RT\left[\frac{\mathrm{In}(1-\phi)+\phi+\chi\phi^2}{V_s}\right] \tag{2.24}$$

Since the hydrogels under investigation are ionic, the mixing potential contributes little to the equilibrium swelling of the hydrogel. In addition, Eqn. (2.24) does not differ from the general Flory-Huggins equation used to describe the mixing potential.

ii. *Elastic potential*

$$\Delta\mu_{elastic} = -G'\left(\begin{array}{c}\frac{1}{2}r - \frac{\left(1-(1/N)+(0.4/N^2)+(0.32/N^3)\right)}{r^{1/3}} + \left(-\frac{1}{N}+\frac{2.6}{N^2}-\frac{1.72}{N^3}\right)r^{1/3} \\ +\left(-\frac{2.2}{N^2}-\frac{8.84}{N^3}\right)r+\left(\frac{6.84}{N^3}\right)r^{5/3}\end{array}\right) \tag{2.25}$$

r is the mass swelling ratio (see Section 2.9 for details), G', is the shear elastic modulus, and N is the number of chitosan saccharide units per elastically active chain. Defined mathematically as:

$$N = \frac{c_c}{c_g} \tag{2.26}$$

where c_c and c_g are the molar concentrations of chitosan and genipin respectively. From Eqn. (2.25), and a series of experiments [135, 159] the authors derived a linear relationship between G' and r. The linearized form of Eqn. (2.25) was used to determine the contribution due to elastic potential. The error between the model predictions and the experimentally determined

swelling ratio could arise from this approximation or the linearization of the Eqn. (2.25). To circumvent this concern, this study builds on the work of Jahren *et al*. [135] but derives the elastic modulus differently following from Eqn. (2.19).

iii. Ionic potential

$$\Delta\mu_{ionic} = RT\sum_i\left(c_{out}^i - c_{in}^i\right) \tag{2.27}$$

where c_{out}^i and c_{in}^i are the concentration of each ionic species outside and within the hydrogel respectively. Thus, by substituting Eqns. (2.24), (2.25) and (2.27) into Eqn. (2.16) the equilibrium swelling ratio, *r* was determined. One major drawback of this approach is it cannot be used to determine the swelling kinetics of hydrogels.

In general, models developed using this statistical mechanics approach predict the equilibrium volume variation behaviour of stimuli responsive hydrogels. However, their parameters of best fit are often estimated with lots of difficulties and uncertainties. This limits their general use and prediction accuracy. Although some level of agreement between numerical results and experimental data have been achieved in the literature by adjusting some parameters within the models [15].

2.7.2 *Empirical modelling*

Empirical modelling approach describes swelling as the diffusion of water into the polymer matrix, resulting in expansion of the polymer network due to polymer-chain relaxation. The swelling kinetics of hydrogel, modelled through this approach is based on experimental swelling data.

Based on experimental observation, Schott [160, 161] described the rate of diffusion as a second order kinetics given as:

$$\frac{dM_t}{dt} = k_r(M_\infty - M_t)^2 \tag{2.28}$$

Integrating and rearranging parameters gives the following equation:

$$\frac{t}{M_t} = A + Bt \tag{2.29}$$

where M_t is the amount of water uptake at time, t, M_∞ is the equilibrium or maximum amount of water uptake by the polymer gel, k_r is the kinetic rate constant of swelling, $B = 1/M_{\infty,}$ and $A = 1/(k_r {M_\infty}^2) = 1/(dM_t/dt)_{t=0}$ is the reciprocal of the initial swelling rate.

The plot of $\frac{t}{M_t}$ against *t* on the experimental swelling data gives a straight line with slope and intercept as *B* and *A* respectively. Schott's second order swelling kinetic model has been tested and shows good results [162] for hydrogels synthesised from acrylamide, acrylic acid, and *n*-alkyl methacrylate esters cross-linked with 4,4'-di(methacryloyamide) azobenzene.

In addition, power law model [15] proposed for diffusion of water into polymers is given as:

$$M_t/M_\infty = k_r t^n \tag{2.30}$$

where *n* is the diffusion index, which plays a vital role in determining the kinetics (i.e., the rate controlling step) of volume variation of hydrogels. The value of the diffusion index provides information about the phenomenon or mechanism controlling water uptake by the polymeric material.

On one hand, if the rate of solvent diffusion is slower (i.e., the diffusion is the rate-controlling step) than the rate of polymer-chain relaxation, the diffusion index, $n = 0.5$, and the system is considered to exhibit perfect Fickian behaviour or Case 1 transport. However, Wang and co [163] reported *n* values closer to or slightly above 0.5 for Fickian behaviour, while Bajpai and co-workers [164], Bajpai and Giri [165], Wang *et al.* [166], and Denizli *et al.* [167] have demonstrated the possibility of having $n < 0.5$ for Fickian behaviour when the solvent penetration rate is far much slower than the polymer-chain relaxation.

On the other hand, if the polymer-chain relaxation is slower than the diffusion of the solvent in the swollen state, the diffusion index, $n = 1$, and the system is said to exhibit the non-Fickian or Case II transport (i.e., the rate of water uptake is directly proportional to time). The intermediate case (i.e., $0.5 < n < 1$) where the rate of water uptake is directly proportional to t^n, is called the anomalous transport. The power law model describes the swelling behaviour of hydrogels very well for times where $\frac{M_t}{M_\infty} \leq 0.60$, but fails above time values above this range [168]. To complement the power model for time values corresponding to $\frac{M_t}{M_\infty} > 0.60$, a first order kinetic model was proposed [169]:

$$\frac{dM_t}{dt} = k'(M_\infty - M_t) \tag{2.31}$$

where k' is the relaxation rate constant (min^{-1}). Solving Eq. (2.31) gives:

$$M_t/M_\infty = \left(1 - De^{-k't}\right) \tag{2.32}$$

where the constants D and k' are obtained from the slopes and intercepts of the graph of $\ln(1 - M_t/M_\infty)$ against time for t values corresponding to $\frac{M_t}{M_\infty} \geq 0.60$.

Furthermore, continuum mechanics approach was used [146] to derive a model for volume variation of spherical gel as a function of time:

$$\frac{\Delta a(t)}{\Delta a} \cong \frac{6}{\pi} exp\left(-\frac{t}{\tau_1}\right) \tag{2.33}$$

where $\Delta a(t)$ is the deformation of the gel surface over time, Δa is the deformation of the gel surface at equilibrium. Experimentally, τ_1, which is a function of the collective diffusion coefficient of the polymer gel [170], is obtained as the slope of the plot of $\log(\Delta a(t)/\Delta a)$ against t. For details of the derivation, refer to [146]. This model provides a simple method to correlate experimental data from swelling kinetics. Although the model shows good results for swelling studies involving spherically shaped Tetra-PEG gels [170], unfortunately, it cannot offer predictions for non-spherical polymer gels.

The concerns surrounding these empirical models span from their range of accuracy [15, 168], and the fact that they do not account for the influence of electric field (created by the cloud of ions inside and around the hydrogel), and mechanical deformation of the hydrogel.

2.7.3 *Multifield modelling approach*

The multi-field approach to modelling swelling dynamics for hydrogel immersed in an aqueous medium is based on the laws of conservation of mass, charge, and momentum, where the chemical, electrical and mechanical effects are taken into consideration. This approach is based on the work of Wallmersperger and co-workers [41]. Since the volume variation of ionic hydrogels is driven by diffusion of ions between the hydrogel and the surrounding medium, the model developed from this approach couples the Nernst-Plank equation, together with the Poisson equation and the mechanical equation to simulate the diffusive ionic concentration, electric potential, and the deformation of the hydrogel respectively.

The unsteady state Nernst-Plank equation, the Poisson equation, and the unsteady state mechanical equation (for large deformation based on the concept of total Lagrangian) are given as follows:

$$\frac{\partial c_k}{\partial t} + D_k \frac{\partial^2 c_k}{\partial x^2} + \mu_k z_k F \left(c_k \frac{\partial^2 \varphi}{\partial x^2} + \frac{\partial c_k}{\partial x} \cdot \frac{\partial \varphi}{\partial x} \right) = 0 \qquad (k = 1,2,3, \dots N) \qquad (2.34)$$

$$\frac{\partial^2 \varphi}{\partial x^2} = -\frac{F}{\varepsilon \varepsilon_0} \sum_{k=1}^{N} (z_k c_k + z_f c_f) \qquad (2.35)$$

$$\nabla . \boldsymbol{P} + \boldsymbol{b} - \boldsymbol{f} = \rho \dot{\boldsymbol{U}} \qquad (2.36)$$

where D_k is the effective diffusivity (for isotropic diffusion), c_k the concentration, z_k valency, μ_k is the mobility of the k^{th}-species ion, ε_0 is the dielectric constant of vacuum, ε is the relative dielectric constant of the surrounding fluid, F is the Faraday constant, c_f and z_f are the density and the valence of the fixed charge ion inside the hydrogel, $\boldsymbol{b}$ is the body force, $\boldsymbol{f}$ is external force, $\dot{\boldsymbol{U}}$ is acceleration, $\rho \dot{\boldsymbol{U}}$ is inertial force, and ρ is the density of the hydrogel.

The fixed charge density c_f is related to the hydrogel volume variation for anionic and cationic hydrogel respectively [15]:

$$c_f = \frac{1}{H} \frac{c_{f,0} K_a}{(K_a + c_H)} \qquad (2.37)$$

$$c_f = \frac{1}{H} \frac{c_{f,0} c_H}{(K_b + c_H)} \qquad (2.38)$$

where H is the local hydration state of the pH-responsive hydrogel, K_a and K_b are the acid and base dissociation constant of the fixed charged group, $c_{f,0}$ is the initial fixed charge concentration within the hydrogel in its relaxed state, and c_H the concentration of the hydrogen ions inside the hydrogel.

Based on this approach, Li [15] developed a Multi-Effect-Coupling pH-Stimulus (MECpH) model for one-dimensional shape anionic pH-sensitive hydrogels. Suthar [171] developed a multi-field numerical model for simulation of equilibrium swelling of a disc-shaped pH-sensitive anionic hydrogel. However, Kang [172] developed a chemo-electro-mechanical field model by coupling the Nernst–Planck equation together with Donnan theory and elastic mechanics equation to investigate the swelling/deswelling dynamics of pH sensitive hydrogels.

Further, the presence of buffer in the surrounding medium influences the diffusion of hydrogen ion by providing an alternative pathway for the hydrogen ion between the hydrogel and the surrounding medium. To capture the influence of the buffer, Li [15] included additional terms in the continuity equation for hydrogen ions within the hydrogel to obtain the following chemo-electro-mechanical model for swelling kinetics:

Chemical field: Diffusion of hydrogen ion

$$\frac{\partial}{\partial t}\left[Hc_H + \frac{c_{f,0}c_H}{(K_b+c_H)} + \frac{Hc_Tc_H}{(K_B+c_H)}\right] = -\frac{\partial}{\partial X}\left[\alpha\left(\frac{H}{1+H}\right)\left(1+\frac{\bar{D}_{HB}}{\bar{D}_H}\frac{c_T}{(K_B+c_H)}\right)\left(\bar{D}_H\frac{\partial c_H}{\partial x}\right)\right] \quad (2.39)$$

Electric field: Electrostatic potential (Poison equation)

$$\frac{\partial^2\varphi}{\partial x^2} = -\frac{F}{\varepsilon\varepsilon_0}\sum_{k=1}^{N}(z_kc_k + z_fc_f) \quad (2.35')$$

Mechanical field (determines volume ratio in terms of hydration):

$$\frac{\partial}{\partial t} = \frac{\partial}{\partial X}\left[ak'\left(-\frac{\partial(M\varepsilon)}{\partial x} + z_fc_fF\frac{\partial\varphi}{\partial x}\right)\right] \quad (2.40)$$

where H is the hydration, c_T is the total buffer concentration, c_H concentration of hydrogen ion in the hydrogel, K_B is the dissociation constant of the buffer, c_B , $\bar{D}_H$ is the diffusivity of hydrogen ions within the hydrogel $\bar{D}_{HB}$ is the diffusivity of buffer in the hydrogel, M is the bulk modulus of the hydrogel, ε is the compressive strain and k' is hydraulic permeability of the hydrogel.

2.7.4 *Comparison of the different modelling approaches*

The volume variation behaviour of hydrogels can be modelled using either statistical mechanics (thermodynamic modelling) approach, or empirical modelling approach based on experimental swelling data, or the more robust but complex multifield approach. Although the thermodynamic model developed from statistical mechanics standpoint can provide information about the equilibrium volume variation behaviour of hydrogel, they require experimental swelling data for parameters adjustment and cannot provide details about time-

dependent swelling or shrinking behaviour of the hydrogel, which limits their application to only equilibrium swelling or shrinking of hydrogel.

Further, with the availability of time-dependent swelling (experimental) data for hydrogel, empirical models can be employed to predict the mechanism of swelling of the gel. However, their inability to capture influences due to electrostatic interaction for ionic hydrogels, and mechanical deformation due to chemical migration of ions from the surrounding medium to the interior of the hydrogel, limit their general use.

In contrast to the thermodynamic and empirical modelling approaches, the multifield modelling approach can be employed for transient volume variation study of the hydrogel and can account for the influence of electrostatic interactions (between ions inside the hydrogel and the surrounding medium), and mechanical deformation of the hydrogel due to migration of ions. Hence, the reason this modelling approach was deployed in this study.

2.8 Numerical Simulation of Multi-Effect-Coupling Models

A review of the solution methods available in the literature for simulating the volume variation behaviour of stimuli-responsive hydrogels is highlighted in this section. The multi-field model for simulation of the swelling or shrinking behaviour of pH-responsive hydrogels are in the form of coupled Partial Differential Equations (PDEs), with constitutive relations and boundary conditions. The methods to solve this system of equations are largely numerical as the coupled PDEs do not yield themselves well to analytical methods. Usually, an approximation of the equations is formulated typically based on different types of discretization (i.e., numerical) method.

The numerical methods available for solving PDEs are of different types: Finite Difference Method (FDM), Boundary Element Method (BEM), Finite Volume Method (FVM), Finite Element Method (FEM), and the Meshless Method.

Among these methods, FEM and FVM are most widely used for determining the approximate solutions to PDEs for complex geometry. Although, FVM can be used to evaluate PDEs, it is most suited for Computational Fluid Dynamics (CFD) problems.

Traditionally, FEM is employed for simulation of hydrogel deformation [171, 173, 174]. However, Li and co-workers [175] developed a novel approach called the Hermite-cloud

meshless technique for simulation of the response performance of pH-sensitive hydrogels based on one-dimensional domain [42]. The ease and flexibility of implementation of the FEM in commercially available finite element software informs the choice of FEM in this study.

2.8.1 *Basics of finite element method*

Finite Element Analysis (FEA) or FEM is a computational method employed to determine approximate solutions of field problems (i.e., Boundary Value Problems, BVP). The field is the computational domain, while the field variables are the dependent variables in the system of partial differential equations (PDEs). The boundary conditions are the specified values of the field variables or their derivatives on the boundaries of the field. FEM involves modelling a system/structure using small, interconnected elements called finite elements and it is typically characterized by the following steps:

Step 1: Pre-processing

This step involves building the set of PDEs (which captures the physical problem), meshing (which involves discretizing the geometry into specific finite elements defined by nodes and their connections), specifying the material properties, and applying the loads and boundary conditions [176], [177]. Figure 2.11 illustrates the use of a triangular mesh for meshing or modelling a three-dimensional domain, where the points of intersections of the various triangular finite elements represents the node/nodal points.

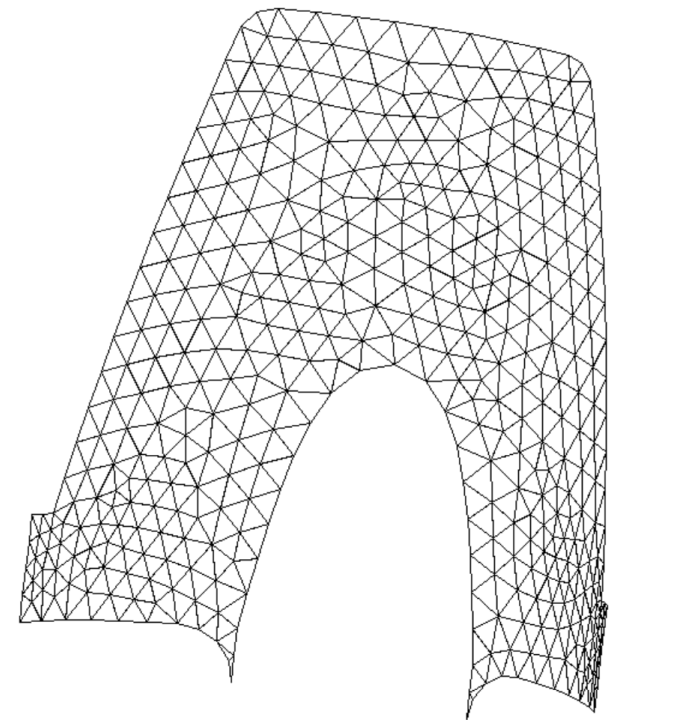

Figure 2.11: Meshing a 3-D geometry using a triangular mesh. Adapted from [178]

The finite elements commonly used for FEA can be one-dimensional (for these elements, one of the dimensions is very large compared with the other two dimensions, e.g., using a line to represent a rod, bar beam, pipe), two-dimensional (when two of the dimensions are very large compared with the third one, e.g., using a quadrilateral or a triangle to represent a plate, membrane etc.), and/or three-dimensional (these elements have all three dimensions comparable e.g., tetra, penta, hex, pyramid representing solids). These elements are shown in Figure 2.12.

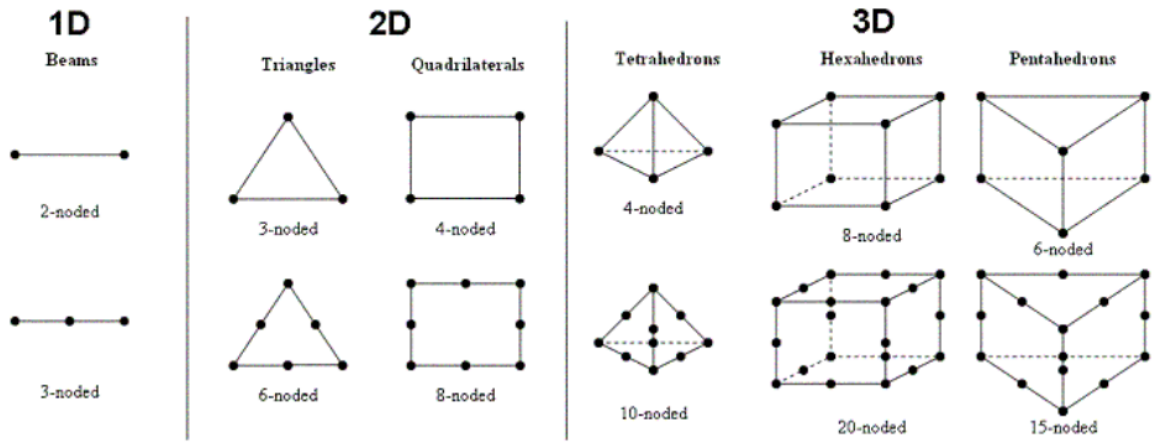

Figure 2.12: Element types with nodes employed for FEA [179]

With these one-, two, and three-dimensional elements, 1D models (which can approximate swelling along the radius of the hydrogel under analysis), 2D models (can approximate swelling in a disc-shaped hydrogel for example, drug in tablet form), and 3D models (deployed for modelling organs and tissues in the body) can be developed and used for simulation studies.

Step 2: Processing

Processing involves deriving a set of linear or nonlinear algebraic equations (from the discretized PDEs in step i above) which can be solved simultaneously to obtain the values of the dependent variables at the nodes. FEM calculates the values of the unknowns (degrees of freedom) at the nodes and then interpolates the results of the entire domain using an interpolation function.

In FEM a continuous quantity such as concentration of a diffusing species or displacement throughout the body, is approximated (through meshing/discretization of the body) by a

discrete model composed of a set of piecewise-continuous functions defined within each finite element. The resulting linear system of algebraic equations is of the form:

$$[K][u] = [f] \tag{2.41}$$

where $[K]$ is the system matrix (in stress analysis it is called the element stiffness matrix).
$[u]$ is the response matrix or the vector of nodal field variables (i.e., the vector of the unknowns)
$[f]$ is the system's input or force vector (i.e., the matrix of the nodal forces).

The processing step in FEM centres on the derivation of equations for each finite element, and calculation of the stiffness matrix. The methods employed for developing the element equations are three: the direct method, the work or energy method, and the methods of weighted residuals.

Direct method is based on force balance on a static body, it is well suited to one-dimensional problems, easy to understand but difficult for computer programming.

The work or energy methods include, the principle of virtual work, the minimum total potential energy, and the Castigliano's theorem [180]. These methods are employed for solid mechanics problems.

The methods of weighted residuals are based on minimizing the error/residual between the exact solution and the approximate solution. The methods include: the collocation, the least squares, the subdomain, and the Galerkin's method. Most commercial software adopts the popular Galerkin's method.

In developing a FEM for hydrogel swelling, Blanco and co-workers [173] adopted the weighted residual method, particularly the Galerkin formulation (explained in detail in Appendix I).

Step 3: Post-processing

This final step involves visualizing and manipulating the results obtained at the processing step. It could display results in form of graphs, surface, or contour plots etc.

2.8.2 *Software implementation of finite element method*

The volume variation behaviour of hydrogels is a multiphysics problem because, as discussed in Section 2.7.3, the swelling or shrinking response of ionic hydrogels in the presence of stimuli (e.g., pH, temperature, etc.,) is affected by the interaction between several distinct fields or physics such as chemical, electrical, and mechanical interactions. Although there are several

software packages (such as MATLAB, ANSYS, ABAQUS, COMSOL, SimScale, Autodesk, OpenFOAM, etc.,) that can be used to solve problems in the form of finite element analysis [181], COMSOL Multiphysics was chosen in this study because of its relative ease in coupling different physics [182]. Section 2.8.3 gives a brief introduction to COMSOL Multiphysics® software as used in this work.

2.8.3 *Introduction to COMSOL Multiphysics*

COMSOL Multiphysics is a versatile software package that offers a convenient means for implementing a wide range of finite element analysis problems. These problems can be solved as standard physics modalities such as chemical diffusion, fluid mechanics, structural mechanics, etc., or as coupled multiphysics problems, such as the case handled in this study. Its coupling capabilities justifies the choice for COMSOL in this study.

In this work, the three physics coupled together were transport of diluted species (representing chemical diffusion), electrostatics under AC/DC interface, and solid mechanics. For details about the mathematics and coupling of these physics to simulate the swelling/shrinking of the anionic and cationic hydrogels in COMSOL Multiphysics, refer to Section 3.1.3.

2.9 Swelling Data

Experimental swelling data often use for model validation studies could come in form of mass swelling ratio, or volume swelling ratio. In other to convert from one form of ratio to the other, this section highlights the mathematical relationship between these ratios.

2.9.1 *Mass swelling ratio*

The mass swelling ratio, m_{SR} is defined as:

$$m_{SR} = \frac{m_t - m_0}{m_0} \tag{2.42}$$

where m_t is mass of the hydrogel gel at time, t, m_0 is mass of the hydrogel at as-prepared state.

2.9.2 *Volume swelling ratio*

The volume swelling ratio, V_{SR} is defined as:

$$V_{SR} = \frac{V_t}{V_0} \tag{2.43}$$

here V_t is the volume of the hydrogel at time, *t*, V_0 is the volume of the hydrogel at as-prepared state. There are other representations such as:

$$V_{SR} = \frac{V_t - V_0}{V_0} \tag{2.44}$$

However, to avoid misinterpretation of Eqn. (2.44) as ratio of water uptake, all through this study, swelling ratio is defined using Eqn. (2.43).

Furthermore, if the density of the fluid is assumed constant, then the mass swelling ratio can be converted to the volume swelling ratio through the relation:

$$\begin{aligned} V_{SR} &= \frac{V_t}{V_0} = \frac{V_0 + V_{f,t}}{V_0} = 1 + \frac{V_{f,t}}{V_0} \\ &= 1 + \left(\frac{m_{f,t}/\rho_f}{m_0/\rho_g} \right) = 1 + \frac{\rho_g}{\rho_f} \frac{m_{f,t}}{m_0} \\ &= 1 + \frac{\rho_g}{\rho_f} \left(\frac{m_t - m_0}{m_0} \right) \\ &= 1 + \frac{\rho_g}{\rho_f} m_{SR} \end{aligned} \tag{2.45}$$

where $V_{f,t}$ is volume of fluid uptake at time, *t*, ρ_g is the density of the hydrogel at as-prepared state, ρ_f is the density of the fluid (assumed constant).

2.10 Engineering Applications of pH-Sensitive Hydrogels

Mathematical or numerical modelling and simulations can aid in the design, construction, and investigation of the volume change behaviour of pH responsive hydrogels used for applications in numerous areas such as wound dressing, drug delivery, tissue engineering, etc.

2.10.1 *Wound dressing*

Microorganism invasion and proliferation can be enhanced by the pH of a wound [183]. For example, *Streptococcus pyogenes, Pseudomonas aeruginosa*, and *Escherichia coli* can grow in a wound of pH values 4.5, 4.4 and 4.3 respectively [184]. Open wounds typically are in the pH range of $6.5 - 8.5$ while chronic wounds exist in pH range of $7.2 - 8.9$ [185]. To enhance the biochemical processes of healing, it is important to monitor the pH of wounds [183, 186] to keep them under control. And one way to do this would be to use pH responsive hydrogels. To form composite products suitable for various kinds of wounds, hydrogels have been included

in the structure of some wound dressing materials [77]. As an example, Figure 2.13 shows different commercially available hydrogel-based wound dressings.

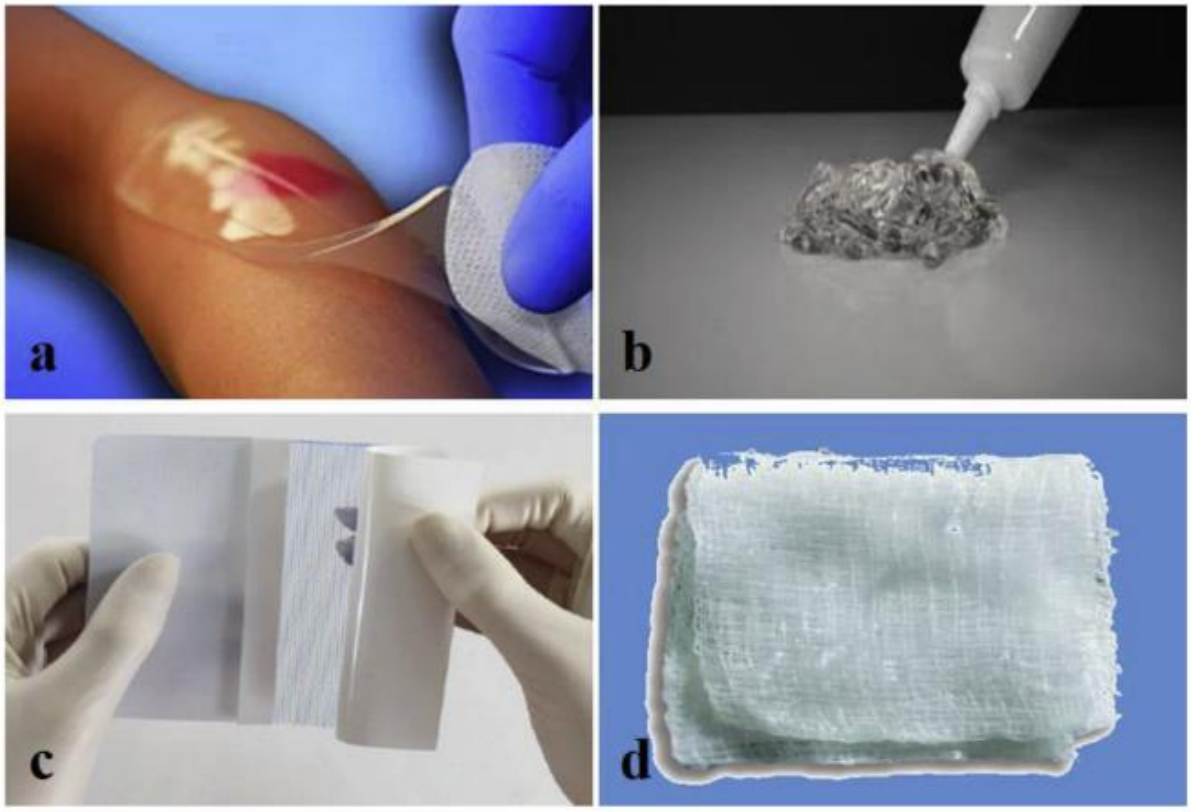

Figure 2.13: Various forms of commercially available hydrogel-based wound dressings. Reprinted from [187].

The different sections in Figure 2.13 represents, (a) Neoheal® hydrogel sheet used for wound dressing, (b) Amorphous gel that can be used for necrotic wounds and burns, (c) Hydrogel film and (d) Hydrogel impregnated gauze.

2.10.2 *Drug delivery*

Hydrogels used in drug delivery applications are either formed outside of the body and used to encapsulate drugs before the hydrogel–drug complex enters the body [9], or they are preformed into micro- or nanoparticles carrying drugs. In some applications, the hydrogels can also be formed *in situ* (i.e., in vivo). pH responsive hydrogels have been identified as suitable carriers in the design of swelling-controlled-drug delivery devices. The ability of hydrogels to dynamically self-modulate and control their volume variation in response to changes in the pH value and ionic strength of the surrounding medium makes them suitable for drug release to

disease sites in the body. For example, in the gastrointestinal tract, pH variation is from $1-3$ in the stomach, and $5-8$ in the small intestine. This variation allows for the use of either anionic or cationic hydrogels to deliver drugs to the target site, while preventing drug release at other sites or healthy tissues. Figure 2.14 shows hydrogel in drug delivery applications.

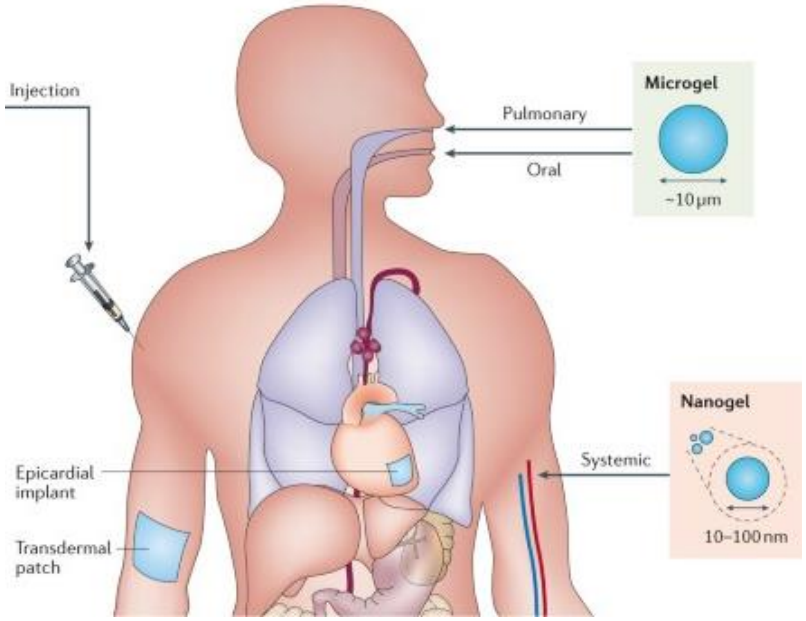

Figure 2.14: Deploying hydrogel via different routes to deliver drugs to various parts of the body. Reprinted from [188].

2.10.3 *Tissue engineering*

Over the past two decades, hydrogels have been used as tissue engineering scaffolds owing to their ability to maintain a distinct 3D structure, provide both mechanical support [24] and a soft tissue-like environment for the cells in the engineered tissues to grow, and allow diffusion of nutrients and cellular waste through the porous structure of hydrogel network [189].

Mathematical modelling and simulation of the volume variation behaviour of hydrogels can provide useful insights that can aid the design and fabrication of hydrogel scaffolds for tissue engineering. During numerical simulation, various hydrogel material properties such as mechanical stability, degree of crosslinking, concentration of crosslinking agent used etc., and the surrounding environmental conditions can be varied to study the response behaviour of hydrogel *in vitro*, with potential application *in vivo*. Figure 2.15 shows how hydrogels are used for cartilage defects repair.

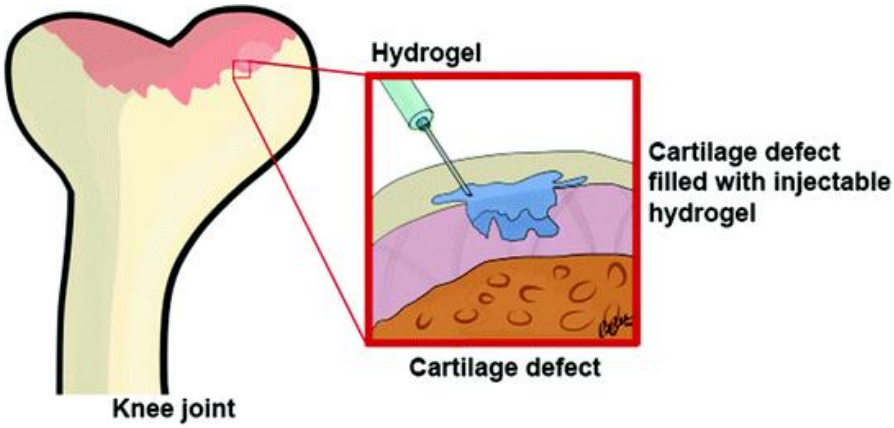

Figure 2.15: Application of injectable hydrogel for cartilage defect repair [190].

2.11 Statement of Economic Impact of this Study

As the experimental side of studying the equilibrium and dynamic swelling behaviour of pH responsive anionic and cationic hydrogels develop, there is a strong need to develop mathematical frameworks for studying the underlying mechanism of the swelling of these hydrogels. For over a decade, methodologies for studying the swelling behaviour of smart hydrogels from a mathematical standpoint are being developed, tested, and have been applied to model the swelling behaviour of stimuli-responsive anionic hydrogels [15]. However, a major challenge to progress in this field, especially in generalising the models to swelling behaviours both anionic and cationic hydrogels of complex geometry is the mathematical complexities behind their numerical solutions.

Furthermore, that sufficient knowledge of some operating parameters (e.g., concentration of the fixed charge group at the backbone of hydrogel) is often lacking and the mathematical complexity behind the multiphysics chemo-electro-mechanical interaction between hydrogel and the surrounding pose a significant challenge for the simulation engineer. However, developing, analysing, and simulating numerical models can provide useful insight for understanding the interplay between the various physics behind swelling and/or shrinking of hydrogels. Ideally mathematical modelling and simulation is performed to complement experimental study, to allow the developed model to be tested, validated and where necessary recalibrated, and the results of the model predictions, could guide the simulation engineer to suggest protocols for improving experimental outcomes.

For example, mathematical modelling of the volume variation behaviour of hydrogels can be used to predict the time evolution of the volume of the different tissue constituents inside an engineered scaffold after implantation in the host tissue [191]. With the aid of mathematical models, one can explore the impact of varying the properties of the scaffold, nutrient and growth factor concentrations [192] *in vitro*, to gain insight into what may likely happen *in vivo* after implantation.

Though *in vivo* studies are the standard for assessing the effectiveness of new treatments proposed for wound healing [193], mathematical modelling and simulation has helped offer insight into the underlying mechanisms behind each stage of the wound healing process [193], [194]. Nonhealing wounds are inconveniencing and are of considerable pain, immobility, leading to a decreased quality of life of patients [195]. Globally, wound healing constitutes the biggest challenge for public health systems, with total spending in the United States alone, for all wound types estimated to be up to $96.8 billion per annum [196].

Therefore, with mathematical modelling, a real-world problem (such as delivering drugs to a targeted disease site, repairing a damaged cartilage, wound healing, etc.,) is simplified to a working model in the form of a system of equations. Such models become a framework for exploring the roles played by individual components characterizing the real-world problem, and when solved, can potentially generate theoretical outcomes that may not have been anticipated otherwise. Thereby stirring further research, streamlining experiments, and saving cost. In addition, they can provide a means to study the impact of varying the values of some key elements/parameters on the real-world problem.

Hence, it is intended that this study will benefits researchers in the field of smart hydrogel modelling, by providing a testbed for exploring the interplay of many parameters controlling the conformational change dynamics of hydrogels synthesised from naturally available polymers with high degree of biocompatibility, biodegradability, and non-toxicity, such as genipin-crosslinked chitosan hydrogels thereby benefitting the society at large by improving patient outcomes.

2.12 Summary of Findings on Literature Review

pH-sensitive hydrogels have found promising applications in areas such as control drug delivery systems, biomaterials for biomedical applications, mechano-chemical sensor, owing to their abilities to swell or shrink in response to pH changes in their surroundings. Depending on the ionisable pendant groups in the polymer network chain, they can be classified as either anionic or cationic hydrogels. The swelling behaviour of hydrogels in general have been modelled in the literature using statistical mechanics, empirical, and multifield approaches for steady state and transient state simulations.

The statistical mechanics or thermodynamics approach has been used to predict the equilibrium volume variation of pH-sensitive genipin crosslinked chitosan hydrogel with lots of adjustment of model parameters required. For example, most of the parameters of the thermodynamic models (for example, $\overline{M_c}$, f_i, $\overline{M_n}$, Ω, $\bar{V}_r$) are difficult to ascertain as they require lots of trial and error to estimate them using experimental data.

In modelling the swelling behaviour of chitosan crosslinked with genipin, glutaraldehyde and polygenipin hydrogels, Jahren *et al.* [135] developed a thermodynamic model whose parameter for example, the concentration of the crosslinking reagent (a parameter that controls swelling, water uptake, and mechanical properties of the hydrogel) can be tuned in the direction of the desired swelling/response. However, the major drawback of the model is the discrepancy (consistently large by a factor of 30) between the model predictions and the experimentally determined swelling ratios. Thus, limiting its application.

For dynamic swelling of pH-sensitive hydrogels, the empirical modelling approach relies on swelling data and cannot be extrapolated beyond the conditions under which the experiment was performed. In addition, the concerns with empirical models are their range of accuracy (for example the power law model describes the swelling behaviour of hydrogels very well for times where $\frac{M_t}{M_\infty} \leq 0.60$, but fails at time values above this range). Furthermore, their inability to describe the contributions of electrostatic and mechanical fields due to the deformation of the hydrogel limits their extent of application.

Literature search reveals that by coupling the chemical, electrical, and mechanical field interactions, the multifield model has the potential to simulate the swelling dynamics of pH responsive hydrogels and provide good predictions for their volume variation. However, the

mathematical complexity associated with numerical simulations involving complex hydrogel geometry remains a challenge that limits their broader applications in real life.

In reviewing the various models for equilibrium and dynamic swelling of pH responsive hydrogels, the gaps in the literature were identified. Thus, drawing from the strength of the thermodynamics model, and overcoming the mathematical complexities associated with the multifield model, a framework that combines a chemo-mechanical model with a thermodynamics model (derived from statistical mechanics approach) is developed in this study for simulation of the dynamic volume variation behaviour of pH responsive cationic (chitosan crosslinked with genipin) hydrogels.

CHAPTER THREE

METHODOLOGY

3.1 Multiphysics Modelling of pH-Sensitive Anionic and Cationic Hydrogels

Hydrogels find applications in areas such as wound healing, drug encapsulating devices, food packaging etc. So, when in contact with external environments, the interplay of the various interacting fields (i.e., chemical, electrical, and mechanical fields) as mentioned in Section 2.7.3 results in conformational changes of the hydrogel. To dynamically control the swelling characteristic property of hydrogels, mathematical models (that capture the underlying multi-physics behind the deformation of the hydrogel) can offer insight that complements experimental studies [197]. This is no doubt the reason numerical modelling approach was employed in this study to simulate the volume variation behaviour of anionic and cationic pH responsive hydrogels in view of deploying these models in various applications where hydrogels play important roles.

The pendant groups of the anionic, and cationic hydrogels whose deformation/volume-variation behaviours were modelled and simulated in this work are carboxylic acid group (-COOH, study 1) and amino group (-NH_2, study 2), respectively. The nonlinear coupled Partial Differential Equations, PDEs with constitutive relation which characterizes the chemo-electro-mechanical behaviour of the hydrogel-environment system were collated from the literature and solved as finite element model using COMSOL Multiphysics software. Values of operating conditions of process parameters, material properties, and boundary conditions obtained from the literature, were used to solve the finite element model. The processes that led to the development of the multiphysics model with which the physical process was simulated are outlined in the following subsections.

3.1.1 *Physical and computational domains*

The geometry or physical domain of the hydrogel used in this work (Figure 3.1a) is a cylindrical-shaped hydrogel immersed in aqueous (buffer) solution. For comparison with other studies, the size of the hydrogel under investigation in Study 1 (involving anionic hydrogel) is of initial diameter of $400\mu m$. However, for Study 2 (involving cationic, genipin crosslinked chitosan hydrogels) the initial size of the hydrogel varied according to the experimental swelling data.

To reduce the computation, symmetry was assumed around the axis so that one half of the cylinder (2D-axisymmteric geometry) was chosen as the computational domain. That is, the region of the actual geometry where computations were performed (Figure 3.1b).

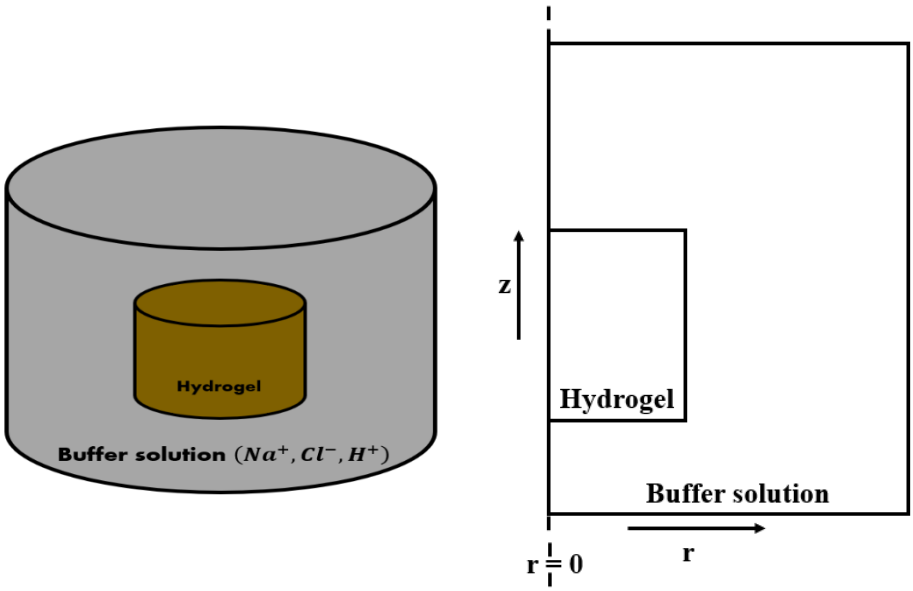

Figure 3.1: (a) Hydrogel immersed in a buffer solution (left) and (b) the computational domains reduced to 2D by axial symmetry (right).

3.1.2 T*he governing equations*

Following from previous discussion in Section 2.7.3, the three most distinct physics considered in the simulation studies performed in this work are chemical transport of diluted ionic species (for conservation of mass), variation of electric potential (representing the conservation of charge), and the mechanical deformation (for conservation of momentum) of the hydrogel in the surrounding medium with varying environmental conditions. Some of these conservation equations were applied over the entire computational domains, while others were selectively applied over its subdomains. The details of how these equations were applied in this work to model the response behaviour of pH-sensitive anionic and cationic hydrogels are provided in the following subsections.

3.1.2.1 *Transport of diffusive ionic species*

Building from the multifield modelling approach described in Section 2.7.3, when hydrogel comes in contact with an aqueous solution, ions in the solution migrate towards the hydrogel due to gradients of ionic concentration, electric potential, and chemical potential in the

hydrogel-solution system. This behaviour is generally described using the Nernst Planck equation [40], [41], given as:

$$\frac{\partial C_k}{\partial t} + D_k \nabla^2 C_k + \mu_k z_k F \nabla C_k \nabla \varphi + \mu_k z_k F C_k \nabla^2 \varphi = 0 \qquad (3.1)$$

$$(k = Na^+, Cl^-, H^+, \dots N)$$

where D_k (m^2/s) is the diffusivity of the k^{th} species, μ_k is the mobility of the k^{th}-species ion.

C_k (mM) is the concentration of *k*th diffusive ionic species, z_k is the *k*th-ionic valence number, φ (V) is the electrostatic potential, *N* is total number of diffusive ionic species. *F*, *R*, *T* are the Faraday's constant ($9.6487 \times 10^4 C/mol$), universal gas constant (8.314 J/mol K), and absolute temperature (K), respectively.

The first term in Eq. (3.1) indicates the change in concentration of k^{th} species within the hydrogel. The second term represents the ionic diffusion due to concentration gradient in the entire domain. The third and fourth terms together represent the migration of ions arising from the gradient of the electric potential in the system. Therefore, the concentration of each species in solution is a function of the bulk concentration and the distribution of electric potential across the entire system domain.

3.1.2.2 *Electrostatics*

The spatial distribution of electric potential in the domain can be described by the Poisson equation given as:

$$\nabla^2 \varphi = -\frac{F}{\varepsilon \varepsilon_0}\left(\sum_{k=1}^{N} z_k c_k + z_f c_f\right) \qquad (3.2)$$

where ε_0 is the dielectric constant of vacuum, ε is the relative dielectric constant of the medium, *F* is the Faraday constant, c_f and z_f are the concentration and the valence of the fixed charge in the hydrogel, respectively. The fixed charge concentration for anionic hydrogel is given as [15]:

$$c_f = \frac{c_{mo}^S}{H} \frac{K_a}{(K_a + [H^+])} \qquad (3.3)$$

For the case of a cationic hydrogel, the fixed charge concentration c_f is [15]:

$$c_f = \frac{c_{mo}^S}{H} \frac{[H^+]}{(K_b + [H^+])} \qquad (3.4)$$

where K_a and K_b are the acid and base dissociation constants of the fixed charged groups, c_{mo}^{s} is the initial concentration of the total ionizable fixed charged group within the unswollen hydrogel, determined by titration using Eqn. (3.6) [15]. In addition, $[H^+]$ is the concentration of the hydrogen ions within the hydrogel, and *H* is the local hydration state of the hydrogel defined as:

$$H = \frac{volume\ of\ fluid\ in\ the\ hydrogel}{volume\ of\ the\ solid\ phase\ of\ the\ hydrogel} = \frac{V_f}{V_s} \tag{3.5}$$

$$c_{mo}^{s} = \frac{\text{moles of ionizable group}}{\text{volume of solid polymer}} = \frac{n}{V_s} \tag{3.6}$$

It is worth noting that, genipin crosslinked chitosan hydrogel, for which the concentration of chitosan, c_{c^+}, is far greater than that of genipin, c_{g^-}, can be considered a cationic hydrogel. For such crosslinked hydrogel, the concentration of the total available ionizable fixed charge group is given as:

$$c_{mo}^{s} = c_{c^+} - c_{g^-} \tag{3.6b}$$

3.1.2.3 *Mechanical deformation*

The mechanical equations employed in this study are based on Lagrangian formulation as against the Eulerian formulation. The latter is based on a controlled volume fixed in space with flux in and out of it, while the former is based on a certain volume of the material being tracked as it translates and deforms [198, 199]. In addition, Lagrangian formulation is made in terms of material/reference coordinate (**X**) while the Eulerian formulation is made in terms of spatial coordinate (**x**). Since Lagrangian description is very suited for analysis of geometrically nonlinear problems, the mechanical equations deployed to describe the deformation of the pH-sensitive hydrogels in this study are based on Lagrangian formulation.

Let **X** denote the original position of a particle of the hydrogel in the undeformed state. At a time, *t*, say the particle has moved to a new position in space, $\mathbf{x} = \mathbf{x}(\mathbf{X}, \mathrm{t})$. this new position is given as:

$$\mathbf{x}(\mathbf{X}, \mathrm{t}) = \mathbf{X} + \mathbf{u}(\mathbf{X}, \mathrm{t}) \tag{3.7}$$

where $\mathbf{u}(\mathbf{X}, \mathrm{t})$ is the displacement (the vector that points away from the original position to the new position). As time, *t* increases, there will be local changes (called strains) in the shape or volume of the hydrogel. Information about changes is contained in the deformation gradient.

The deformation gradient, **F** is a measure of mechanical deformation [200 – 202] experienced by the hydrogel. Mathematically, **F** is defined as:

$$\mathbf{F} = \mathrm{F_{iJ}} = \frac{\partial \mathrm{x_i}}{\partial \mathrm{X_J}} = \frac{\partial \mathbf{x}}{\partial \mathbf{X}} = \frac{\partial(\mathbf{X}+\mathbf{u})}{\partial \mathbf{X}} = \mathbf{I} + \frac{\partial \mathbf{u}}{\partial \mathbf{X}} = \mathbf{I} + \boldsymbol{\nabla}\mathbf{u} \tag{3.8}$$

where **I** is the identity tensor. In matrix form, Eq. (3.8) is rewritten as:

$$\mathbf{F} = \begin{bmatrix} \frac{\partial \mathrm{x}}{\partial \mathrm{X}} & \frac{\partial \mathrm{x}}{\partial \mathrm{Y}} & \frac{\partial \mathrm{x}}{\partial \mathrm{Z}} \\ \frac{\partial \mathrm{y}}{\partial \mathrm{X}} & \frac{\partial \mathrm{y}}{\partial \mathrm{Y}} & \frac{\partial \mathrm{y}}{\partial \mathrm{Z}} \\ \frac{\partial \mathrm{z}}{\partial \mathrm{X}} & \frac{\partial \mathrm{z}}{\partial \mathrm{Y}} & \frac{\partial \mathrm{z}}{\partial \mathrm{Z}} \end{bmatrix} = \begin{bmatrix} 1 & 0 & 0 \\ 0 & 1 & 0 \\ 0 & 0 & 1 \end{bmatrix} + \begin{bmatrix} \frac{\partial \mathrm{u}}{\partial \mathrm{X}} & \frac{\partial \mathrm{u}}{\partial \mathrm{Y}} & \frac{\partial \mathrm{u}}{\partial \mathrm{Z}} \\ \frac{\partial \mathrm{v}}{\partial \mathrm{X}} & \frac{\partial \mathrm{v}}{\partial \mathrm{Y}} & \frac{\partial \mathrm{v}}{\partial \mathrm{Z}} \\ \frac{\partial \mathrm{w}}{\partial \mathrm{X}} & \frac{\partial \mathrm{w}}{\partial \mathrm{Y}} & \frac{\partial \mathrm{w}}{\partial \mathrm{Z}} \end{bmatrix} = \begin{bmatrix} 1 + \frac{\partial \mathrm{u}}{\partial \mathrm{X}} & \frac{\partial \mathrm{u}}{\partial \mathrm{Y}} & \frac{\partial \mathrm{u}}{\partial \mathrm{Z}} \\ \frac{\partial \mathrm{v}}{\partial \mathrm{X}} & 1 + \frac{\partial \mathrm{v}}{\partial \mathrm{Y}} & \frac{\partial \mathrm{v}}{\partial \mathrm{Z}} \\ \frac{\partial \mathrm{w}}{\partial \mathrm{X}} & \frac{\partial \mathrm{w}}{\partial \mathrm{Y}} & 1 + \frac{\partial \mathrm{w}}{\partial \mathrm{Z}} \end{bmatrix} \tag{3.9}$$

Eq. (3.9) shows that the deformation gradient provides information about the local deformation of the hydrogel. The first column of the matrix shows that the deformation tensor can provide insight into the orientation of a line segment in the undeformed body, d**X** as it is stretched into a line segment on the deformed body, d**x**, since from Eq. (3.8) we have that:

$$\mathrm{d}\mathbf{x} = \mathbf{F}\mathrm{d}\mathbf{X} \tag{3.10}$$

Mathematically, the deformation gradient, **F**, is the Jacobian matrix of the transformation from the undeformed state **X** to the deformed state **x** [203, 204]. From this, we can define a local volume scale factor J, as the determinant of the deformation gradient tensor.

$$\mathrm{J}(\mathbf{X}, \mathrm{t}) = \det(\mathbf{F}) = \frac{dV}{dV_0} \tag{3.11}$$

This determinant is a measure of how the volume of the hydrogel has changed with deformation. That is why it is called the volume ratio. J is equivalent to the local hydration defined earlier in Eq. (3.5).

To develop the mechanical balance equation, consider an undeformed hydrogel of volume V_0, the momentum balance equation can be expressed in the following differential form:

$$\rho_{\mathrm{gel}} \frac{\partial^2 \mathrm{u_i}}{\partial \mathrm{t}^2} = \mathrm{f_{v,i}} + \frac{\partial \mathrm{P_{iJ}}}{\partial \mathbf{X_J}} \tag{3.12}$$

In tensor notation:

$$\rho_{gel}\frac{\partial^2 \mathbf{u}}{\partial t^2} = \mathbf{f_v} + \boldsymbol{\nabla_X}.\mathbf{P^T} \tag{3.13}$$

where $\mathbf{f_v}$ is the force per unit volume, ρ_{gel} is the mass density in the reference/material configuration (density of the hydrogel), and the velocity field is computed from the displacement field, **u**, as:

$$\mathbf{v} = \frac{\partial \mathbf{u}(\mathbf{X},t)}{\partial t} \tag{3.14}$$

Further, **P** is the first Piola-Kirchoff (PK1) stress tensor, it relates forces acting in the current or deformed configuration to the elemental areas in the reference or undeformed configuration [205]. The first Piola-Kirchoff stress tensor, **P** is related to the Cauchy stress tensor, σ (or true stress tensor as it represents a true measure of the force per unit area in the current/deformed or spatial configuration) by the equation:

$$\mathbf{P} = J\sigma\mathbf{F^{-T}} \tag{3.15}$$

Although Cauchy stress, σ is symmetric, deformation gradient **F**, is not. Thus, PK1 stress tensor is asymmetric. This lack of symmetry is the reason PK1 is not employed in modelling the deformation of materials. To get an alternative but symmetric stress measure explains the need for second Piola-Kirchoff (PK2) stress tensor, S, defined as [206, 207]:

$$\mathbf{S} = J\mathbf{F}^{-1}\sigma\mathbf{F^{-T}} \tag{3.16}$$

From Eq. (3.16), since σ is symmetric, then PK2 stress tensor is symmetric, meaning that:

$$\mathbf{S} = \mathbf{S^T} \tag{3.17}$$

In terms of material moduli tensor, PK2 can take the form:

$$\boldsymbol{S} = \boldsymbol{C}:\boldsymbol{E} \tag{3.18}$$

where **C** is the material moduli tensor which for plane stress (the boundary load is applied only in the x-y plane) is given as:

$$\boldsymbol{C} = \frac{E}{(1-v^2)}\begin{bmatrix} 1 & v & 0 \\ v & 1 & 0 \\ 0 & 0 & (1-v)/2 \end{bmatrix} \tag{3.19}$$

where the *E* is the Young's modulus and *v* is the Poisson's ratio. The Green-Lagrangian strain tensor $\boldsymbol{E}$ is given as:

$$\boldsymbol{E} = \frac{1}{2}(\boldsymbol{F^T}.\boldsymbol{F} - \boldsymbol{I}) \tag{3.20}$$

Substituting Eqns. (3.15) into (3.16) gives that the first and second Piola-Kirchoff stress tensors are related thus:

$$\mathbf{P} = \mathbf{FS} \tag{3.21}$$

Hence, the momentum balance equation, from Eqn. (3.12), becomes:

$$\rho_{\text{gel}} \frac{\partial^2 \mathbf{u}}{\partial t^2} = \mathbf{F_v} + \boldsymbol{\nabla_X}.\mathbf{FS} \tag{3.23}$$

Substituting Eq. (3.8) into Eq. (3.23) gives the momentum balance equation as:

$$\rho_{\text{gel}} \frac{\partial^2 \mathbf{u}}{\partial t^2} = \boldsymbol{\nabla_X}.(\mathbf{I} + \boldsymbol{\nabla}\mathbf{u})\mathbf{S} + \mathbf{F_v} \tag{3.24}$$

The boundary load, $\mathbf{F_v}$, is a function of the osmotic pressure due to counterions in the hydrogel-solution system. This osmotic pressure can be calculated thus:

$$P_{osmotic} = RT \sum_{k=1}^{N} (c_{k,gel} - c_{k,sol}) \tag{3.25}$$

where subscripts k, gel and k, sol represent the k^{th} ionic species in the hydrogel and the surrounding solution, respectively.

3.1.3 *Modelling and simulation in COMSOL multiphysics*

A finite element model of the anionic and cationic pH-sensitive hydrogel in buffer solution was developed and simulated in a commercial finite element software, COMSOL Multiphysics. The field equations and the corresponding multiphysics modules employed in the simulation study to develop the FEA model are:

3.1.3.1 *Physics*

- Transport of Diluted Species (TDS): This physics defined for both domains, represents the Nernst Planck equation, Eq. (3.1). It solves for the concentration profiles of the ionic species in the system.
- Electrostatics (AC/DC interface): This physics defined for both the hydrogel and the buffer solution subdomains, solves the Poisson equation, Eq. (3.2), for the distribution of electric potential (φ) in both domains, with electroneutrality assumed in the buffer solution:

- Solid Mechanics: This physics defined only for the hydrogel domain, solves the mechanical balance equation, Eq. (3.24) for the displacement/deformation (**u**) of the hydrogel.

3.1.3.2 *Boundary conditions*

The 2D axisymmetric domain (representing the physical geometry), the associated boundary conditions, and the meshed computational domains are shown in Figure 3.2.

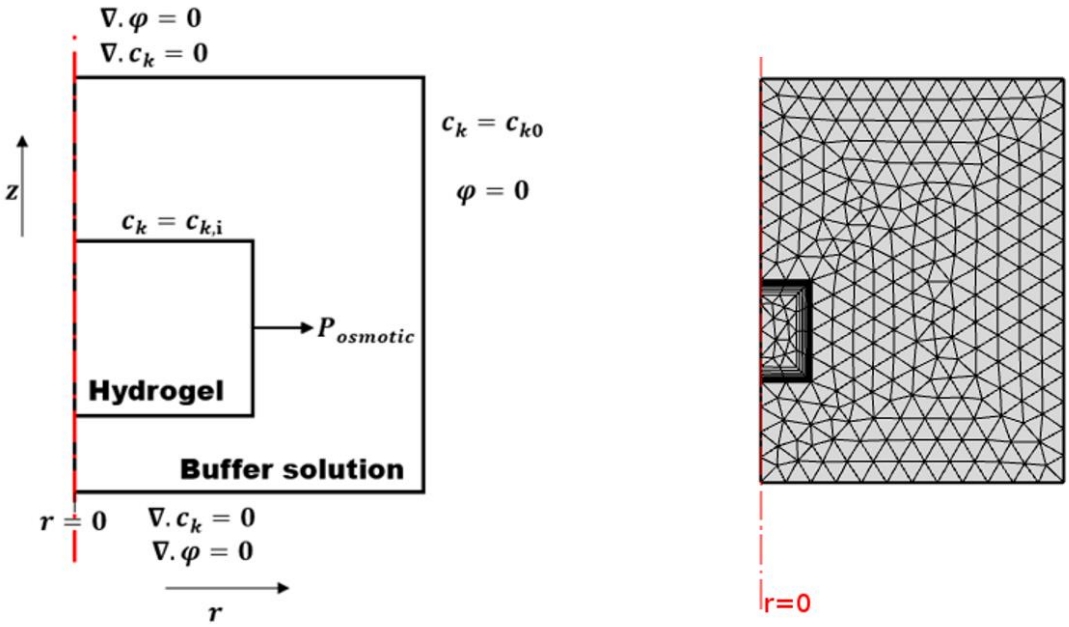

Figure 3.2: The modelling domains along with relevant boundary conditions (left) and the meshed domains (right).

Boundary: Corners of the hydrogel

Type	Mathematics	Physics equation
Symmetry	$\frac{\partial c_k}{\partial r} = 0$	Nernst Planck
Zero charge	$\frac{\partial \varphi}{\partial r} = 0$	Poisson
Rollers		Mechanical
• vertical	$u_r = 0, u_z \; is \; free$	
• horizontal	$u_r \; is \; free, u_z = 0$	

To be able to compare computational results with published data (for the case where hydrogels were confined in a microchannel to allow for deformation in the radial direction only), roller

boundary conditions were imposed at the top and bottom of the hydrogel to constrain displacement in the axial direction.

Boundary: Sides of the solution

Type	Mathematics	Physics equation
No flux	$\frac{\partial c_k}{\partial r} = 0$	Nernst Planck
Zero charge	$\frac{\partial \varphi}{\partial r} = 0$	Poisson

Boundary: Hydrogel-Buffer interface

Type	Mathematics	Physics equation
Concentration	$c_k = continuous$	Nernst Planck
Boundary load	$P_{osmotic} = RT(\sum_{k=1}^{N}(c_k^h - c_k^s))$	Mechanical deformation
Displacement	$r = R + u_r, z = Z + u_z$	Moving mesh

Boundary: Buffer end

Type	Mathematics	Physics equation
Concentration	$c_k = c_{k0}$	Nernst Planck
Ground	$\varphi = 0$	Poisson
Displacement	$u_r = 0, u_z = 0$	Moving mesh

3.1.3.3 ***Material properties and process parameters***

The material properties and process parameters used for the simulation studies were obtained from the literature and experimental studies. For multiphysics simulation of the swelling behaviour of pH-sensitive anionic hydrogels (study 1) the parameters used are detailed in Table 3.1, while parameters used for studying swelling behaviour of pH-responsive cationic hydrogels (study 2) are outlined in Table 3.2.

Table 3.1: Values of parameters used for simulation study 1

Property/parameter	Value	Description	Source
r	200 μm	radius of the gel	[15]
ϵ	80	Dielectric constant	[15]
T	298 K	Temperature	
z_f	-1	Valency of fixed charge	
c_{mo}^{s}	1800 mM	initial fixed charge density	[15]
K_a	$10^{-4.5}$ mM	Dissociation constant of Carboxylic acid group	[15]
D_{Na}	$9.31 \times 10^{-9} m^2/s$	Diffusion coefficient Na^+	
D_{Cl}	$9.31 \times 10^{-9} m^2/s$	Diffusion coefficient Cl^-	
D_{H_2}	$9.31 \times 10^{-9} m^2/s$	Diffusion coefficient H^+	
v	0.43	Poisson's ratio	[15]
F	$9.6487 \times 10^4 C/mol$	Faraday Constant	
ρ_{gel}	1200 kg/m^3	Density of dry hydrogel	
pH	$2 - 12$	pH of the bathing solution	

As mentioned previously, the same platform used to model the equilibrium swelling behaviour of pH-responsive anionic hydrogels was adapted and used for modelling the swelling behaviour of pH-sensitive cationic hydrogels.

Table 3.2: Values of parameters used for simulation study 2

Property/parameter	Value	Description	Source
r	200 μm	radius of the gel	[15]
ϵ	80	Dielectric constant	[15]
T	298 K	Temperature	
z_f	+1	Valency of fixed charge	
c_{mo}^{s}	1800 mM	initial fixed charge density	[15]
K_b	1.0x10^{-5} mol/m^3	Dissociation constant of amine group	[135]
D_{Na}	$9.31 \times 10^{-9} m^2/s$	Diffusion coefficient Na^+	
D_{Cl}	$9.31 \times 10^{-9} m^2/s$	Diffusion coefficient Cl^-	
D_{H_2}	$9.31 \times 10^{-9} m^2/s$	Diffusion coefficient H^+	
v	0.43	Poisson's ratio	[15]
F	$9.6487 \times 10^4 C/mol$	Faraday Constant	
ρ_{gel}	1200 kg/m^3	Density of dry hydrogel	
pH	$2 - 12$	pH of the medium	

3.1.3.4 *Choice of solver*

The two general approaches employed by COMSOL Multiphysics software to solve nonlinear systems of equations are the Fully Coupled or the Segregated approach [208]. The former being the default solver for most 2D and 2D-axisymmetrical problems, solves in a single iteration for all unknowns in the model by taking into consideration all coupling terms between all unknowns in the multiphysics problem. While memory intensive, it does results in the most robust convergence.

The segregated approach on the other hand solves the problem sequentially, assuming each physics as a standalone problem thereby ignoring the coupling terms between the different physics. It offers the advantage of being less memory demanding. Although the segregated approach is cheaper in terms of memory, it is unsuitable for the problem under consideration due to the strong interaction within the various physics (i.e., the various physics are not standalone) describing the system under consideration, the Fully Coupled approach was adopted for this reason.

Therefore, the transport of diluted species, electrostatics, and the solid mechanics interfaces in the software, representing the Nernst Planck, Poisson, and Mechanical deformation equations respectively, were fully coupled and solved as stationary problem using the PARDISO-Direct solver. This Fully Coupled approach uses the Newton-Raphson iteration scheme to converge at the desired solution.

3.2 Modelling Equilibrium Swelling of pH-Sensitive Chitosan-Genipin Hydrogels

Having modelled in Section 3.1, the equilibrium swelling behaviour of pH-sensitive anionic and cationic hydrogels using a multi-field approach, this section approaches the equilibrium swelling of cationic hydrogels (specifically genipin crosslinked chitosan hydrogel) from a statistical mechanics' standpoint. The reasoning behind this approach is to incorporate the concentration of the crosslinking agent as a tuneable parameter in the model, and to study its influence on the equilibrium swelling ratio.

Consider a crosslinked electrically charged hydrogel in its as-prepared state, fully immersed in a bathing solvent, as shown in Figure 3.3. The hydrogel swells as a result a of the competition between three driving forces: the force that causes the solvent particle to mix with polymer

chain, F_{mix} , the force that prevents the polymer chain from stretching, $F_{elastic}$, and the force due to electrostatic interactions between ions in surrounding medium and those in the hydrogel.

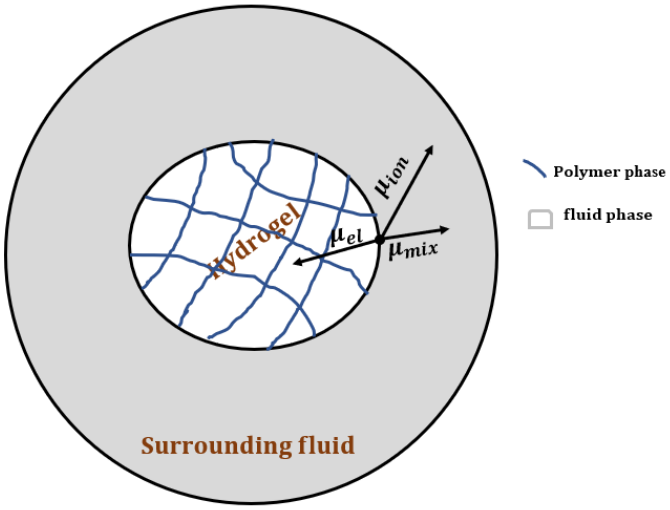

Figure 3.3: Pressures generated on an electrically charged hydrogel in aqueous environment

From Figure 3.3, while the energy due to mixing and ionic interaction both drive the swelling of the hydrogel, the elastic energy prevents indefinite swelling of the gel which eventually balances the energy terms as equilibrium is reached. At equilibrium, the change in total free energy during swelling/deswelling of the gel is 0. That is, the osmotic pressure balance due to mixing, elastic deformation, and the counterions in the gel-solution system is given as:

$$\mu_{mix} + \mu_{elastic} + \mu_{ionic} = 0 \tag{3.26}$$

3.2.1 *The mixing potential*, μ_{mix}

When the hydrogel is immersed in a bathing medium, the driving force, F_{mix}, allows the hydrogel to take up solvent molecules (in the bathing medium) and swell. The osmotic pressure due to free energy of mixing (μ_{mix}) is evaluated as a change in the free energy of mixing (ΔG_{mix}) when changing the number of moles of solvent (n_s) at a constant number of moles of polymers in the system (n_p) [146].

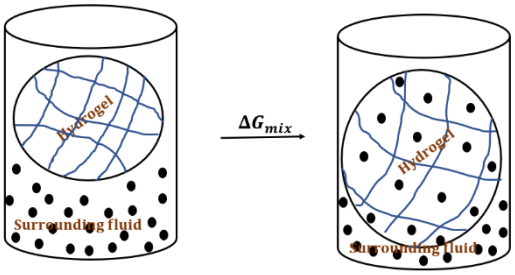

Figure 3.4: Hydrogel-Solvent mixing

$$\mu_{mix} = -\frac{N_A}{V_s}\left(\frac{\partial \Delta G_{mix}}{\partial n_s}\right)_{n_p} \tag{3.27}$$

where N_A is Avogadro's constant, V_s is the molar volume of the solvent molecule. It is obvious from Eq. (3.27) that, the number of polymer molecules in the crosslinked hydrogel, n_p does not change, but the number of solvent molecules, n_s changes. The change in free energy of mixing is given as:

$$\Delta G_{mix} = \Delta H - T\Delta S \tag{3.28}$$

where ΔS is the difference in entropy before an after mixing, and ΔH is the enthalpy change due to mixing of the polymer and the solvents.

Flory and Huggins [138] proposed that ΔG_{mix} of the gel has the form:

$$\Delta G_{mix} = nkT[(1-\phi)\mathrm{In}(1-\phi) + \chi\phi(1-\phi)] \tag{3.29}$$

where *n* is the total number of molecules, *k* is the Boltzmann's constant, χ is the Flory-Huggins interaction parameter, and ϕ is the polymer volume fraction of the swollen hydrogel (at equilibrium).

Substituting Eq. (3.29) into Eq. (3.27), gives μ_{mix} as:

$$\mu_{mix} = -\frac{N_A kT}{V_s}[\mathrm{In}(1-\phi) + \phi + \chi\phi^2] \tag{3.30}$$

It is worth noting that as the hydrogel swells, the polymer volume fraction, ϕ, changes during swelling, but the volume of the polymer phase of the hydrogel (that is the solid phase), V_p does not change.

This implies that the volume of the hydrogel at equilibrium swelling state is related to the initial polymer volume fraction in the following way:

$$\phi_0 = \frac{V_p}{V(t=0)}, \text{and } \phi_{eq} = \frac{V_p}{V(t=\infty)} \tag{3.31}$$

$$V_{eq} = \phi_0/\phi_{eq} \tag{3.32}$$

where ϕ_0, ϕ_{eq}, and V_{eq} are the polymer volume fraction at as-prepared state, polymer volume fraction at equilibrium swelling, and the equilibrium volume swelling ratio (volume of the gel at equilibrium swelling, with respect to the original volume at as-prepared state).

Since chitosan and genipin both contribute to the polymer volume fraction of the crosslinked hydrogel, then the polymer volume fraction of the crosslinked network at as-prepared state, ϕ_0 is given as:

$$\phi_0 = \frac{\left(\frac{\%c_c}{\rho_c}\upsilon_c + \frac{\%c_g}{\rho_g}\upsilon_g\right)}{\left[\frac{\%c_c}{\rho_c}\upsilon_c + \frac{\%c_g}{\rho_g}\upsilon_g + \left(\frac{\left(100-(\%c_c+\%c_g)\right)}{\rho_w}\upsilon_w\right)\right]} \tag{3.33}$$

Substituting Eq. (3.33) into Eq. (3.32) gives the equilibrium polymer volume fraction of the swollen hydrogel, ϕ_{eq} as:

$$\phi_{eq} = \frac{1}{V_{eq}}\left\{\frac{\left(\frac{\%c_c}{\rho_c}\upsilon_c + \frac{\%c_g}{\rho_g}\upsilon_g\right)}{\left[\frac{\%c_c}{\rho_c}\upsilon_c + \frac{\%c_g}{\rho_g}\upsilon_g + \left(\frac{\left(100-(\%c_c+\%c_g)\right)}{\rho_w}\upsilon_w\right)\right]}\right\} \tag{3.34}$$

where $\%c_c$ and $\%c_g$ are concentrations (% wt/v) of chitosan and genipin (crosslinking agent) solutions, respectively. υ_c, and υ_g, are and υ_w are the volumes of chitosan solution, genipin solution, and water used, respectively. ρ_c, ρ_g, and ρ_w are densities of chitosan, genipin, and water, respectively.

3.2.2 *The Elastic potential*, $\mu_{elastic}$

In similar form to Eq. (3.27), the osmotic pressure due to elastic deformation is a function of the change in the elastic energy when the number of solvent molecules entering the hydrogel increase as the number of polymer network strands inside the hydrogel is constant:

$$\mu_{elastic} = -\frac{N_A}{V_s}\left(\frac{\partial \Delta G_{elastic}}{\partial n_s}\right)_{n_p} \tag{3.35}$$

$\Delta G_{elastic}$ can be obtained from the affine network model for idea chains as [146]:

$$\Delta G_{elstic} = \frac{3v_0V_0kT}{2}(\lambda^2 - 1 - ln\lambda) \tag{3.36}$$

where v_0 is the number of network strands in the polymer network, V_0 is the original volume of the hydrogel, and λ is the uniaxial stretch ($\lambda = l/l_0$). l and l_0 are the new and original lengths of the gel, respectively.

Differentiating Eq. (3.36) w.r.t n_s gives:

$$\left(\frac{\partial \Delta G_{elstic}}{\partial n_s}\right)_{n_p} = \left(\frac{\partial \Delta G_{elstic}}{\partial \lambda}\right)_{n_p}\left(\frac{\partial \lambda}{\partial n_s}\right)_{n_p} = \frac{3v_0V_0kT}{2}(2\lambda - \frac{1}{\lambda})\left(\frac{\partial \lambda}{\partial n_s}\right)_{n_p} \tag{3.37}$$

$$\lambda^3 = V_{eq} = \frac{V(t=\infty)}{V(t=0)} = \frac{V(t=0)+n_sV_s}{V(t=0)} \tag{3.38}$$

Differentiating Eq. (3.38) w.r.t n_s gives:

$$3\lambda^2\left(\frac{\partial \lambda}{\partial n_s}\right)_{n_p} = \frac{V_s}{V_0} \tag{3.39}$$

Substituting Eq. (3.39) into Eq. (3.37) gives:

$$\left(\frac{\partial \Delta G_{elstic}}{\partial n_s}\right)_{n_p} = \frac{v_0V_0kT}{2}\left(2\lambda - \frac{1}{\lambda}\right)\lambda^{-2}\frac{V_s}{V_0} = \frac{v_0V_skT}{2}(\lambda^{-3} - 2\lambda^{-1}) \tag{3.40}$$

Substituting Eq. (3.40) into Eq. (3.35) gives:

$$\mu_{elastic} = -N_Av_0kT(\lambda^{-1} - 0.5\lambda^{-3}) \tag{3.41}$$

In terms of equilibrium swelling volume, Eq. (3.41) can be rewritten as:

$$\mu_{elastic} = N_Av_0kT(0.5{V_{eq}}^{-1} - {V_{eq}}^{-1/3}) \tag{3.42}$$

For affine network model, the number density of effective network strands, $v_0(\mathrm{m}^{-3})$ is related to the shear modulus, *G* in the following way:

$$G = v_0kT \tag{3.43}$$

Substituting Eq. (3.43) into Eq. (3.42) gives:

$$\mu_{elastic} = N_AG(0.5{V_{eq}}^{-1} - {V_{eq}}^{-1/3}) \tag{3.44}$$

3.2.3 *The Ionic potential*, μ_{ionic}

For ionic hydrogels, this potential is the most dominant of all the competing potentials. As the crosslinked hydrogel encounters the aqueous medium, the ionic interaction between ions in the hydrogel and those in the bathing medium causes the pores/mesh size of the gel network to increase (for swelling) allowing the solvent molecules in the bathing medium to drift into the hydrogel.

Further, the functional groups at the backbone of the crosslinked gel (such as amine for chitosan, and carboxylic acid for genipin) become ionized, and the hydrophilic nature of these ionized groups tend to attract more water molecules from the aqueous medium into the hydrogel, thereby causing the hydrogel to further swell.

The osmotic pressure due to counterions in the hydrogel-solution system as a function of the ionic strength of the environment is [15]:

$$\mu_{ionic} = RTV_s\left(\frac{\alpha^2 c_f^2}{4I}\right) \tag{3.45}$$

where α is the degree of dissociation of the amino group on the chitosan chain, c_f the concentration of the available ionizable group on chitosan chain, I is the ionic strength of the surrounding medium. The degree of ionization, α, and ionic strength, I can be evaluated using the relations:

$$K_a = \left(\frac{\alpha^2 c_{mo}}{1-\alpha}\right) \tag{3.46}$$

where K_a is the dissociation constant for the fixed charge (amine) group on the chitosan network.

$$Chit - NH_2 + H^+ \leftrightharpoons Chit - NH_3^+ \tag{3.47}$$

Therefore, the equilibrium constant, for the reaction K_a is:

$$K_a = \frac{[Chit{-}NH_3^+]}{[Chit{-}NH_2][H^+]} \tag{3.48}$$

Rearranging Eq. (3.46) gives:

$$\alpha^2 c_{mo} + K_a\alpha - K_a = 0 \tag{3.49}$$

Solving Eq. (3.49) gives:

$$\alpha = \frac{-K_a + \sqrt{{K_a}^2 + 4K_a c_{mo}}}{2c_{mo}} \tag{3.50}$$

For cationic hydrogels, the concentration of the ionizable groups, c_f in the swollen genipin crosslinked chitosan hydrogel is:

$$c_f = \frac{(c_{c+} - c_{g-})}{V_{eq}} \frac{C_{H+}}{(K_a + C_{H+})} \tag{3.51}$$

The ionic strength of the surrounding medium is calculated thus:

$$I = \frac{1}{2}\sum_i^n c_i {z_i}^2 \tag{3.52}$$

where c_i is the molar concentration of ion i (M, mol/m^3), and z_i is the charge number of that ion in the swelling medium.

Therefore, the total pressure (μ) of the charged crosslinked hydrogel at equilibrium swelling condition is given by:

$$\mu = -\frac{N_A kT}{V_s}\left[\mathrm{In}(1-\phi_e) + \phi_e + \chi {\phi_e}^2\right] + N_A G\left(0.5{V_{eq}}^{-1} - {V_{eq}}^{-1/3}\right) + RTV_s\left(\frac{\alpha^2 c_f^2}{4I}\right) = 0 \tag{3.53}$$

However, the shear modulus, G of the swollen hydrogel is related to the equilibrium volume swelling ratio by the expression [146]:

$$G = G_0 {V_{eq}}^{-1/3} \tag{(3.54)}$$

where, G_0 is the shear modulus of the gel at as-prepared state.

3.2.4 *Parameters used for simulation of equilibrium swelling of chitosan-genipin hydrogel*

The parameters used for simulation of the equilibrium model developed for genipin crosslinked chitosan hydrogel are outlined in Table 3.3.

Table 3.3: Values of parameters used in the simulation of the statistical mechanics' model

Name	Value	Unit	Description
N_A	6.02214076×10²³	mol^{-1}	Avogadro's constant
k	1.380649 × 10^{-23}	J/K	Boltzmann's constant
G_0	15	kPa	Shear modulus of the gel (for the starting gel)
T	298	K	temperature
z_c^f	1		valence of fixed charge, chitosan ($R-NH_2^+$)
pH	2 -13		pH range of the surrounding medium
K_b	1.0x10^{-5}	mol/m^3	Dissociation constant of Chitosan's amine group [135]
ρ_{gel}	1200	kg/m^3	density of the crosslinked starting gel
R	8.3145	$J.K^{-1}mol^{-1}$	general gas constant
V_s	0.00612	m^3/mol	Molar volume of solvent [135]
χ	0.48		Interaction parameter [135]

3.2.5 *Solution algorithm*

Newton Raphson's numerical scheme employed to obtain an approximate solution to the single variable nonlinear model equations developed in this section is detailed in Appendix II.

3.3 Modelling the Swelling Kinetics of pH-Sensitive Chitosan-Genipin Hydrogels

In Section 3.1, a multifield model for studying the equilibrium volume variation of anionic hydrogels (PHEMA) was developed. Further, the simulation platform for the anionic hydrogel was adapted to simulate the swelling behaviour of pH-responsive cationic hydrogels (genipin-chitosan hydrogels). To circumvent the challenges associated with modelling the equilibrium volume variation during shrinking of the hydrogel (such as having to manually change the boundary conditions at the interface of the hydrogel and the surrounding medium), the equilibrium volume variation of cationic hydrogels (chitosan-genipin) was modelled thermodynamically from a statistical mechanics standpoint in Section 3.2.

Having studied (in Section 3.2) how genipin crosslinked chitosan hydrogels swell or shrink to an equilibrium volume in response to pH variation in the environment. The next consideration

is how fast, and how long it takes the crosslinked cationic hydrogels to attain the equilibrium volume. To solve this problem, let us consider a crosslinked hydrogel of volume, $V(\boldsymbol{r}, t)$ bounded by the closed surface (A), immersed in a bathing medium, deforming as the fluid in the surrounding medium permeates through the hydrogel.

The mass of an elemental volume of the hydrogel (i.e., the differential mass of the hydrogel comprising the fluid and polymer phases) is:

$$dm = \phi\rho_p dV + (1-\phi)\rho_f dV \tag{3.55}$$

where ρ_p is the specific density of the polymer (assumed constant), ρ_f is the specific density of the fluid within the hydrogel (assumed constant here, but not necessarily the density of the fluid in the surrounding medium), and ϕ is the polymer volume fraction of the hydrogel defined as:

$$\phi = \frac{V_p}{V} \tag{3.56}$$

where V_p is the volume of the polymer phase of the hydrogel, and V is the total volume of the fluid phase, V_f and the polymer phase, V_p.

Dividing Eq. (3.55) by dV gives the density of the hydrogel, ρ_g as:

$$\rho_g = \phi\rho_p + (1-\phi)\rho_f \tag{3.57}$$

3.3.1 The conservation of mass equation

The continuity equation (mass conservation) in differential form, written separately for the constituent parts of the hydrogel gives:

The general form (continuity equation): $\frac{\partial\rho}{\partial t} + \nabla.(\rho\boldsymbol{u}) = 0$ (3.58)

Polymer phase: $\frac{\partial\rho_p}{\partial t} + \nabla.\left(\rho_p\boldsymbol{v}_p\right) = 0$ (3.59)

$$\frac{\partial(\phi\rho_p)}{\partial t} + \nabla.\left(\left(\phi\rho_p\right)\boldsymbol{v}_p\right) = 0 \tag{3.60}$$

where are ρ_p and $\boldsymbol{v}_p$ are the density of the polymer phase and the velocity of the polymer phase (or chain) respectively. Evaluating the derivative gives:

$$\rho_p \frac{\partial \phi}{\partial t} + \rho_p \nabla . \left(\phi \boldsymbol{v}_p\right) = 0 \tag{3.61}$$

Fluid phase: $\frac{\partial \rho_f}{\partial t} + \nabla . \left(\rho_f \boldsymbol{v}_f\right) = 0$ (3.62)

$$\frac{\partial \left((1-\phi)\rho_f\right)}{\partial t} + \nabla . \left(\left((1-\phi)\rho_f\right)\boldsymbol{v}_p\right) = 0 \tag{3.63}$$

where are ρ_f and $\boldsymbol{v}_f$ are the density of the fluid phase and the velocity of the fluid phase respectively. Evaluating the derivative gives:

$$\rho_f \frac{\partial [(1-\phi)]}{\partial t} + \rho_f \nabla . \left[(1-\phi)\boldsymbol{v}_f\right] = 0 \tag{3.64}$$

Dividing both equations by their respective densities give:

$$\frac{\partial \phi}{\partial t} + \nabla . \left(\phi \boldsymbol{v}_p\right) = 0 \tag{3.65}$$

$$\frac{\partial [(1-\phi)]}{\partial t} + \nabla . \left[(1-\phi)\boldsymbol{v}_f\right] = 0 \tag{3.66}$$

Combining Eq. (3.65) and Eq. (3.66) gives the compressibility relation (i.e., the densities of the polymer, and the fluid phases are constant):

$$\nabla . \left[\phi \boldsymbol{v}_p + (1-\phi)\boldsymbol{v}_f\right] = 0 \tag{3.66}$$

Therefore, the equation of continuity and its condition of incompressibility for the polymer network are:

$$\frac{\partial \phi}{\partial t} + \nabla . \left(\phi \boldsymbol{v}_p\right) = 0 \tag{3.65′}$$

$$\nabla . \left[\phi \boldsymbol{v}_p + (1-\phi)\boldsymbol{v}_f\right] = 0 \tag{3.66′}$$

It is important to note that, although the polymer volume fraction, ϕ, changes with time during swelling, the volume of the polymer phase of the hydrogel, V_p does not change. This implies that:

$$\left.\begin{matrix} \phi_0 = \frac{V_p}{V(0)} \\ \phi(t) = \frac{V_p}{V(t)} \end{matrix}\right\} \tag{3.67}$$

where ϕ_0, $\phi(t)$, and $V(t)$ are the initial polymer volume fraction, polymer volume fraction at time, t, and the total volume of the hydrogel at any time, *t*, respectively.

3.3.2 The Darcy law

To define a relationship between the velocity of the polymer, v_p, and that of the fluid, v_f, we apply the Darcy law for porous medium, given by:

$$\boldsymbol{v}_f - \boldsymbol{v}_p = -\kappa_0(\phi)\nabla p \tag{3.68}$$

where ∇p is the pressure drop, the Darcy velocity, $\boldsymbol{v}_f - \boldsymbol{v}_p$, is written as the velocity of the fluid relative to the polymer, the Darcy constant is given as [209]:

$$\kappa_0(\phi) = \frac{(1-\phi)}{\zeta(\phi)} \tag{3.69}$$

3.3.3 Mechanical balance equation

The governing mechanical equation for nonlinear problems, such as large deformation of hydrogel is given as:

$$\rho \frac{\partial^2 \boldsymbol{u}}{\partial t^2} - \nabla . \boldsymbol{P} + \boldsymbol{b} - \boldsymbol{f} = 0 \tag{3.70}$$

where $\boldsymbol{u}$ is the displacement vector of a 3-dimensional body undergoing deformation, ρ is the density of the hydrogel, $\boldsymbol{P}$ is the first Piola–Kirchhoff stress tensor, $\boldsymbol{b}$ is body force, $\boldsymbol{f}$ is the external force.

Since the volume variation of hydrogel is a slow, and gradual process, with no external force, the first, third, and fourth terms in Eq. (3.70) can be ignored. Hence,

$$\nabla . \boldsymbol{P} = 0 \tag{3.71}$$

For simplicity, let us assume small deformation of the hydrogel. Then the elastic theory can be used to describe the hydrogel's deformation. Thus, Eq. (3.71) is rewritten in terms of the Cauchy stress tensor, $\boldsymbol{\sigma}$ as:

$$\nabla . \boldsymbol{\sigma} = 0 \tag{3.72}$$

Eq. (3.72) rewritten in terms of the stress components is given as:

$$\begin{pmatrix} \frac{\partial \sigma_{11}}{\partial x_1} + \frac{\partial \sigma_{12}}{\partial x_2} + \frac{\partial \sigma_{13}}{\partial x_3} \\ \frac{\partial \sigma_{21}}{\partial x_1} + \frac{\partial \sigma_{22}}{\partial x_2} + \frac{\partial \sigma_{23}}{\partial x_3} \\ \frac{\partial \sigma_{31}}{\partial x_1} + \frac{\partial \sigma_{32}}{\partial x_2} + \frac{\partial \sigma_{33}}{\partial x_3} \end{pmatrix} = 0 \tag{3.73}$$

Since the hydrogel under study is a porous material, Eq. (3.72) could be modified to give:

$$\nabla.(\boldsymbol{\sigma} - p\mathbf{I}) = 0 \tag{3.74}$$

where *p* is the osmotic pressure acting at the surface of the hydrogel, because of the tendency of the hydrogel to absorb more surrounding solvent.

Hence, the mathematical model for the coupled mass transport and mechanical deformation of the hydrogel are Eq. (3.65), (3.66), (3.68), and Eq. (3.74).

3.3.4 Stress tensor

The stress tensor ($\boldsymbol{\sigma}$) is related to the displacement vector ($\boldsymbol{u}$), shear modulus (G), and the bulk modulus (K) in the following way:

$$\boldsymbol{\sigma}_{ij} = (\underbrace{K\nabla.\boldsymbol{u}\delta_{ij}}_{\substack{stress\ due\\ to\\ volume\\ variation}} + \underbrace{2G(u_{ik} - \frac{1}{3}\nabla.\boldsymbol{u}\delta_{ij})}_{\substack{stress\ due\ to\\ shear\ deformation}} \tag{3.75}$$

where the component of the displacement is:

$$u_{ij} = \left(\frac{\partial u_k}{\partial x_i} + \frac{\partial u_i}{\partial x_j}\right) \tag{3.76}$$

Substituting Eq. (3.76) into (3.75) gives a more compact form Eq. (3.72) or (3.73) as:

$$\begin{pmatrix} (K + G/3)\frac{\partial}{\partial x_1}\nabla\boldsymbol{u} + G\Delta\boldsymbol{u} \\ (K + G/3)\frac{\partial}{\partial x_2}\nabla\boldsymbol{u} + G\Delta\boldsymbol{u} \\ (K + G/3)\frac{\partial}{\partial x_3}\nabla\boldsymbol{u} + G\Delta\boldsymbol{u} \end{pmatrix} = 0 \tag{3.77}$$

Replacing the operation $\Delta\boldsymbol{u}$ by $\nabla^2\boldsymbol{u}$ gives:

$$[(K + G/3)\nabla\nabla\boldsymbol{u} + G\nabla^2\boldsymbol{u}] = 0 \tag{3.78}$$

3.3.5 The free energy density equation

For a temperature induced swelling, the elastic free energy density is a function of deformation gradient and temperature [209]. That is:

$$A = A(F_{ij}, T) \tag{3.79}$$

However, the hydrogel under study is pH responsive, which means Eq. (3.79) must be modified to the form:

$$A = A(F_{ij}, pH) \tag{3.80}$$

This quite agrees with what is observed experimentally about the material properties of swollen hydrogel. The elastic and shear moduli of hydrogel during swelling depend on the pH of the surrounding fluid [210].

The free energy density for an isotropic material is given as:

$$\mathrm{A} = \frac{1}{2}K\left(\frac{\partial u_k}{\partial x_k}\right)^2 + \frac{1}{4}G\left(\frac{\partial u_i}{\partial x_j} + \frac{\partial u_j}{\partial x_i} - \frac{2}{3}\delta_{ij}\frac{\partial u_k}{\partial x_k}\right)^2 \tag{3.81}$$

Changing the pH of the surrounding fluid from a value pH_1 to pH_2 will require that Eq. (3.81) be modified to the form:

$$\mathrm{A} = A_0 + \frac{1}{2}K\left[\frac{\partial u_k}{\partial x_k} - \alpha_{12}(pH)\right]^2 + \frac{1}{4}G\left(\frac{\partial u_i}{\partial x_j} + \frac{\partial u_j}{\partial x_i} - \frac{2}{3}\delta_{ij}\frac{\partial u_k}{\partial x_k}\right)^2 \tag{3.82}$$

From Eq. (3.75), the stress tensor becomes:

$$\sigma_{ij} = K\left(\frac{\partial u_k}{\partial x_k}\right)\delta_{ij} - K\alpha_{12}(pH)\delta_{ij} + G\left(\frac{\partial u_i}{\partial x_j} + \frac{\partial u_j}{\partial x_i} - \frac{2}{3}\delta_{ij}\frac{\partial u_k}{\partial x_k}\right) \tag{3.83}$$

where the pH-induced deformation coefficient is given as:

$$\alpha_{12}(pH) = \frac{V_{eq}(pH_2) - V(t=0)}{V(t=0))} \tag{3.84}$$

Eq. (3.81) shows that, α_{12} requires the knowledge of the final equilibrium volume, V_{eq}, and initial unswollen volume, V_0, of the hydrogel.

3.3.6 Geometry

Since the deformation of the hydrogel under study was measured by changes in the diameter of the hydrogel, we would assume a linearized elastic cylindrical hydrogel undergoing deformation in the radial direction only (that is, one-dimensional domain).

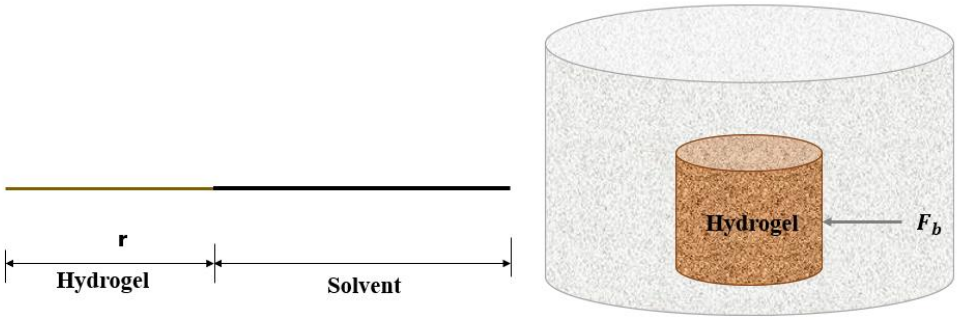

Figure 3.5: Hydrogel submerged in fluid: Physical geometry (right), and computational domain (left)

3.3.7 Model analysis

The model equations for the dynamics of the hydrogel are:

$$\frac{\partial \phi}{\partial t} + \nabla.(\phi \boldsymbol{v}_p) = 0 \qquad (3.65')$$

$$\nabla.[\phi \boldsymbol{v}_p + (1-\phi)\boldsymbol{v}_f] = 0 \qquad (3.66')$$

$$\boldsymbol{v}_f - \boldsymbol{v}_p = -\kappa_0(\phi)\nabla p \qquad (3.68')$$

$$\nabla.(\boldsymbol{\sigma} - p\mathbf{I}) = 0 \qquad (3.74')$$

Expanding Eq. $(3.66')$ gives:

$$\phi \nabla.\boldsymbol{v}_p + \boldsymbol{v}_p \nabla\phi - \boldsymbol{v}_f \nabla\phi + (1-\phi)\nabla.\boldsymbol{v}_f = 0 \qquad (3.85)$$

For small deformation, the polymer volume fraction does not change spatially (i.e., $\nabla\phi = 0$), therefore Eq. (3.85) becomes:

$$\phi \nabla.\boldsymbol{v}_p + (1-\phi)\nabla.\boldsymbol{v}_f = 0 \qquad (3.86)$$

Let the displacement of the hydrogel at a point $\boldsymbol{x}$ be $\boldsymbol{u}\,(\boldsymbol{x},t)$. Then the velocity, $\boldsymbol{v}_p$, of the polymer phase of the hydrogel is:

$$\boldsymbol{v}_p = \frac{\partial \boldsymbol{u}}{\partial t} \tag{3.87}$$

The velocity of the fluid phase, $\boldsymbol{v}_f$, can be obtained from Darcy's law by substituting Eq. (3.87) into $(3.68')$:

$$\boldsymbol{v}_f = -\kappa_0(\phi)\nabla p + \left(\frac{\partial u}{\partial t}\right) \tag{3.88}$$

Substituting Eq. (3.88) into (3.86) gives:

$$\phi\nabla.\left(\frac{\partial \boldsymbol{u}}{\partial t}\right) + (1-\phi)\nabla.\left(\frac{\partial \boldsymbol{u}}{\partial t}\right) - \kappa_0(\phi)(1-\phi)\nabla^2 p = 0 \tag{3.89}$$

Rearranging Eq. (3.89) gives that:

$$\nabla.\left(\frac{\partial \boldsymbol{u}}{\partial t}\right) = \kappa\nabla^2 p \tag{3.90}$$

where κ is defined as:

$$\kappa = \kappa_0(\phi)(1-\phi) = \frac{(1-\phi)^2}{\zeta(\phi)} \tag{3.91}$$

The governing mechanical balance equation is:

$$\nabla.(\boldsymbol{\sigma} - p\mathbf{I}) = 0 \tag{3.74'}$$

Expanding Eq. $(3.74')$ gives:

$$\nabla.\sigma = \nabla p \tag{3.92}$$

Substituting Eq.(3.92) into the stress tensor, Eq. (3.78), gives:

$$(K + G/3)\nabla\nabla\boldsymbol{u} + G\nabla^2\boldsymbol{u} = \nabla p \tag{3.93}$$

Factorizing the LHS of Eqn. (3.93) for the one dimensional problem gives Eq. (3.93) as:

$$\frac{\partial p}{\partial x} = \left(K + \frac{4G}{3}\right)\frac{\partial^2 u}{\partial x^2} \tag{3.94}$$

Eq. (3.94) is not solvable in the current form, since there are two dependent variables in it.

3.3.8 Boundary conditions

To solve the derived equation, Eq. (3.94), the following boundary conditions (depicted in Fig. 3.6) are defined for the chemo-mechanical conditions of the hydrogel-solvent system.

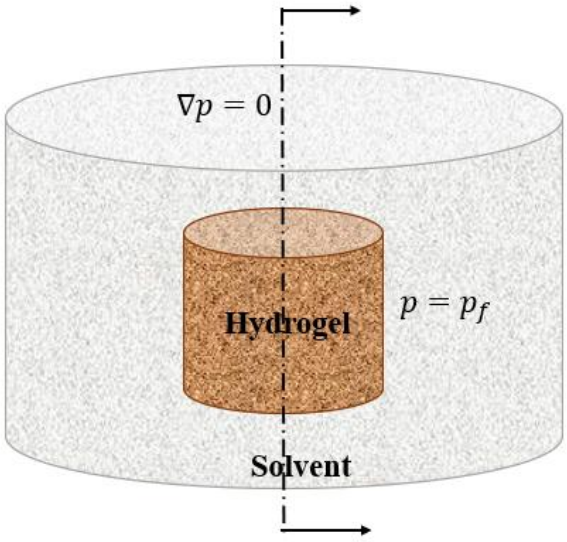

Figure 3.6: Hydrogel submerged in a solvent, showing boundary conditions.

- ***Chemical boundary condition***

At the centre of the hydrogel, due to symmetry, the pressure gradient is zero. Mathematically:

$$\nabla p = 0 \tag{3.95}$$

At the other end of the hydrogel, since the fluid can move freely through the boundary, then, the pressure inside the gel, p must be equal to the pressure in the surrounding fluid at the hydrogel-solvent boundary. That is:

$$p = p_f \tag{3.96}$$

- ***Mechanical boundary condition***

At the hydrogel-solution boundary, the force per unit area, F_b, acting at the surface of the hydrogel is given as:

$$(\boldsymbol{\sigma} - p\mathbf{I}).\,\mathbf{n} = F_b \tag{3.97}$$

From Eq. (3.94), the mechanical boundary condition for unaxial deformation of the hyrogel is:

$$(\sigma_{ii} - p) = F_b = -p_{ext} \tag{3.98}$$

where σ_{ii} is the stress acting in the *x*-direction, and p_{ext} is the solvent pressure acting at the boundary between the solvent and the hydrogel.

Therefore, from Eq. (3.98), the pressure, p, inside the hydrogel is:

$$p = \sigma_{ii} + p_{ext} \tag{3.99}$$

From Eq. (3.83), for pH-induced swelling, the stress σ_{ii}, acting in the *x*-direction is given as:

$$\sigma_{ii} = \left(K + \frac{4G}{3}\right)\frac{\partial u}{\partial x} - K\alpha_{12}(pH) \tag{3.100}$$

Combining Eq. (3.99) and (3.100) gives:

$$\frac{\partial u}{\partial x} = \frac{1}{\left(K+\frac{4G}{3}\right)}[p - p_{ext} + K\alpha_{12}(pH)] \tag{3.101}$$

Differentiating Eq. (3.101) w.r.t time, gives:

$$\frac{\partial}{\partial t}\left(\frac{\partial u}{\partial x}\right) = \frac{1}{\left(K+\frac{4G}{3}\right)}\frac{\partial p}{\partial t} \tag{3.102}$$

Rearranging the LHS of Eq. (3.90) gives:

$$\frac{\partial}{\partial t}\left(\frac{\partial u}{\partial x}\right) = \kappa\nabla^2 p \tag{3.103}$$

Substituting Eq. (3.103) into Eq. (3.102) gives:

$$\frac{\partial p}{\partial t} = \kappa\left(K + \frac{4G}{3}\right)\frac{\partial^2 p}{\partial x^2} \tag{3.104}$$

Eqn. (3.104) models the pressure distribution within the hydrogel in spatial and temporal coordinates. It is perceived to be the summation of the pressures due to mixing, elasticity, and ionic interaction between the hydrogel and the medium as explained in Section 3.2.

In comparison with Eq. (3.94), Eq. (3.104) is solvable in its current form to obtain $p(x,t)$ using the following boundary and initial conditions.

- Boundary conditions: $x = 0,\ \frac{\partial p}{\partial x} = 0$ (symmetry) (3.105)

$$x = a,\ p = p_{ext} \text{ (free)} \tag{3.106}$$

- Initial condition: In the initial state when the gel is immersed in the solvent, $\frac{\partial u}{\partial x} = 0$. Therefore, from Eq. (3.101), the pressure inside the hydrogel, in the initial condition (i.e., $\partial u/\partial x = 0$), is:

$$p(x,0) = p_{ext} - K\alpha_{12}(pH) \tag{3.107}$$

Assuming the external medium is very dilute that it can be considered an ideal solution, then the external solvent pressure can be obtained as follows:

$$p_{ext} = \rho_{ext} RT/M_f \tag{3.108}$$

where ρ_{ext}, M_f , and T are the density, molecular weight, and the temperature, respectively of the surrounding medium (this could be alcohol, water, etc).

3.3.9 Model simulation

The partial differential equation, Eq. (3.104) with the associated boundary conditions, Eq. (3.105) – (3.107), was solved as a 1-dimensional axisymetrical problem using finite element method (in COMSOL Multiphysics software) to obtain the pressure inside the gel as a function of time, $p(x,t)$.

The change in radius of the gel, Δa is given by $u(a,t)$, which can be obtained from Eq. (3.101):

$$\Delta a(t) = a(t) - a(0) = u(a,t) = \int_0^a \frac{\partial u}{\partial x}.dx$$

$$= \frac{1}{\left(K+\frac{4G}{3}\right)} \int_0^a [p(x,t) - p_{ext} + K\alpha_{12}(pH)]\, dx \tag{3.109}$$

At equilibrium swelling of the hydrogel, the pressure outside the gel is equal to the pressure inside the gel. Therefore, the change in the radius of the gel at equilibrium, calculated from Eq. (3.109) is:

$$\Delta a_\infty = a(\infty) \frac{K}{\left(K+\frac{4G}{3}\right)} \alpha_{12}(pH) \tag{3.110}$$

From Eq. (3.110) the unaxial swelling ratio can be calculated:

$$\frac{\Delta a_{\infty}}{a(0)} = \frac{a(\infty) - a(0)}{a(0)} = \frac{a(\infty)}{a(0)}\left[\frac{K}{\left(K + \frac{4G}{3}\right)}\right]\alpha_{12}(pH)$$

$$\frac{a(\infty)}{a(0)}\left\{1 - \left[\frac{K\alpha_{12}(pH)}{\left(K + \frac{4G}{3}\right)}\right]\right\} = 1$$

Therefore, the equilibrium uniaxial swelling ratio is:

$$\frac{a(\infty)}{a(0)} = \frac{\left(K+\frac{4G}{3}\right)}{\left[\left(K+\frac{4G}{3}\right) - K\alpha_{12}(pH)\right]} \tag{3.111}$$

The solution steps are outlined below:

Step 1: Pressure distribution within the hydrogel was obtained by solving Eq. (3.104), with finite element method using COMSOL Multiphysics Equation-based approach.

For optimized time-step in the dynamic simulation, the three different time-stepping methods underneath transient operation in COMSOL multiphysics (the implicit Backward Differentiation Formula (BDF), Generalized Alpha Methods (GAM), and the explicit Runge–Kutta) were considered. Of these three, the BDF method was adopted in this study because, this time-step implicit solver uses backward differentiation formulas with variable discretization order and automatic step-size selection with good stability and have been reported to be suited to problems involving diffusion, convection, and reactions [208, 211]. The time-step control scheme for the BDF method is given as:

$$\|\bar{e}_k\|_{WRMS}^2 = \frac{1}{M}\sum_j \frac{1}{N_j}\sum_i \frac{\left|\bar{e}_{k,i}(q)\right|^2}{(A_i + R|U_i^k|)^2} < 1 \tag{3.112}$$

The criterion used in this work is:

$$|\bar{e}_k| \leq A + R|U^k| \tag{3.113}$$

for an absolute tolerance, *A*, and a relative tolerance, *R.* The local truncation error estimate, $\bar{e}_{k,i}$ for the scaled or unscaled field component U_i^k at time t_k, and the scaled and unscaled absolute tolerance A_i.

Step 2

Numerical integration (composite Simpson's rule) was employed to obtain the change in radius of the hydrogel as a function of time. That is, the area under the curve, of Eq. (3.109).

$$\Delta a(t) = \int_{a_1}^{a_2} f(x)\,dx \approx \frac{\Delta x}{3}\left(f(x_0) + 4f(x_1) + 2f(x_2) + \cdots + 4f(x_{n-1}) + f(x_n)\right) \quad (3.114)$$

The error in the integration method (3.114) is:

$$\varepsilon = \frac{(a_2 - a_1)}{180}(\Delta x)^4 f^{iv}(\xi) \quad (3.115)$$

where ξ is some number between a_1 and a_2, and $\Delta x = a_2 - a_1/n$ is the strip length of each subdivision.

Therefore, the pressure distribution, $p(x,t)$, within the hydrogel obtained at step 1, was inserted into Eqn. (3.109) to determine the change in the radius of the hydrogel, $\Delta a(t)$, using step 2.

3.3.10 *Parameters and variables used for simulation of swelling kinetics*

The parameters used for simulation of the dynamic swelling/deswelling of genipin crosslinked chitosan hydrogels are given in Table 3.4.

Table 3.4: Values of parameters used for simulation of the dynamic model

Name	Expression/Value	Description
a	2 - 20[mm]	Radius of the gel (unswollen)
T	20[℃]	Temperature
M_f	0.0180153[kg/mol]	Molecular weight of the fluid (water)
R	8.3145[J/mol/K]	General gas constant
ρ_f	1000[kg/m^3]	Density of the fluid (water)
G	15[kPa]	Shear moduli
K	80[kPa]	Bulk moduli
p_{ext}	$\rho_{ext}RT/M_f$	External (solvent) pressure
D_{cop}	$(K + 4\,G/3)$	Coperative diffusion constant

3.4 Optimization Model for Equilibrium Swelling of Chitosan/Genipin Hydrogel

In most applications, it is desirable to know the optimum conditions for equilibrium swelling of the crosslinked hydrogel. We address such concern in this section by first identifying the parameters that affect equilibrium swell volume, then use central composite response surface design to develop an optimization model that connects those parameters with the equilibrium swell volume.

Some key parameters that influence the equilibrium swelling of the crosslinked hydrogel are the concentration of the crosslinking agent, $\%c_g$, the polymer-solvent interaction parameter, χ, ionic strength, *I*, and pH of the surrounding medium. Therefore, the relationship between these parameters and the equilibrium swell ratio, V_{eq}, is given as:

$$V_{eq} = \mathrm{f}\left(\%c_g, \chi, I, pH\right) \tag{3.116}$$

3.4.1 *Operating conditions of the parameters*

- Genipin concentration, $\%c_g$: Since chitosan concentration was set at 1 wt.%, that of genipin was in the range $0.2\ \text{wt.}\% - 0.6\ \text{wt.}\%$.
- Polymer-solvent interaction, χ: The range of the operating conditions for this parameter was set 20% above and below the nominal value (i.e., $\chi = 0.48$) obtained from the literature [135]. Therefore, the range used is: $0.384 - 0.576$
- Ionic strength of the surrounding medium, *I*: based on the work of Li [15], this was set in the range, $300\text{mM} - 900\text{mM}$
- pH of the surrounding medium: the range of pH used was set at 20% above and below the nominal value of the pH for simulated body fluid ($pH = 7.4$). Therefore, the range used is: $5.92 - 8.88$ (so that the pH of tumorous tissue, 6.4 – 7.0, is within this range in the case of targeted drug release.

With these operating conditions, a central composite response surface design (full) was used to generate thirty (30) data sets. These data sets were then plugged into the equilibrium swelling simulation platform (developed in Section 3.2) to determine the value for the corresponding response variable, V_{eq}. Furthermore, with the aid of Design Expert statistical software, a regression-based optimization model was developed. The operational or response surface (design) matrix is detailed in Appendix III.

3.4.2 *Model development*

The regression model employed to study the optimum equilibrium swelling conditions of genipin crosslinked chitosan hydrogel, was developed using Response Surface Methodology (RSM) with the aid of Design Expert software following the steps outlined below.

- ❖ The value of the response (for each design run) obtained from simulation of the thermodynamics model developed in Section 3.2 was plugged into the appropriate column design layout view of the software.
- ❖ The response variable was transformed to obtain the best model statistics (i.e., R^2, R^2_{Adj}, R^2_{Pred}, p-value, F-test, etc.). With F-test, we determined the group of variables that are jointly significant. P-value, which must be less than the alpha level (in this work, alpha = 0.05) is the probability that the results obtained happened by chance. Predicted Residual Error Sum of Squares (PRESS) statistic gives an estimate of how the model performs on hold-out data, using only in-sample data [212].
- ❖ To automatically eliminate undesirable model terms, backward elimination regression (with alpha = 0.05) was employed for model process order (such as, 2FI, quadratic, cubic).
- ❖ With Analysis of Variance (ANOVA) the most suited coefficients of the quadratic-type regression model were determined as:

$$V_{SR} = a_0 + a_1x_1 + a_2x_2 + a_3x_3 + \cdots + a_{12}x_1x_2 + a_{13}x_1x_3 \ + \cdots + a_{11}{x_1}^2 + a_{22}{x_2}^2 + \cdots \quad (3.117)$$

Where V_{SR} is the estimated volume swell ratio of the crosslinked hydrogel, $x_1, x_2, x_{3,}$ ... are the factors/parameters (i.e., genipin concentration, polymer-solvent interaction parameter, pH, and ionic strength of the surrounding medium). The constants a_0, represents the mean (intercept); a_1, a_2, a_3 ..., are the linear effects; a_{12}, a_{13}, a_{23}, ... are the interaction effects, while a_{11}, a_{22}, a_{33}, ... are the quadratic effects.

3.5 Error Propagation and Uncertainties

Uncertainties and errors can cause simulation results to deviate significantly from their true values. To substantiate the level of accuracy accompanying the simulation results in this work, errors and uncertainties in the modelling process or model parameters were taken into consideration. Uncertainty is a potential deficiency that arises from poor knowledge of the modelling process or model parameters. Whereas error is a recognizable deficiency that is not caused by poor knowledge of the modelling process. The important errors considered and taken

into consideration in this study include: the iterative convergence errors and the discretization errors.

Iterative convergence errors come to play due to the stopping criteria of the iterative method adopted in the simulation study. Since the system of equations modelled in this work is nonlinear, the solution was arrived at using Damped Newton iterative method. Steady state simulation of hydrogel swelling in COMSOL Multiphysics was performed using the stationary direct linear system solver. The error convergence criteria were fixed at 1×10^{-5}.

Discretization errors occur because the continuum chemo-electro-mechanical field PDEs are represented by an approximate discrete finite element model. To achieve a consistent simulation result (such that the solution is insensitive to the mesh size) within reasonable computation time, finer mesh was used in both the hydrogel and solution (i.e., the external environment) domains, whereas extremely fine boundary layer mesh was employed at the hydrogel-solution interface (refer to Figure 3.2). The sharp concentration gradient at the interface between hydrogel and the buffer solution was modelled using a hyperbolic tangent profile to polish the variation in concentration.

3.6 Performance Evaluation of the Developed Models

In this work, models have been developed on one hand, for predicting the volume variation behaviours of pH-sensitive anionic and cationic hydrogels. On the other hand, to determine the optimum conditions for equilibrium swelling of cationic hydrogels. Further, to evaluate the performance or prediction capabilities of these models, the data used were obtained from swelling experiments performed in the laboratory and some from the literature. Furthermore, for the optimization model, validation data were generated (i.e., synthetic data) using 2-level factorial design of experiment. The details of the model validation procedure are provided in the following sub-sections.

3.6.1 *Validation with swelling experiment data*

Two sets of data obtained from the literature [15, 135], and from experimental swelling measurements for anionic, and cationic (genipin crosslinked chitosan) hydrogels, respectively were used to evaluate the performance of the numerical models developed in this work. The performances of the models were ascertained by comparing these datasets with simulation results.

3.6.2 *Evaluation using interpolation and extrapolation datasets*

Two sets of data obtained by interpolation and extrapolation (of the range of operating conditions of the model parameters) through two (2)-level Factorial Design (Res V), resulting in twelve (12) runs, were used to evaluate the performance/robustness of the regression-based model developed in Section 3.4.

3.6.2.1 *Interpolation test*

Operating conditions for the interpolation dataset was created and plugged into the equilibrium swelling simulation platform to generate response data for the interpolation test. The upper boundary (UB) and lower boundary (LB) of the interpolation dataset are 10% below and 10% above the original upper and lower boundary operating conditions used to develop the model respectively.

That is, the lower boundary (LB) for the interpolation dataset, was 110% LB of original while the upper boundary (UB) was 90% UB of the (original) operating conditions. The response data for the interpolation datasets were compared with the model predictions at the same design points.

3.6.2.2 *Extrapolation test*

In a bid to check the robustness of the regression model (developed for equilibrium swelling studies) outside the range of operating conditions, extrapolation dataset was generated and plugged into the equilibrium swelling simulation platform to generate response data for the extrapolation test.

For the extrapolation test, the lower boundary (LB) for the interpolation dataset, was 95% LB of original while the upper boundary (UB) was 105% UB of the (original) operating conditions. The response data for the extrapolation datasets were compared with the model predictions at the same design points.

In addition to the statistical criteria discussed in Section 3.4.2, the accuracy or acceptability of the models' predictions was determined by evaluating the coefficient of determination (R^2) and the percent relative error (ϵ_r) produced when the models when compared with experimental data, trained and untrained datasets (for the regression-based model). The performance criteria are calculated using the following equations:

$$R^2 = 1 - \frac{\sum_{i=1}^{n}(y-y_p)^2}{\sum_{i=1}^{n}(y-\bar{y})^2} \tag{3.118}$$

$$\varepsilon_r = \frac{|Experiment-Simulation|}{Experiment} \times 100 \tag{3.119}$$

where y_p, is the predicted value of the dependent variable and y is the experimental value.

CHAPTER FOUR

RESULTS AND DISCUSSION

Multiphysics Simulation for Equilibrium Swelling of pH-Sensitive Anionic Hydrogel

The multiphysics model developed in Section 3.1 for equilibrium swelling of pH-sensitive anionic hydrogels are analysed, and the simulation results discussed in this chapter. The model incorporates the Poisson-Nernst-Planck (PNP) equations, which represents the diffusion and migration of ionic species in the system (i.e., hydrogel and the surrounding medium), together with the equilibrium mechanical equation for deformation of the hydrogel. The simulation results presented and discussed here are for the equilibrium swelling of a case-study anionic hydrogel (PHEMA) described in Section 2.3.

4.1 Model Validation for pH-Sensitive Anionic Hydrogels

To evaluate the performance of the numerical model developed in this study for equilibrium swelling of pH-sensitive anionic (PHEMA) hydrogels, steady state simulations were performed on a two-dimensional axisymmetric domain (representing the cylindrical shape hydrogel) and the results were compared with experimental data obtained from the work of Beebe *et al.* [213]. To justify this comparison, reference is made to the experimental procedure followed by Beebe *et al.* [213] to generate the data. The PHEMA hydrogel was synthesised in a microchannel covered at the top and bottom with two pieces of glasses to constrain axial displacement. Hence, the reason a cylindrical-shape hydrogel constrained at the top and bottom using rollers (refer to boundary conditions in Section 3.1.3.2) was chosen as the geometry for the simulation study.

In the experiment, the PHEMA hydrogel formed in a microchannel had an initial diameter of $400\mu m$. Further, it was observed that, on submerging the hydrogel in a surrounding fluid of ionic strength 300mM, it instantaneously swelled to a certain degree (a condition referred to as initial hydration state) then attained equilibrium swelling state before being subjected to changes in the pH of the surrounding medium. In keeping track of the volume variation of the hydrogel, the diameter of the cylindrical hydrogel was recorded as a function of the pH of the surrounding fluid (see the diamond markers on Figure 4.1). To reproduce this swelling scenario mathematically, the multifield equations (discussed in Section 3.1) in their steady state form that is, Eq. (3.1), (3.2), and (3.24); together with the auxiliary equations, Eq. (3.3) and (3.25)

and the computational domain with its associated boundary conditions detailed in Section 3.1.3.2, and parameters values provided in Table 3.1 were solved numerically as a finite element problem using COMSOL Multiphysics software. The simulation was performed to obtain the volume variation (in terms of diameter changes) as a function of pH (see the triangle markers on Figure 4.1, with the broken line plotted to aid visualization).

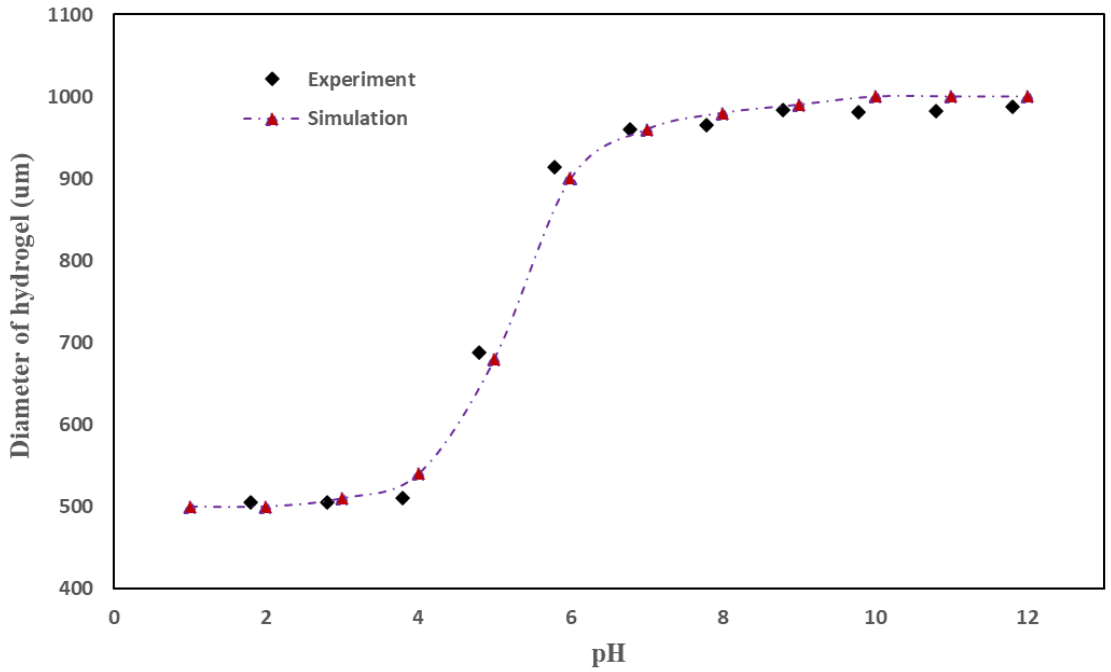

Figure 4.1 Validation against experimental studies by Beebe *et al.* [213] for equilibrium swelling of PHEMA hydrogel as a function pH

In the region of acidity (as seen in Figure 4.1), as the pH of the surrounding medium increases from 2 to 7, the hydrogel remains unchanged in size at very low pH, and slowly begins to swell in response to pH variation. However, the swelling becomes more pronounced as the pH value enters the range of 4 to 6.5. The swelling (which is due to charge build-up within the hydrogel) results from the protonation of the pendant carboxylic acid ($RCOO^-$) groups at the backbone of the PHEMA hydrogel. This charge build-up causes electrostatic repulsion which influences the osmotic balance between the hydrogel and the external environment, causing moisture and positively charged ions in the surrounding medium to penetrate the hydrogel. As the pH of the surrounding medium approaches 7, the protonation of the carboxylic acid group of PHEMA approaches the saturation state, therefore, further increase in the pH does not result in significant volume variation of the hydrogel. In conclusion, from the analysis of Figure 4.1, it is obvious that the simulation results compare very well with the experimental data. Hence, the model has the potential to offer predictions for equilibrium swelling of anionic (PHEMA)

hydrogels and the simulation platform can be deployed or adapted to model the volume variation behaviour of pH responsive cationic hydrogels.

4.2 Steady State Swelling of pH-Sensitive Anionic Hydrogels

This section details steady state simulation for equilibrium swelling of the pH-sensitive anionic (PHEMA) hydrogels with a closer look at the influence of the properties of the hydrogel or conditions of the surrounding medium. Simulations were performed (using input data obtained from the literature as prescribed in Table 3.1) to highlight the effects of initial fixed charge concentration of the hydrogel and effects of pH variation of the surrounding medium on the equilibrium swelling of PHEMA hydrogels.

4.2.1 *Effect of initial fixed charge concentration on swelling of anionic hydrogel*

The degree of ionisation of the fixed charge groups at the backbone of the PHEMA hydrogel and the nature (i.e., positive, or negative) of the mobile ions in the surrounding medium, contribute to the overall swelling of the hydrogel. From Eqn. (3.2) and (3.3), it is clear that the initial fixed charge concentration, c_{mo}^{s}, of the hydrogel contributes significantly to the Poison-Nernst-Planck equation hence the need to study its effect on the swelling of anionic (PHEMA) hydrogels. The cylindrical pH responsive hydrogel under study is immersed in a medium that is made of sodium chloride (NaCl) and hydrochloric acid (HCl) solution with a slight buffer to stablize the solution pH and swelling rate (Fig. 3.1). Therefore, the mobile ions in solution are sodium (Na^+), hydrogen (H^+), and chloride (Cl^-) ions.

As the initial fixed charge concentration increase (calculated using Eqn. (3.6)) from 1200 $\mathrm{mol/m^3}$ to 2400 $\mathrm{mol/m^3}$, at the same pH of the surrounding medium, the affinity of the carboxylic acid group $(\mathrm{RCOO^-})$ for cations tends to increase leading to the diffusion of more mobile ions with opposite sign from the surrounding solution into the hydrogel. Fig. 4.2- 4.3 show that the mobile cations, sodium (Na^+) and hydrogen (H^+) ions, tend to have higher concentrations within the hydrogel than in the surrounding solution, due to the negative fixed charge group bound to the backbone of the hydrogel attracting postively charged ions from the solution into the interior of the hydrogel.

Since the concentration of the fixed charge group drops from an initially high value at the center of the hydrogel to a zero value at the surface of the hydrogel, the concentrations of the cations tend to be higher at the center of the hydrogel than it is at the surface of the hydrogel (3D plots). Even though the swelling of the hydrogel is not very pronouced for low pH values (the line

plots), the effect of increasing the initial fixed charge concentration at the backbone of the hydrogel could still be observed.

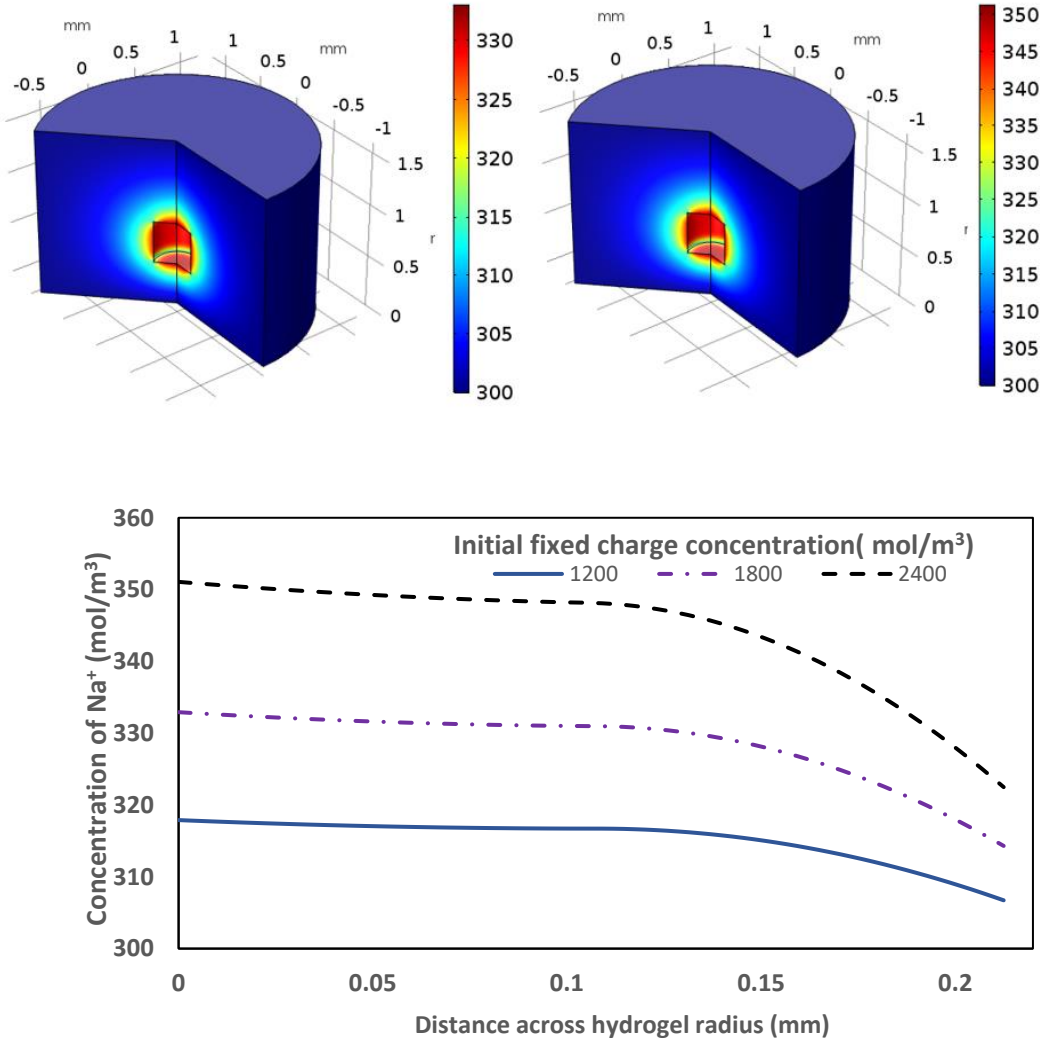

Figure 4.2: 3D plots for concentration (mol/m^3) distributions of Na^+ in the system for initial fixed charge ($RCOO^-$) concentration 1800 mol/m^3(left) and 2400 mol/m^3 (right), and 1D plot (down) in acidic medium of pH = 2.

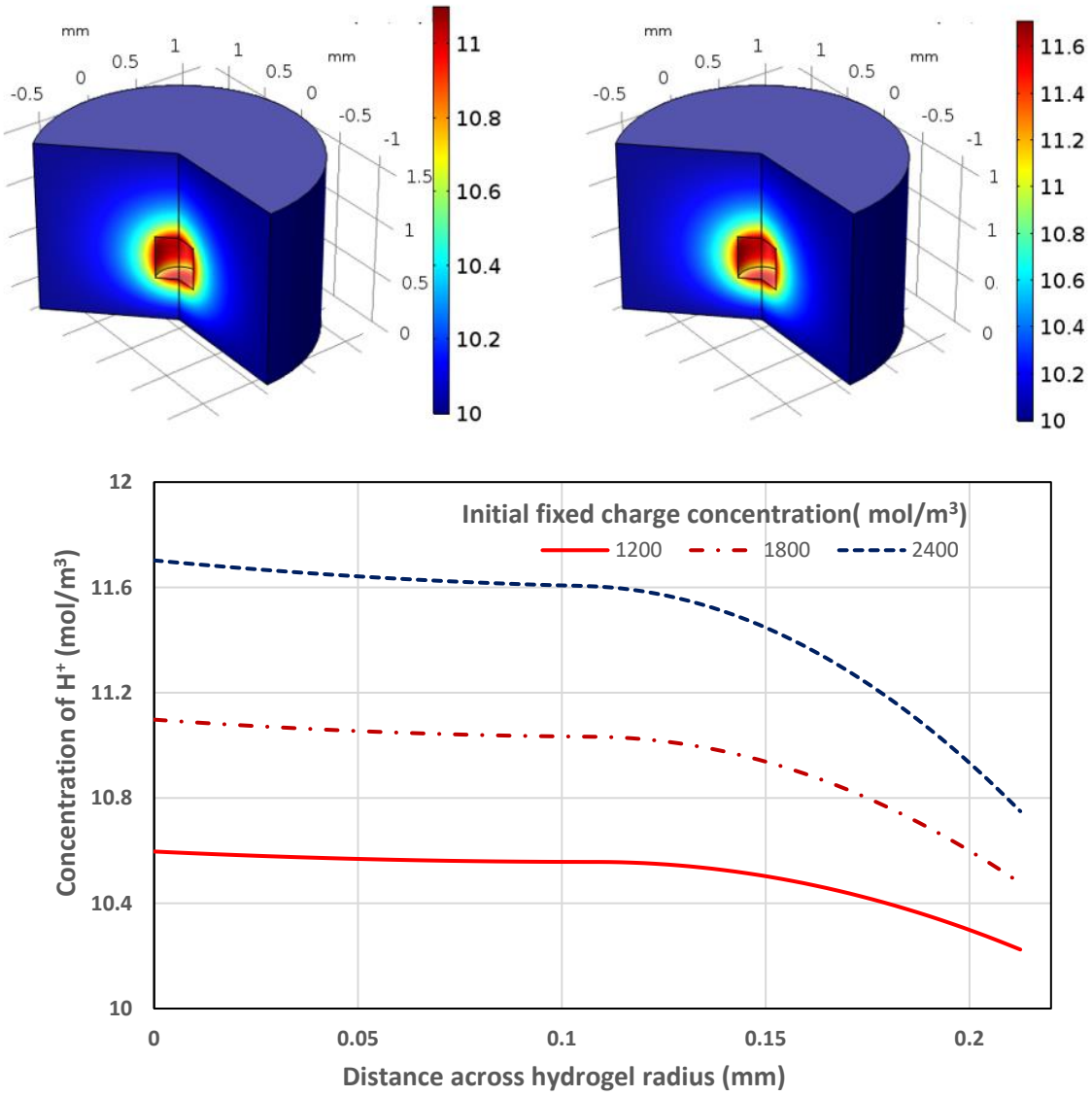

Figure 4.3: 3D plots for concentration (mol/m^3) distributions of H^+ in the system for initial fixed charge ($RCOO^-$) concentration 1800 mol/m^3(left) and 2400 mol/m^3 (right), and 1D plot (down) in acidic medium of pH = 2.

Conversly, Fig. 4.4 shows that increasing the initial fixed charge concentration from 1200 mol/m^3 to 2400 mol/m^3, causes the mobile chloride (Cl^-) anion to deplet within the hydrogel as a result of the repulsion between the negative fixed charge group and the mobile anions migrating from the surrrounding medium to the interior of the hydrogel. Hence, the concentration of the Cl^- is higher in the solution phase than it is within the hydrogel.

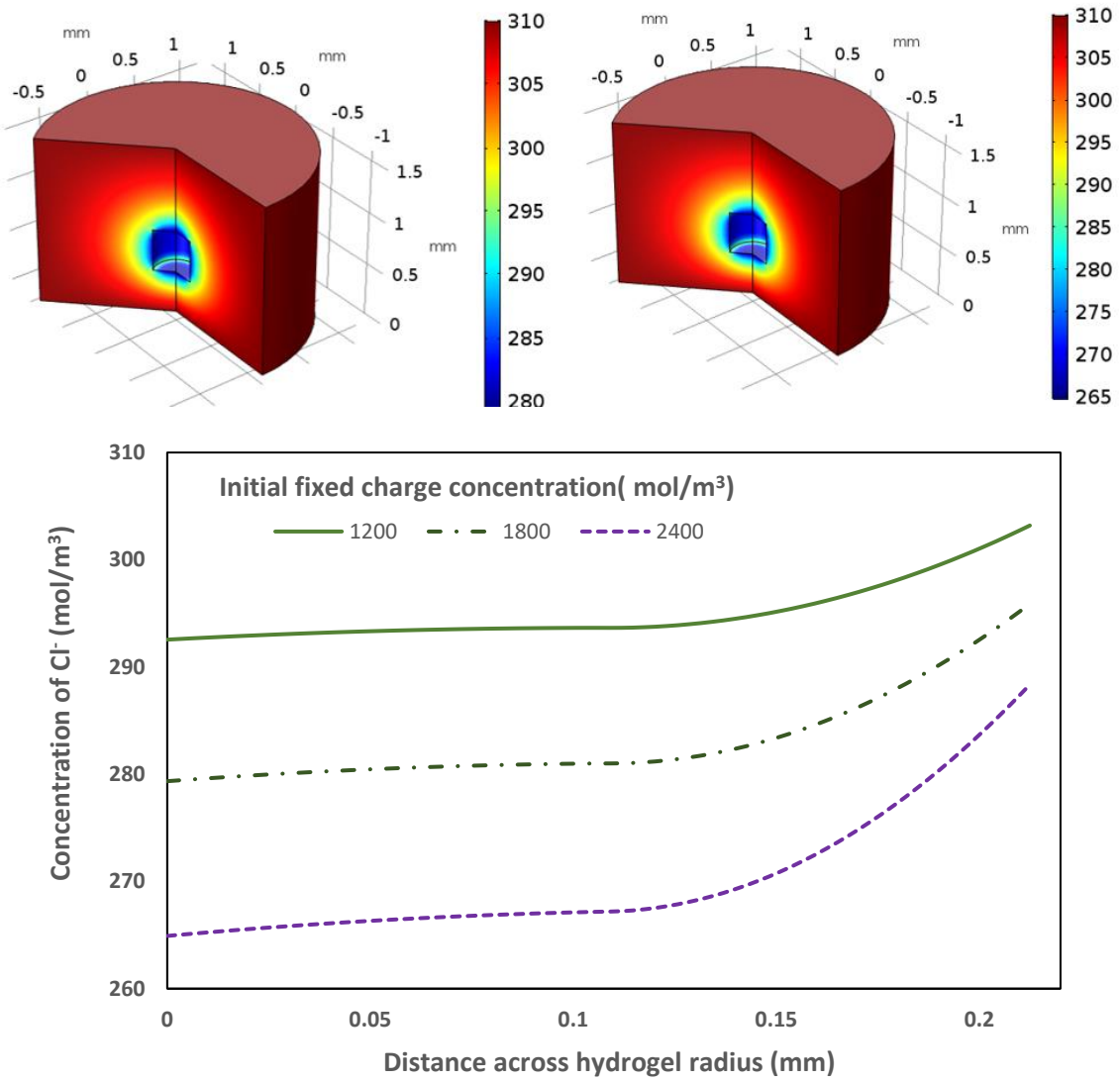

Figure 4.4: 3D plots for concentration (mol/m^3) distributions of Cl^- in the system for initial fixed charge ($RCOO^-$) concentration 1800 mol/m^3(left) and 2400 mol/m^3 (right), and 1D plot (down) in acidic medium of pH = 2.

The trend of the plots (Figs. 4.2- 4.4) which shows that as the concentrations of the mobile cations decrease from the center of the hydrogel, that of the mobile anions increase from the center of the hydrogel to the surface of the hydrogel (as the initial fixed charge concentration at the backbone of the hydrogel increase) is intuitively correct and corroborate with the work reported elsewhere [41, 90]

It is obsereved from Fig. 4.5 that increasing the initial fixed charge concentration from 1200 mol/m^3 to 2400 mol/m^3, causes the electric potential within the hydrogel to drop in value but increase along the radius of the hydrogel. The electric field distribution in the surrounding medium is not taken into consideration since electroneutrality was assumed in the medium. The low electric potential at the center and high potential at the surface of the hydrogel may be due to the high interractions between the fixed charge group and the mobile counterions (e.g Na^+) at the center and a low interraction at the surface of the hydrogel.

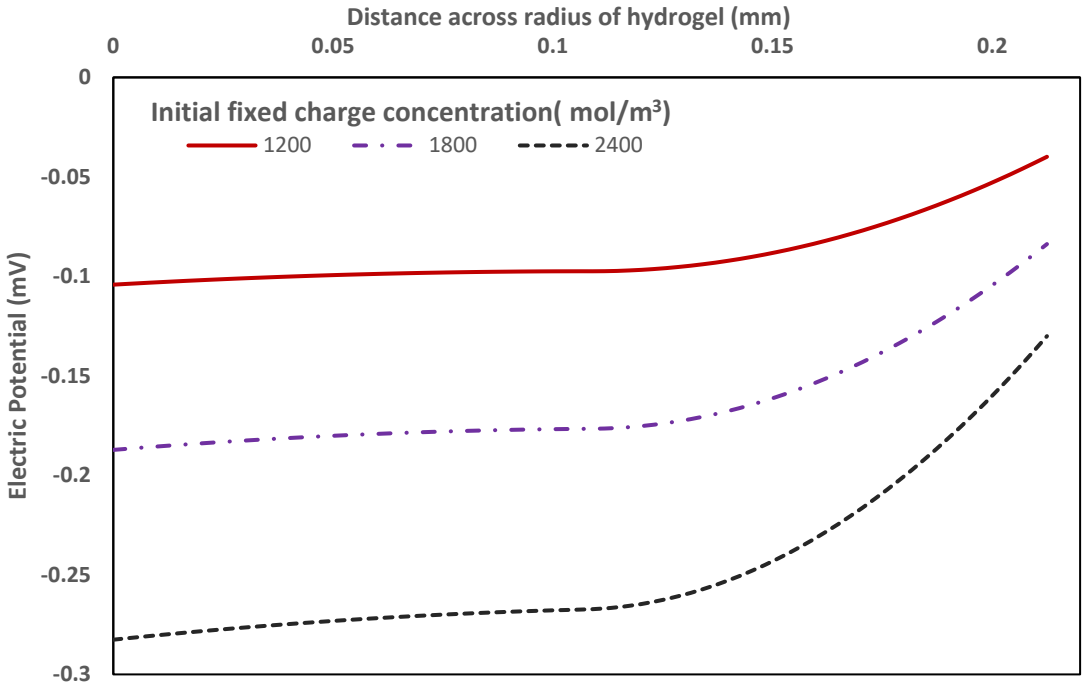

Figure 4.5: Electric potential distribution profiles as a function of initial fixed charge concentration in in acidic medium of pH = 2

Mechanically, increasing the initial fixed charge concentration from 1200 mol/m^3 to 2400 mol/m^3, causes an increase in displacement along the radius of the hydrogel. As shown in Fig. 4.6, at constant pH, the hydrogel deforms more at high initial fixed charge concentration due to the increased affinity for mobile counterions diffusing from the surrounding medium into the interior of the hydrogel. The pull for more mobile ions increases the ionic cloud within the hydrogel leading to higher osmotic pressure which ultimately drives higher swelling of the hydrogel.

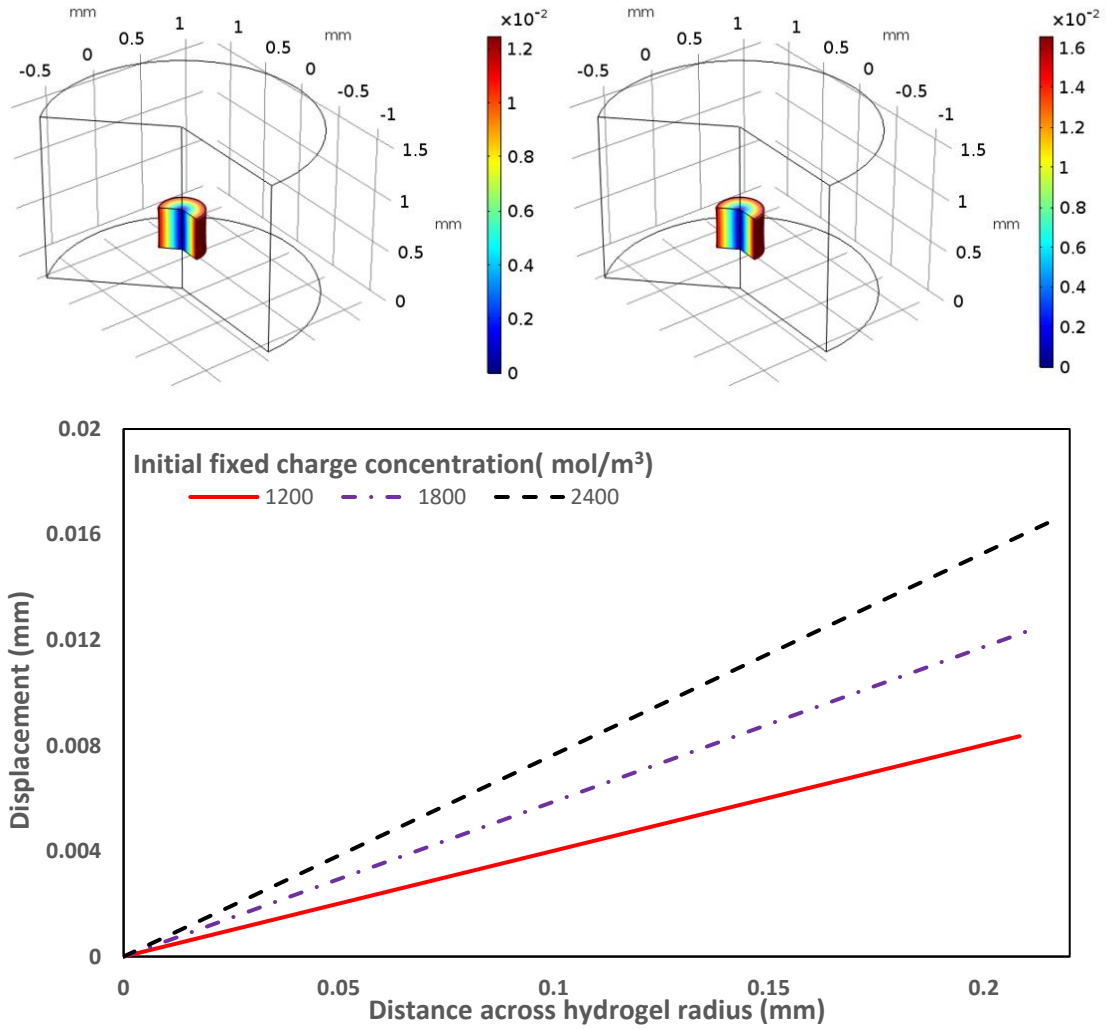

Figure 4.6: 3D plots for displacement as a function of initial fixed charge ($RCOO^-$) concentration 1800 mol/m^3(left) and 2400 mol/m^3 (right), and 1D plot (down) in acidic medium of pH = 2.

4.2.2 Effect of pH variation on equilibrium swelling of anionic hydrogel

Varying the pH of the surrounding medium at a specific initial fixed charge concentration, influences the equilibrium swelling of the hydrogel more in the alkaline medium. As seen in Fig. 4.7 – 4.8, deformation is highest at alkaline pH. This is the idea behind the use of anionic hydrogel-based materials for controlled drug release to regions of the body that require release of therapeutics at alkaline pH. These materials encapsulating therapeutics will resist deformation/swelling in the stomach where the pH is acidic (i.e., varies from 1 to 3), and effectively transport the drugs through the small intestines to the target tissue with alkaline pH.

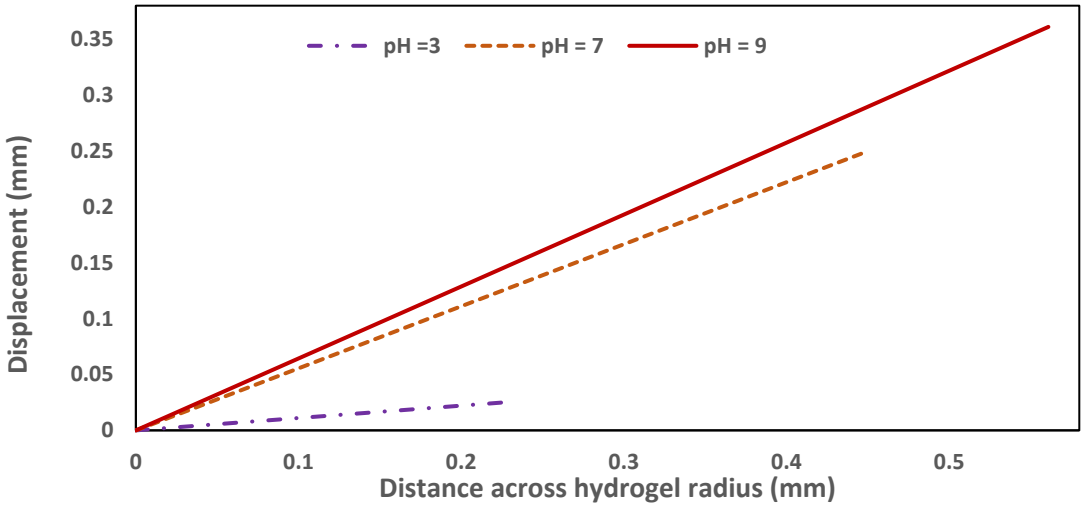

Figure 4.7: Displacement (1D) across the radius of the hydrogel at different pH of the bathing medium for ionizable fixed charge concentration of 2400 mol/m^3

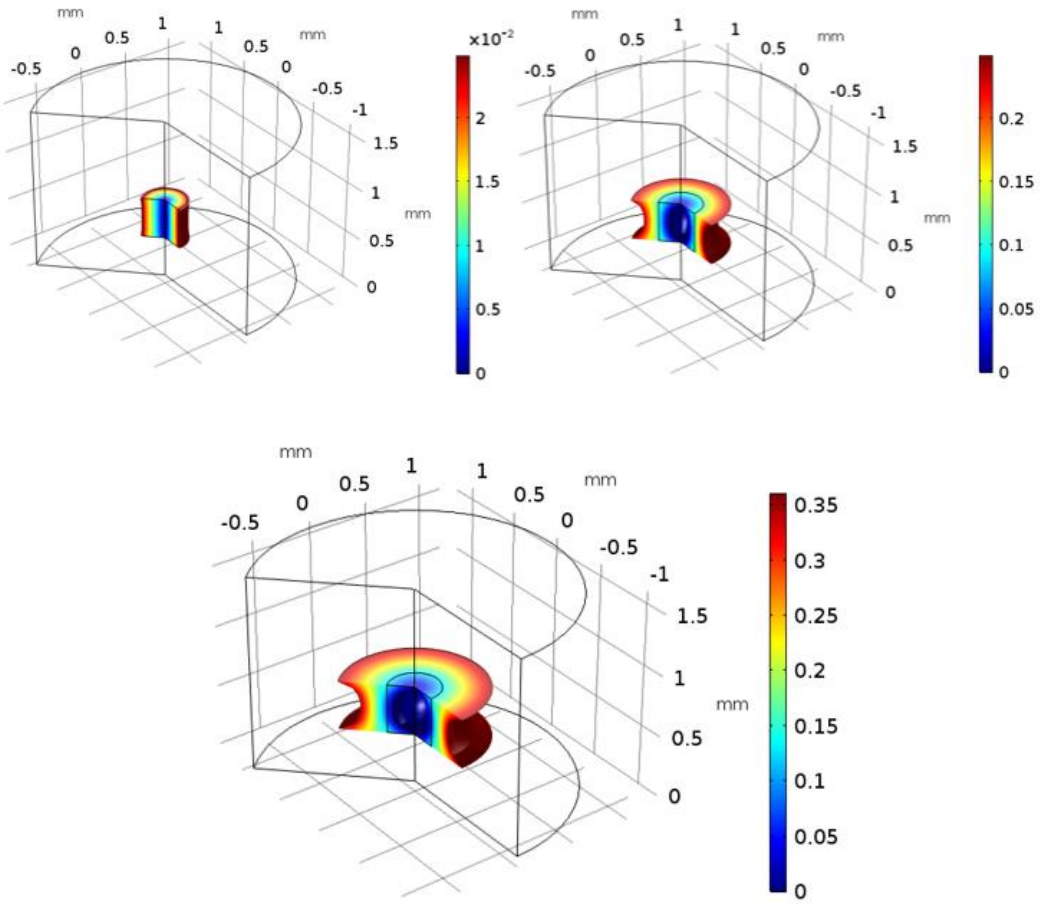

Figure 4.8: Displacement (3D) across the radius of the hydrogel as a function of pH at ionizable fixed charge concentration of 2400 mol/m^3 for pH =3 (left), 7 (right), and 9 (down).

Fig. 4.9 shows that the radius of the anionic hydrogel resist changes to environmental pH values less than 4 and begins to change significantly as the pH of the surrounding medium varies from 4 to 8, thereafter remains almost unchanged. This behaviour results from the increase in ionization of the pendant group as the pH of the surrounding medium increase.

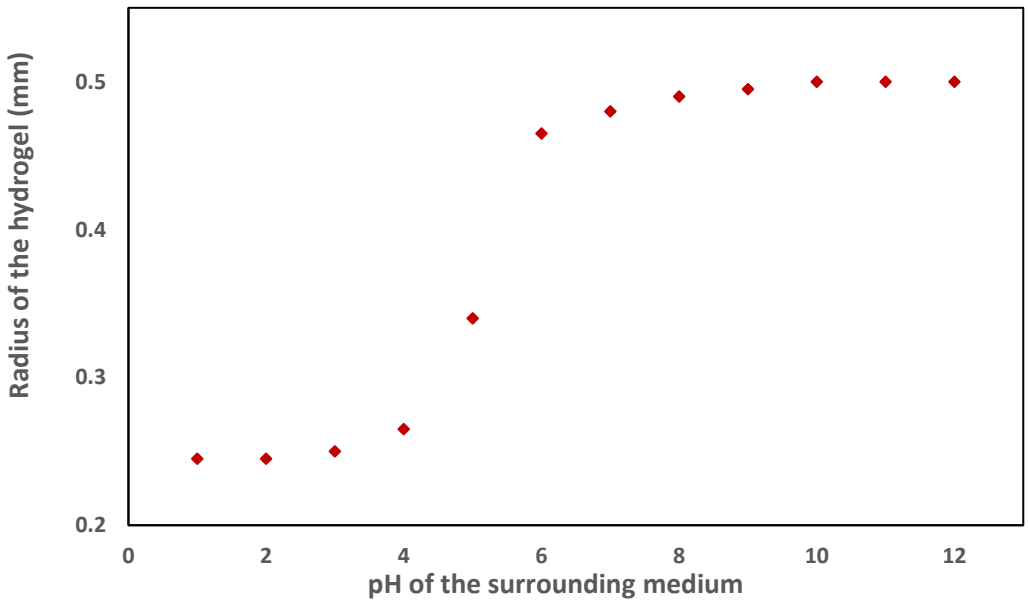

Figure 4.9: Radius of the hydrogel as a function of pH of the surrounding medium

4.3 Reflection

In this chapter, a multifield numerical model has been developed using COMSOL Multiphysics software package based on the famous Poisson-Nernst-Plank formulation in combination with mechanical (deformation) equation. The model describes the equilibrium swelling behaviour of anionic hydrogels, and its prediction capability was tested against experimental, equilibrium swelling data for PHEMA hydrogels. Though the model validation was performed for one-dimensional equilibrium swelling of PHEMA hydrogel, the model, based on the chosen geometry/computational domain, can be adapted to predict two- or three-dimensional volume variation behaviour of other pH responsive hydrogels.

Further, due to model stiffness (i.e., the solution of one or more equations in the system vary rapidly, while others vary slowly) and instability (i.e., a small perturbation in the initial data for the model leads to large variations in the response variable), obtaining consistent dynamic solutions of the model based on the prescribed conditions and geometry was very challenging. However, with the steady state solution, insights into the equilibrium volume variation

behaviour of the hydrogel under study can be derived, and the framework can be adapted to model the volume variation behaviour of pH responsive cationic hydrogels.

CHAPTER FIVE

RESULTS AND DISCUSSION

Multiphysics Simulation for Equilibrium Swelling of pH-Sensitive Cationic Hydrogel

The COMSOL multiphysics-based model developed in Section 3.1 for pH-sensitive anionic hydrogels was adapted for various operating conditions and applied to a case study pH-sensitive cationic hydrogel. The cationic hydrogel studied and analysed is genipin (fixed charged group, -COOH) crosslinked with chitosan (fixed charged group, $–NH_2$) hydrogel. Since genipin is anionic, chitosan is cationic, the hydrogel formed is cationic because the concentration of chitosan used all through was greater than that of genipin.

The governing equations (3.1), (3.2), and (3.24) representing the Nernst Planck, Poisson, and momentum balance equations respectively were solved on the computational domain, Fig. 3.1b, under steady state conditions.

The constitutive relations used for the simulations were Eqns. (3.4), (3.5), (3.6), and (3.25) corresponding to the fixed charge concentration for cationic hydrogels, local hydration state of the hydrogel, total available ionizable fixed charge group in the network, and the osmotic pressure respectively. The results of the steady state simulation are analysed and discussed in this chapter.

5.1 Steady State Swelling/Deswelling of pH-Sensitive Cationic Hydrogels

In a similar fashion to the simulation of equilibrium volume variation of a pH responsive anionic hydrogel (PHEMA), discussed in Chapter 4. A one-dimensional (cylindrical) steady-state simulations were performed for predicting the equilibrium volume variation behaviour of pH-sensitive genipin crosslinked chitosan hydrogel of initial diameter of $400\mu m$.

As stated previously, the pH-sensitive cationic hydrogel swells when the pH of the solution is less than the pK_b of the ionic group at the backbone of the hydrogel. The parameters used for the simulation are presented in Table 3.1. Before swelling, the hydrogel has a radius of 200 μm, as seen in Fig. 5.1. As the hydrogel is placed in acidic medium, for example pH = 4, it swells to an equilibrium size of radius 352 μm as shown by the elongation in the horizontal axis.

Figures 5.1 and 5.2 give the distributive profile of the ionic concentrations of the diffusing species along the radius of the hydrogel for acidic and alkaline media respectively.

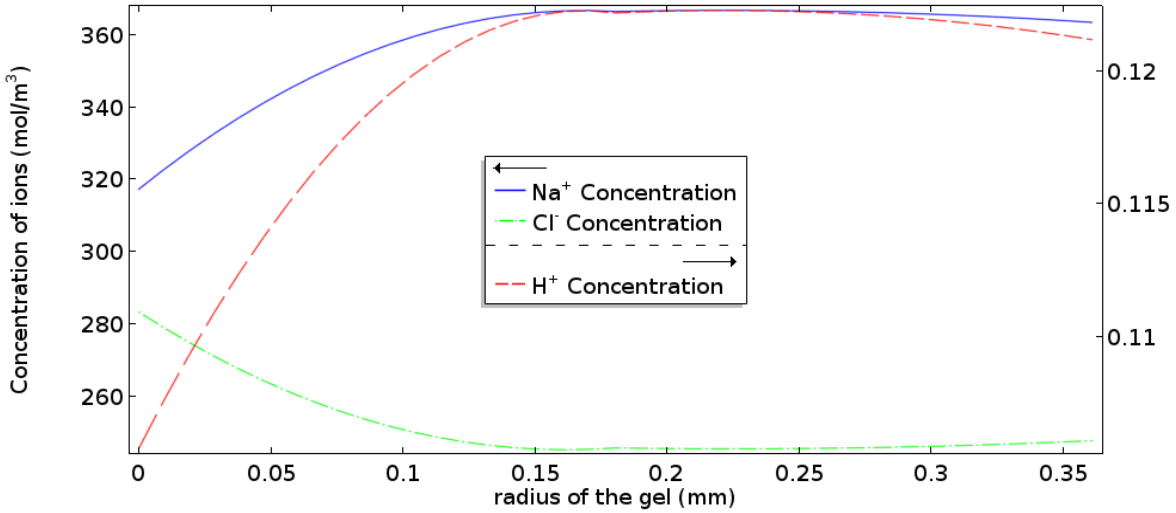

Figure 5.1: Concentration (mol/m^3) distributions of ions in the system for acidic medium of pH 4

From the distributive patterns of the concentrations of the mobile cations (Na^+, and H^+), and mobile anions (Cl^-), it is obvious that the concentrations of the cations are lower at the center of the hydrogel and begins to increase towards the surface of the hydrogel. This could be attributed to the positively charged group at the backbone of the hydrogel network. This positive ion tends to repel cations from entering the interior of the hydrogel while attracting

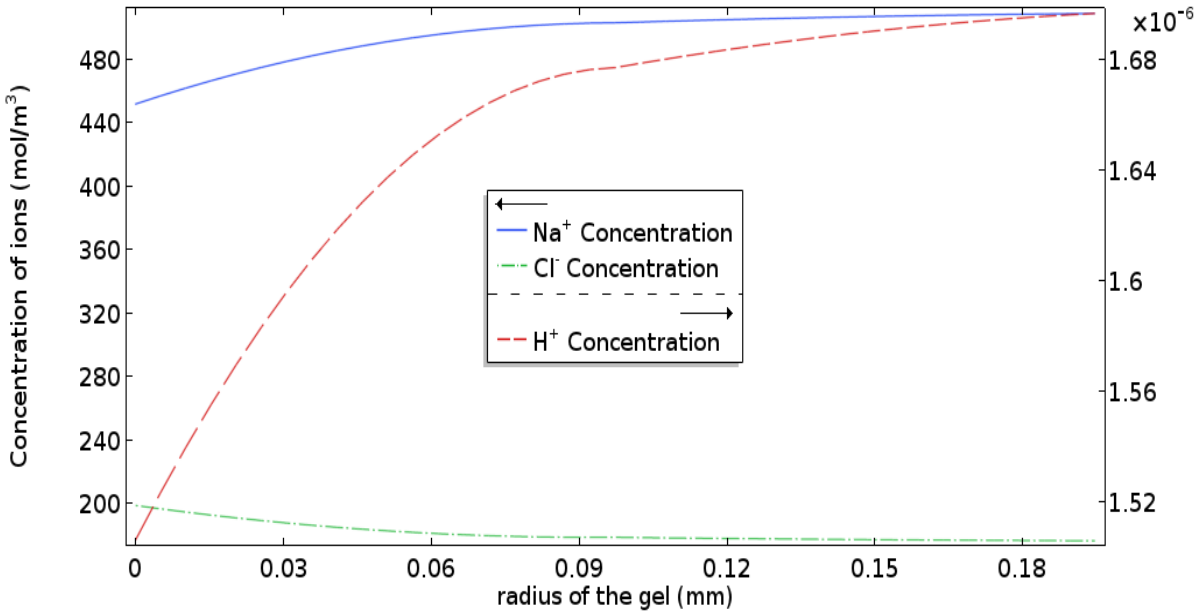

Figure 5.2: Concentration (mol/m^3) distributions of ions in the system for alkaline medium of pH 9

anions in the solution into the interior of the hydrogel, creating a cloud of ions within the hydrogel. The difference in concentrations of the ions within and outside the hydrogel

generates an osmotic pressure that causes the hydrogel to swell with the aim of redistributing the mobile ions within the hydrogel and the external medium until equilibrium is reached.

In alkaline medium, for example pH 9, the hydrogel appears to shrink from an initial radius of 0.2 mm to an equilibrium radius of 0.19 mm. In comparing the behaviour of the hydrogel in alkaline medium with that in acidic medium, the distributive concentrations profiles, show that, the concentration of sodium ion, Na^+ is higher while that of chloride ion, Cl^- is lower for the alkaline medium.

5.2 Effect of Increasing Initial Fixed Charge Concentration of the Crosslinking Agent

Increasing the initial fixed charge density of genipin at a specific initial fixed charge density of chitosan can influence the swelling property of the hydrogel. To study this effect, Figures 5.3, 5.4, 5.5, and 5.6 are the simulation plots for the mechanical displacement, sodium ion, chloride ion, and hydrogen ion concentrations profiles along the radius of the hydrogel as a function of genipin ionizable fixed charge concentration within the hydrogel.

A 0.2 mm genipin crosslinked hydrogel submerged in an acidic medium of pH 4, experiences less swelling as the initial fixed charge density of genipin (at a constant chitosan fixed charge density) increases from an initial value of 500 mol/m^3 to 1500 mol/m^3.

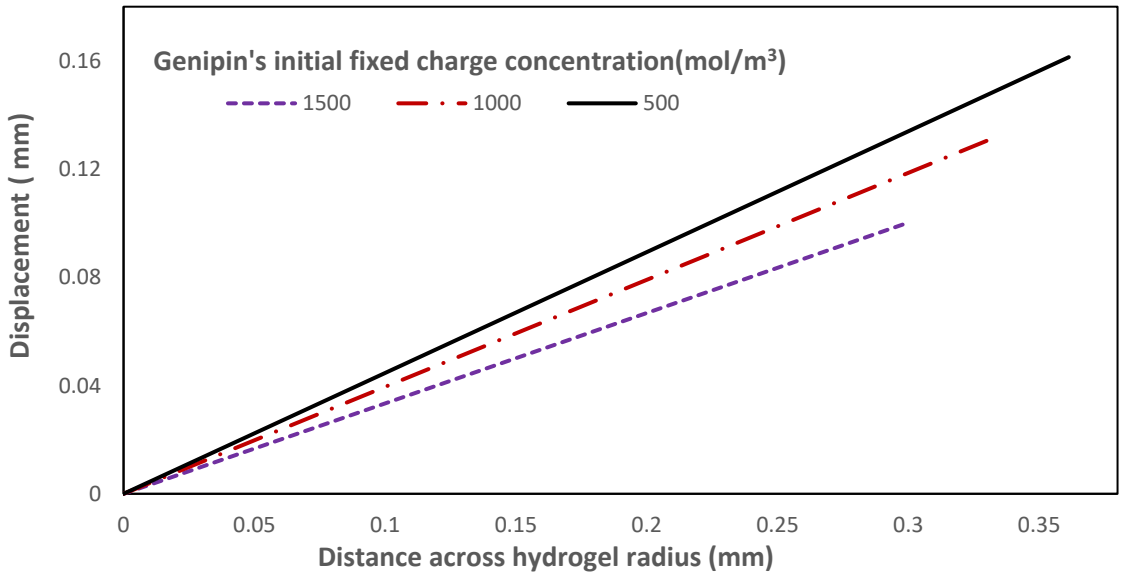

Figure 5.3: Displacement as a function of genipin's initial fixed charge ($RCOO^-$) concentration at a specific chitosan's initial fixed charge ($–NH_2$) concentration of 1800 mol/m^3 for pH = 4

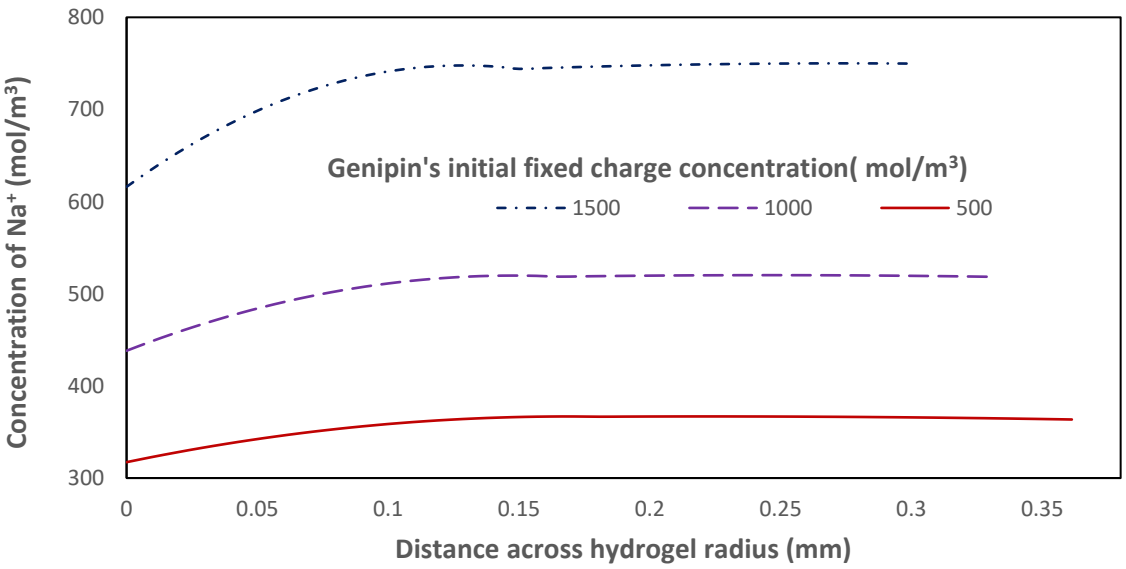

Figure 5.4: Concentration (mol/m^3) distributions of Na^+ in the system as a function of genipin's initial fixed charge ($RCOO^-$) concentration at a specific chitosan's initial fixed charge ($–NH_2$) concentration of 1800 mol/m^3 for pH = 4

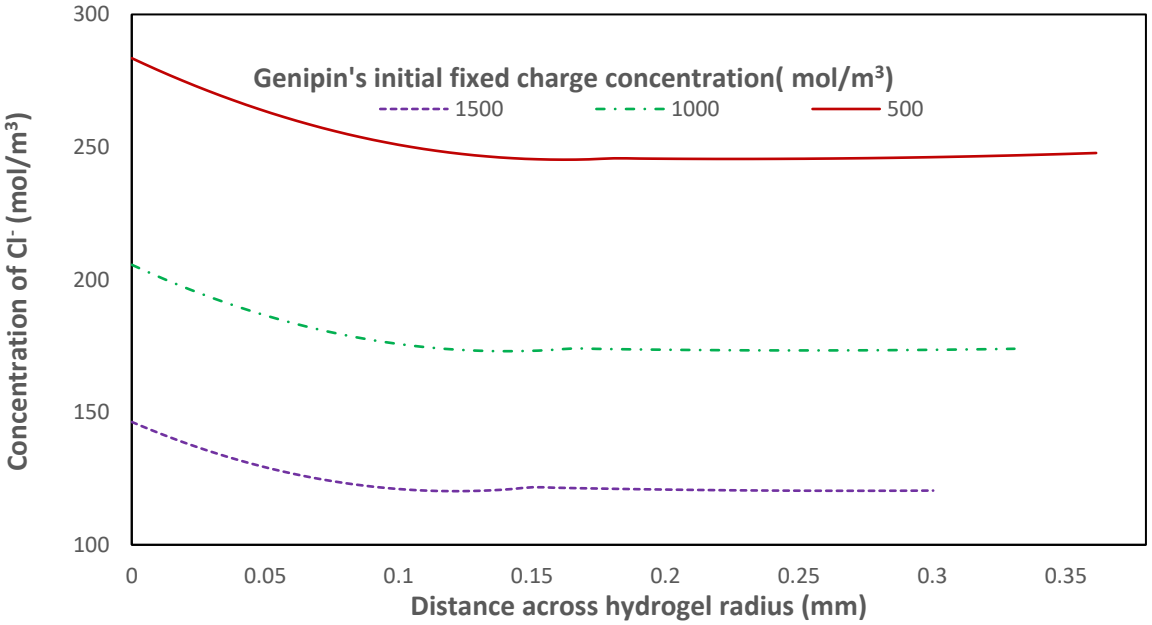

Figure 5.5: Concentration (mol/m^3) distributions of Cl^- in the system as a function of genipin's initial fixed charge ($RCOO^-$) concentration at a specific chitosan's initial fixed charge ($–NH_2$) concentration of 1800 mol/m^3 for pH = 4

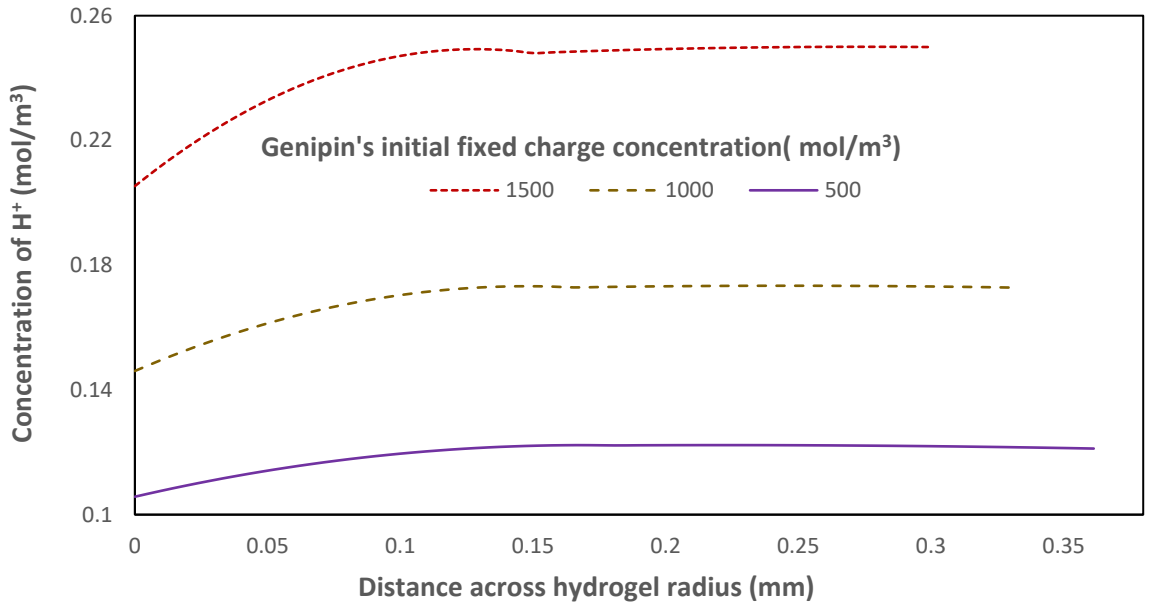

Figure 5.6: Concentration (mol/m^3) distributions of H^+ in the system as a function of genipin's initial fixed charge ($RCOO^-$) concentration at a specific chitosan's initial fixed charge ($–NH_2$) concentration of 1800 mol/m^3 for pH = 4

Although increasing the initial fixed charge density increases the concentration of the diffusing ions entering the hydrogel, it leads to a decrease in the degree of swelling of the hydrogel.

5.3 Effect of pH Variation on Equilibrium Swelling of Cationic Hydrogel

The property of cationic hydrogels to reversibly swell or shrink in response to changes in the pH of the surrounding medium makes them useful in a wide range of applications such as the design of controlled drug delivery systems.

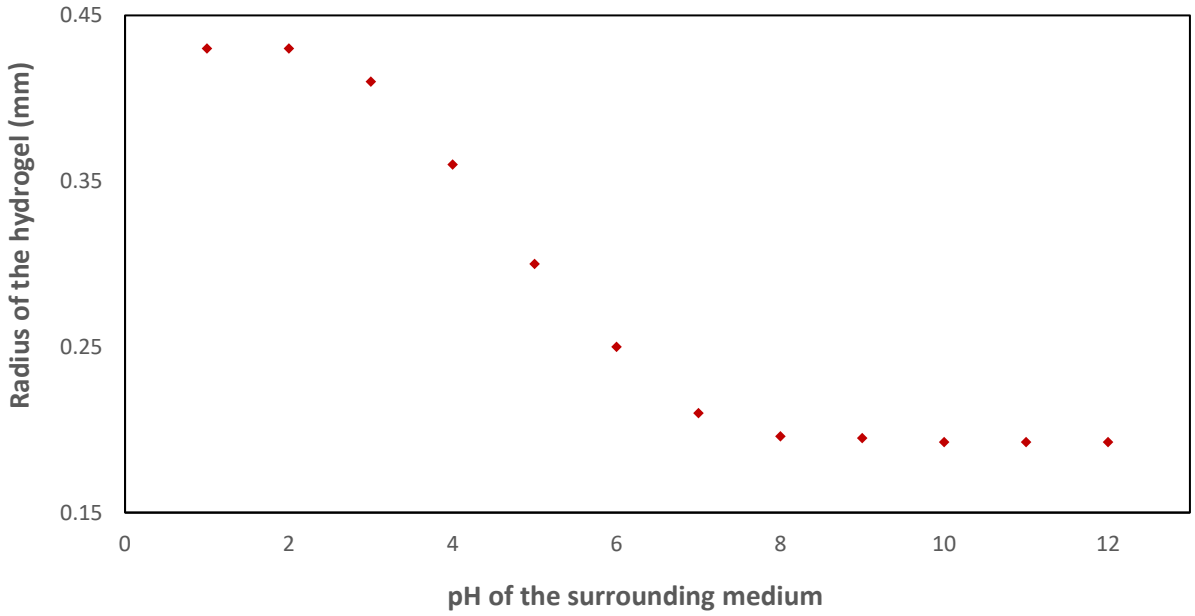

Figure 5.7: Radius of the hydrogel as a function of the pH of the surrounding medium for equilibrium swelling

As can be seen in Fig. 5.7 and Fig 5.8, the cationic hydrogel swells in solutions whose pH is within the acidic range and shrink in solutions with pH within the alkaline range. In drug delivery applications, these materials can be used to prevent drug delivery in alkaline medium, but in acidic region such as tumour site they can swell to aid drug release.

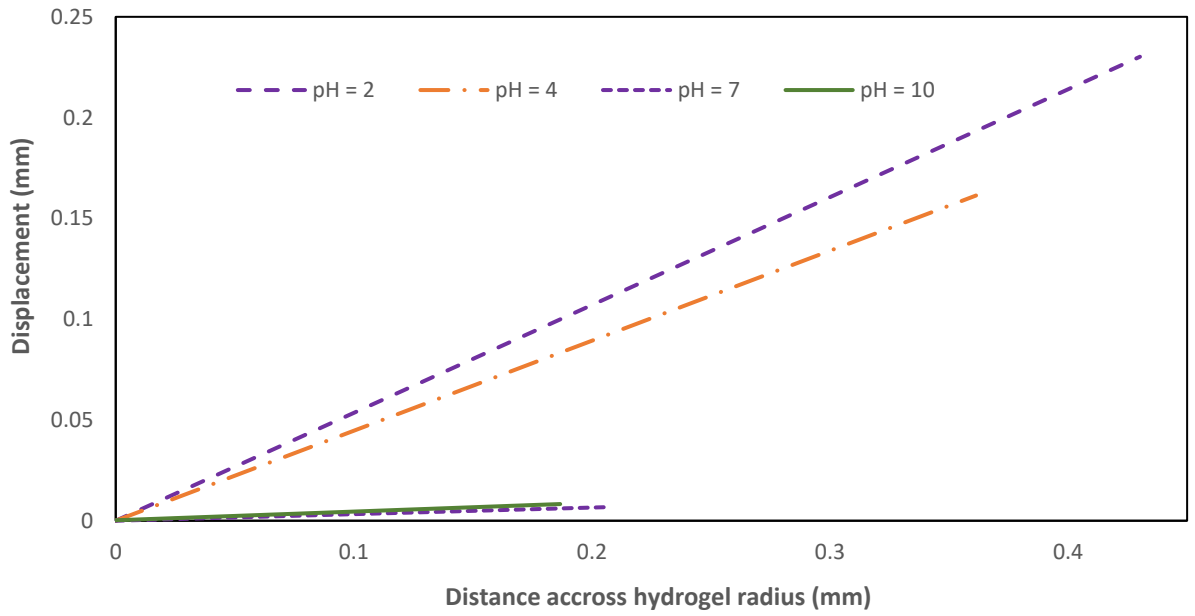

Figure 5.8: Displacement as a function of pH along the radius of the hydrogel

5.4 Limitations

Following on from Chapter 4, the simulation platform developed for studying the equilibrium swelling behaviour of pH-sensitive anionic hydrogels was adapted and applied to simulate the equilibrium volume variation of pH responsive cationic hydrogels. The primary aim of this study was to model and simulate the dynamic volume variation behaviour of pH responsive cationic hydrogels. However, the difficulty associated with performing dynamic solutions for anionic hydrogels places a limitation on the use of this multifield chemo-electro-mechanical approach to simulate and predict time-dependent volume variation behaviour of pH responsive cationic, genipin-crosslinked chitosan hydrogels.

Although steady state solutions were obtained for volume variation of pH responsive cationic hydrogels, the reversible swelling-shrinking property of cationic hydrogels makes it challenging to automate the model as the gel moves from acidic pH medium to alkaline pH medium. To generate equilibrium solutions for all pH values, it was required to manually change the mechanical boundary conditions at the hydrogel-surrounding interface, since osmotic pressure acting at the interface changes direction as the gel moves from acidic pH medium (where swelling occurs) to alkaline pH medium (where shrinking occurs).

CHAPTER SIX

RESULTS AND DISCUSSION
Simulation of the Thermodynamics Model Developed for Equilibrium Swelling of Genipin Crosslinked Chitosan Hydrogels

The multiphysics numerical model developed for studying the volume variation behaviour of anionic (PHEMA) hydrogels (results analysed and discussed in Chapter 4) was adapted to simulate the volume variation behaviour of cationic (genipin crosslinked chitosan) hydrogels (discussed in Chapter 5). However, to overcome the computational challenges encountered during simulation of the cationic (genipin crosslinked chitosan) hydrogels in alkaline region (where the hydrogel shrinks significantly), an alternative approach that uses thermodynamics was employed to model the equilibrium volume variation of the crosslinked hydrogel. The thermodynamics model developed from a statistical mechanics standpoint in Section 3.2 for equilibrium volume variation behaviour of genipin crosslinked chitosan hydrogel was simulated under various operating conditions, and the results are analysed, discussed, and validated in this chapter.

6.1 Response of the Interacting Potentials to pH Variation of the Medium

Genipin crosslinked chitosan hydrogel placed in a bathing medium will continue to swell until there is osmotic pressure balance due to mixing, elastic deformation, and the counterions in the system, according to Eqn. (3.26). The effects of varying the concentration of the crosslinker (i.e., genipin) and pH of the surrounding medium on the contributing potentials/pressures μ_{mix} , $\mu_{elastic}$, and μ_{ionic}, were studied, and the behaviour is shown in Fig. 6.1 – 6.2.

Solving Eqns. (3.34) - (3.53) iteratively gives the equilibrium swell volume, V_{eq}, which makes the summation of all the contributing potentials zero, satisfying the condition of Eqn. (3.26).

As shown in Fig. 6.1, the mixing potential (circle marker) appears to have a negligible effect on the total potential of the hydrogel, whereas the elastic and ionic potentials decreased and increased (respectively) relative to each other. The crosslinked hydrogel under study is an electrically charged hydrogel. Therefore, as the potential due to ionic interactions increases, the potential due to elastic deformation will increase correspondingly to counteract its effect. The mixing potential has negligible effect on the overall swelling (as shown in Fig. 6.2) because, the potentials due to elastic deformation and ionic interactions are far much higher than the potential due to mixing.

Furthermore, increasing the concentration of genipin from (a) 5mM through (b) 7.5mM to (c) 10mM at constant chitosan concentration tends to increase the potential within the hydrogel (see Fig. 6.1) due to increased ionic interaction between the mobile ions in solution and those bound to the polymer network. However, this increase in concentration of the crosslinking reagent tends to toughen the polymer network leading to a decrease in equilibrium swelling of the hydrogel as the concentration increase from (a) 5 mM through (b) 7.5 mM to (c) 10 mM as depicted in Fig. 6.2.

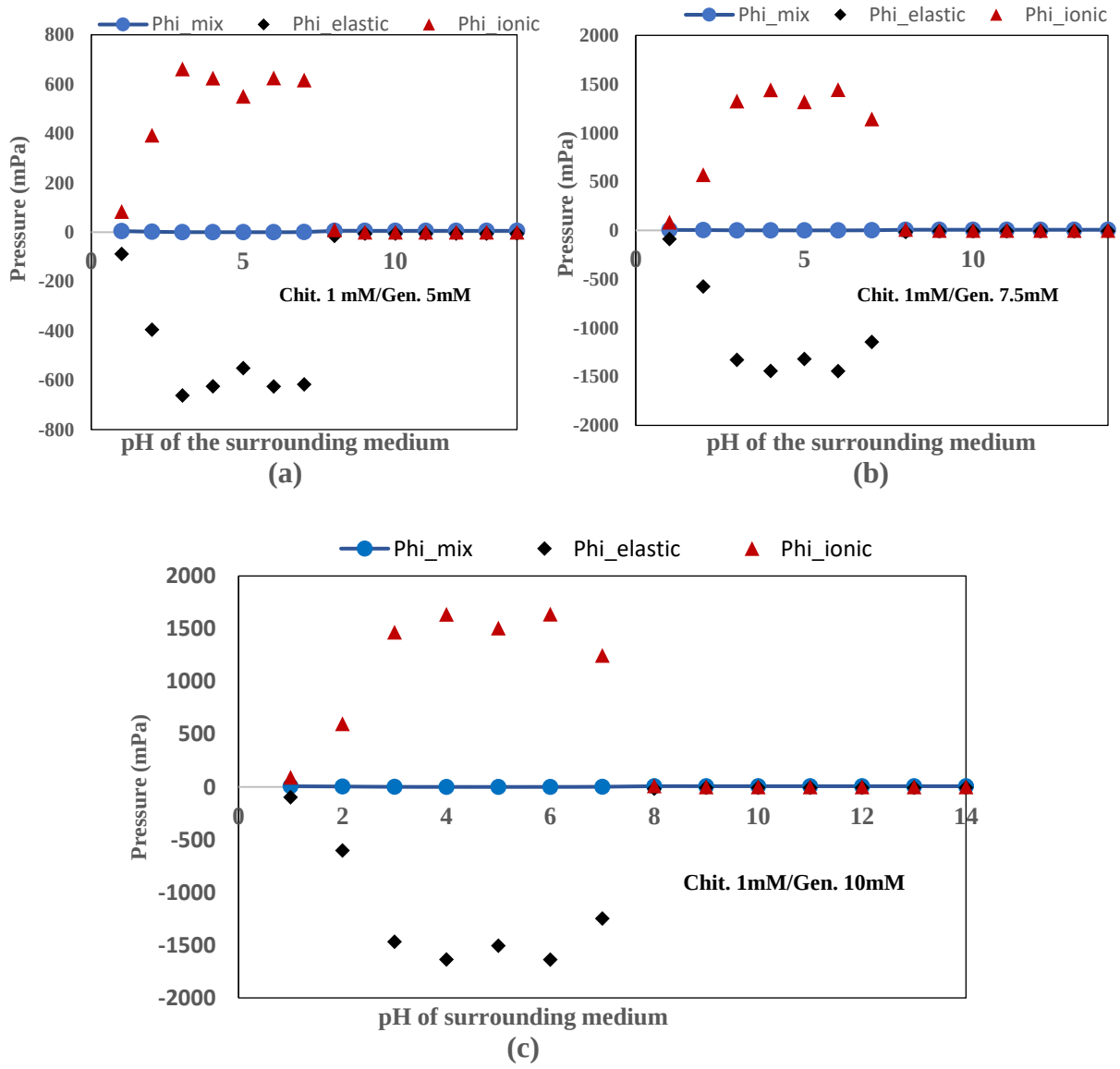

Figure 6.1 Potentials as a function of pH of the surrounding medium at different genipin concentration (a) 5 mM (b) 7.5 mM (c) 10 mM

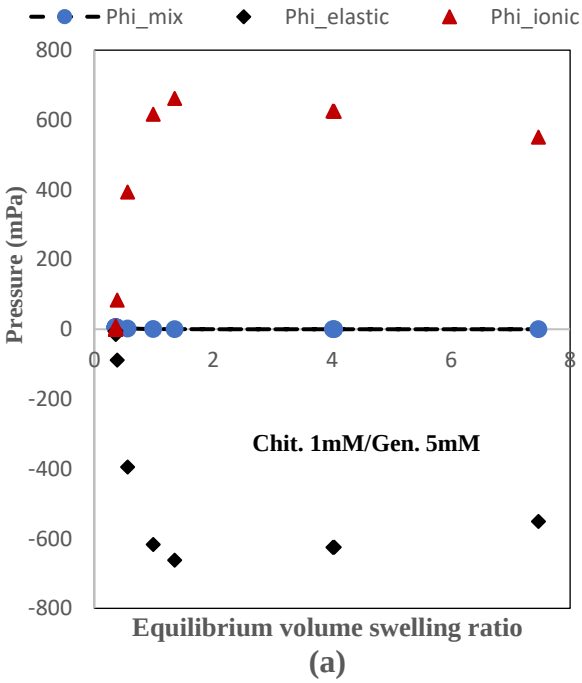

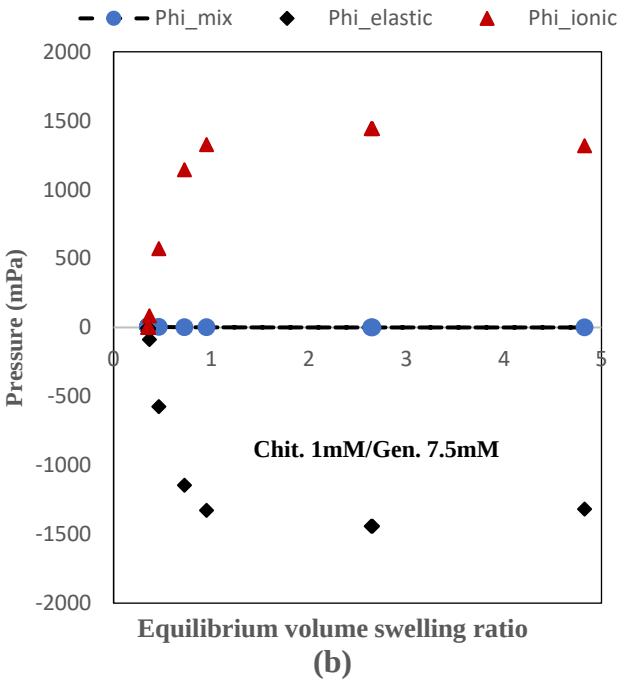

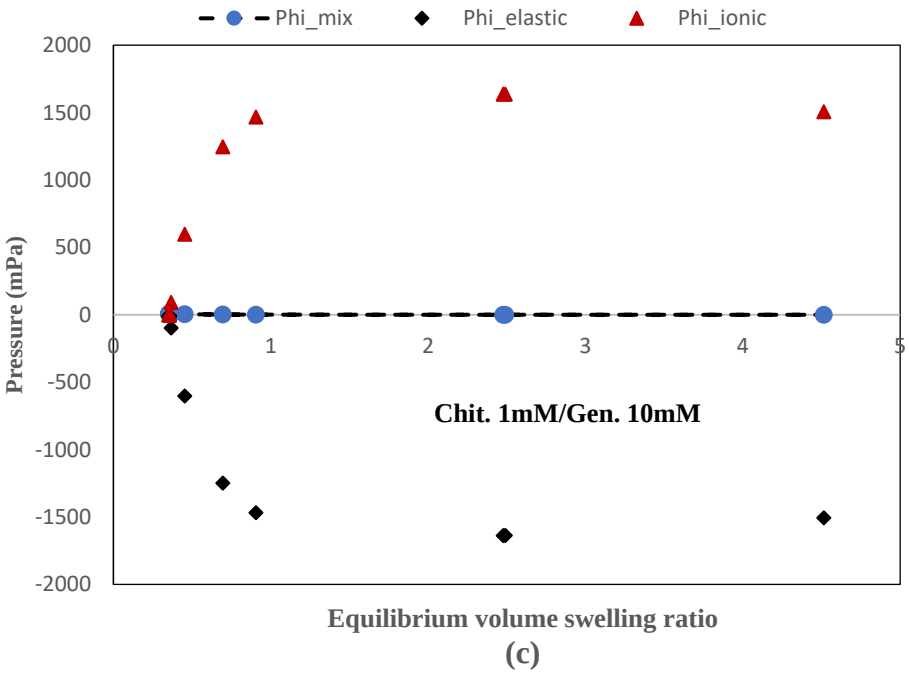

Figure 6.2: Potentials as a function of equilibrium swell ratio at different genipin concentration (a) 5 mM (b) 7.5 mM (c) 10 mM.

6.2 Model Validation

Two sets of data were used to evaluate the performance of the equilibrium model developed (from statistical mechanics approach) for swelling studies involving genipin crosslinked chitosan hydrogel. The first dataset was obtained from the experimental studies by Jahren *et al.* [159], involving hydrogels synthesised from chitosan crosslinked with genipin. In generating this data, Jahren, and co-workers [159] made stock solutions for chitosan (from 2 and 3 wt.% chitosan dissolved in 1% acetic acid in deionized water) and for genipin (0.01M, 0.015M, 0.020M, 0.050M, and 0.10M genipin solution in 1% acetic acid). 10ml of the stock chitosan solutions were mixed with 10ml of the genipin solution and poured into a 10 cm diameter Petri dish for gelling. After gelation, discs of 15mm diameter and 2.5mm depth were cut off from the parent gel for swelling studies. For the swelling experiments, large baths containing aqueous solutions of various pH were prepared. For the acidic baths the pH was adjusted by adding small amount of 1M laboratory-grade HCl while for the alkaline baths 2 M laboratory-grade NaOH was used. The hydrogel samples were monitored for twenty-four hours to equilibrate and attained a constant weight. The degree of swelling was determined using Eqn. (2.36). To convert the data to a form useable in this work, Eqn. (2.39) was used to transform the data from mass swelling ratio to volume swelling ratio. On the other hand, the second dataset was obtained from experimental swelling data (from our laboratory, Novakovic's group) involving chitosan crosslinked with genipin hydrogels. The experimental procedure for the hydrogel synthesis and swelling experiments are detailed in the works by Vo *et al*. [133] and Vukajlović [214].

6.2.1 *Performance evaluation using literature data*

The performance of the thermodynamics model (derived from statistical mechanics approach) developed in Section 3.2 for equilibrium swelling of genipin crosslinked chitosan hydrogels was evaluated using data obtained from the experimental work of Jahren *et al.* [135]. Fig. 6.3 shows how the simulated equilibrium swelling ratio correlates with the literature values. The discrepancies in the profiles and the equilibrium swelling ratio between the experimental (literature data) and the model simulation values in acidic pH range may be attributed to the crosslinked hydrogel behaving like a network of stiff rods [215] in low pH of the surrounding medium.

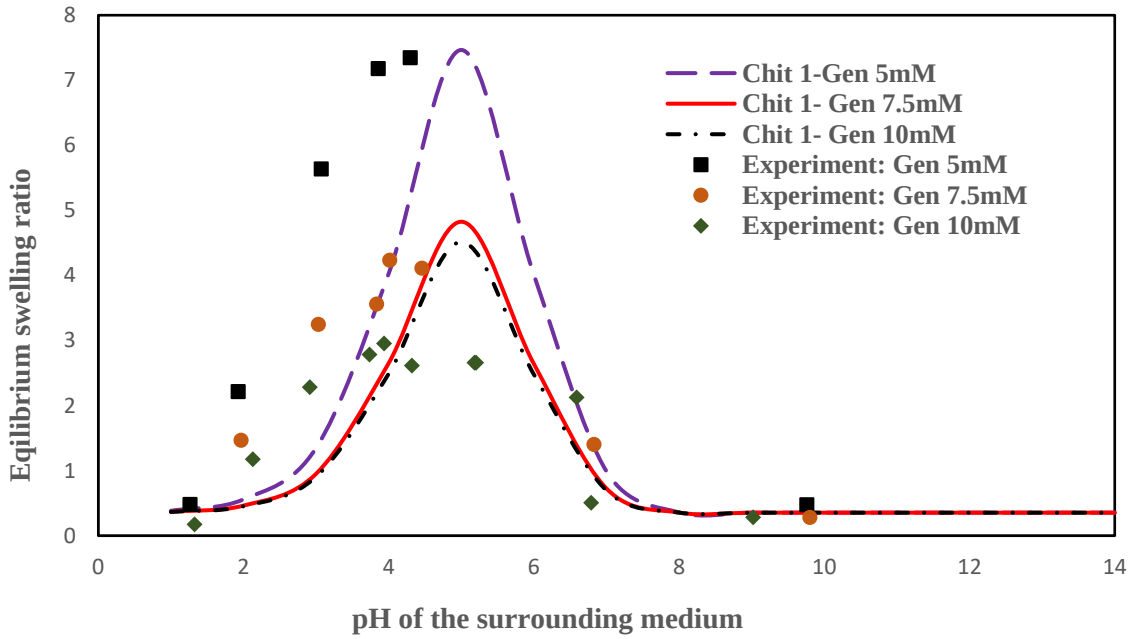

Figure 6.3: Equilibrium swell ratio for experimental [135] versus simulated as a function of the surrounding pH for different concentration of genipin used.

6.2.2 *Performance evaluation using laboratory deswelling data*

Conformational change experiments were performed in three trials for genipin crosslinked chitosan hydrogels in Simulated Body Fluid, SBF (pH = 7.4). Table 6.1 compares the average equilibrium swell volume ratio obtained from experiment with that predicted by the model for different degree of crosslinking used.

Swelling experiment was performed for chitosan-genipin hydrogels with different degree of crosslinking, as shown in Table 6.1. For example, x40, x80, x120, and x160 represent chitosan to genipin molar ratio of 1:40, 1:80, 1:120, and 1:160 respectively.

Table 6.1: Comparison between experiment and model prediction for deswelling in SBF

Gel Type	V_{SR} (Actual)	V_{SR} (Pred)	Error (%)
x40	0.837111639	0.836135	0.11667
x80	0.417730389	0.420062	-0.55817
x120	0.246110284	0.373562	-51.7862
x160	0.196565682	0.358027	-82.1414

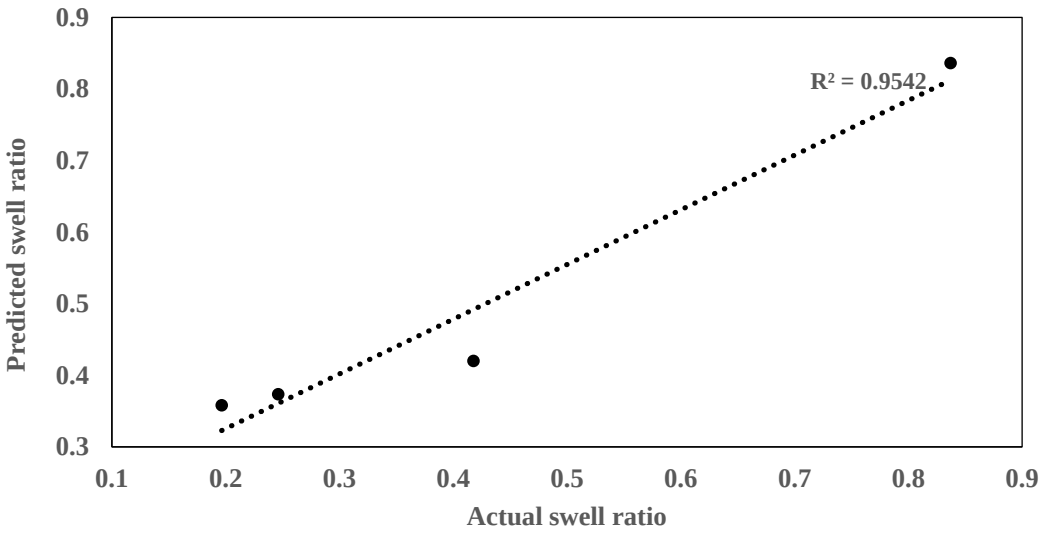

Figure 6.4: Plot of actual volume swell ratio against predicted volume swell ratio in SBF medium

It is clear from Table 6.1 that the model gives good prediction at low concentration of the crosslinking agent. For x40, and x80 type hydrogels, percentage relative error is less than 1%, whereas, at high crosslinking concentration, the error between model predictions and experimentally observed swelling ratio becomes large. This behaviour is expected because the model assumes gaussian statistical behaviour (i.e., the rubber elasticity theory) for the crosslinked hydrogels. For this reason, this model is limited to applications requiring the use of genipin crosslinked hydrogels with low crosslink density, since the limitations have negligible effects on the model's capability to predict accurately the response behaviour of the hydrogel.

Figure 6.4 compares the average of the three trials of the equilibrium swell volume ratio obtained experimentally (at the pH of 7.4) with the value obtained from simulation at the same pH for the different degree of crosslinking. From Table 6.1 and Fig. 6.4, it can be deduced that the model can offer good predictions for equilibrium swell volume ratio involving low genipin concentration.

6.3 Effects of Increasing Concentration of Crosslinking Agent

Having validated the performance of the thermodynamics model developed for studying the volume variation behaviour of cationic (genipin crosslinked chitosan) hydrogels, let's consider further the influence of varying the crosslink density of genipin on the swelling or deswelling behaviour of the crosslinked hydrogels. The concentration of the crosslinking reagent is a key

parameter that has significant effect on the swelling behaviour of stimuli responsive hydrogels. Varying the concentration of the crosslinking reagent affects both the structure and elasticity of the hydrogels, which in turn controls the mechanical properties of the hydrogel. The degree of swelling of the hydrogel reduces significantly as the amount of crosslinker increases.

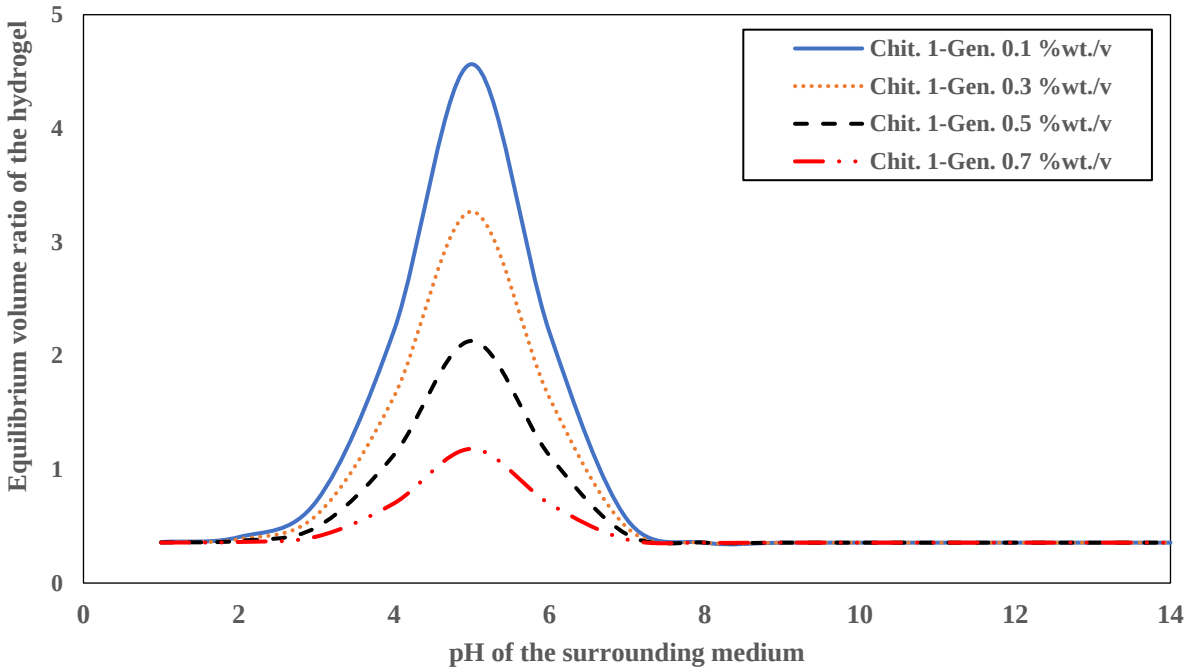

Figure 6.5: Influence of concentration of crosslinking agent on equilibrium swell ratio as a function of pH

Fig. 6.5 is plotted for the equilibrium swell ratio as a function of pH for various concentrations of genipin. It is obvious from the plot that, increasing the concentration of genipin increases the mechanical strength, which evidently decreases the swelling degree of the hydrogels. This increased mechanical strength is due to the weak van der Waals intermolecular bonds being partially replaced by the strong covalent bonds as the amount of crosslinking agent increase.

6.4 Effect of Surrounding Media on Equilibrium Swelling

The nature of the ions in the surrounding medium plays an important role in the swelling behaviour of the crosslinked hydrogel. The ions in the swelling medium can alter the polymer-polymer, polymer-water, water-ion, and ion-polymer interactions in the system thereby affecting the degree of swelling in the different media.

When the hydrogel is immersed in a buffered solution, the ions in the surrounding medium diffuse into the hydrogel leading to a chemical reaction between the diffusive mobile ions and

the ionizable groups attached on the backbone of the hydrogel. The redistribution of ionic concentrations within the interior of the hydrogel creates a cloud of ions inside the hydrogel leading to osmotic pressure build up due to the difference in ionic concentrations between the hydrogel and the surrounding medium. This osmotic pressure drives the swelling and shrinking of the hydrogel. The swelling/deswelling in turn leads to redistribution of ions within the hydrogel. This cycle continues until equilibrium swelling or shrinking is attained.

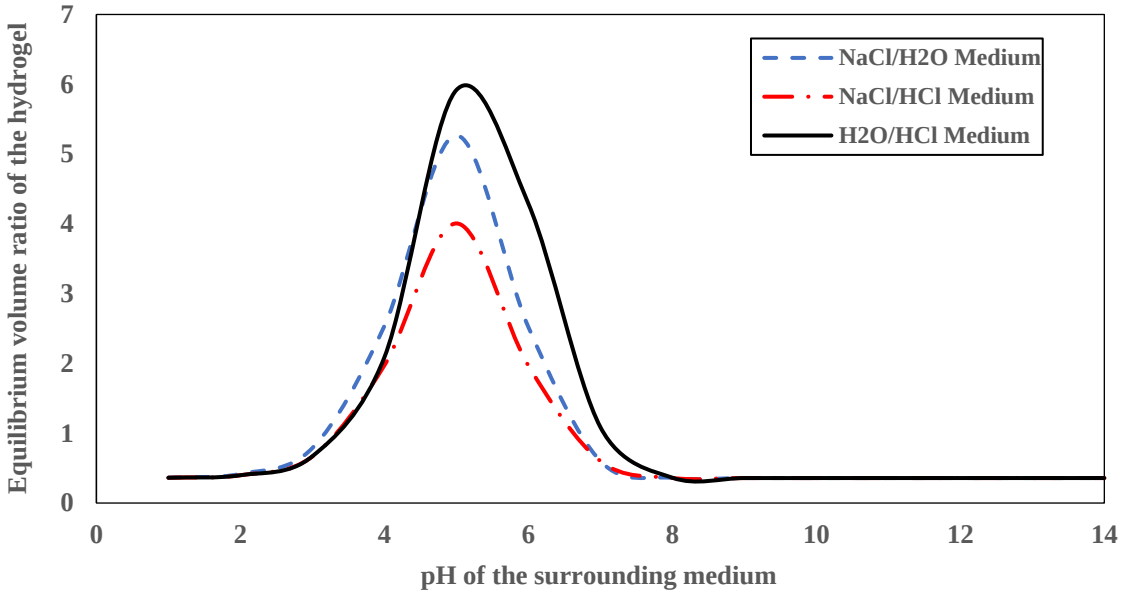

Figure 6.6: Influence of environment/solution type on equilibrium swelling ratio as a function of pH.

Fig. 6.6 shows that, although the crosslinked hydrogel tends to swell maximally in dilute hydrochloric acid solution (i.e., H_2O/HCl medium), the response to pH variation was the fastest in dilute sodium chloride solution (i.e., NaCl/H_2O) due to the affinity of sodium ions in solution for the polar groups at the backbone of the hydrogel. The high equilibrium swelling ratio of the dilute hydrochloric acid solution could be attributed to the availability of more hydrogen ions for protonation of the fixed charged group at the hydrogel network.

6.5 Effects of Increasing the Ionic Strength of the Surrounding Medium

pH sensitive hydrogels respond differently to variations in the ionic strength of the surrounding medium. Figure 6.7 and 6.8 demonstrates theoretically the effect of ionic strength of the surrounding medium on the equilibrium swell ratio of the crosslinked hydrogel at constant

genipin and chitosan concentration, and identical modulus of elasticity and initial fixed charge concentration.

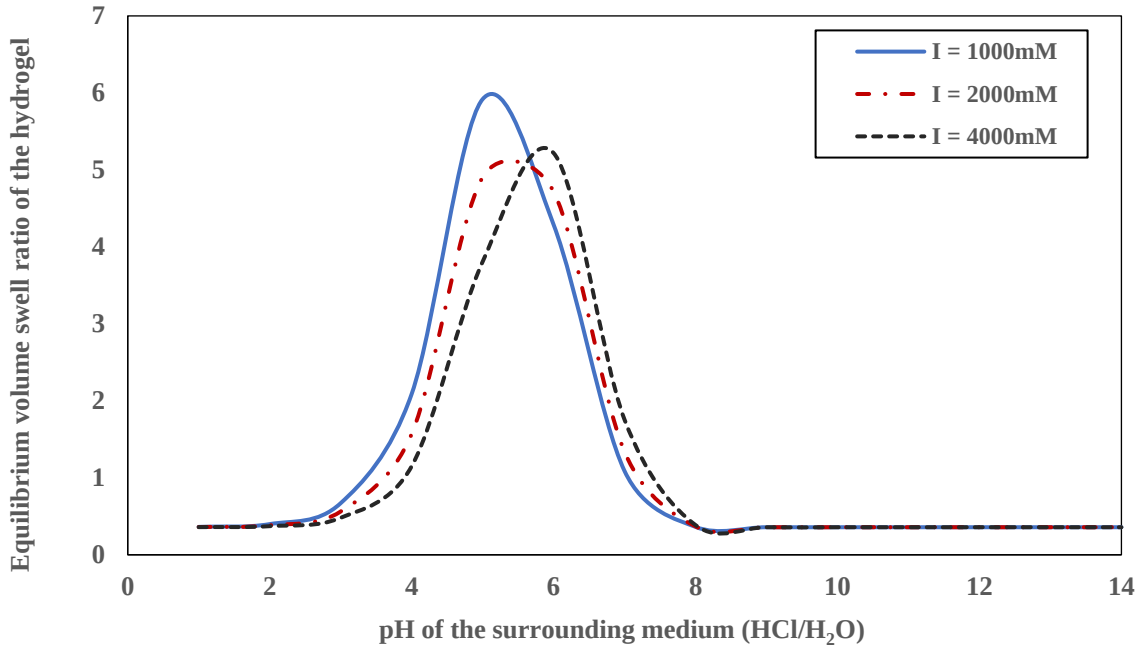

Figure 6.7: Influence of ionic strength on equilibrium volume swell ratio as a function of pH of surrounding dilute acid medium.

The highest curves for both figures (i.e., Fig. 6.7 and 6.8) correspond to solution with ionic strength of 1000mM, while subsequently lower curves are associated with higher values of ionic strength, increasing from 2000 mM to 4000 mM. Increasing the ionic strength of the surrounding medium increases the tendency of the fixed charged group at the backbone of the hydrogel to repel the mobile cations in the solution from entering the interior of the hydrogel. This eventually leads to shrinking of the hydrogel, as evident in the Fig. 6.8. Although the behaviour seems slightly different for Fig. 6.7, this implies that the hydrogen (H^+) ions play-

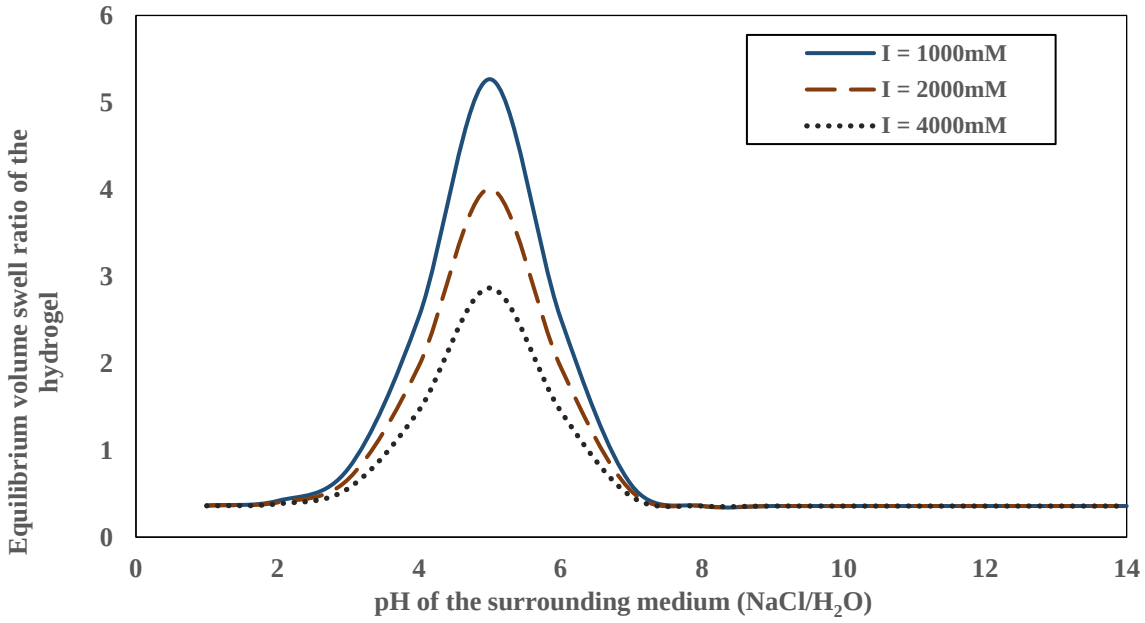

Figure 6.8: Influence of ionic strength on equilibrium volume swell ratio as a function of pH of surrounding sodium chloride solution

an important role in the association and dissociation process of the fixed charge group for swelling/deswelling of hydrogels in dilute acid solution.

6.6 Reflection

To overcome the computational challenges encountered while trying to adapt the multifield numerical model (results in Chapter 4) for studying the volume variation behaviour of anionic hydrogels to suit the simulation of the swelling−shrinking behaviour of cationic hydrogels (Chapter 5), an alternative approach was employed. The alternative approach derived a thermodynamic model (using statistical mechanics method) for the equilibrium volume variation behaviour of cationic crosslinked hydrogels. Besides overcoming the mathematical difficulties associated with the multifield approach, one major advantage of this modelling approach is the easy with which the concentration of the crosslinking reagent was incorporated into the model as a tuneable parameter.

Moreover, one limitation of the thermodynamic model, Eq. (3.53), developed in Section 3.2, is the high dependence on laboratory data for model recalibration and validation. This is due to uncertainties in some of the model parameters such as N_c, the average number of segments in the polymer chain network, χ, is the polymer-solvent interaction parameter, c_f, the charge density of crosslinked hydrogel, etc., therefore requiring uncertainty quantification. However,

its theoretical predictions offer some insight (such as influence of ions in the medium on equilibrium swelling) that could be difficult to observe otherwise.

CHAPTER SEVEN

RESULTS AND DISCUSSION

Simulation for Dynamic Swelling of Genipin Crosslinked Chitosan Hydrogel

The main goal of this work was to model and simulate the swelling/deswelling dynamics of cationic (genipin crosslinked chitosan) hydrogels. Due to numerical issues (bothering around stability and model stiffness) associated with the use of the multiphysics approach that involves coupled Poisson-Nernst-Planck and mechanical equation, an alternative approach that combines the thermodynamics model (developed in Section 3.2) with the chemo-mechanical model (developed in Section 3.3) to model the time-dependent swelling/deswelling of the cationic (genipin crosslinked chitosan) hydrogels was employed. The theoretical approach adopted in this study to determine the dynamic volume-variation of the crosslinked hydrogels, uses the initial and final/equilibrium states of the swollen or shrunk hydrogel to determine the time-dependent states/volumes of the hydrogel between initial and final volumes. Hence, results for simulation of dynamic volume-variation depend on either theoretically generated data from Chapter 6 (thermodynamics model data) or experimentally determined equilibrium swelling/shrinking data.

7.1 Model Validation

The swelling dynamics of genipin crosslinked chitosan hydrogels discussed in Section 3.3 is governed by the model equation, Eqn. (3.101) that describes the pressure distribution within the hydrogel due to chemo-mechanical interactions between species inside the hydrogel and those in the external medium. By using the initial condition, boundary conditions, and constitutive equation, an equation that describes the volume variation of the crosslinked hydrogel, Eqn. (3.106) was derived. This equation was solved numerically as a finite element problem using COMSOL Multiphysics software (refer to Section 3.3.9 for details). To examine the validity of the dynamic model developed (in Section 3.3), laboratory (time-dependent) data from swelling experiments (gravimetric) performed by Vo *et al*. [133] to examine the pH responsiveness of genipin crosslinked chitosan hydrogels in different buffer solutions: glycine (pH 2), phthalate (pH 4), and phosphate (pH 7) were used. For insight into how the data used for validation were generated, reference is made to the experimental procedure employed by Vo and co-workers [133] .

Chitosan powder was dissolved in a 1% (v/v) acetic acid solution to obtain a solution with a concentration of 1.5% (w/v). Genipin was dissolved in distilled water to produce a 0.5% (w/v)

solution. Thereafter, hydrogels were prepared using 1ml chitosan solution (1.5 % w/v), and 0.2 ml genipin solution (0.5% w/v). On gelation, the weight of each hydrogel was recorded, and the hydrogels placed in the bathing medium (buffer solution) for swelling. The weight of each hydrogel was recorded at time intervals (1, 2, 3, 4, 5, 6, 7, 8, 9,10, 24, 48, and 72hr) and the mass swelling ratio determined using Eqn. (3.36). The mass swelling ratio data were converted to volume swelling ratio data using Eqn. (3.39).

The model for studying the conformational change dynamics of pH-responsive genipin crosslinked chitosan hydrogel was validated using experimental data for pH 2 (Figure 7.1), pH 4 (Figure 7.2), and pH 7 (Figure 7.3).

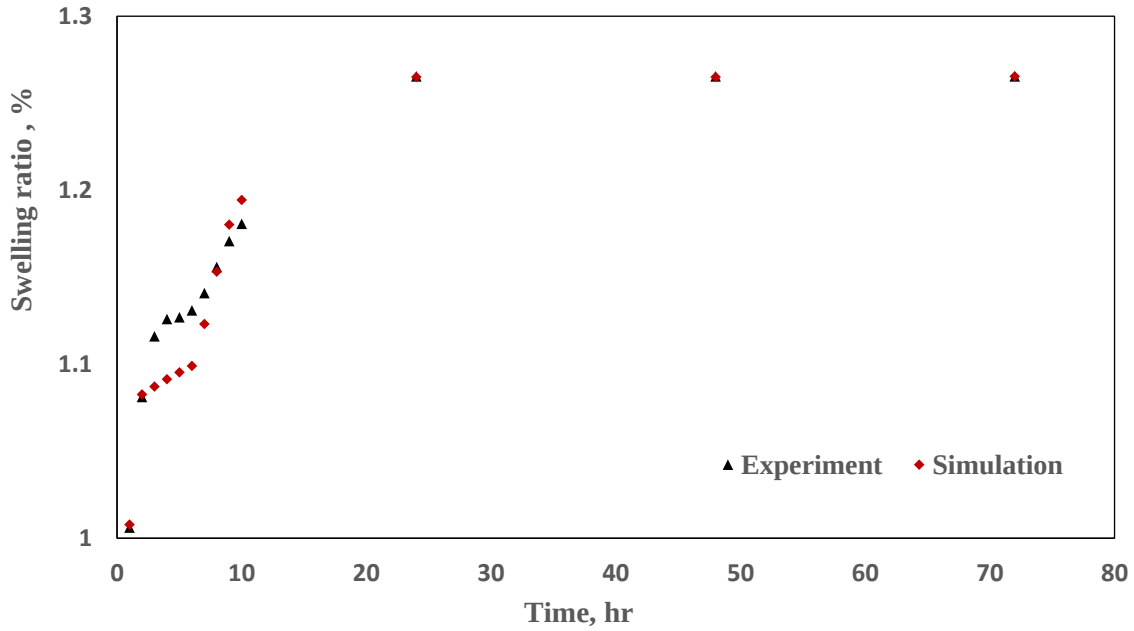

Figure 7.1: Comparison between laboratory data and simulation results for dynamic swelling of genipin crosslinked chitosan hydrogel in a medium of pH 2

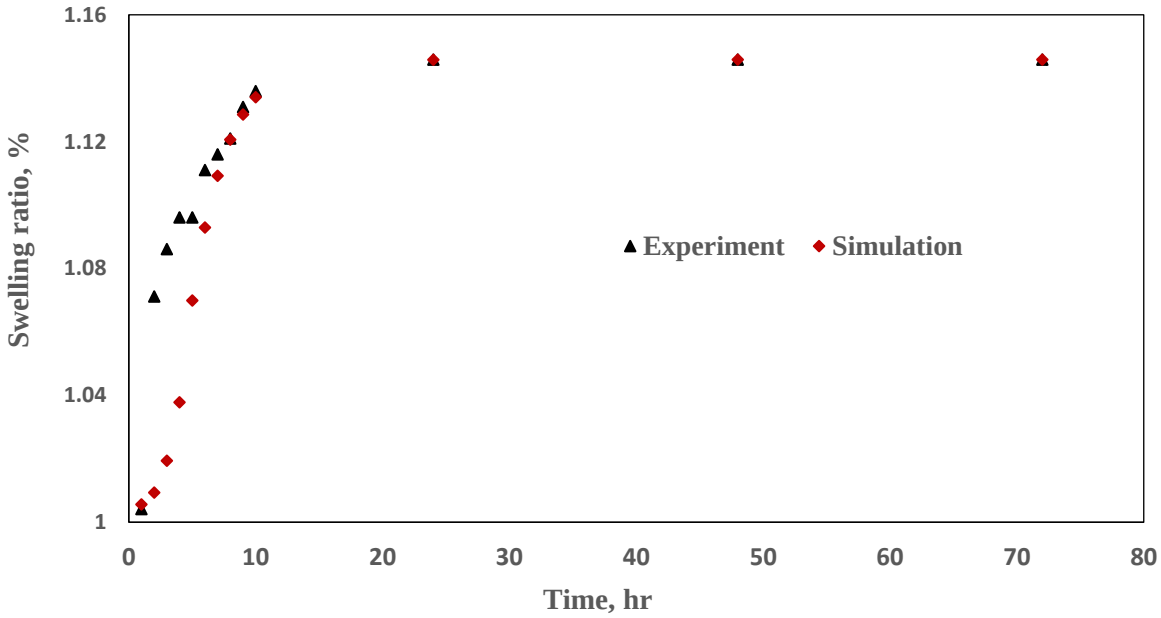

Figure 7.2: Comparison between laboratory data and simulation results for dynamic swelling of genipin crosslinked chitosan hydrogel in a medium of pH 4

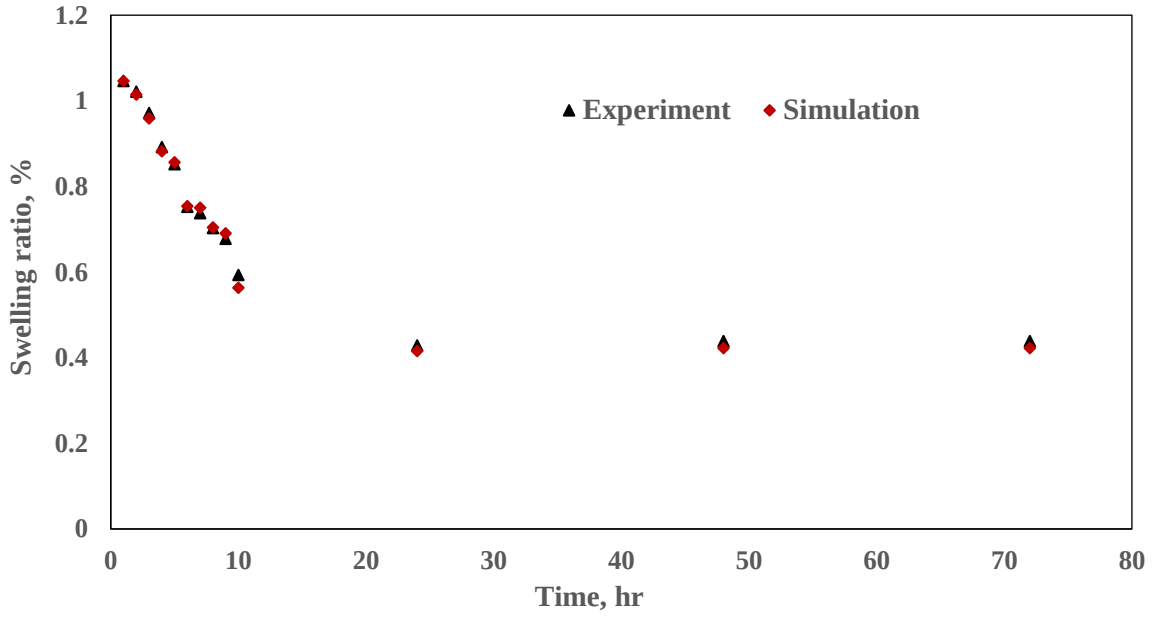

Figure 7.3: Comparison between laboratory data and simulation results for dynamic deswelling of genipin crosslinked chitosan hydrogel in a medium of pH 7

The comparison between the simulated values and the experimental results illustrated in Figure 7.1 – 7.3 shows that the model has the potential to be used for prediction of the conformational change dynamics of genipin crosslinked chitosan hydrogels.

7.2 Parametric Study of Dynamic Swelling/Deswelling of Chitosan Genipin Hydrogel

Although the responsive performance of the crosslinked hydrogel under study is largely pH dependent, other effects also must be taken into consideration as they can affect the conformational change dynamics of hydrogels.

7.2.1 *Effect of initial size of the hydrogel*

Figure 7.4 compares the swelling behaviour of three hydrogel samples of same crosslinked densities but different sizes. Hydrogels of sizes 10 mm, 15 mm, and 20 mm with the same degree of crosslinking (Chit. 1: Gen 0.3% w/v) placed in the same bathing medium of pH 4, and allowed to swell to equilibrium, was studied for dynamic swelling behaviour.

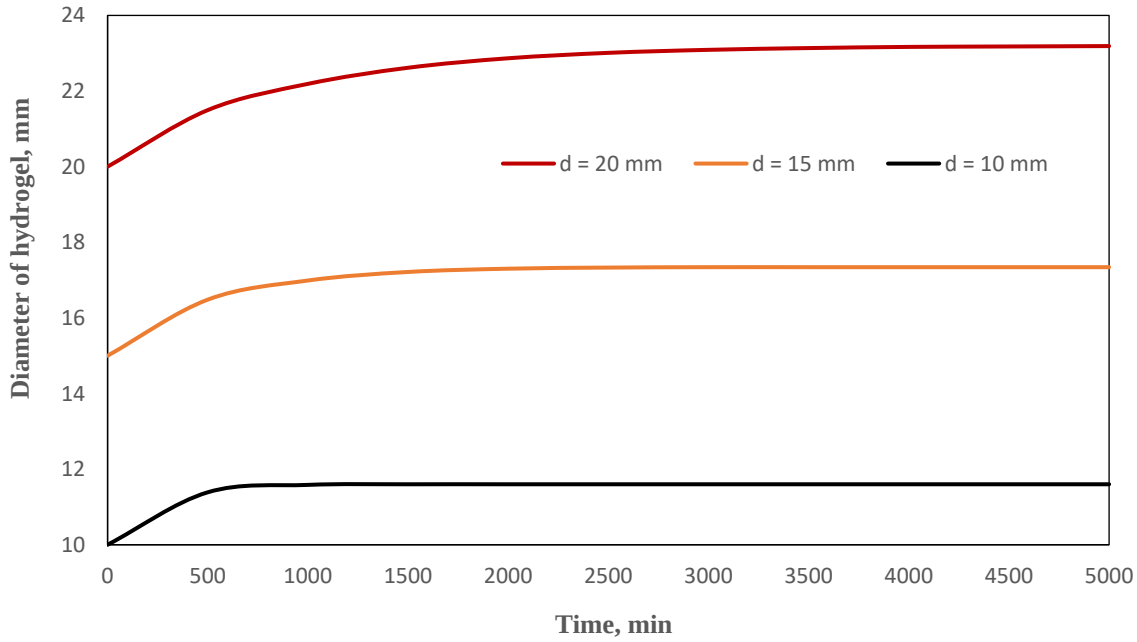

Figure 7.4: Influence of initial size on the swelling dynamics of genipin crosslinked chitosan hydrogel

As seen in Figure 7.4, the 10 mm diameter hydrogel attained equilibrium swell volume in far much lesser time than the other larger sizes. Which agrees with Djabourov and co-workers [216] that, reducing the size of the hydrogel from macroscopic to micro-particles hydrogel can accelerate the swelling rate of the hydrogel. The implication of this is that, for some applications involving controlled drug delivery, it is better to use smaller size hydrogels because they will attain equilibrium swelling in a short time. Thus, releasing the drug at the targeted site quicker than the larger sized hydrogels.

7.2.2 *Effect of initial polymer volume fraction of the hydrogel*

For the same initial size of the hydrogel (20 mm) but different polymer volume fraction (obtained using Eqn. (3.33)), the swelling dynamics of the crosslinked hydrogel was studied. As seen in Figure 7.5, the hydrogel with higher polymer volume fraction attains equilibrium in a shorter time compared with hydrogels of lower polymer volume fraction.

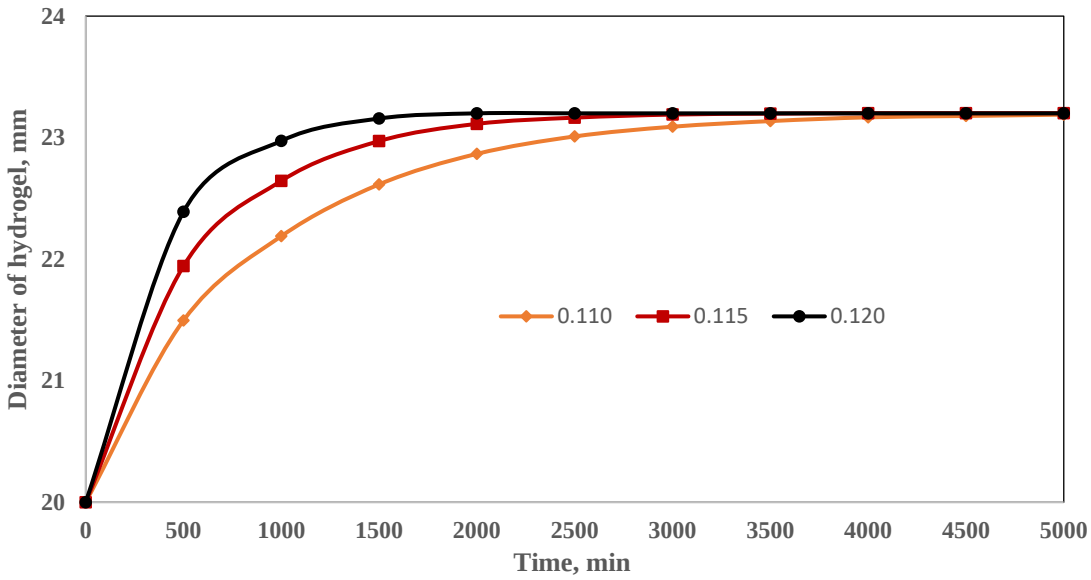

Figure 7.5: Influence of initial polymer volume fraction on the swelling dynamics of genipin crosslinked chitosan hydrogel

Therefore, in applications where the time to reach equilibrium swell volume is a key parameter, the polymer volume fraction of the crosslinked hydrogel must be carefully chosen alongside other parameters that can influence optimum swelling of the hydrogel.

7.2.3 *Effect of pH variation on dynamic swelling*

For the same size of the hydrogel (3.81mm), same chitosan concentration (0.9 ml of 1.5% w/v), and same genipin concentration (0.1ml of 0.5% w/v) used for the study, the time evolution of the diameter of the hydrogel at different pH values of the surrounding medium is shown in Figure 7.6.

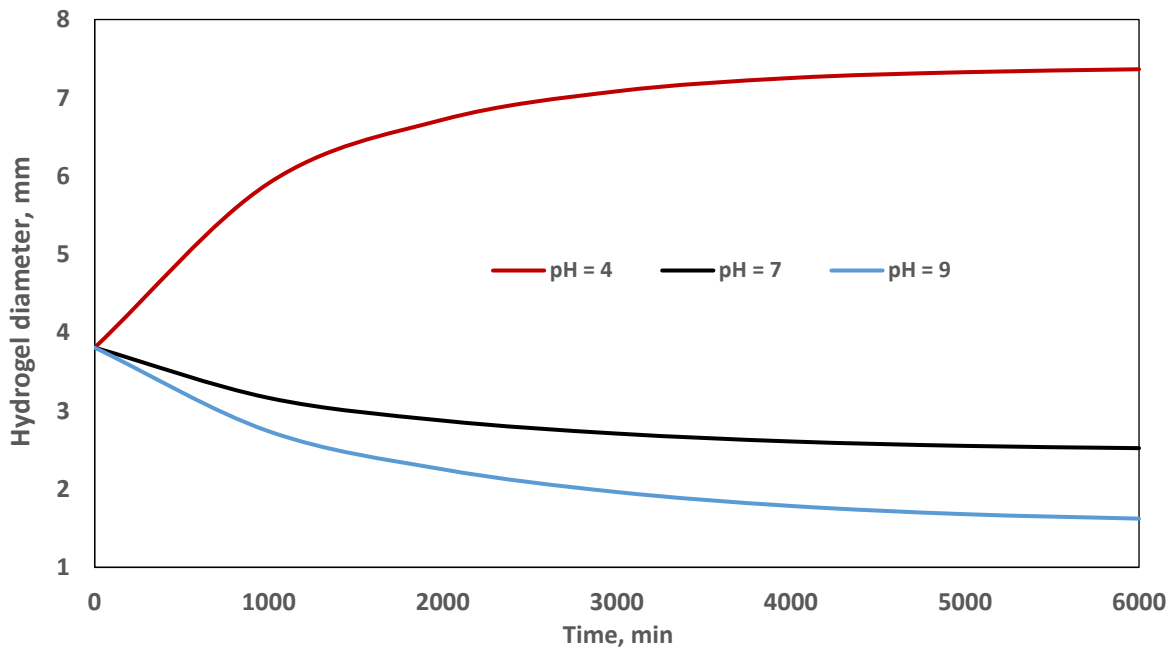

Figure 7.6: Dynamic response of chitosan-genipin hydrogel as a function of pH of the surrounding medium

Depending on the application, genipin crosslinked chitosan hydrogels can be tailored to swell or shrink significantly in response to pH variation in the surrounding medium. The swelling ability of the hydrogel decreased considerably at lower acidity. This can be attributed to the cationic nature of the crosslinked hydrogel. At a low pH, the polymer chains ionize to accommodate the diffusion of moisture-bearing-ions in the surrounding medium through the osmotic effect.

7.2.4 *Effect of varying crosslinker concentration on dynamic swelling*

The effects of varying genipin concentration on the equilibrium swell ratio of the hydrogel was studied in Section 6.3. For dynamic swelling/deswelling study, the values of the equilibrium swelling ratios taken from Section 6.3 for different concentrations of genipin (0.1, 0.3, 0.5, and 0.7 % w/v) at constant chitosan concentration (as shown on Figure 6.5) were used to simulate the dynamic model for surrounding medium of pH 6.

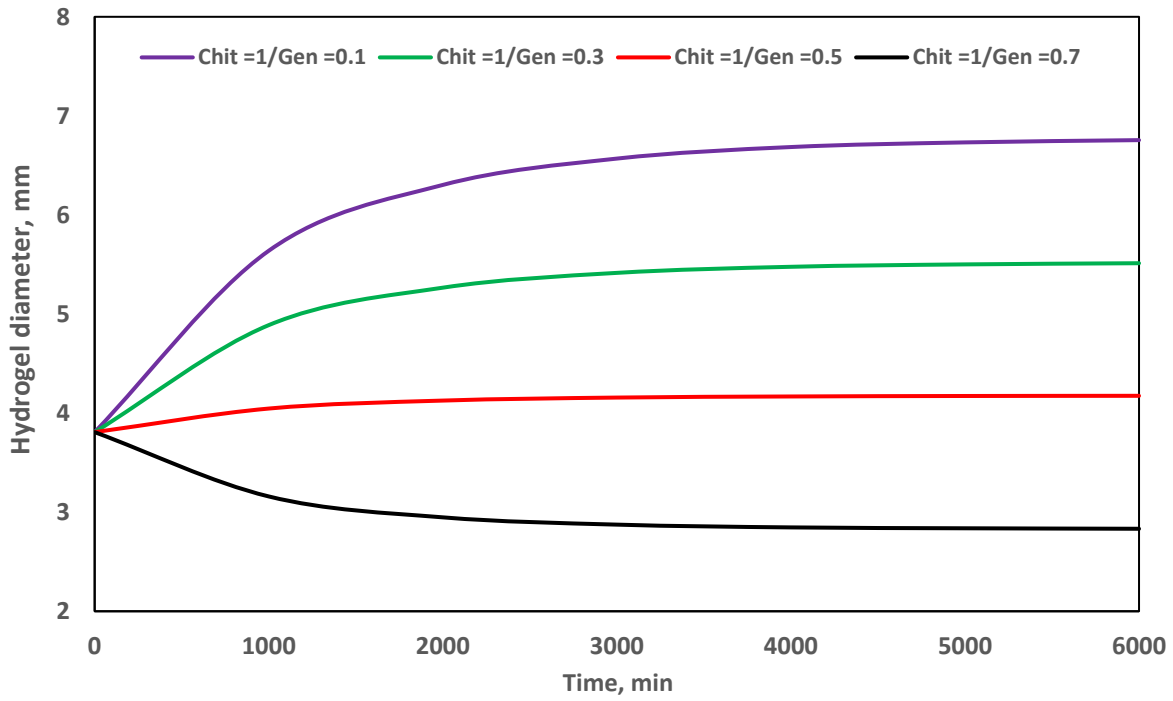

Figure 7.7: Dynamic swelling/shrinking of the hydrogel as a function of genipin concentration at pH 6

Figure 7.7 shows that the swelling capacity of the hydrogel decreased with increasing concentration of the crosslinking reagent. The swelling response is fastest for the hydrogel with the lowest crosslink density. This is attributed to the mechanical strength of the hydrogel being higher at high crosslink density, making the hydrogel's response to swelling lowest at the highest crosslink density.

7.3 Swelling Kinetics of Chitosan Genipin Hydrogels

To describe the swelling kinetics of the cationic hydrogel under study (genipin crosslinked chitosan hydrogels), using the model developed for dynamic swelling study, a gel size 3.808mm and composition (0.9 ml of 1.5 % w/v chitosan and 0.1 ml of 0.5 % w/v genipin) was simulated. The simulation results were compared with experimental data for same gel size and composition as shown in Table 7.1 (worst-case percent relative error in the model prediction is 3.75%). Further, having validated the model's performance in Figure 7.8, by plotting the actual versus predicted values ($R^2 = 0.9919$), the swelling kinetics was determined using the Schott second order model.

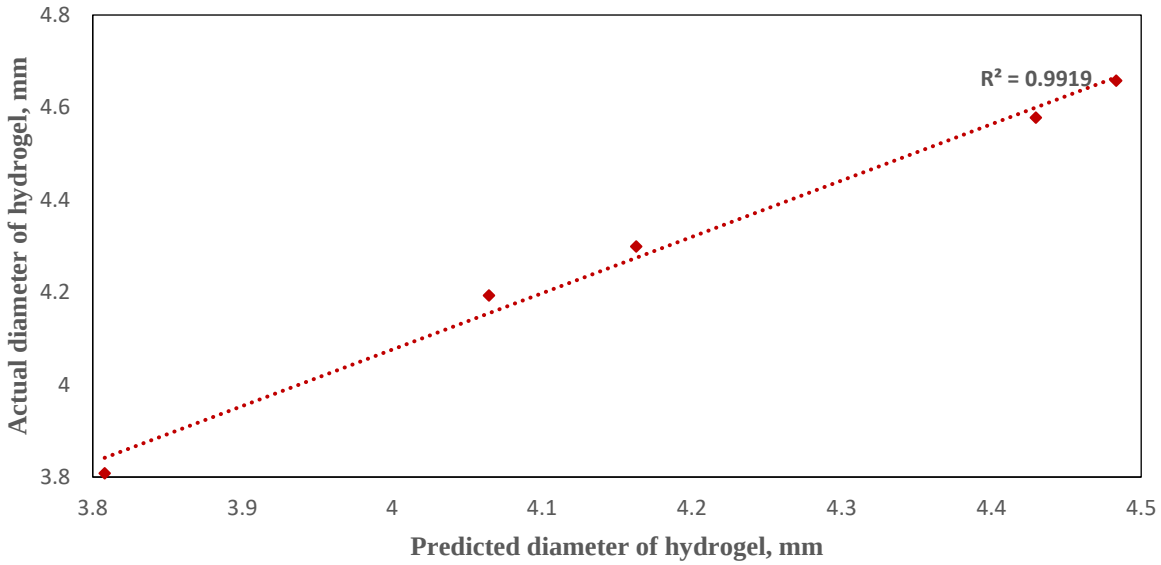

Figure 7.8: Plot of actual vs predicted diameter for dynamic swelling of genipin crosslinked chitosan hydrogel for swelling in pH 2

Table 7.1: Error estimation in dynamic model prediction (swelling)

Time, min	d_{pred} (mm)	d_{actual} (mm)	error (%)
0	3.808	3.808	0
180	4.0646	4.193	3.0618
360	4.1629	4.299	3.1655
1440	4.4297	4.578	3.2398
2880	4.4833	4.658	3.7502

Applying the simulation swelling data to Schott [160] second order kinetic model, Eqn. (2.19), gives a linear relation between the inverse of swelling rate (t/M_t) and the swelling time as shown in Figure 7.9. The results demonstrates that the swelling of genipin crosslinked chitosan hydrogels in buffer solution of pH 2 follows Schott's theoretical model with kinetic rate constant of swelling (described in Section 2.6.2), $k_r = 0.349$, calculated using Eqn. (2.19).

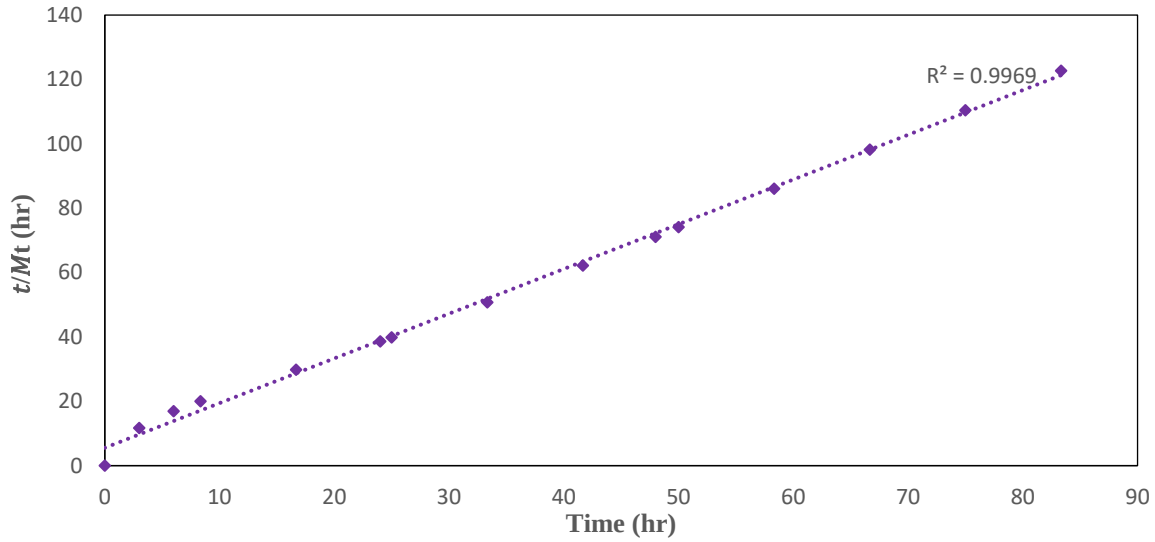

Figure 7.9: Reciprocal of rates of swelling as a function of the swelling time in a medium of pH 2

For different initial size of the hydrogel, Figure 7.10 shows the variation of the inverse swelling rates as function of swelling time for the hydrogel (whose composition was earlier defined) swelling in a medium of pH 2. From Eqn. (2.19) the swelling behaviour of the hydrogels depends on two constants A and B, the initial swelling rate, and the equilibrium swell size, respectively. These constants control the entire swelling process.

Figure 7.10 demonstrates how well the Schott's model agrees with the model developed in this study for describing the swelling kinetics of genipin crosslinked chitosan hydrogels. The high R^2 value indicates that the swelling process described by the developed model is of second order kinetics. The dotted trendlines (lines of best fits for the data sets) on Figure 7.10 are added to aid visualization, they do not represent actual data points.

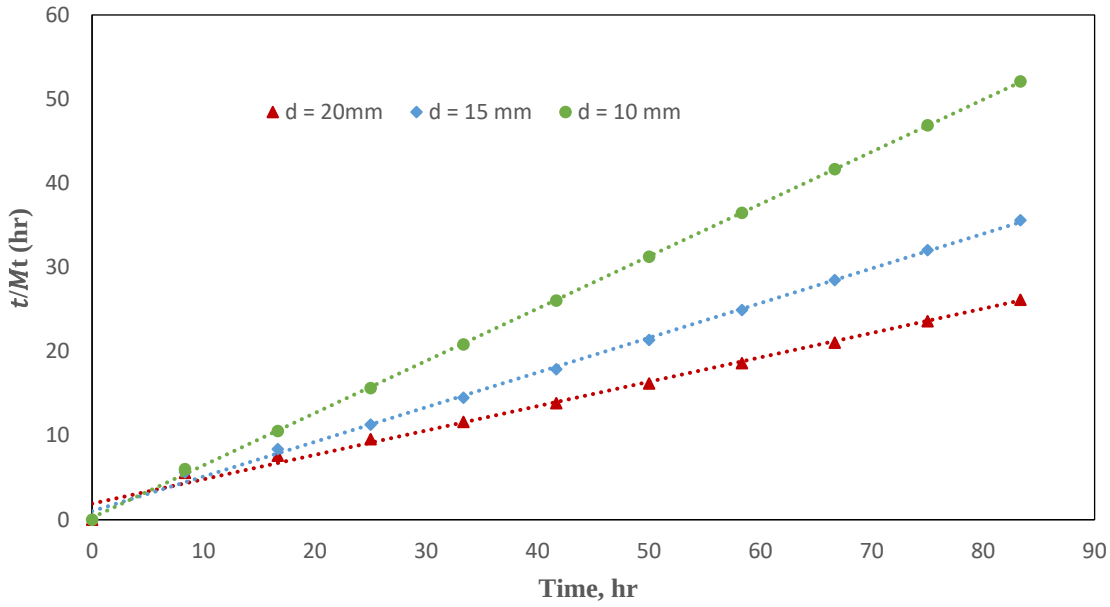

Figure 7.10: Inverse of rates of swelling as a function of the swelling time for swelling in a medium of pH 2, for different initial gel size.

Furthermore, kinetic rate constant of swelling (described in Section 2.6.2), k_r for the different gel sizes are 0.04415, 0.1697, 1.5898 for the 20 mm, 15 mm, and 10 mm, hydrogels respectively. Hence, the smaller the hydrogel the faster the swelling response, a concept employed for nanoparticle drug delivery of pharmaceuticals.

7.4 Take Away

The primary goal of this study was to model and simulate the swelling−shrinking dynamics of cationic (genipin-crosslinked chitosan) hydrogels. Due to numerical issues mentioned in Section 7.1, an alternative approach that combines the strength of the thermodynamic model (developed in Section 3.2) with the chemo-mechanical model (developed in Section 3.3) to model the time-dependent swelling/deswelling behaviour of the cationic (genipin crosslinked chitosan) hydrogels was employed. This theoretical framework uses the initial and final/equilibrium states of the swollen or shrunk hydrogel to determine the pH-induced deformation coefficient (α_{12}), Eq. (3.84), which in turn is used to determine the time-dependent states/volumes of the hydrogel between the initial and final volumes, Eq. (3.109).

With the framework developed in this study for numerical simulation of the volume variation behaviour of pH responsive cationic hydrogels (though can be adapted to simulate the swelling behaviour of pH-sensitive anionic hydrogels) a software can be developed using the algorithm

depicted in Figure 7.11. The algorithm combines both the thermodynamic and chemo-mechanical models on same platform for automation of the prediction of volume variation behaviour of crosslinked hydrogels.

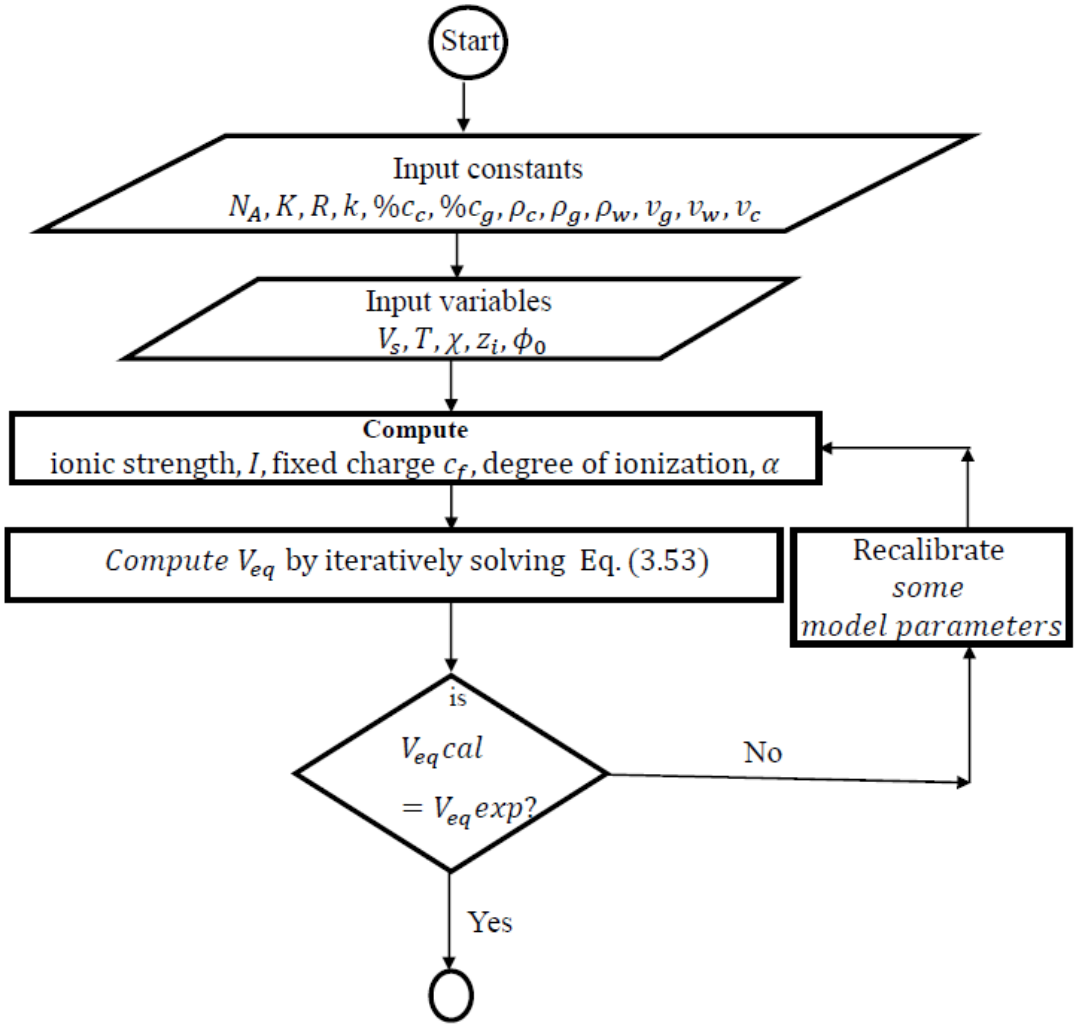

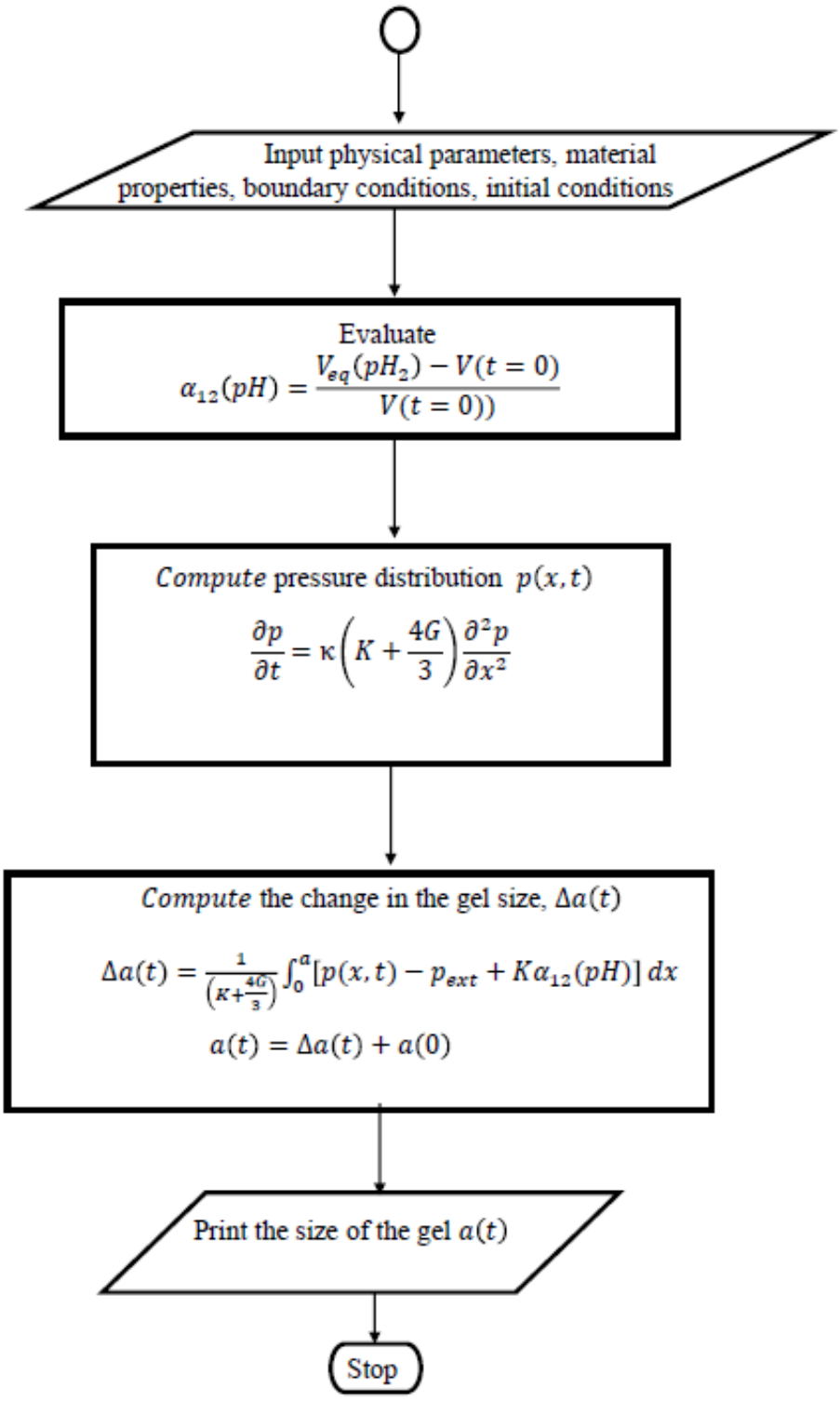

Figure 7. 11: Algorithm for developing a software that automatically predicts the dynamic volume variation of pH-sensitive hydrogels.

In general, the thermo-chemo-mechanical model gives a fundamental knowledge of what is happening within the hydrogel (something that could be missed or overlooked during experimentation) such as:

i. different bathing media of the same pH value yielding different degrees of hydrogel swelling.
ii. the initial concentration of the fixed charge group at the backbone of hydrogel impacts on the swelling of the gel.
iii. the initial polymer volume fraction of hydrogel impacting its swelling dynamics.
iv. the concentration of ions varying radially, something that may impact on drug delivery through the gel.
v. confirming that the initial size of hydrogel affects the swelling kinetics of the gel.

CHAPTER EIGHT

RESULTS AND DISCUSSION

Optimum Equilibrium Swelling of Genipin Crosslinked Chitosan Hydrogel

As discussed in Section 2.4, the swelling extent of chitosan-based hydrogels depends on some key parameters such as the pH of the environment, density of the crosslinking reagent, ionic strength of the surrounding medium, etc. To determine the conditions of parameters for optimum equilibrium swell volume of genipin crosslinked chitosan hydrogel, these parameters were carefully selected as described in Section 3.4.

The model developed in Section 3.2 for equilibrium swelling of genipin crosslinked chitosan hydrogel was simulated for various operating conditions of the above-mentioned parameters. Using the simulation data, central composite design-based optimization models were developed as described in Section 3.4 and the results are analysed, discussed, and validated in this chapter.

8.1 Estimation of Model Capabilities

For swelling or shrinking (of the crosslinked hydrogel) in a surrounding fluid that contains compounds such as NaCl, $NaHCO_3$, KCl, $K_2HPO_4.3H_2O$, $MgCl_2.6H_2O$, HCl, $CaCl_2$, and Na_2SO_4 that constitute a simulated body fluid [217], a regression model was developed following the steps outlined in Section 3.4. The parametric model (quadratic) developed for predicting equilibrium volume swell ratio, V_{SR}, is:

$$\frac{1}{\sqrt{V_{SR}}} = -18.41435 + 0.17587\%c_g - 1.57033\chi - 1.05722 \times 10^{-3} I + 5.23779pH - 0.26710\%c_g pH + 0.043395\chi pH - 4.77669 \times 10^{-5} IpH + 2.72860\%{c_g}^2 + 1.96805\chi^2 + 1.23321 \times 10^{-6} I^2 - 0.32601pH^2 \quad (8.1)$$

Eqn. (8.1) shows that pH is the most sensitive factor, and the three response surfaces (in terms of untransformed variables) that can be constructed from this model are as shown in Figs 8.1, 8.2, and 8.3.

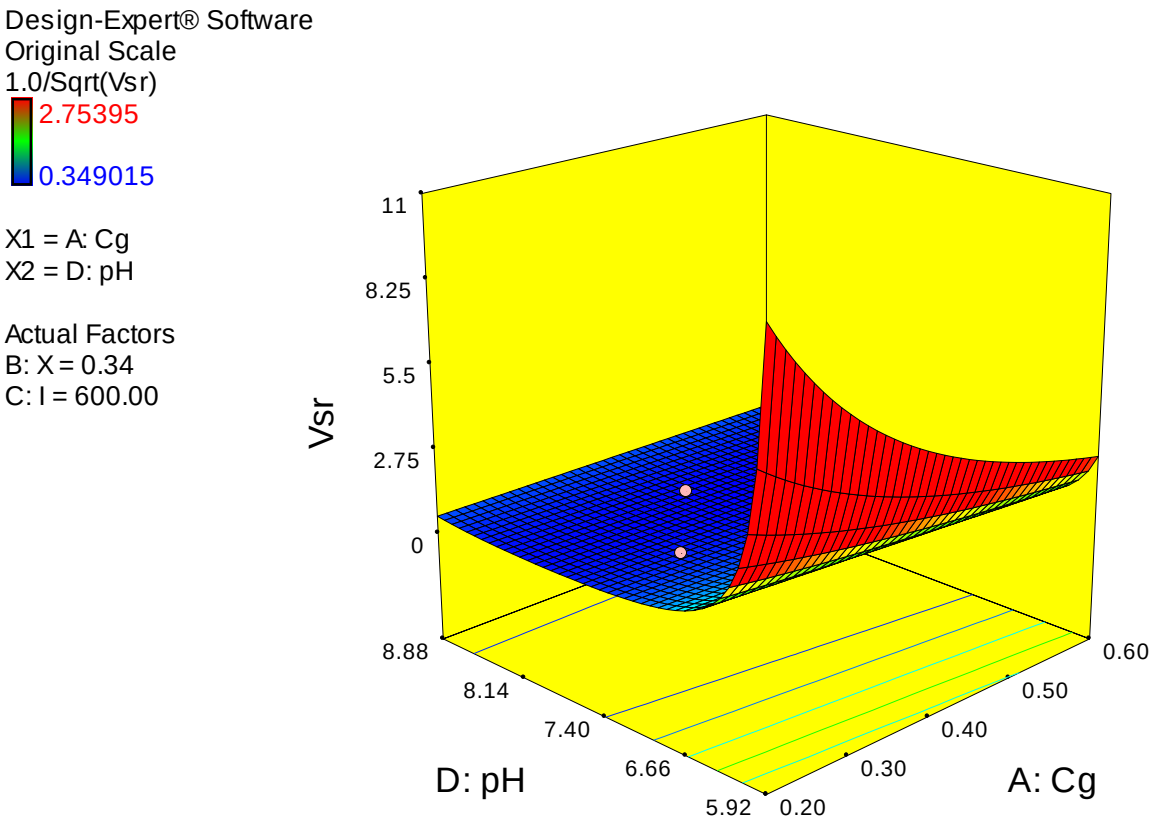

Figure 8.1: Response surface showing the influence of the pH and genipin concentration on the equilibrium swelling ratio.

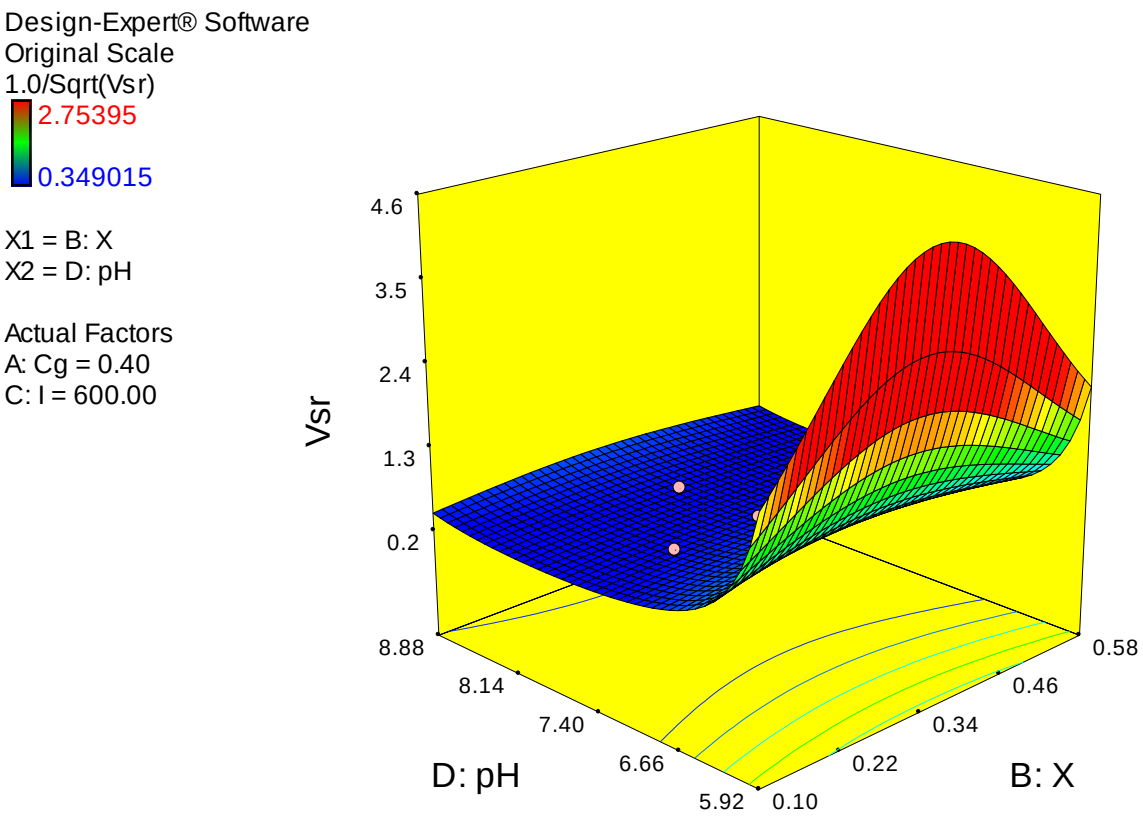

Figure 8.2: Response surface showing the influence of the pH and solvent interaction parameter on the equilibrium swelling ratio.

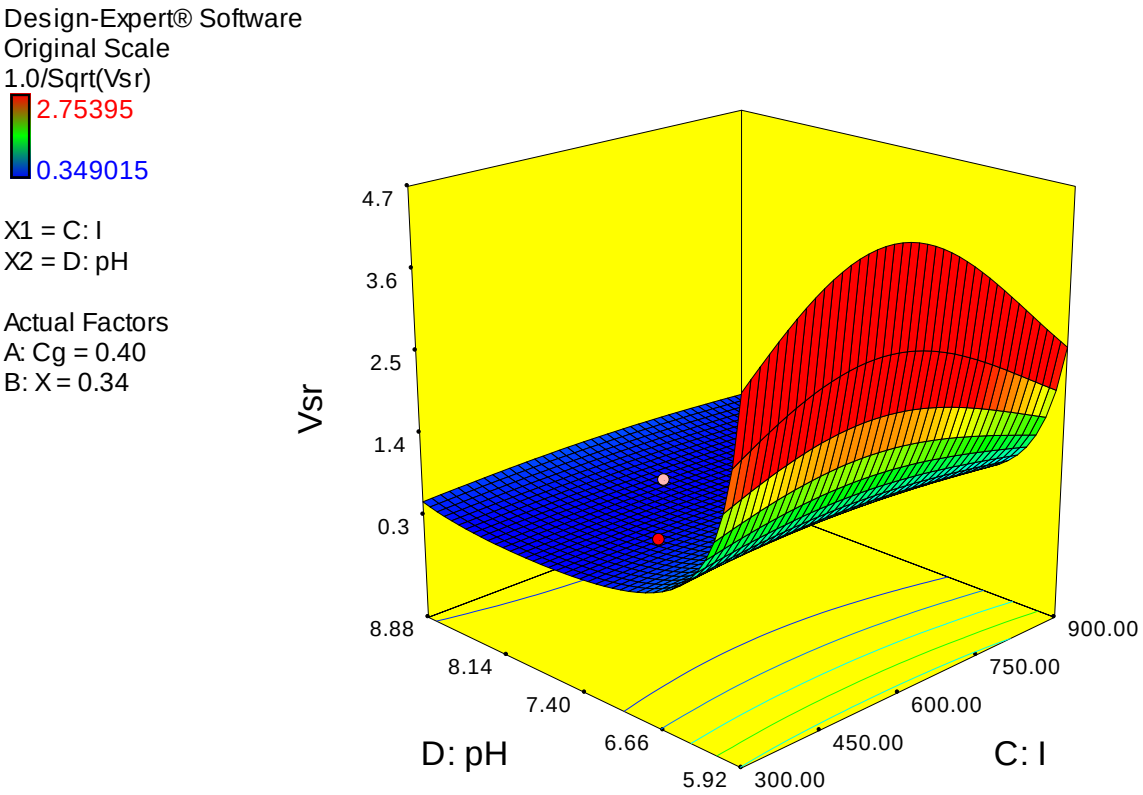

Figure 8.3: Response surface showing the influence of the pH and ionic strength of the swelling medium on the equilibrium swelling ratio

From the parametric model, the corresponding contours for the response surfaces are shown in Figs 8.4, 8.5, and 8.6.

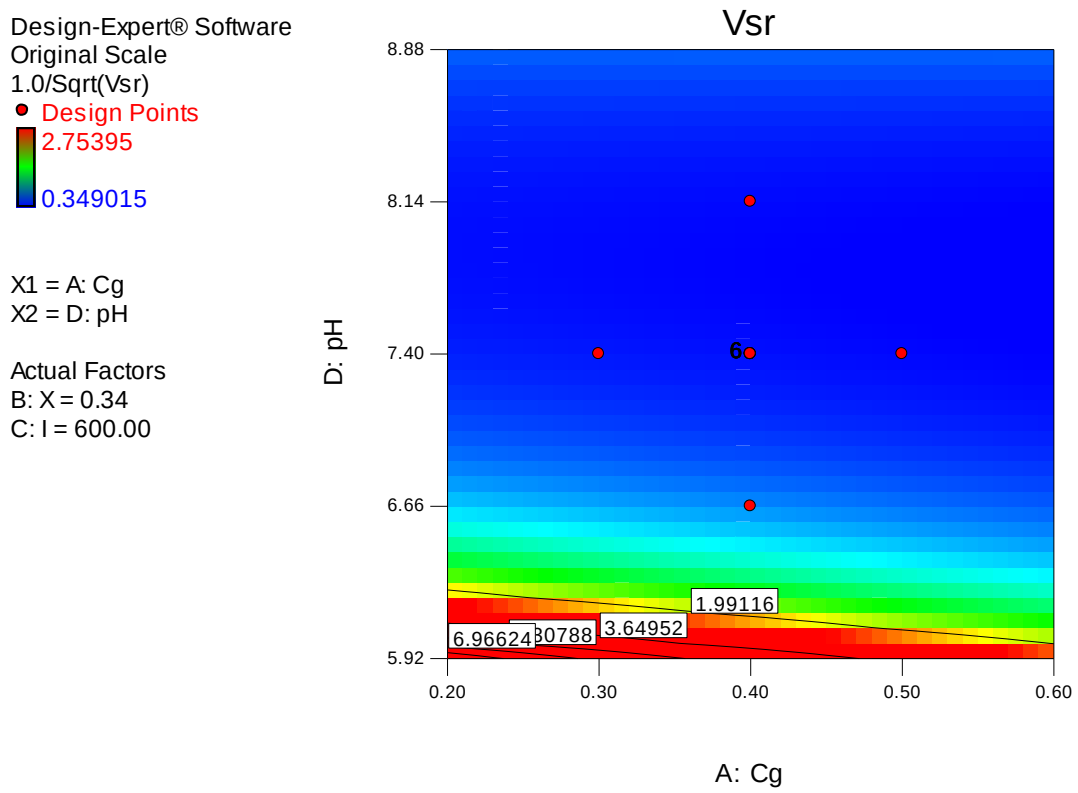

Figure 8.4: Contour representation of the influence of the pH and genipin concentration on the equilibrium swelling ratio.

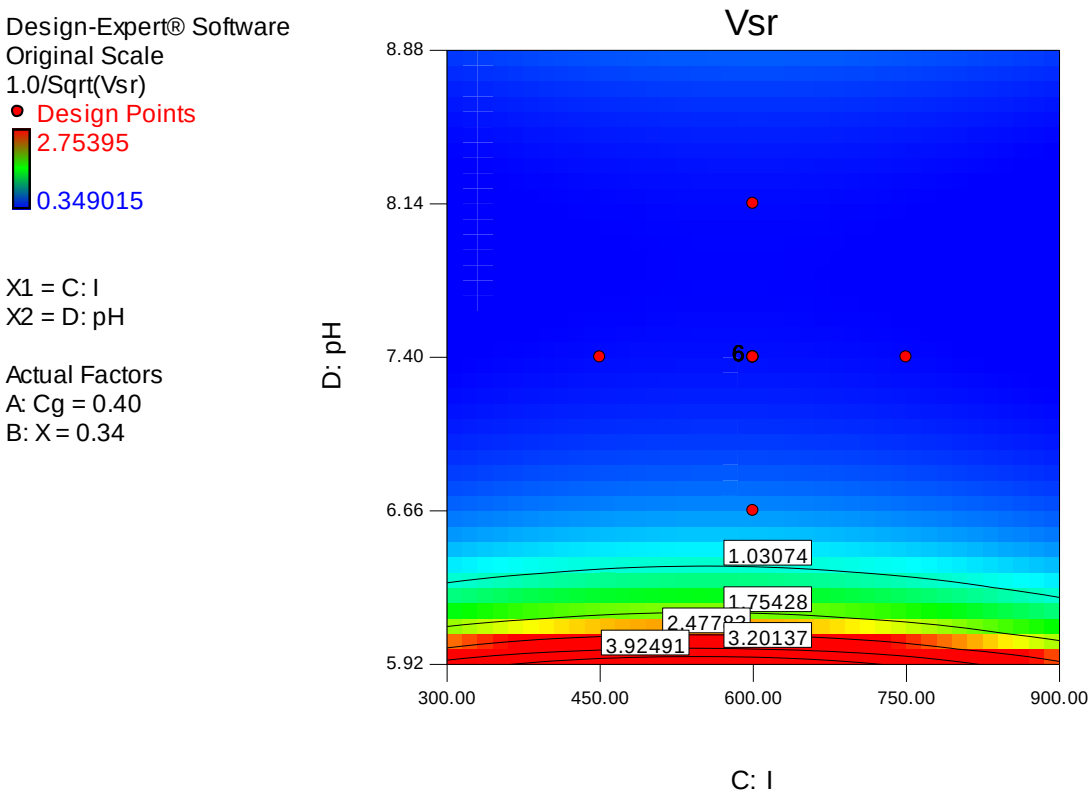

Figure 8.5: Contour representation of the influence of the pH and ionic strength on the equilibrium swelling ratio.

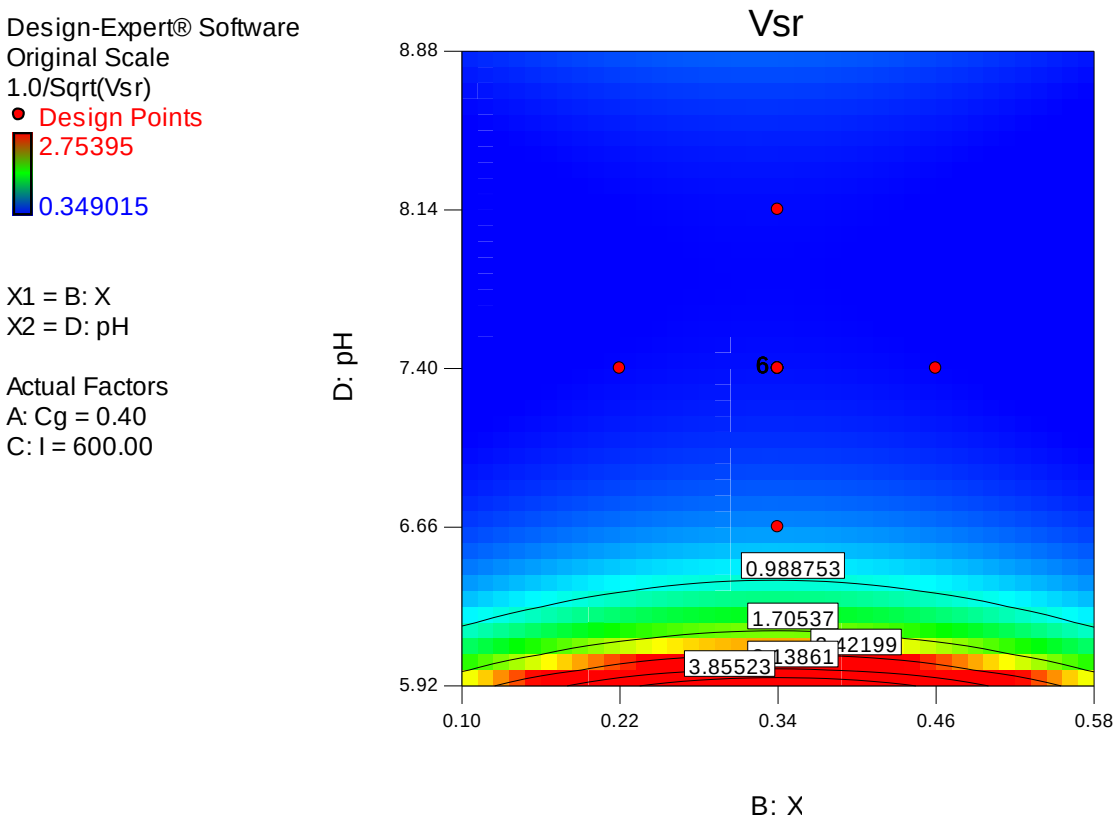

Figure 8.6: Contour representation of the influence of the pH and solvent interaction parameter on the equilibrium swelling ratio.

Figures 8.1- 8.2 show the estimation capabilities of the developed model with respect to the data sets used to build the optimization model. Table 8.1 shows the model statistics and worst-case absolute and relative error estimation.

Table 8.1: Model statistics in terms of trained data

Statistics	**Value**
R^2	0.9987
R^2_{Adj}	0.9979
R^2_{Pred}	0.9962
Adeq. Precision	96.681
PRESS	0.017
Absolute error (worst-case)	0.0902
Relative error (worst-case)	5.54%

With F-value = 1228.27, and *p* values (of "Prob > F") less than 0.0001 show that the model terms in Eq. (8.1) are significant. The predicted versus actual plot, Fig 8.7, showing how well the optimization model Eqn. (8.1), in its untransformed variable state explains variation in the trained dataset. The normal probability plot, which shows the normality of residuals is shown in Fig. 8.8.

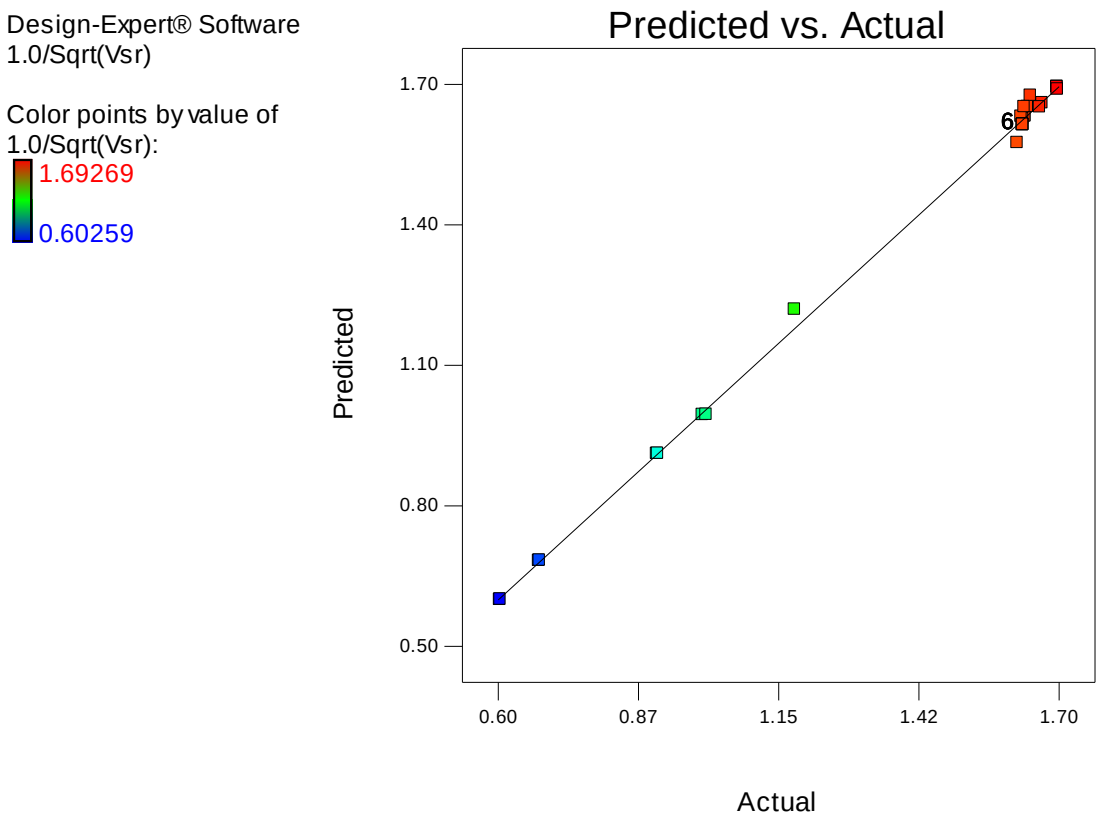

Figure 8.7: Predicted vs Actual for the training dataset.

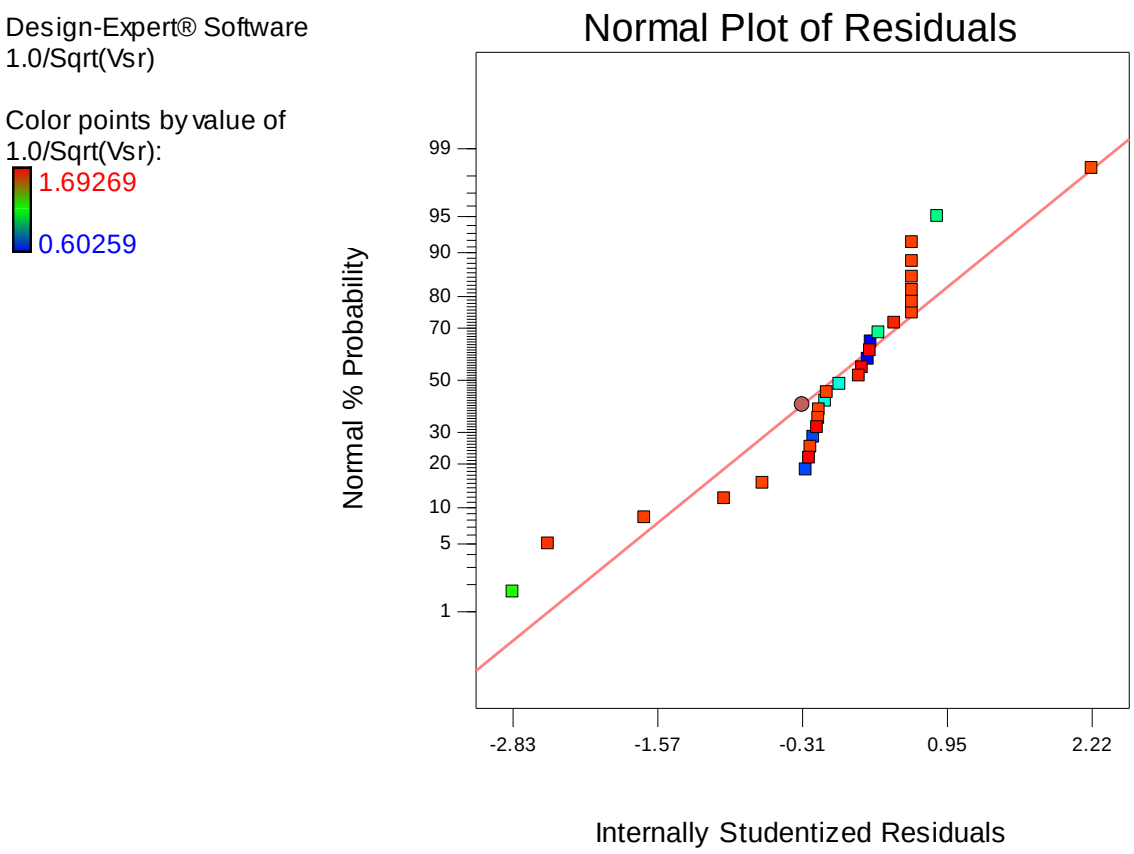

Figure 8.8: Normal probability plot of the studentized residuals

8.2 Optimum Equilibrium Swell Ratio

Based on the operating conditions (Section 3.4.1) used to develop the optimization model, Eqn. (8.1), the optimum conditions for swelling of genipin crosslinked chitosan hydrogel is shown on the response plots (Figs 8.1 – 8.3). The surrounding fluid is a medium whose pH is allowed to vary slightly from the pH of normal body tissue or simulated body fluid.

The surface plots with their corresponding contour plots show that as the pH of the surrounding medium drops below the pH of simulated body fluid, the equilibrium swell ratio of the hydrogel approaches a maximum value at low concentration of the crosslinking agent. The optimum condition for equilibrium swelling ratio of the hydrogel for a specific case (for example, during drug delivery to tumorous site) is estimated to fall in the region: $pH = 5.92, \%c_g = 0.2$ wt%, $I = 600$mM, $\chi = 0.34$. The implication of this is that the optimization model, on proper calibration with laboratory data (and well-defined range of operating conditions), has the potential to be used for studies involving targeted drug delivery. For example, at tumour

sites, where the pH is below that of healthy or normal body tissue, the parameters of the model can be tuned to stimulate enhanced swelling of the hydrogel for optimum release of the encapsulated drugs.

8.3 Performance Evaluation of The Model

The model's estimation capabilities or robustness were evaluated with respect to untrained datasets obtained from simulation (with 2-factor design interpolation data and extrapolation data) as described in Section 3.6.2.

8.3.1 Interpolation Test

The behaviour of the regression model to untrained datasets within the range of original operating conditions is demonstrated in Figure 8.9.

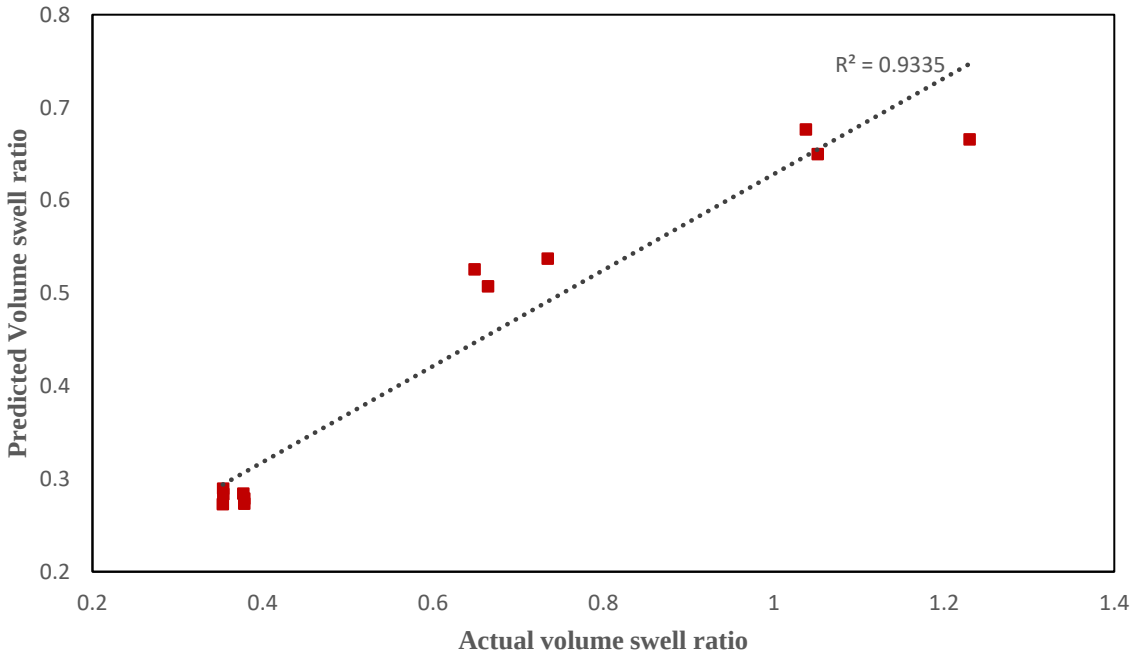

Figure 8.9: Interpolation test on regression model: Actual and predicted equilibrium volume swell ratio.

The interpolation capability of the optimization model, Eqn. (8.1) was tested by evaluating its predictive capacity using a set of simulated data (described in Section 3.6.2) different from those used to develop the model. It is obvious from Fig. 8.9 that the model's predictions are good in response to operating conditions different from, but within the range of the original operating conditions used to build the model. Thus, the model is both accurate and generally

adequate for the purpose of predicting equilibrium swelling ratio, and for estimating optimum conditions of equilibrium swelling of the crosslinked hydrogel.

8.3.2 Extrapolation Test

The extrapolation capability of the regression model was tested by evaluating its predictive ability using a set of simulated data (described in Section 3.6.2) outside the range of datasets used to develop the model. It is evident from Fig. 8.10 that, as the operating conditions of the swelling/deswelling process drift 5% outside the original conditions used to build the regression model, that the model prediction capabilities drop.

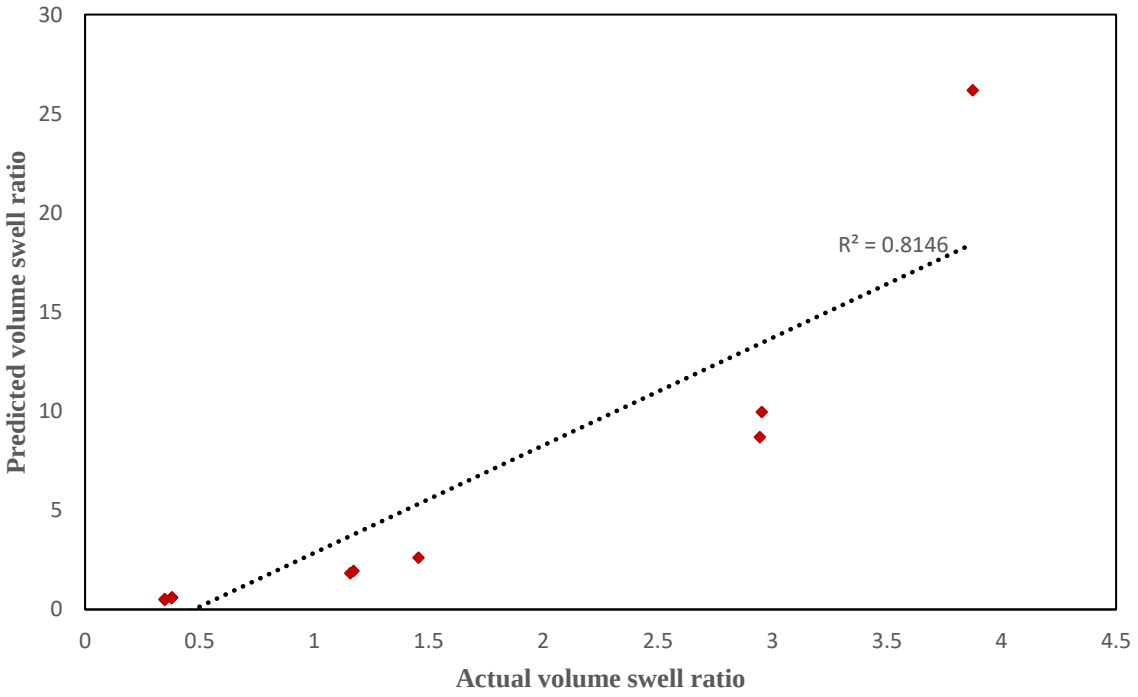

Figure 8.10: Extrapolation test on regression model: Actual and predicted equilibrium volume swell ratio.

The high sensitivity of the model's response is explained by the erratic behaviour demonstrated by the model in estimating the equilibrium swell ratio outside the range of original operating conditions. Therefore, the model is inaccurate to handle $\geq 5\%$ deviation from the original operating conditions used to build the optimization model, generally inadequate for estimating equilibrium swell ratio outside the original operating conditions.

8.4 Limitations

Although the mathematical framework presented in this chapter can be improved further, the mathematical ideology behind it can potentially be applied to predict and optimize drug release from crosslinked hydrogels. The limitation to its use is hugely dependent on the robustness of the numerical model from which the optimization model was developed. For example, the optimization model analysed and discussed here was built from the thermodynamic model (discussed in Chapter 6) whose limitations have already been discussed in Section 6.6.

CHAPTER NINE

CONCLUSION AND FUTHER WORK

9.1 Synopsis

The swelling property of pH responsive hydrogels is controlled by the chemical, electrical, and mechanical fields interaction. To describe the conformational change dynamics of genipin crosslinked chitosan hydrogels, a mathematical or numerical model that captures these interacting fields is required. Poisson Nernst Planck and mechanical equations have proven to be a suitable mathematical model(s) and have been adapted to anionic hydrogels and solved numerically under steady state conditions for equilibrium swelling studies [15, 40, 41, 171, 218].

In Section 3.1 a methodology that employs Poisson Nernst Planck and mechanical equations to model the equilibrium swelling behaviour of anionic hydrogels was described. In Chapter 4, the performance of the numerical model developed for equilibrium swelling of pH-sensitive anionic (PHEMA) hydrogels was evaluated. Steady-state simulations were conducted on a two-dimensional axisymmetric domain (representing a cylindrical-shape hydrogel constrained at the top and bottom using rollers) and the results were compared with experimental data obtained from the work of Beebe *et al.* [213]. The justification for the comparison is based on the method employed to synthesize the PHEMA hydrogel. The gel was synthesised in a microchannel covered at the top and bottom with two pieces of glasses to constrain axial displacement. The closeness between the simulation (model) results and the experimental data (refer to Figure 4.1) shows that the model has the potential to offer predictions for equilibrium swelling of anionic (PHEMA) hydrogels, and that the simulation platform could be adapted to model the volume variation behaviour of pH responsive cationic hydrogels. Moreover, the simulation/model platform can be deployed to model and simulate the responsive behaviour of other anionic hydrogels. In terms of application, the model can be deployed in pH sensing devices for monitoring and control purposes, and for design of drug delivery devices where the biomaterial (hydrogel) is expected to swell in alkaline medium.

Moving from anionic to cationic hydrogels, the same model platform developed for anionic hydrogels was adapted (by altering the equation for fixed charge concentration) to cationic hydrogels. The results of the steady state simulations are presented in Chapter 5. However, obtaining a dynamic simulation was difficult owing to numerical issues such as stability and

stiffness of the model equations. Although steady state solutions were obtained, each time the pH of the surrounding medium changed from acidic to alkaline, it was required to manually change the boundary conditions especially during deformation due to shrinking of the hydrogel. To circumvent these challenges, a new approach that utilizes the initial and final equilibrium states of the crosslinked hydrogel to predict the time-dependent volume variation of the hydrogel between both states was adopted.

Finally, to determine the optimum conditions for equilibrium swelling of genipin crosslinked chitosan hydrogel, statistical optimization was employed to develop a Response Surface Design model. The methodology is described in Section 3.4 and the results for a case where the hydrogel is submerged in a simulated body fluid are presented in Chapter 8.

9.2 Conclusions

The main highlight of this study is the utilization of a novel modelling strategy as an alternative to the traditional modelling approach (i.e., coupling PNP with mechanical equation) for predicting the volume variation behaviour of smart hydrogels. Although the traditional approach suits anionic hydrogels well, there are accompanying challenges during implementation with cationic hydrogels owing to the strong reversible swelling behaviour of cationic hydrogels. The alternative approach provided in this study, which combines thermodynamic model with chemo-mechanical model, contributes to knowledge in the field of hydrogel modelling, as it helps to overcome the computational difficulties associated with applying the traditional approach used for modelling anionic hydrogels. A challenge that has restricted studies involving cationic hydrogels to mainly experimentation.

The thermodynamic-based model developed using Statistical Mechanics approach described in Section 3.2, estimates the equilibrium swell ratio of cationic (genipin crosslinked chitosan) hydrogels. With the value of the equilibrium swell ratio, the chemo-mechanical model (derived in Section 3.3) then predicts the dynamic volume variation of cationic (genipin crosslinked chitosan) hydrogels. One advantage of the numerical model is that it allows for the concentration of the crosslinking reagent (a very important parameter that controls the mechanical property and swelling capability of the crosslinked hydrogel) to be tuned during

dynamic studies to predict the effect of concentration variation on the volume variation behaviour of pH responsive cationic hydrogels.

The simulation results (for equilibrium swelling) presented in Chapter 6 were compared with literature and laboratory data, and the model showed good agreement ($R^2 = 0.9542$ and worst-case percent relative error $= 0.56$ for hydrogels with low genipin crosslinked ratio). Therefore, the closeness between model predictions and experimental values does not only show that the model has the potential to be deployed for equilibrium studies involving cationic (genipin crosslinked chitosan) hydrogels, but it also shows that the approach employed in this study is an improvement on the original work of Jahren *et al.* [135].

Furthermore, dynamic simulation results presented in Chapter 7 were validated using experimental data for time-dependent studies involving genipin crosslinked chitosan hydrogel. The closeness between model predictions and experimental results confirms qualitatively, the potential of the model for predicting the dynamic volume variation of pH responsive cationic (genipin crosslinked chitosan) hydrogels. Therefore, by incorporating pharmaceutical compounds, or combining cationic hydrogels with DNA through conjugation (to release the DNA) or varying the concentration of the crosslinking reagent to create scaffolds of new tissues, the model can be adapted to simulate applications such as targeted drug delivery, gene delivery, and tissue engineering respectively.

Moreover, the swelling kinetic studies performed in Section 7.3 revealed that the swelling of genipin crosslinked chitosan hydrogel (in a medium of pH 2) followed the Schott [160] second order kinetic model with kinetic rate constant of swelling, $k_r = 0.349$, and $R^2 = 0.9969$. In applications, this model can be deployed to predict the time-dependent volume variation behaviour of other cationic hydrogels. In addition, the model can be employed in the design of swelling-controlled drug release systems and chemical sensors where the hydrogel is expected to swell in acidic pH and shrink in alkaline pH of the surrounding.

For hydrogel submerged in a simulated body fluid, the optimum condition for equilibrium swell ratio of the hydrogel for a specific case (e.g., during drug delivery to tumorous site) is estimated to fall in the region: $pH = 5.92, \%c_g = 0.2$ wt%$, I = 600$mM$, \chi = 0.34$. The implication of this is that the optimization model, on proper calibration with laboratory data (and well-defined range of operating conditions), has the potential to be used for studies involving targeted drug

delivery. Hence, it is concluded that the model can be used to evaluate the influence of a range of parameters which can be tuned to stimulate enhanced swelling of the cationic, genipin crosslinked chitosan hydrogel for optimum release of any encapsulated therapeutics.

9.3 Further Work

This study provides a theoretical framework for predicting the conformational change dynamics of cationic hydrogels; a case study of genipin crosslinked chitosan hydrogels. Though the approach employed in this study is new and has been evaluated satisfactory via simulation, it is recommended for further study that the model be calibrated further with laboratory data to improve its performance.

In addition, to measure the dynamics of volume variation in more than one direction, it is recommended that the model be extended to predict volume variation behaviour in more than one direction (i.e., for 2D or 3D models) to handle more complicated scenarios. Further, a software could be developed that can handle simulations involving the thermodynamics and chemo-mechanical models together on one platform, using the algorithm in Figure 7.11.

Furthermore, the model developed in this study could be adapted to model the volume variation behaviour of other cationic hydrogels and be further deployed to model pH-sensitive swelling-controlled drug delivery devices by including the drug molecule among the non-ionic diffusing species.

REFERENCES

[1] S. Rowlands and S. Searle, “Contraceptive implants: current perspectives,” *Open Access J Contracept*, no. September 2014, p. 73, 2014, doi: 10.2147/oajc.s55968.

[2] M. Ashtikar, K. Nagarsekar, and A. Fahr, “Transdermal delivery from liposomal formulations – Evolution of the technology over the last three decades,” *Journal of Controlled Release*, vol. 242, pp. 126–140, 2016, doi: 10.1016/j.jconrel.2016.09.008.

[3] Y. N. Kalia and R. H. Guy, “Modeling transdermal drug release,” *Adv Drug Deliv Rev*, vol. 48, no. 2–3, pp. 159–172, 2001, doi: 10.1016/S0169-409X(01)00113-2.

[4] A. Z. Wilczewska, K. Niemirowicz, K. H. Markiewicz, and H. Car, “Nanoparticles as drug delivery systems.,” *Pharmacol Rep*, vol. 64, no. 5, pp. 1020–1037, 2012, doi: 10.1016/s1734-1140(12)70901-5.

[5] K. E. Uhrich, S. M. Cannizzaro, R. S. Langer, and K. M. Shakesheff, “Polymeric Systems for Controlled Drug Release,” *Chem Rev*, vol. 99, no. 11, pp. 3181–3198, 1999, doi: 10.1021/cr940351u.

[6] D. Bhowmik, H. Gopinath, B. P. Kumar, S. Duraivel, and K. P. S. Kumar, “Controlled Release Drug Delivery Systems,” *The Pharma Journal*, vol. 1, no. 10, pp. 24–32, 2012.

[7] N. Kamaly, B. Yameen, J. Wu, and O. C. Farokhzad, “Degradable Controlled-Release Polymers and Polymeric Nanoparticles: Mechanisms of Controlling Drug Release.,” *Chem Rev*, vol. 116, no. 4, pp. 2602–2663, Feb. 2016, doi: 10.1021/acs.chemrev.5b00346.

[8] J. Li and D. J. Mooney, “Designing hydrogels for controlled drug delivery,” *Nat Rev Mater*, vol. 1, no. 12, Oct. 2016, doi: 10.1038/NATREVMATS.2016.71.

[9] T. R. Hoare and D. S. Kohane, “Hydrogels in drug delivery: Progress and challenges,” *Polymer (Guildf)*, vol. 49, no. 8, pp. 1993–2007, 2008, doi: 10.1016/j.polymer.2008.01.027.

[10] B. Baroli, “Hydrogels for Tissue Engineering and Delivery of Tissue-Inducing Substances,” *J Pharm Sci*, vol. 96, no. 9, pp. 2197–2223, 2007, doi: https://doi.org/10.1002/jps.20873.

[11] C. He, S. W. Kim, and D. S. Lee, “In situ gelling stimuli-sensitive block copolymer hydrogels for drug delivery,” *Journal of Controlled Release*, vol. 127, no. 3, pp. 189–207, 2008, doi: 10.1016/j.jconrel.2008.01.005.

[12] Y. Qiu and K. Park, “Environment-sensitive hydrogels for drug delivery,” *Adv Drug Deliv Rev*, vol. 64, no. SUPPL., pp. 49–60, 2012, doi: 10.1016/j.addr.2012.09.024.

[13] F. Ganji, M. J. Abdekhodaie, and A. Ramazani, “Gelation time and degradation rate of chitosan-based injectable hydrogel,” *J Solgel Sci Technol*, vol. 42, no. 1, pp. 47–53, 2007, doi: 10.1007/s10971-006-9007-1.

[14] E. M. Ahmed, “Hydrogel: Preparation, characterization, and applications: A review,” *J Adv Res*, vol. 6, no. 2, pp. 105–121, 2015, doi: 10.1016/j.jare.2013.07.006.

[15] H. Li, *Smart Hydrogel Modelling*. New York, 2010.

[16] N. Sood, A. Bhardwaj, S. Mehta, and A. Mehta, "Stimuli-responsive hydrogels in drug delivery and tissue engineering," *Drug Deliv*, vol. 23, no. 3, pp. 758–780, 2016, doi: 10.3109/10717544.2014.940091.

[17] M. Fathi, J. Barar, A. Aghanejad, and Y. Omidi, "Hydrogels for ocular drug delivery and tissue engineering.," *Bioimpacts*, vol. 5, no. 4, pp. 159–164, 2015, doi: 10.15171/bi.2015.31.

[18] N. R. Johnson and Y. Wang, "Drug delivery systems for wound healing.," *Curr Pharm Biotechnol*, vol. 16, no. 7, pp. 621–629, 2015, doi: 10.2174/1389201016666150206113720.

[19] C. Alvarez-Lorenzo and A. Concheiro, "Smart drug delivery systems: From fundamentals to the clinic," *Chemical Communications*, vol. 50, no. 58. pp. 7743–7765, 2014. doi: 10.1039/c4cc01429d.

[20] "Birth Control Implant: Advantages and Disadvantages." [Online]. Available: https://www.invitra.com/en/birth-control-implant/

[21] K. Ita, *Transdermal Drug Delivery: Concepts and Application*. Elsevier, 2020. doi: 10.1016/B978-0-12-822550-9.00013-2.

[22] J. Z. Ziyuan Li, Yanzi Zhou, Tianyue Li, "Stimuli-responsive hydrogels: Fabrication and biomedicalapplications," *View*, vol. 3, no. 2, pp. 1–26, 2021.

[23] Y. Zhang and Y. Huang, "Rational Design of Smart Hydrogels for Biomedical Applications," *Front Chem*, vol. 8, 2021, doi: 10.3389/fchem.2020.615665.

[24] S. Mantha *et al.*, "Smart Hydrogels in Tissue Engineering and Regenerative Medicine.," *Materials (Basel)*, vol. 12, no. 20, Oct. 2019, doi: 10.3390/ma12203323.

[25] M. Mahinroosta, Z. Jomeh Farsangi, A. Allahverdi, and Z. Shakoori, "Hydrogels as intelligent materials: A brief review of synthesis, properties and applications," *Mater Today Chem*, vol. 8, pp. 42–55, 2018, doi: https://doi.org/10.1016/j.mtchem.2018.02.004.

[26] S. Bhaladhare and D. Das, "Cellulose: a fascinating biopolymer for hydrogel synthesis," *J. Mater. Chem. B*, vol. 10, no. 12, pp. 1923–1945, 2022, doi: 10.1039/D1TB02848K.

[27] D. A. Gyles, L. D. Castro, J. O. C. Silva, and R. M. Ribeiro-Costa, "A review of the designs and prominent biomedical advances of natural and synthetic hydrogel formulations," *Eur Polym J*, vol. 88, pp. 373–392, 2017, doi: https://doi.org/10.1016/j.eurpolymj.2017.01.027.

[28] F. Ahmadi, Z. Oveisi, S. M. Samani, and Z. Amoozgar, "Chitosan based hydrogels: characteristics and pharmaceutical applications.," *Res Pharm Sci*, vol. 10, no. 1, pp. 1–16, 2015.

[29] D. I. Sánchez-Machado, J. López-Cervantes, Ma. A. Correa-Murrieta, R. G. Sánchez-Duarte, P. Cruz-Flores, and G. S. de la Mora-López, "Chapter 4.2 - Chitosan," in

Nonvitamin and Nonmineral Nutritional Supplements, S. M. Nabavi and A. S. Silva, Eds., Academic Press, 2019, pp. 485–493. doi: https://doi.org/10.1016/B978-0-12-812491-8.00064-3.

[30] S. Zivanovic, R. H. Davis, and D. A. Golden, "8 - Chitosan as an antimicrobial in food products," in *Handbook of Natural Antimicrobials for Food Safety and Quality*, T. M. Taylor, Ed., in Woodhead Publishing Series in Food Science, Technology and Nutrition. Oxford: Woodhead Publishing, 2015, pp. 153–181. doi: https://doi.org/10.1016/B978-1-78242-034-7.00008-6.

[31] J. Lizardi-Mendoza, W. M. Argüelles Monal, and F. M. Goycoolea Valencia, "Chapter 1 - Chemical Characteristics and Functional Properties of Chitosan," in *Chitosan in the Preservation of Agricultural Commodities*, S. Bautista-Baños, G. Romanazzi, and A. Jiménez-Aparicio, Eds., San Diego: Academic Press, 2016, pp. 3–31. doi: https://doi.org/10.1016/B978-0-12-802735-6.00001-X.

[32] F. Shahidi, "16 - Chitin and chitosan from marine by-products," in *Maximising the Value of Marine By-Products*, F. Shahidi, Ed., in Woodhead Publishing Series in Food Science, Technology and Nutrition. Woodhead Publishing, 2007, pp. 340–373. doi: https://doi.org/10.1533/9781845692087.2.340.

[33] J. C. Buendia, "Chitin from shell waste," no. 4, 1999.

[34] J. P. Martínez, M. P. Falomir, and D. Gozalbo, "Chitin: A Structural Biopolysaccharide with Multiple Applications," *eLS*, 2014, doi: 10.1002/9780470015902.a0000694.pub3.

[35] V. P. Santos, N. S. S. Marques, P. C. S. V. Maia, M. A. B. de Lima, L. de O. Franco, and G. M. de Campos-Takaki, "Seafood waste as attractive source of chitin and chitosan production and their applications," *Int J Mol Sci*, vol. 21, no. 12, pp. 1–17, 2020, doi: 10.3390/ijms21124290.

[36] S. Dimida, C. Demitri, V. M. de Benedictis, F. Scalera, F. Gervaso, and A. Sannino, "Genipin-cross-linked chitosan-based hydrogels: Reaction kinetics and structure-related characteristics," *J Appl Polym Sci*, vol. 132, no. 28, 2015, doi: 10.1002/app.42256.

[37] M. J. Moura, M. M. Figueiredo, and M. H. Gil, "Rheology of Chitosan and Genipin Solutions," in *Advanced Materials Forum IV*, in Materials Science Forum, vol. 587. Trans Tech Publications Ltd, 2008, pp. 27–31. doi: 10.4028/www.scientific.net/MSF.587-588.27.

[38] S. Matcham and K. Novakovic, "Fluorescence imaging in genipin crosslinked chitosan-poly(vinyl pyrrolidone) hydrogels," *Polymers (Basel)*, vol. 8, no. 11, pp. 1–10, 2016, doi: 10.3390/polym8110385.

[39] R. A. A. Muzzarelli, "Genipin-crosslinked chitosan hydrogels as biomedical and pharmaceutical aids," *Carbohydr Polym*, vol. 77, no. 1, pp. 1–9, 2009, doi: https://doi.org/10.1016/j.carbpol.2009.01.016.

[40] T. Wallmersperger, B. Kroeplin, J. Holdenried, and R. W. Guelch, "Coupled multifield formulation for ionic polymer gels in electric fields," in *Smart Structures and*

Materials 2001: Electroactive Polymer Actuators and Devices, Y. Bar-Cohen, Ed., SPIE, 2001, pp. 264–275. doi: 10.1117/12.432655.

[41] T. Wallmersperger, B. H. Kröplin, and R. W. Gülch, "Coupled chemo-electro-mechanical formulation for ionic polymer gels—numerical and experimental investigations," *Mechanics of Materials*, vol. 36, pp. 411–420, 2004.

[42] H. Li, Y. K. Yew, T. Y. Ng, and K. Y. Lam, "Meshless steady-state analysis of chemo-electro-mechanical coupling behavior of pH-sensitive hydrogel in buffered solution," *Journal of Electroanalytical Chemistry*, vol. 580, no. 1, pp. 161–172, 2005, doi: https://doi.org/10.1016/j.jelechem.2005.03.034.

[43] X. Zhou, Y. C. Hon, S. Sun, and A. F. T. Mak, "Numerical simulation of the steady-state deformation of a smart hydrogel under an external electric field," *Smart Mater Struct*, vol. 11, no. 3, pp. 459–467, May 2002, doi: 10.1088/0964-1726/11/3/316.

[44] S. Chatterjee and P. Chi-leung Hui, "Stimuli-Responsive Hydrogels: An Interdisciplinary Overview," *Hydrogels - Smart Materials for Biomedical Applications*, no. November, 2019, doi: 10.5772/intechopen.80536.

[45] T. Hiratani, O. Kose, W. Y. Hamad, and M. J. Maclachlan, "Stable and sensitive stimuli-responsive anisotropic hydrogels for sensing ionic strength and pressure," *Mater Horiz*, vol. 5, no. 6, pp. 1076–1081, 2018, doi: 10.1039/c8mh00586a.

[46] R. Liang, H. Yu, L. Wang, L. Lin, N. Wang, and K.-U.-R. Naveed, "Highly Tough Hydrogels with the Body Temperature-Responsive Shape Memory Effect.," *ACS Appl Mater Interfaces*, vol. 11, no. 46, pp. 43563–43572, Nov. 2019, doi: 10.1021/acsami.9b14756.

[47] O. Werzer, S. Tumphart, R. Keimel, P. Christian, and A. M. Coclite, "Drug release from thin films encapsulated by a temperature-responsive hydrogel.," *Soft Matter*, vol. 15, no. 8, pp. 1853–1859, Feb. 2019, doi: 10.1039/c8sm02529k.

[48] H. M. El-Husseiny *et al.*, "Smart/stimuli-responsive hydrogels: Cutting-edge platforms for tissue engineering and other biomedical applications.," *Mater Today Bio*, vol. 13, p. 100186, Jan. 2022, doi: 10.1016/j.mtbio.2021.100186.

[49] B. Mishra, M. Upadhyay, S. Reddy Adena, B. Vascant, and M. Muthu, "Hydrogels: An Introduction to a Controlled Drug Delivery Device, Synthesis and Application in Drug Delivery and Tissue Engineering," *Austin J Biomed Eng*, vol. 4, no. 1, pp. 1037–1, 2017.

[50] L. I. Georgi Stoychev, Alina Kirillova, "Light-Responsive Shape-Changing Polymers," *Adv Opt Mater*, vol. 7, no. 16, pp. 1–30, 2019.

[51] Z. Jiang *et al.*, "Strong, Self-Healable, and Recyclable Visible-Light-Responsive Hydrogel Actuators.," *Angew Chem Int Ed Engl*, vol. 59, no. 18, pp. 7049–7056, Apr. 2020, doi: 10.1002/anie.201916058.

[52] S. Mallawarachchi, V. Gejji, L. S. Sierra, H. Wang, and S. Fernando, "Electrical Field Reversibly Modulates Enzyme Kinetics of Hexokinase Entrapped in an Electro-

Responsive Hydrogel.," *ACS Appl Bio Mater*, vol. 2, no. 12, pp. 5676–5686, Dec. 2019, doi: 10.1021/acsabm.9b00748.

[53] W. Shi, J. Huang, R. Fang, and M. Liu, "Imparting Functionality to the Hydrogel by Magnetic-Field-Induced Nano-assembly and Macro-response.," *ACS Appl Mater Interfaces*, vol. 12, no. 5, pp. 5177–5194, Feb. 2020, doi: 10.1021/acsami.9b16770.

[54] A. C. Manjua, V. D. Alves, J. G. Crespo, and C. A. M. Portugal, "Magnetic Responsive PVA Hydrogels for Remote Modulation of Protein Sorption.," *ACS Appl Mater Interfaces*, vol. 11, no. 23, pp. 21239–21249, Jun. 2019, doi: 10.1021/acsami.9b03146.

[55] J. Hu *et al.*, "A pH-responsive hydrogel with potent antibacterial activity against both aerobic and anaerobic pathogens.," *Biomater Sci*, vol. 7, no. 2, pp. 581–584, Jan. 2019, doi: 10.1039/c8bm01211c.

[56] A. Bhat, J. M. Amanor-Boadu, and A. Guiseppi-Elie, "Toward Impedimetric Measurement of Acidosis with a pH-Responsive Hydrogel Sensor.," *ACS Sens*, vol. 5, no. 2, pp. 500–509, Feb. 2020, doi: 10.1021/acssensors.9b02336.

[57] M. Rizwan *et al.*, "pH Sensitive Hydrogels in Drug Delivery: Brief History, Properties, Swelling, and Release Mechanism, Material Selection and Applications.," *Polymers (Basel)*, vol. 9, no. 4, Apr. 2017, doi: 10.3390/polym9040137.

[58] H. Haidari, Z. Kopecki, A. T. Sutton, S. Garg, A. J. Cowin, and K. Vasilev, "pH-Responsive 'Smart' Hydrogel for Controlled Delivery of Silver Nanoparticles to Infected Wounds.," *Antibiotics (Basel)*, vol. 10, no. 1, Jan. 2021, doi: 10.3390/antibiotics10010049.

[59] A. Hendi *et al.*, "Healthcare applications of pH-sensitive hydrogel-based devices: A review," *Int J Nanomedicine*, vol. 15, pp. 3887–3901, 2020, doi: 10.2147/IJN.S245743.

[60] R. Zhang, M. Tang, A. Bowyer, R. Eisenthal, and J. Hubble, "A novel pH- and ionic-strength-sensitive carboxy methyl dextran hydrogel.," *Biomaterials*, vol. 26, no. 22, pp. 4677–4683, Aug. 2005, doi: 10.1016/j.biomaterials.2004.11.048.

[61] H. Vihola, A. Laukkanen, H. Tenhu, and J. Hirvonen, "Drug release characteristics of physically cross-linked thermosensitive poly(N-vinylcaprolactam) hydrogel particles," *J Pharm Sci*, vol. 97, no. 11, pp. 4783–4793, 2008, doi: https://doi.org/10.1002/jps.21348.

[62] J. W. Lee, F. Hua, and D. S. Lee, "Thermoreversible gelation of biodegradable poly(epsilon-caprolactone) and poly(ethylene glycol) multiblock copolymers in aqueous solutions.," *J Control Release*, vol. 73, no. 2–3, pp. 315–327, Jun. 2001, doi: 10.1016/s0168-3659(01)00297-8.

[63] L. Klouda and A. G. Mikos, "Thermoresponsive hydrogels in biomedical applications.," *Eur J Pharm Biopharm*, vol. 68, no. 1, pp. 34–45, Jan. 2008, doi: 10.1016/j.ejpb.2007.02.025.

[64] S. Purushotham and R. v Ramanujan, “Thermoresponsive magnetic composite nanomaterials for multimodal cancer therapy,” *Acta Biomater*, vol. 6, no. 2, pp. 502–510, 2010, doi: https://doi.org/10.1016/j.actbio.2009.07.004.

[65] A. K. Bajpai, S. K. Shukla, S. Bhanu, and S. Kankane, “Responsive polymers in controlled drug delivery,” *Prog Polym Sci*, vol. 33, no. 11, pp. 1088–1118, 2008, doi: https://doi.org/10.1016/j.progpolymsci.2008.07.005.

[66] A. D. M. and A. Wilkinson, “Compendium of Chemical Terminology, 2nd ed. (the ‘Gold Book’),” *The IUPAC Compendium of Chemical Terminology*, p. 7280, 1997, doi: 10.1351/goldbook.ut07280.

[67] A. Bilia, V. Carelli, G. di Colo, and E. Nannipieri, “In vitro evaluation of a pH-sensitive hydrogel for control of GI drug delivery from silicone-based matrices,” *Int J Pharm*, vol. 130, no. 1, pp. 83–92, 1996, doi: https://doi.org/10.1016/0378-5173(95)04297-0.

[68] A. R. Hibbins *et al.*, “Design of a Versatile pH-Responsive Hydrogel for Potential Oral Delivery of Gastric-Sensitive Bioactives.,” *Polymers (Basel)*, vol. 9, no. 10, Sep. 2017, doi: 10.3390/polym9100474.

[69] W. Jian, D. Hui, and D. Lau, “Nanoengineering in biomedicine: Current development and future perspectives,” *Nanotechnology Reviews*, vol. 9, no. 1. De Gruyter Open Ltd, pp. 700–715, Jan. 01, 2020. doi: 10.1515/ntrev-2020-0053.

[70] Y. Qiu and K. Park, “Environment-sensitive hydrogels for drug delivery,” *Adv Drug Deliv Rev*, vol. 53, no. 3, pp. 321–339, 2001, doi: https://doi.org/10.1016/S0169-409X(01)00203-4.

[71] D. Schmaljohann, “Thermo- and pH-responsive polymers in drug delivery,” *Adv Drug Deliv Rev*, vol. 58, no. 15, pp. 1655–1670, 2006, doi: https://doi.org/10.1016/j.addr.2006.09.020.

[72] P. Gupta, K. Vermani, and S. Garg, “Hydrogels: from controlled release to pH-responsive drug delivery,” *Drug Discov Today*, vol. 7, no. 10, pp. 569–579, 2002, doi: https://doi.org/10.1016/S1359-6446(02)02255-9.

[73] L. Xu *et al.*, “Biodegradable pH-responsive hydrogels for controlled dual-drug release,” *J. Mater. Chem. B*, vol. 6, no. 3, pp. 510–517, 2018, doi: 10.1039/C7TB01851G.

[74] A. S. Hoffman, “Hydrogels for biomedical applications,” *Adv Drug Deliv Rev*, vol. 64, no. SUPPL., pp. 18–23, 2012, doi: 10.1016/j.addr.2012.09.010.

[75] Q. Chai, Y. Jiao, and X. Yu, “Hydrogels for Biomedical Applications: Their Characteristics and the Mechanisms behind Them.,” *Gels*, vol. 3, no. 1, Jan. 2017, doi: 10.3390/gels3010006.

[76] M.-H. Cai *et al.*, “Design and Development of Hybrid Hydrogels for Biomedical Applications: Recent Trends in Anticancer Drug Delivery and Tissue Engineering,” *Front Bioeng Biotechnol*, vol. 9, 2021, doi: 10.3389/fbioe.2021.630943.

[77] E. Caló and V. V Khutoryanskiy, “Biomedical applications of hydrogels: A review of patents and commercial products,” *Eur Polym J*, vol. 65, pp. 252–267, 2015, doi: https://doi.org/10.1016/j.eurpolymj.2014.11.024.

[78] S. J. Buwalda, “Bio-based composite hydrogels for biomedical applications,” *Multifunctional Materials*, vol. 3, no. 2, p. 22001, May 2020, doi: 10.1088/2399-7532/ab80d6.

[79] C. R. Lynch, P. P. D. Kondiah, Y. E. Choonara, L. C. du Toit, N. Ally, and V. Pillay, “Hydrogel Biomaterials for Application in Ocular Drug Delivery,” *Front Bioeng Biotechnol*, vol. 8, 2020, doi: 10.3389/fbioe.2020.00228.

[80] A. C. Daly, L. Riley, T. Segura, and J. A. Burdick, “Hydrogel microparticles for biomedical applications,” *Nat Rev Mater*, vol. 5, no. 1, pp. 20–43, 2020, doi: 10.1038/s41578-019-0148-6.

[81] H. Chang, C. Li, R. Huang, R. Su, W. Qi, and Z. He, “Amphiphilic hydrogels for biomedical applications,” *J. Mater. Chem. B*, vol. 7, no. 18, pp. 2899–2910, 2019, doi: 10.1039/C9TB00073A.

[82] P. Vaupel, F. Kallinowski, and P. Okunieff, “Blood flow, oxygen and nutrient supply, and metabolic microenvironment of human tumors: a review.,” *Cancer Res*, vol. 49, no. 23, pp. 6449–6465, Dec. 1989.

[83] A. A. Deshpande, C. T. Rhodes, and M. Danish, “Intravaginal drug delivery,” *Drug Dev Ind Pharm*, vol. 18, no. 11–12, pp. 1225–1279, 1992, doi: 10.3109/03639049209046329.

[84] J. Fallingborg, “Intraluminal pH of the human gastrointestinal tract.,” *Dan Med Bull*, vol. 46, no. 3, pp. 183–196, Jun. 1999.

[85] L. Li *et al.*, “Injectable and Biodegradable pH-Responsive Hydrogels for Localized and Sustained Treatment of Human Fibrosarcoma.,” *ACS Appl Mater Interfaces*, vol. 7, no. 15, pp. 8033–8040, Apr. 2015, doi: 10.1021/acsami.5b00389.

[86] N. Ninan, A. Forget, V. P. Shastri, N. H. Voelcker, and A. Blencowe, “Antibacterial and Anti-Inflammatory pH-Responsive Tannic Acid-Carboxylated Agarose Composite Hydrogels for Wound Healing,” *ACS Appl Mater Interfaces*, vol. 8, no. 42, pp. 28511–28521, Oct. 2016, doi: 10.1021/acsami.6b10491.

[87] B. Yıldız, B. Is, and M. Kıs, “pH-Sensitive Dimethylaminoethyl Methacrylate(DMAEMA)/Acrylamide (AAm) Hydrogels: Synthesis andAdsorption from Uranyl Acetate Solutions,” *J Appl Polym Sci*, vol. 88, pp. 2028–2031, 2002.

[88] M. C. Koetting, J. T. Peters, S. D. Steichen, and N. A. Peppas, “Stimulus-responsive hydrogels: Theory, modern advances, and applications,” *Materials Science and Engineering: R: Reports*, vol. 93, pp. 1–49, 2015, doi: https://doi.org/10.1016/j.mser.2015.04.001.

[89] T. Li, J. Shen, Z. Zhang, S. Wang, and D. Wei, “A poly(2-(dimethylamino)ethyl methacrylate-co-methacrylic acid) complex induced route to fabricate a super-

hydrophilic hydrogel and its controllable oil/water separation," *RSC Adv.*, vol. 6, no. 47, pp. 40656–40663, 2016, doi: 10.1039/C6RA01820C.

[90] S. K. De and N. R. Aluru, "A chemo-electro-mechanical mathematical model for simulation of pH sensitive hydrogels," *Mechanics of Materials*, vol. 36, no. 5, pp. 395–410, 2004, doi: https://doi.org/10.1016/S0167-6636(03)00067-X.

[91] S. Hirotsu, "Coexistence of phases and the nature of first-order phase transition in poly-N-isopropylacrylamide gels," in *Responsive Gels: Volume Transitions II*, K. Dušek, Ed., Berlin, Heidelberg: Springer Berlin Heidelberg, 1993, pp. 1–26. doi: 10.1007/BFb0021126.

[92] K. Qu *et al.*, "Structures, properties, and applications of zwitterionic polymers," *ChemPhysMater*, 2022, doi: https://doi.org/10.1016/j.chphma.2022.04.003.

[93] R. Wei *et al.*, "Bidirectionally pH-Responsive Zwitterionic Polymer Hydrogels with Switchable Selective Adsorption Capacities for Anionic and Cationic Dyes," *Ind Eng Chem Res*, vol. 57, no. 24, pp. 8209–8219, Jun. 2018, doi: 10.1021/acs.iecr.8b01027.

[94] Q. Shao *et al.*, "Differences in Cationic and Anionic Charge Densities Dictate Zwitterionic Associations and Stimuli Responses," *J Phys Chem B*, vol. 118, no. 24, pp. 6956–6962, Jun. 2014, doi: 10.1021/jp503473u.

[95] S. Liu, J. Tang, F. Ji, W. Lin, and S. Chen, "Recent Advances in Zwitterionic Hydrogels: Preparation, Property, and Biomedical Application," *Gels*, vol. 8, no. 1, 2022, doi: 10.3390/gels8010046.

[96] L. Brannon-Peppas and N. A. Peppas, "Equilibrium swelling behavior of dilute ionic hydrogels in electrolytic solutions," *Journal of Controlled Release*, vol. 16, no. 3, pp. 319–329, 1991, doi: https://doi.org/10.1016/0168-3659(91)90009-3.

[97] B. A. Firestone and R. A. Siegel, "Kinetics and mechanisms of water sorption in hydrophobic, ionizable copolymer gels," *J Appl Polym Sci*, vol. 43, no. 5, pp. 901–914, 1991.

[98] M. R. Bayat and M. Baghani, "A review on swelling theories of pH-sensitive hydrogels," *Journal of Intelligent Material Systems and Structures*, vol. 32, no. 18–19. SAGE Publications Ltd, pp. 2349–2365, Nov. 01, 2021. doi: 10.1177/1045389X21995880.

[99] J. R. Saunders, S. Abu-Salih, T. Khaleque, S. Hanula, and W. Moussa, "Modeling theories of intelligent hydrogel polymers," *J Comput Theor Nanosci*, vol. 5, no. 10, pp. 1942–1960, 2008, doi: 10.1166/jctn.2008.1001.

[100] L. A. Sharpe, A. M. Daily, S. D. Horava, and N. A. Peppas, "Therapeutic applications of hydrogels in oral drug delivery.," *Expert Opin Drug Deliv*, vol. 11, no. 6, pp. 901–915, Jun. 2014, doi: 10.1517/17425247.2014.902047.

[101] L. Liu, W. Yao, Y. Rao, X. Lu, and J. Gao, "pH-Responsive carriers for oral drug delivery: challenges and opportunities of current platforms.," *Drug Deliv*, vol. 24, no. 1, pp. 569–581, Nov. 2017, doi: 10.1080/10717544.2017.1279238.

[102] Y. S. Casadio, D. H. Brown, T. v. Chirila, H. B. Kraatz, and M. v. Baker, "Biodegradation of poly(2-hydroxyethyl methacrylate) (PHEMA) and poly{(2-hydroxyethyl methacrylate)-co-[poly(ethylene glycol) methyl ether methacrylate]} hydrogels containing peptide-based cross-linking agents," *Biomacromolecules*, vol. 11, no. 11, pp. 2949–2959, 2010, doi: 10.1021/bm100756c.

[103] T. D. Dziubla, M. C. Torjman, J. I. Joseph, M. Murphy-Tatum, and A. M. Lowman, "Evaluation of porous networks of poly(2-hydroxyethyl methacrylate) as interfacial drug delivery devices," *Biomaterials*, vol. 22, no. 21, pp. 2893–2899, 2001, doi: 10.1016/S0142-9612(01)00035-7.

[104] G. H. Hsiue, J. A. Guu, and C. C. Cheng, "Poly(2-hydroxyethyl methacrylate) film as a drug delivery system for pilocarpine," *Biomaterials*, vol. 22, no. 13, pp. 1763–1769, 2001, doi: 10.1016/S0142-9612(00)00336-7.

[105] L. G. Bach, Md. R. Islam, Y. T. Jeong, Y. S. Gal, and K. T. Lim, "Synthesis and characterization of chemically anchored adenosine with PHEMA grafted gold nanoparticles," *Appl Surf Sci*, vol. 258, no. 7, pp. 2816–2822, 2012, doi: https://doi.org/10.1016/j.apsusc.2011.10.140.

[106] M. F. Passos *et al.*, "pHEMA hydrogels Synthesis, kinetics and in vitro tests," *J Therm Anal Calorim*, vol. 125, no. 1, pp. 361–368, 2016, doi: 10.1007/s10973-016-5329-6.

[107] O. WICHTERLE and D. LÍM, "Hydrophilic Gels for Biological Use," *Nature*, vol. 185, no. 4706, pp. 117–118, 1960, doi: 10.1038/185117a0.

[108] M. Zare, A. Bigham, M. Zare, H. Luo, E. Rezvani Ghomi, and S. Ramakrishna, "pHEMA: An Overview for Biomedical Applications.," *Int J Mol Sci*, vol. 22, no. 12, Jun. 2021, doi: 10.3390/ijms22126376.

[109] M. F. Passos *et al.*, "PHEMA Hydrogels Obtained by Infrared Radiation for Cartilage Tissue Engineering," *International Journal of Chemical Engineering*, vol. 2019, p. 4249581, 2019, doi: 10.1155/2019/4249581.

[110] H. Ayhan and F. Ayhan, "Water based PHEMA hydrogels for controlled drug delivery," *Turkish Journal of Biochemistry*, vol. 43, no. 3, pp. 228–239, 2018, doi: doi:10.1515/tjb-2017-0250.

[111] L. Ferreira, M. M. Vidal, and M. H. Gil, "Evaluation of poly(2-hydroxyethyl methacrylate) gels as drug delivery systems at different pH values," *Int J Pharm*, vol. 194, no. 2, pp. 169–180, 2000, doi: 10.1016/S0378-5173(99)00375-0.

[112] G. R. Deen and X. J. Loh, "Stimuli-Responsive Cationic Hydrogels in Drug Delivery Applications," *Gels*, vol. 4, no. 1, p. E13, Feb. 2018, doi: 10.3390/gels4010013.

[113] P. Ferruti, M. A. Marchisio, and R. Duncan, "Poly(amido-amine)s : Biomedical Applications," *Macromol. Rapid Commun*, vol. 23, no. 5/6, pp. 332–355, 2002.

[114] N. A. Peppas, P. Bures, W. Leobandung, and H. Ichikawa, "Hydrogels in pharmaceutical formulations," *European Journal of Pharmaceutics and Biopharmaceutics*, vol. 50, no. 1, pp. 27–46, 2000, doi: 10.1016/S0939-6411(00)00090-4.

[115] W. Wei, H. Li, C. Yin, and F. Tang, “Research progress in the application of in situ hydrogel system in tumor treatment.,” *Drug Deliv*, vol. 27, no. 1, pp. 460–468, Dec. 2020, doi: 10.1080/10717544.2020.1739171.

[116] S. Komatsu, M. Tago, Y. Ando, T.-A. Asoh, and A. Kikuchi, “Facile preparation of multi-stimuli-responsive degradable hydrogels for protein loading and release,” *Journal of Controlled Release*, vol. 331, pp. 1–6, 2021, doi: https://doi.org/10.1016/j.jconrel.2021.01.011.

[117] G. R. Shin, H. E. Kim, J. H. Kim, S. Choi, and M. S. Kim, “Advances in injectable in situ-forming hydrogels for intratumoral treatment,” *Pharmaceutics*, vol. 13, no. 11, pp. 1–15, 2021, doi: 10.3390/pharmaceutics13111953.

[118] H. Wu, S. Liu, L. Xiao, X. Dong, Q. Lu, and D. L. Kaplan, “Injectable and pH-Responsive Silk Nanofiber Hydrogels for Sustained Anticancer Drug Delivery,” *ACS Appl Mater Interfaces*, vol. 8, no. 27, pp. 17118–17126, Jul. 2016, doi: 10.1021/acsami.6b04424.

[119] C. Bastiancich, P. Danhier, V. Préat, and F. Danhier, “Anticancer drug-loaded hydrogels as drug delivery systems for the local treatment of glioblastoma,” *Journal of Controlled Release*, vol. 243, pp. 29–42, 2016, doi: https://doi.org/10.1016/j.jconrel.2016.09.034.

[120] C. Nishi, N. Nakajima, and Y. Ikada, “In vitro evaluation of cytotoxicity of diepoxy compounds used for biomaterial modification,” *J Biomed Mater Res*, vol. 29, no. 7, pp. 829–834, 1995, doi: 10.1002/jbm.820290707.

[121] D. P. Speer, M. Chvapil, C. D. Eskelson, and J. Ulreich, “Biological effects of residual glutaraldehyde in glutaraldehyde-tanned collagen biomaterials,” *J Biomed Mater Res*, vol. 14, no. 6, pp. 753–764, 1980, doi: 10.1002/jbm.820140607.

[122] A. A. D. N. Pomari, T. L. D. A. Montanheiro, C. P. de Siqueira, R. S. Silva, D. B. Tada, and A. P. Lemes, “Chitosan hydrogels crosslinked by genipin and reinforced with cellulose nanocrystals: Production and characterization,” *Journal of Composites Science*, vol. 3, no. 3, 2019, doi: 10.3390/jcs3030084.

[123] N. R. Kildeeva, P. A. Perminov, L. v Vladimirov, V. v Novikov, and S. N. Mikhailov, “About mechanism of chitosan cross-linking with glutaraldehyde,” *Russ J Bioorg Chem*, vol. 35, no. 3, pp. 360–369, 2009, doi: 10.1134/S106816200903011X.

[124] R. Shah, P. Stodulka, K. Skopalova, and P. Saha, “Dual Crosslinked Collagen/Chitosan Film for Potential Biomedical Applications,” *Polymers (Basel)*, vol. 11, no. 12, 2019, doi: 10.3390/polym11122094.

[125] M. F. Butler, Y. F. Ng, and P. D. A. Pudney, “Mechanism and kinetics of the crosslinking reaction between biopolymers containing primary amine groups and genipin,” *J Polym Sci A Polym Chem*, vol. 41, no. 24, pp. 3941–3953, 2003, doi: 10.1002/pola.10960.

[126] N. Kildeeva *et al.*, “Influence of genipin crosslinking on the properties of Chitosan-based films,” *Polymers (Basel)*, vol. 12, no. 5, 2020, doi: 10.3390/POLYM12051086.

[127] D. Vukajlovic, O. Bretcanu, and K. Novakovic, “Fabrication and characterization of two types of bone composites made of chitosan-genipin hydrogel and Bioglass 45S5,” *Open Ceramics*, vol. 8, p. 100174, 2021, doi: https://doi.org/10.1016/j.oceram.2021.100174.

[128] C. J. Nwosu, G. A. Hurst, and K. Novakovic, “Genipin Cross-Linked Chitosan-Polyvinylpyrrolidone Hydrogels: Influence of Composition and Postsynthesis Treatment on pH Responsive Behaviour,” *Advances in Materials Science and Engineering*, vol. 2015, p. 621289, 2015, doi: 10.1155/2015/621289.

[129] K. Chung, M. A. Birch, and K. Novakovic, “Genipin-crosslinked Chitosan Hydrogels as Scaffolds for Mammalian Cell Growth,” *Int J Adv Sci Eng Technol*, vol. 6, no. 1, p. 8, 2018.

[130] N. T. N. Vo, L. Huang, H. Lemos, A. L. Mellor, and K. Novakovic, “Genipin-crosslinked chitosan hydrogels: Preliminary evaluation of the in vitro biocompatibility and biodegradation,” *J Appl Polym Sci*, vol. 138, no. 34, p. 11, May 2021, doi: 10.1002/app.50848.

[131] G. A. Hurst and K. Novakovic, “A facile in situ morphological characterization of smart genipin-crosslinked chitosan–poly(vinyl pyrrolidone) hydrogels,” *J Mater Res*, vol. 28, no. 17, pp. 2401–2408, 2013, doi: 10.1557/jmr.2013.134.

[132] G. A. Hurst, “The Studies of Genipin-Crosslinked Chitosan-poly(vinyl pyrrolidone) Hydrogels as Smart pH Responsive Materials,” Newcastle University, United Kingdom, 2016. [Online]. Available: http://hdl.handle.net/10443/3284

[133] N. T. N. Vo, L. Huang, H. Lemos, A. Mellor, and K. Novakovic, “Poly(ethylene glycol)-interpenetrated genipin-crosslinked chitosan hydrogels: Structure, pH responsiveness, gelation kinetics, and rheology,” *J Appl Polym Sci*, vol. 137, no. 41, pp. 1–16, 2020, doi: 10.1002/app.49259.

[134] A. M. Heimbuck *et al.*, “Development of Responsive Chitosan–Genipin Hydrogels for the Treatment of Wounds,” *ACS Appl Bio Mater*, vol. 2, no. 7, pp. 2879–2888, 2019, doi: 10.1021/acsabm.9b00266.

[135] S. L. Jahren, M. F. Butler, S. Adams, and R. E. Cameron, “Predictive modelling of the swelling behaviour of polyelectrolytic chitosan hydrogels,” *Carbohydr Polym*, vol. 86, no. 2, pp. 769–773, 2011, doi: 10.1016/j.carbpol.2011.05.021.

[136] S. Rajput and N. K. Thakur, “Rock Properties,” *Geological Controls for Gas Hydrate Formations and Unconventionals*, pp. 131–164, Jan. 2016, doi: 10.1016/B978-0-12-802020-3.00005-9.

[137] M. L. Huggins, “Principles of Polymer Chemistry.,” *J Am Chem Soc*, vol. 76, no. 10, p. 2854, 1954, doi: 10.1021/ja01639a090.

[138] P. J. Flory, *Principles of polymer chemistry*. ITHACA, NEW YORK: Cornell University Press, 1953. doi: 10.1093/jaoac/49.4.744.

[139] T. Wallmersperger, F. K. Wittel, M. D’Ottavio, and B. Kröplin, “Multiscale Modeling of Polymer Gels—Chemo-Electric Model versus Discrete Element Model,” *Mechanics*

of Advanced Materials and Structures, vol. 15, no. 3–4, pp. 228–234, 2008, doi: 10.1080/15376490801907731.

[140] A. Hüther, X. Xu, and G. Maurer, "Swelling of n-isopropyl acrylamide hydrogels in water and aqueous solutions of ethanol and acetone," *Fluid Phase Equilib*, vol. 219, no. 2, pp. 231–244, 2004, doi: https://doi.org/10.1016/j.fluid.2003.08.002.

[141] J. Bluhm, S. Serdas, and J. Schröder, "Theoretical framework of modeling of ionic EAPs within the Theory of Porous Media," *Archive of Applied Mechanics*, vol. 86, no. 1, pp. 3–19, 2016, doi: 10.1007/s00419-015-1110-8.

[142] J. Bluhm, "Modelling of saturated thermo-elastic porous solids with different phase temperatures," in *Porous Media: Theory, Experiments and Numerical Applications*, W. Ehlers and J. Bluhm, Eds., Berlin, Heidelberg: Springer Berlin Heidelberg, 2002, pp. 87–118. doi: 10.1007/978-3-662-04999-0_2.

[143] J. R. Barber, *Contact Mechanics*. in Solid mechanics and its applications ; 250. 2018.

[144] V. L. Popov and E. Willert, "James R. Barber: Contact Mechanics," *Tribol Lett*, vol. 66, no. 2, p. 73, 2018, doi: 10.1007/s11249-018-1028-8.

[145] A. Gugliuzza, "Solvent Swollen Polymer," in *Encyclopedia of Membranes*, E. Drioli and L. Giorno, Eds., Berlin, Heidelberg: Springer Berlin Heidelberg, 2016, pp. 1801–1802. doi: 10.1007/978-3-662-44324-8_1407.

[146] T. Sakai, *Physics of Polymer Gels*. John Wiley & Sons, 2020. [Online]. Available: https://books.google.co.uk/books?id=2XPTDwAAQBAJ

[147] W. Kuhn, "Dependence of the average transversal on the longitudinal dimensions of statistical coils formed by chain molecules," *Journal of Polymer Science*, vol. 1, no. 5, pp. 380–388, 1946, doi: 10.1002/pol.1946.120010505.

[148] H. M. James and E. Guth, "Simple presentation of network theory of rubber, with a discussion of other theories," *Journal of Polymer Science*, vol. 4, no. 2, pp. 153–182, Apr. 1949, doi: 10.1002/pol.1949.120040206.

[149] K. Nishi, H. Noguchi, T. Sakai, and M. Shibayama, "Rubber elasticity for percolation network consisting of Gaussian chains," *Journal of Chemical Physics*, vol. 143, no. 18, 2015, doi: 10.1063/1.4935395.

[150] P. J. Flory and B. Erman, "Theory of elasticity of polymer networks. 3," *Macromolecules*, vol. 15, no. 3, pp. 800–806, 1982, doi: 10.1021/ma00231a022.

[151] M. Doi, "Explanation for the 3.4-power law for viscosity of polymeric liquids on the basis of the tube model," *Journal of Polymer Science Part B*, vol. 21, pp. 667–684, 1983.

[152] F. Horkay and G. B. McKenna, "Polymer Networks and Gels," in *Physical Properties of Polymers Handbook*, J. E. Mark, Ed., New York, NY: Springer New York, 2007, pp. 497–523. doi: 10.1007/978-0-387-69002-5_29.

[153] A. Kloczkowski, J. E. Mark, and B. Erman, "A Diffused-Constraint Theory for the Elasticity of Amorphous Polymer Networks. 1. Fundamentals and Stress-Strain

Isotherms in Elongation," *Macromolecules*, vol. 28, no. 14, pp. 5089–5096, 1995, doi: 10.1021/ma00118a043.

[154] H. M. James and E. Guth, "Theory of the Increase in Rigidity of Rubber during Cure," *jcp*, vol. 15, no. 9, pp. 669–683, Sep. 1947, doi: 10.1063/1.1746626.

[155] A. Katchalsky and I. Michaeli, "Polyelectrolyte gels in salt solutions," *Journal of Polymer Science*, vol. 15, no. 79, pp. 69–86, 1955, doi: 10.1002/pol.1955.120157906.

[156] J. Rička and T. Tanaka, "Swelling of Ionic Gels: Quantitative Performance of the Donnan Theory," *Macromolecules*, vol. 17, no. 12, pp. 2916–2921, 1984, doi: 10.1021/ma00142a081.

[157] L. Brannon-Peppast, "EQUILIBRIUM SWELLING HYDROGELS OF pH-SENSITIVE," *Chemical Engineering*, vol. 46, no. 3, pp. 715–722, 1991, [Online]. Available: http://www.sciencedirect.com/science/article/B6TFK-444P1P4-H1/2/e866d771afcdad2db5bfa0e86fa92cc6

[158] and Ö. K. T. Çaykara, U. Bozkaya, "Network Structure and Swelling Behavior of Poly (acrylamide / crotonic acid) Hydrogels in," *Polymer*. pp. 1656–1664, 2003.

[159] S. L. Jahren, M. F. Butler, S. Adams, and R. E. Cameron, "Swelling and viscoelastic characterisation of pH-responsive chitosan hydrogels for targeted drug delivery," *Macromol Chem Phys*, vol. 211, no. 6, pp. 644–650, 2010, doi: 10.1002/macp.200900560.

[160] H. Schott, "Swelling kinetics of polymers," *Journal of Macromolecular Science, Part B*, vol. 31, no. 1, pp. 1–9, 1992, doi: 10.1080/00222349208215453.

[161] H. Schott, "Kinetics of swelling of polymers and their gels," *J Pharm Sci*, vol. 81, no. 5, pp. 467–470, 1992, doi: https://doi.org/10.1002/jps.2600810516.

[162] Y. Yin, Y. Yang, and H. Xu, "Swelling behavior of hydrogels for colon-site drug delivery," *J Appl Polym Sci*, vol. 83, no. 13, pp. 2835–2842, 2002.

[163] J. Wang, W. Wu, and Z. Lin, "Kinetics and thermodynamics of the water sorption of 2-hydroxyethyl methacrylate/styrene copolymer hydrogels," *J Appl Polym Sci*, vol. 109, no. 5, pp. 3018–3023, 2008, doi: https://doi.org/10.1002/app.28403.

[164] A. K. Bajpai, J. Bajpai, and S. Shukla, "Water sorption through a semi-interpenetrating polymer network (IPN) with hydrophilic and hydrophobic chains," *React Funct Polym*, vol. 50, no. 1, pp. 9–21, 2002, doi: https://doi.org/10.1016/S1381-5148(01)00085-2.

[165] A. K. Bajpai and A. Giri, "Swelling dynamics of a macromolecular hydrophilic network and evaluation of its potential for controlled release of agrochemicals," *React Funct Polym*, vol. 53, no. 2, pp. 125–141, 2002, doi: https://doi.org/10.1016/S1381-5148(02)00168-2.

[166] C. Wang, B. Yu, B. Knudsen, J. Harmon, F. Moussy, and Y. Moussy, "Synthesis and performance of novel hydrogels coatings for implantable glucose sensors.," *Biomacromolecules*, vol. 9, no. 2, pp. 561–567, Feb. 2008, doi: 10.1021/bm701102y.

[167] B. K. Denizli, H. K. Can, Z. M. O. Rzaev, and A. Guner, “Preparation conditions and swelling equilibria of dextran hydrogels prepared by some crosslinking agents,” *Polymer (Guildf)*, vol. 45, no. 19, pp. 6431–6435, 2004, doi: https://doi.org/10.1016/j.polymer.2004.07.067.

[168] F. Ganji, S. Vasheghani-Farahani, and E. Vasheghani-Farahani, “Theoretical description of hydrogel swelling: A review,” *Iranian Polymer Journal (English Edition)*, vol. 19, no. 5, pp. 375–398, 2010.

[169] A. R. Berens and H. B. Hopfenberg, “Diffusion and relaxation in glassy polymer powders: 2. Separation of diffusion and relaxation parameters,” *Polymer (Guildf)*, vol. 19, no. 5, pp. 489–496, 1978, doi: 10.1016/0032-3861(78)90269-0.

[170] T. Fujiyabu, F. Toni, X. Li, U.-I. Chung, and T. Sakai, “Three cooperative diffusion coefficients describing dynamics of polymer gels.,” *Chem Commun (Camb)*, vol. 54, no. 50, pp. 6784–6787, Jun. 2018, doi: 10.1039/c8cc01357h.

[171] K. J. Suthar, “Simulation, synthesis, and characterization of hydrogels and nanocomposite gels,” Western Michigan University, 2009. [Online]. Available: https://search.proquest.com/docview/305029264?accountid=10267%5Cnhttp://resolver.library.cornell.edu/net/openurl?ctx_ver=Z39.88-2004&ctx_enc=info:ofi/enc:UTF-8&rfr_id=info:sid/ProQuest+Dissertations+%26+Theses+Global&rft_val_fmt=info:ofi/fmt:kev:mtx:disse

[172] B. Kang, Y. Dai, X. Shen, and D. Chen, “Dynamical modeling and experimental evidence on the swelling/deswelling behaviors of pH sensitive hydrogels,” *Mater Lett*, vol. 62, no. 19, pp. 3444–3446, 2008, doi: https://doi.org/10.1016/j.matlet.2008.02.075.

[173] A. Blanco, G. González, E. Casanova, M. E. Pirela, and A. Briceño, “Mathematical Modeling of Hydrogels Swelling Based on the Finite Element Method,” *Appl Math (Irvine)*, vol. 04, no. 08, pp. 161–170, 2013, doi: 10.4236/am.2013.48a022.

[174] J. C. Kurnia, E. Birgersson, and A. S. Mujumdar, “Computational Study of pH-sensitive Hydrogel-based Microfluidic Flow Controllers,” *J Funct Biomater*, vol. 2, no. 3, pp. 195–212, 2011, doi: 10.3390/jfb2030195.

[175] H. Li, T. Y. Ng, J. Q. Cheng, and K. Y. Lam, “Hermite–Cloud: a novel true meshless method,” *Comput Mech*, vol. 33, no. 1, pp. 30–41, 2003, doi: 10.1007/s00466-003-0497-1.

[176] R. M. Pidaparti, *Engineering Finite Element Analysis*, vol. 1, no. 1. Morgan & Claypool, 2017. doi: 10.2200/s00761ed1v01y201703mec001.

[177] J. Bonet and R. D. Wood, *Nonlinear Continuum Mechanics for Finite Element Analysis*, 2 ed. Cambridge University Press, 2008. [Online]. Available: https://books.google.co.uk/books?id=V5Zf1rVeeEsC

[178] M. Rees, “Combining quadrilateral and triangular meshing using the advancing front approach,” *... of the 6th International Meshing Roundtable, Park City, ...*, 1997, [Online]. Available:

http://citeseerx.ist.psu.edu/viewdoc/download?doi=10.1.1.43.1606&rep=rep1&type=pdf

[179] V. Hooda, “Pre-processing for the suspension assembly of a car for NVH in ANSA,” 2022.

[180] D. L. Logan, *A First Course in the Finite Element Method*, 6th ed. Cengage Learning, 2017. [Online]. Available: https://books.google.co.uk/books?id=KptPymzHa%5C_gC

[181] V. Kanade, “What Is Finite Element Analysis? Working, Software, and Applications,” 2022.

[182] A. Davoodalhosseini, “COMSOL, ANSYS or ABAQUS.” [Online]. Available: https://comsolink.com/en/comsol-vs-ansys-vs-abaqus/#:~:text=If you want to create,the time%2C we recommend COMSOL.

[183] V. K. Shukla, D. Shukla, S. K. Tiwary, S. Agrawal, and A. Rastogi, “Evaluation of pH measurement as a method of wound assessment.,” *J Wound Care*, vol. 16, no. 7, pp. 291–294, 2007, doi: 10.12968/jowc.2007.16.7.27062.

[184] G. T. Gethin, S. Cowman, and R. M. Conroy, “The impact of Manuka honey dressings on the surface pH of chronic wounds,” in *International Wound Journal*, May 2008, pp. 185–194. doi: 10.1111/j.1742-481X.2007.00424.x.

[185] S. L. Percival, S. McCarty, J. A. Hunt, and E. J. Woods, “The effects of pH on wound healing, biofilms, and antimicrobial efficacy,” *Wound repair and regeneration : official publication of the Wound Healing Society [and] the European Tissue Repair Society*, vol. 22, no. 2. pp. 174–186, 2014. doi: 10.1111/wrr.12125.

[186] L. A. Schneider, A. Korber, S. Grabbe, and J. Dissemond, “Influence of pH on wound-healing: A new perspective for wound-therapy?,” *Archives of Dermatological Research*, vol. 298, no. 9. pp. 413–420, Feb. 2007. doi: 10.1007/s00403-006-0713-x.

[187] S. H. Aswathy, U. Narendrakumar, and I. Manjubala, “Commercial hydrogels for biomedical applications,” *Heliyon*, vol. 6, no. 4. Elsevier Ltd, Apr. 01, 2020. doi: 10.1016/j.heliyon.2020.e03719.

[188] J. Li and D. J. Mooney, “Designing hydrogels for controlled drug delivery,” *Nature Reviews Materials*, vol. 1, no. 12. Nature Publishing Group, Oct. 18, 2016. doi: 10.1038/natrevmats.2016.71.

[189] J. Zhu and R. E. Marchant, “Design properties of hydrogel tissue-engineering scaffolds,” *Expert Review of Medical Devices*, vol. 8, no. 5. pp. 607–626, Sep. 2011. doi: 10.1586/erd.11.27.

[190] C. Celik, V. T. Mogal, J. H. P. Hui, X. J. Loh, and W. S. Toh, “Injectable Hydrogels for Cartilage Regeneration,” 2018, pp. 315–337. doi: 10.1007/978-981-10-6077-9_12.

[191] G. Lemon *et al.*, “Mathematical modelling of tissue-engineered angiogenesis,” *Math Biosci*, vol. 221, no. 2, pp. 101–120, Oct. 2009, doi: 10.1016/j.mbs.2009.07.003.

[192] I. Burova, I. Wall, and R. J. Shipley, “Mathematical and computational models for bone tissue engineering in bioreactor systems,” *J Tissue Eng*, vol. 10, Feb. 2019, doi: 10.1177/2041731419827922.

[193] S. N. Menon and J. A. Flegg, “Mathematical Modeling Can Advance Wound Healing Research,” *Adv Wound Care (New Rochelle)*, vol. 10, no. 6, pp. 328–344, Jun. 2021, doi: 10.1089/wound.2019.1132.

[194] J. A. Sherratt and J. C. Dallon, “Theoretical models of wound healing: past successes and future challenges,” *C R Biol*, vol. 325, no. 5, pp. 557–564, May 2002, doi: 10.1016/S1631-0691(02)01464-6.

[195] J. A. Thackham, D. L. S. McElwain, and R. J. Long, “The use of hyperbaric oxygen therapy to treat chronic wounds: A review,” *Wound Repair and Regeneration*, vol. 16, no. 3. pp. 321–330, May 2008. doi: 10.1111/j.1524-475X.2008.00372.x.

[196] S. R. Nussbaum *et al.*, “An Economic Evaluation of the Impact, Cost, and Medicare Policy Implications of Chronic Nonhealing Wounds,” *Value in Health*, vol. 21, no. 1, pp. 27–32, Jan. 2018, doi: 10.1016/j.jval.2017.07.007.

[197] N. K. Moses NO, Franklin F, Zivkovic V, “Multiphysics Simulation of the Swelling Kinetics of pH-Responsive Anionic Hydrogels,” in *COMSOL Conference 2020 Europe*, 2022, pp. 1–2.

[198] B. E. Rapp, “Chapter 10 - Conservation of Mass: The Continuity Equation,” in *Microfluidics: Modelling, Mechanics and Mathematics*, B. E. Rapp, Ed., in Micro and Nano Technologies. Oxford: Elsevier, 2017, pp. 265–271. doi: https://doi.org/10.1016/B978-1-4557-3141-1.50010-1.

[199] W. D. Nix, “Interface Stresses,” in *Encyclopedia of Materials: Science and Technology*, K. H. J. Buschow, R. W. Cahn, M. C. Flemings, B. Ilschner, E. J. Kramer, S. Mahajan, and P. Veyssière, Eds., Oxford: Elsevier, 2001, pp. 4136–4141. doi: https://doi.org/10.1016/B0-08-043152-6/00727-0.

[200] S. E. Bechtel and R. L. Lowe, “Chapter 3 - Kinematics: Motion and Deformation,” in *Fundamentals of Continuum Mechanics*, S. E. Bechtel and R. L. Lowe, Eds., Boston: Academic Press, 2015, pp. 75–114. doi: https://doi.org/10.1016/B978-0-12-394600-3.00003-4.

[201] S. E. Bechtel and R. L. Lowe, “Chapter 1 - What Is a Continuum?,” in *Fundamentals of Continuum Mechanics*, S. E. Bechtel and R. L. Lowe, Eds., Boston: Academic Press, 2015, pp. 3–4. doi: https://doi.org/10.1016/B978-0-12-394600-3.00001-0.

[202] J. Bergström, “4 - Continuum Mechanics Foundations,” in *Mechanics of Solid Polymers*, J. Bergström, Ed., William Andrew Publishing, 2015, pp. 131–207. doi: https://doi.org/10.1016/B978-0-323-31150-2.00004-2.

[203] C. D. Coman, “Kinematics,” in *Continuum Mechanics and Linear Elasticity: An Applied Mathematics Introduction*, Dordrecht: Springer Netherlands, 2020, pp. 121–160. doi: 10.1007/978-94-024-1771-5_2.

[204] C. D. Coman, *Compatibility of the Infinitesimal Deformation Tensor*, vol. 238. 2020. doi: 10.1007/978-94-024-1771-5_6.

[205] J. N. (Junuthula N. Reddy, *An introduction to continuum mechanics : with applications*. New York: Cambridge University Press, 2008.

[206] M. H. Sadd, "Chapter 4 - Force and Stress," in *Continuum Mechanics Modeling of Material Behavior*, M. H. Sadd, Ed., Academic Press, 2019, pp. 111–138. doi: https://doi.org/10.1016/B978-0-12-811474-2.00004-6.

[207] W. M. Lai, D. Rubin, and E. Krempl, "CHAPTER 4 - Stress and Integral Formulations of General Principles," in *Introduction to Continuum Mechanics (Fourth Edition)*, W. M. Lai, D. Rubin, and E. Krempl, Eds., Fourth Edi.Boston: Butterworth-Heinemann, 2010, pp. 155–200. doi: https://doi.org/10.1016/B978-0-7506-8560-3.00004-9.

[208] C. Multiphysics, *Introduction to COMSOL Multiphysics*. 2019.

[209] D. Masao, "Gel Dynamics," *J Physical Soc Japan*, vol. 78, no. 5, p. 52001, 2009, doi: 10.1143/JPSJ.78.052001.

[210] F. Horkay, M.-H. Han, I. S. Han, I.-S. Bang, and J. J. Magda, "Separation of the effects of pH and polymer concentration on the swelling pressure and elastic modulus of a pH-responsive hydrogel.," *Polymer (Guildf)*, vol. 47, no. 21, pp. 7335–7338, Oct. 2006, doi: 10.1016/j.polymer.2006.08.037.

[211] J.-P. Weiss, "Automatic Time Step and Order Selection in Time-Dependent Problems," *https://www.Comsol.Com/Blogs/Automatic-Time-Step-and-Order-Selection-in-Time-Dependent-Problems/*. p. 10, 2019.

[212] T. Tarpey, "A Note on the Prediction Sum of Squares Statistic for Restricted Least Squares," *Am Stat*, vol. 54, no. 2, pp. 116–118, 2000, doi: 10.1080/00031305.2000.10474522.

[213] D. J. Beebe *et al.*, "Functional hydrogel structures for autonomous flow control inside microfluidic channels.," *Nature*, vol. 404, no. 6778, pp. 588–590, Apr. 2000, doi: 10.1038/35007047.

[214] D. Vukajlovic, "Chitosan-Bioglass and chitosan-apatite-wollastonite composites for bone tissue engineering," Newcastle University, 2021.

[215] J. R. MITCHELL, "the Rheology of Gels," *J Texture Stud*, vol. 11, no. 4, pp. 315–337, 1980, doi: 10.1111/j.1745-4603.1980.tb01312.x.

[216] M. Djabourov, K. Nishinari, and S. B. Ross-Murphy, *Physical Gels from Biological and Synthetic Polymers*. Cambridge University Press, 2013. doi: 10.1017/CBO9781139024136.

[217] G. D. P. and I. B. Elisabetta Tranquillo, Federico Barrino, "Sol–Gel Synthesis of Silica-Based Materials with Different Percentages of PEG or PCL and High Chlorogenic Acid Content," *Materials*, vol. 12, no. 1, p. 12, 2019.

[218] H. Li, T. Y. Ng, Y. K. Yew, and K. Y. Lam, “Modeling and Simulation of the Swelling Behavior of pH-Stimulus-Responsive Hydrogels,” *Biomacromolecules*, vol. 6, no. 1, pp. 109–120, 2005, doi: 10.1021/bm0496458.

[219] S. S. Rao, “Chapter 5 - Derivation of Element Matrices and Vectors,” in *The Finite Element Method in Engineering (Sixth Edition)*, S. S. Rao, Ed., Sixth Edit.Butterworth-Heinemann, 2018, pp. 173–212. doi: https://doi.org/10.1016/B978-0-12-811768-2.00005-5.

[220] S. S. Rao, “Chapter 6 - Assembly of Element Matrices and Vectors, and Derivation of System Equations,” in *The Finite Element Method in Engineering (Sixth Edition)*, S. S. Rao, Ed., Sixth Edit.Butterworth-Heinemann, 2018, pp. 213–256. doi: https://doi.org/10.1016/B978-0-12-811768-2.00006-7.

[221] S. S. Rao, “Chapter 7 - Numerical Solution of Finite Element Equations,” in *The Finite Element Method in Engineering (Sixth Edition)*, S. S. Rao, Ed., Sixth Edit.Butterworth-Heinemann, 2018, pp. 257–292. doi: https://doi.org/10.1016/B978-0-12-811768-2.00007-9.

[222] T. Sakai, “Swelling and Deswelling,” in *Physics of Polymer Gels*, Wiley, 2020, pp. 77–107. doi: 10.1002/9783527346547.ch4.

[223] Anton Paar, “The principles of dynamic light scattering,” *International Organization for Standarization*, p. 2020, 2020, [Online]. Available: https://wiki.anton-paar.com/in-en/the-principles-of-dynamic-light-scattering/%0Ahttps://wiki.anton-paar.com/us-en/the-principles-of-dynamic-light-scattering/%0Ahttps://wiki.anton-paar.com/en/the-principles-of-dynamic-light-scattering/%0Ahttps://wiki.anton

[224] A. Alizadeh, C. A. Nieto de Castro, and W. A. Wakeham, “The theory of the Taylor dispersion technique for liquid diffusivity measurements,” *Int J Thermophys*, vol. 1, no. 3, pp. 243–284, 1980, doi: 10.1007/BF00517126.

[225] F. Horkay, M. H. Han, I. S. Han, I. S. Bang, and J. J. Magda, “Separation of the effects of pH and polymer concentration on the swelling pressure and elastic modulus of a pH-responsive hydrogel,” *Polymer (Guildf)*, vol. 47, no. 21, pp. 7335–7338, Oct. 2006, doi: 10.1016/j.polymer.2006.08.037.

[226] C. W. Pyun and M. Fixman, “Frictional coefficient of polymer molecules in solution,” *J Chem Phys*, vol. 41, no. 4, pp. 937–944, 1964, doi: 10.1063/1.1726036.

APPENDIX I

GALERKIN FINITE ELEMENT FORMULATION APPLIED TO HYDROGEL DEFORMATION

I.1 General Concept

Suppose a 1D problem modelled as a differential equation takes the form:

$$f(\varphi) = g, \qquad 0 \leq x \leq 1$$

subject to the boundary conditions $\varphi(0) = 0,\ \varphi(1) = a$

Let us divide the domain of the equation using line elements with linear interpolation model and apply the various steps of the FEM to find the solution.

Procedure:

For the Galerkin Finite Element technique,

$$\sum_{e=1}^{E} \int_{x_i}^{x_j} [N^e]^T . R^{(e)} dx = 0$$

where

R is the residual defined as:

$$R = [f\left(\underline{\varphi}\right) - g]$$

Step1: Let us discretize the domain ($x = 0\ to\ x = 1$) using (a) three nodes and two elements of equal length and (b) four nodes and three elements.

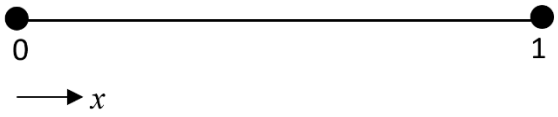

Figure I1: Solution domain

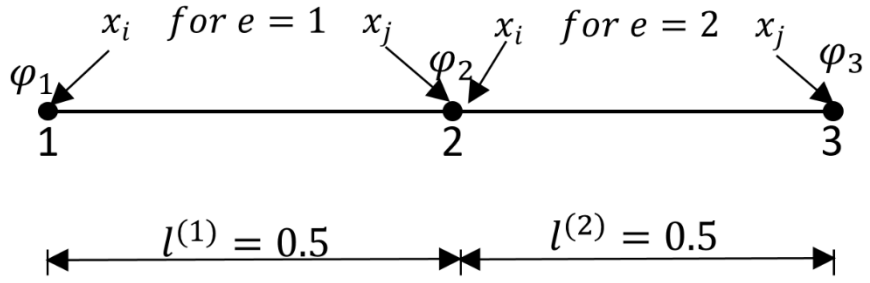

$$\vec{\boldsymbol{\varphi}}^{\mathbf{1}} = \begin{Bmatrix} \varphi_i^{(1)} \\ \varphi_j^{(1)} \end{Bmatrix} = \begin{Bmatrix} \varphi_1 \\ \varphi_2 \end{Bmatrix};\ \vec{\boldsymbol{\varphi}}^{\mathbf{2}} = \begin{Bmatrix} \varphi_i^{(2)} \\ \varphi_j^{(2)} \end{Bmatrix} = \begin{Bmatrix} \varphi_2 \\ \varphi_3 \end{Bmatrix}$$

Figure I1(a) Two element discretized domain [219]

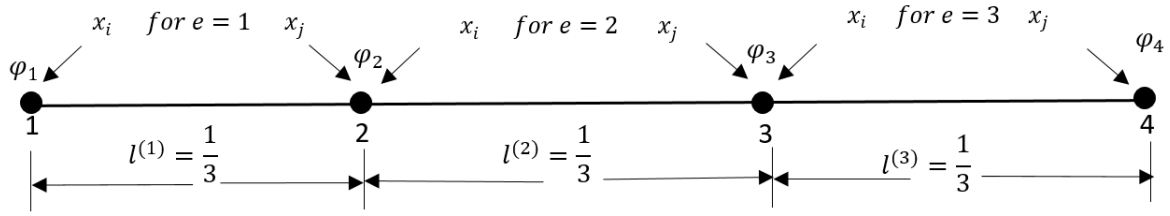

$$\vec{\boldsymbol{\varphi}}^{\mathbf{1}} = \begin{Bmatrix} \varphi_i^{(1)} \\ \varphi_j^{(1)} \end{Bmatrix} = \begin{Bmatrix} \varphi_1 \\ \varphi_2 \end{Bmatrix};\ \vec{\boldsymbol{\varphi}}^{\mathbf{2}} = \begin{Bmatrix} \varphi_i^{(2)} \\ \varphi_j^{(2)} \end{Bmatrix} = \begin{Bmatrix} \varphi_2 \\ \varphi_3 \end{Bmatrix};\ \vec{\boldsymbol{\varphi}}^{\mathbf{3}} = \begin{Bmatrix} \varphi_i^{(3)} \\ \varphi_j^{(3)} \end{Bmatrix} = \begin{Bmatrix} \varphi_3 \\ \varphi_4 \end{Bmatrix}$$

Figure I1(b) Two element discretized domain [219]

Step2: Assume a linear interpolation model within element e for variation of the field variable, that is:

$$\varphi(x) = [N(x)]\vec{\boldsymbol{\varphi}}^{\boldsymbol{e}} = N_i(\boldsymbol{x})\varphi_i^{(e)} + N_j(\boldsymbol{x})\varphi_j^{(e)}$$

where

$N_i(x) = \frac{x_j - x}{l^{(e)}}$,

$N_j(x) = \frac{x - x_i}{l^{(e)}}$,

$\vec{\boldsymbol{\varphi}}^{(\boldsymbol{e})} = \begin{Bmatrix} \varphi_i^{(e)} \\ \varphi_j^{(e)} \end{Bmatrix}$ is the vector of nodal unknowns or degrees of freedom

$l^{(e)}$ is the elemental length, $\varphi_i^{(e)}$ and $\varphi_j^{(e)}$ are the values of $\varphi(x)$ at the nodes $i(x = x_i)$ and $j(x = x_j)$, respectively; and *i* and *j* are the first and second (global) nodes of the element e.

I.2 Application to Hydrogel Deformation

The mathematical model describing the diffusion and migration of ions across the hydrogel and its environment is the Poisson Nernst Planck (PNP) given as:

$$\frac{\partial^2 C_i}{\partial x^2} + \frac{\mu_i F z_i}{D_i}\frac{\partial C_i}{\partial x}\frac{\partial \varphi}{\partial x} - \frac{F z_i C_i}{D_i}\left\{\frac{F}{\varepsilon \varepsilon_0}\left(\sum z_i C_i + z_f C_f\right)\right\}$$

i = 1, 2, 3 (I-1)

subject to the boundary conditions

$$\frac{\partial C_i(0)}{\partial x} = 0,\ \frac{\partial \varphi(0)}{\partial x} = 0,$$
$$C_i(L) = C_{i0},\ \varphi(L)=0$$

(I-2)

where

$$C_f = \frac{K_a C_{mo}^s}{H(K_a + CH^+)}$$

(I-3)

The discretized domain is shown in Figure I2, below:

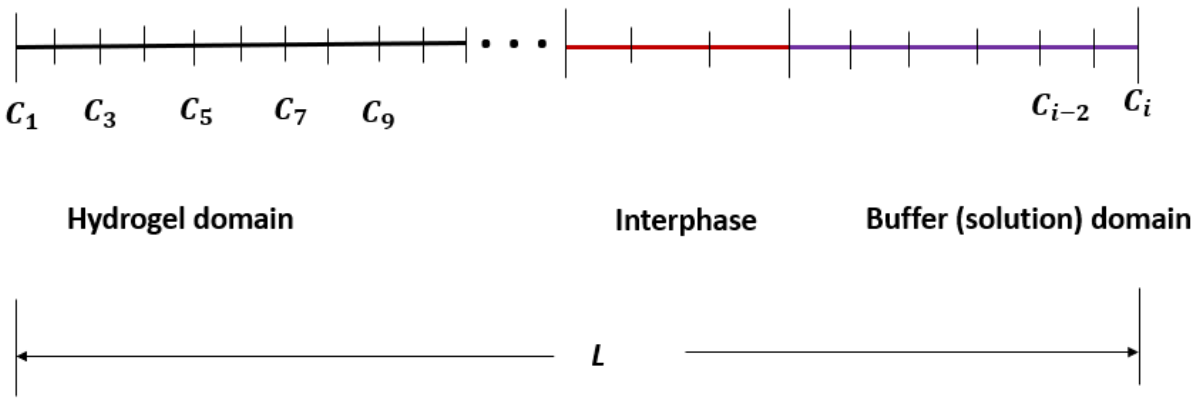

Figure I2: Discretized domain for hydrogel, gel-solution interphase, and the solution

The Galerkin technique requires that:

$$\iiint R^{(e)} N_j^{(e)} dV^{(e)} = 0,$$

$$j = 1, 2, 3, \ldots, n \tag{I-4}$$

where the residue:

$$R = \left(\frac{\partial^2 C_i}{\partial x^2} + \frac{\mu_i F z_i}{D_i} \frac{\partial C_i}{\partial x} \frac{\partial \varphi}{\partial x} - \frac{F z_i C_i}{D_i} \left\{ \frac{F}{\varepsilon \varepsilon_0} \left(\sum z_i C_i + z_f C_f \right) \right\} \right) \tag{I-5}$$

For a 1D problem, we have that:

$$\int_0^L R N_k(x) dx = 0$$

$$k = i, j \tag{I-6}$$

or

$$\sum_{e=1}^{E} \int_{x_i}^{x_j} \left[N^{(e)} \right]^T R^{(e)} dx = 0 \tag{I-7}$$

where

E is the number of elements, and x_i and x_j are the values of *x* at the first and the second nodes of element e, respectively.

Assuming a linear variation of concentration of each species in solution, C_i within each finite element, that is:

$$C_i^{(e)}(x) = N_k(x) C_k^{(e)} + N_{k+1}(x) C_{k+1}^{(e)} \tag{I-8}$$

where

$$N^{(e)} = [N_k(x) \;\; N_{k+1}(x)] \tag{I-9}$$

and

$$N_k(x) = (x_{k+1} - x)/l^{(e)} \tag{I-10}$$

$$N_{k+1}(x) = (x - x_k)/l^{(e)} \tag{I-11}$$

I.2.1 *Hydrogel domain*

Evaluating Eq.(I-7), for an element within the hydrogel domain gives:

$$\int_{x_k}^{x_{k+1}} \left[N^{(e)}\right]^T \left(\frac{\partial^2 C_i^{(e)}}{\partial x^2} + \frac{\mu_i F z_i}{D_i} \frac{\partial C_i^{(e)}}{\partial x} \frac{\partial \varphi^{(e)}}{\partial x} - \frac{F z_i C_i^{(e)}}{D_i} \left\{ \frac{F}{\varepsilon \varepsilon_0} \left(\sum z_i C_i^{(e)} + z_f C_f \right) \right\} \right) dx \tag{I-12}$$

Expanding the integral gives:

$$\int_{x_k}^{x_{k+1}} \left[N^{(e)}\right]^T \frac{\partial^2 C_i^{(e)}}{\partial x^2} dx + \frac{\mu_i F z_i}{D_i} \int_{x_k}^{x_{k+1}} \left[N^{(e)}\right]^T \frac{\partial C_i^{(e)}}{\partial x} \frac{\partial \varphi^{(e)}}{\partial x} dx - \frac{F^2 z_i}{\varepsilon \varepsilon_0 D_i} \int_{x_k}^{x_{k+1}} \left[N^{(e)}\right]^T C_i^{(e)} \left(\sum z_i C_i^{(e)} + z_f C_f \right) dx \tag{I-13}$$

Applying integration by parts to Eq. (I-13) gives, the first term:

$$\int_{x_k}^{x_{k+1}} \left[N^{(e)}\right]^T \frac{\partial^2 C_i^{(e)}}{\partial x^2} dx = \left[N^{(e)}\right]^T \frac{\partial C_i^{(e)}}{\partial x} \Big|_{x_k}^{x_{k+1}} - \int_{x_k}^{x_{k+1}} \frac{\partial \left[N^{(e)}\right]^T}{\partial x} \frac{\partial C_i^{(e)}}{\partial x} dx \tag{I-14}$$

second term:

$$\frac{\mu_i F z_i}{D_i} \int_{x_k}^{x_{k+1}} \left[N^{(e)}\right]^T \frac{\partial C_i^{(e)}}{\partial x} \frac{\partial \varphi^{(e)}}{\partial x} dx = \frac{\mu_i F z_i}{D_i} \int_{x_k}^{x_{k+1}} \left[N^{(e)}\right]^T \frac{\partial C_i^{(e)}}{\partial x} \left\{ -\frac{F}{\varepsilon \varepsilon_0} \int_{x_k}^{x_{k+1}} \left(\sum z_i C_i^{(e)} + z_f C_f \right) \right\} dx \tag{I-15}$$

third term:

$$-\frac{F^2 z_i}{\varepsilon \varepsilon_0 D_i} \int_{x_k}^{x_{k+1}} \left[N^{(e)}\right]^T C_i^{(e)} \left(\sum z_i C_i^{(e)} + z_f C_f \right) dx \tag{I-16}$$

I.2.2 *Hydrogel-Buffer interface domain*

For an element within the interface (assuming linear variation of $C_i^{(e)}$ with Heaviside function for smoothing the sharp concentration gradient).

Recall Eq. (I-12);

$$\int_{x_k}^{x_{k+1}} \left[N^{(e)}\right]^T \left(\frac{\partial^2 C_i^{(e)}}{\partial x^2} + \frac{\mu_i F z_i}{D_i} \frac{\partial C_i^{(e)}}{\partial x} \frac{\partial \varphi^{(e)}}{\partial x} - \frac{F z_i C_i^{(e)}}{D_i} \left\{ \frac{F}{\varepsilon \varepsilon_0} \left(\sum z_i C_i^{(e)} + z_f C_f \right) \right\} \right) dx$$

The concentration of the fixed charge drops from an initial value of C_s^{mo} inside the gel to a value of zero at the boundary of the gel. Thus, we assume $C_f = 0$ at the interface. Hence, Eq. (I-12) becomes:

$$\int_{x_{k_I}}^{x_{k_I+1}} \left[N_I^{(e)}\right]^T \left(\frac{\partial^2 C_i^{(e)}}{\partial x^2} + \frac{\mu_i F z_i}{D_i} \frac{\partial C_i^{(e)}}{\partial x} \frac{\partial \varphi^{(e)}}{\partial x} - \frac{F z_i C_i^{(e)}}{D_i} \left\{ \frac{F}{\varepsilon \varepsilon_0} \sum z_i C_i^{(e)} \right\} \right) dx \tag{I-17}$$

The integration above gives for the first term:

$$\left[N_I^{(e)}\right]^T \frac{\partial C_i^{(e)}}{\partial x} \Big|_{x_{k_I}}^{x_{k_I+1}} - \int_{x_{k_I}}^{x_{k_I+1}} \frac{\partial \left[N_I^{(e)}\right]^T}{\partial x} \frac{\partial C_i^{(e)}}{\partial x} dx \tag{I-18}$$

second term:

$$-\frac{\mu_i F^2 z_i}{\varepsilon \varepsilon_0 D_i} \int_{x_{k_I}}^{x_{k_I+1}} \left[N_I^{(e)}\right]^T \frac{\partial C_i^{(e)}}{\partial x} \left\{ \int_{x_{k_I}}^{x_{k_I+1}} \sum z_i C_i^{(e)} \right\} dx \tag{I-19}$$

third term

$$-\frac{\mu_i F^2 z_i}{\varepsilon \varepsilon_0 D_i} \int_{x_{k_I}}^{x_{k_I+1}} \left[N_I^{(e)}\right]^T C_i^{(e)} \left\{ \int_{x_{k_I}}^{x_{k_I+1}} \sum z_i C_i^{(e)} \right\} dx \tag{I-20}$$

I.2.3 *Buffer domain*

Similarly, for an element within the buffer domain, the integrals are:

first term:

$$\left[N_B^{(e)}\right]^T \frac{\partial C_i^{(e)}}{\partial x} \Big|_{x_{k_B}}^{x_{k_B+1}} - \int_{x_{k_B}}^{x_{k_B+1}} \frac{\partial \left[N_B^{(e)}\right]^T}{\partial x} \frac{\partial C_i^{(e)}}{\partial x} dx$$

(I-21)

second term:

$$-\frac{\mu_i F^2 z_i}{\varepsilon\varepsilon_0 D_i}\int_{x_B}^{x_{k_B+1}}\left[N_B^{(e)}\right]^T\frac{\partial C_i^{(e)}}{\partial x}\left\{\int_{x_{k_B}}^{x_{k_B+1}}\sum z_i C_i^{(e)}\right\}dx$$

(I-22)

third term

$$-\frac{\mu_i F^2 z_i}{\varepsilon\varepsilon_0 D_i}\int_{x_{k_B}}^{x_{k_B+1}}\left[N_B^{(e)}\right]^T C_i^{(e)}\left\{\int_{x_{k_I}}^{x_{k_I+1}}\sum z_i C_i^{(e)}\right\}dx$$

(I-23)

I.2.4 *Evaluation of the integral for the hydrogel domain*

The integrals are all evaluated as follows:

$$\frac{\partial\left[N^{(e)}\right]^T}{\partial x}=\frac{d}{dx}\begin{Bmatrix}(x_{k+1}-x)/l^{(e)}\\(x-x_k)/l^{(e)}\end{Bmatrix}=\frac{1}{l^{(e)}}\begin{Bmatrix}-1\\1\end{Bmatrix}$$

(I-24)

$$\frac{\partial C_i^{(e)}}{\partial x}=\frac{d}{dx}\left(\left[N^{(e)}\right]\vec{C}_i^{(e)}\right)=\vec{C}_i^{(e)}\frac{d}{dx}\left[N^{(e)}\right]=\frac{1}{l^{(e)}}\begin{bmatrix}-1 & 1\end{bmatrix}\begin{Bmatrix}C_{i,k}^{(e)}\\C_{i,k+1}^{(e)}\end{Bmatrix}$$

(25)

Using Eq. (I-24) and Eq. (I-25), Eq.(I-14) can be rewritten as:

$$\begin{aligned}
&\int_{x_k}^{x_{k+1}}\left[N^{(e)}\right]^T\frac{\partial^2 C_i^{(e)}}{\partial x^2}dx\\
&\quad=\left[N^{(e)}\right]^T\frac{\partial C_i^{(e)}}{\partial x}\Big|_{x_k}^{x_{k+1}}-\int_{x_k}^{x_{k+1}}\left(\left[\frac{1}{l^{(e)}}\begin{Bmatrix}-1\\1\end{Bmatrix}\right].\left[\frac{1}{l^{(e)}}\begin{bmatrix}-1 & 1\end{bmatrix}\begin{Bmatrix}C_{i,k}^{(e)}\\C_{i,k+1}^{(e)}\end{Bmatrix}\right]\right)dx\\
&\quad=\left[N^{(e)}\right]^T\frac{\partial C_i^{(e)}}{\partial x}\Big|_{x_k}^{x_{k+1}}-\frac{1}{(l^{(e)})^2}\int_{x_k}^{x_{k+1}}\begin{bmatrix}1 & -1\\-1 & 1\end{bmatrix}\begin{bmatrix}C_{i,k}^{(e)}\\C_{i,k+1}^{(e)}\end{bmatrix}dx\\
&\quad=\left[N^{(e)}\right]^T\frac{\partial C_i^{(e)}}{\partial x}\Big|_{x_k}^{x_{k+1}}-\frac{1}{(l^{(e)})^2}.\begin{bmatrix}1 & -1\\-1 & 1\end{bmatrix}\begin{bmatrix}C_{i,k}^{(e)}\\C_{i,k+1}^{(e)}\end{bmatrix}.\int_{x_k}^{x_{k+1}}1dx\\
&\quad=\left[N^{(e)}\right]^T\frac{\partial C_i^{(e)}}{\partial x}\Big|_{x_k}^{x_{k+1}}-\frac{1}{(l^{(e)})^2}.\begin{bmatrix}1 & -1\\-1 & 1\end{bmatrix}\begin{bmatrix}C_{i,k}^{(e)}\\C_{i,k+1}^{(e)}\end{bmatrix}.(x_{k+1}-x_k)
\end{aligned}$$

(I-26)

The first term in Eq. (I-26) contributes to the assembled vector $\vec{P}$ if only the derivatives $(\partial C_i/\partial x)$ at the nodal points are specified otherwise they are neglected [219]. At $x_k = 0$, there are no flux conditions, and since the values of the directives at nodal points is unknown, the first term is ignored. Hence Eq. (I-26) becomes:

$$\int_{x_k}^{x_{k+1}} \left[N^{(e)}\right]^T \frac{\partial^2 C_i^{(e)}}{\partial x^2} dx = \frac{1}{l^{(e)}} \begin{bmatrix} 1 & -1 \\ -1 & 1 \end{bmatrix} \begin{bmatrix} C_{i,k}^{(e)} \\ C_{i,k+1}^{(e)} \end{bmatrix}$$

(I-27)

Rewriting Eq. (I-15) incorporating the integrals yield:

$$\frac{\mu_i F z_i}{D_i} \int_{x_k}^{x_{k+1}} \left[N^{(e)}\right]^T \frac{\partial C_i^{(e)}}{\partial x} \frac{\partial \varphi^{(e)}}{\partial x} dx$$
$$= \frac{\mu_i F z_i}{D_i} \int_{x_k}^{x_{k+1}} \left(\begin{Bmatrix} (x_{k+1} - x)/l^{(e)} \\ (x - x_k)/l^{(e)} \end{Bmatrix} \cdot \left\{ \frac{1}{l^{(e)}} [-1 \quad 1] \begin{Bmatrix} C_{i,k}^{(e)} \\ C_{i,k+1}^{(e)} \end{Bmatrix} \right\} \cdot \left\{ -\frac{F}{\varepsilon \varepsilon_0} \int_{x_k}^{x_{k+1}} \left(\sum z_i C_i + z_f C_f \right) \right\} \right) dx$$

(I-28)

where

$$\int_{x_k}^{x_{k+1}} \left(\sum z_i C_i + z_f C_f \right) = \int_{x_k}^{x_{k+1}} \left(\sum z_i C_i + z_f C_f \right) dx = \left(\sum z_i C_i + z_f C_f \right) \int_{x_k}^{x_{k+1}} 1 dx$$
$$= \left(\sum z_i C_i + z_f C_f \right) l^{(e)}$$

(I-29)

From the conservation of total mass/charge, it has been assumed that the total concentration of the ions in the whole domain is constant.

Eq. (I-28) rewritten as:

$$\frac{\mu_i F z_i}{D_i}\int_{x_k}^{x_{k+1}}\left[N^{(e)}\right]^T\frac{\partial C_i^{(e)}}{\partial x}\frac{\partial \varphi^{(e)}}{\partial x}dx$$

$$=\frac{\mu_i F z_i}{D_i}\int_{x_k}^{x_{k+1}}\left(\begin{Bmatrix}(x_{k+1}-x)/l^{(e)}\\(x-x_k)/l^{(e)}\end{Bmatrix}\cdot\left\{\frac{1}{l^{(e)}}\begin{bmatrix}-1 & 1\end{bmatrix}\begin{Bmatrix}C_{i,k}^{(e)}\\C_{i,k+1}^{(e)}\end{Bmatrix}\right\}\right.$$

$$\left.\cdot\left\{-\frac{F}{\varepsilon\varepsilon_0}\left(\sum z_i C_i+z_f C_f\right)l^{(e)}\right\}\right)dx$$

$$=\frac{\mu_i F^2 z_i l^{(e)}}{2\varepsilon\varepsilon_0 D_i}\left\{\left(\sum z_i C_i+z_f C_f\right)\begin{bmatrix}1 & -1\\1 & -1\end{bmatrix}\begin{Bmatrix}C_{i,k}^{(e)}\\C_{i,k+1}^{(e)}\end{Bmatrix}\right\}$$

(I-30)

Revisiting Eq.(I-16) incorporating the integrals give:

$$-\frac{F^2 z_i}{\varepsilon\varepsilon_0 D_i}\int_{x_k}^{x_{k+1}}\left[N^{(e)}\right]^T C_i^{(e)}\left(\sum z_i C_i+z_f C_f\right)dx$$

$$=-\frac{F^2 z_i}{\varepsilon\varepsilon_0 D_i}\int_{x_k}^{x_{k+1}}\left[N^{(e)}\right]^T\left[N^{(e)}\right]\vec{C}_i^{(e)}\left(\sum z_i C_i+z_f C_f\right)dx$$

$$=-\frac{F^2 z_i l^{(e)}}{6\varepsilon\varepsilon_0 D_i}\left(\sum z_i C_i+z_f C_f\right)\begin{bmatrix}2 & 1\\1 & 2\end{bmatrix}\begin{Bmatrix}C_{i,k}^{(e)}\\C_{i,k+1}^{(e)}\end{Bmatrix}$$

(I-31)

Therefore, the element characteristic matrix for the hydrogel domain obtained from the combination of Eq. (I-27), Eq. (I-30) and Eq. (I-31) is:

$$\left[K_H^{(e)}\right]=\frac{1}{l_H^{(e)}}\begin{bmatrix}1 & -1\\-1 & 1\end{bmatrix}+\frac{\mu_i F^2 z_i l_H^{(e)}}{2\varepsilon\varepsilon_0 D_i}\left\{\left(\sum z_i C_i+z_f C_f\right)\begin{bmatrix}1 & -1\\1 & -1\end{bmatrix}\right\}$$

$$-\frac{F^2 z_i l_H^{(e)}}{6\varepsilon\varepsilon_0 D_i}\left(\sum z_i C_i+z_f C_f\right)\begin{bmatrix}2 & 1\\1 & 2\end{bmatrix}$$

(I-32)

I.2.5 *Evaluation of the integral for the interface and buffer domains*

The finite element equation for the hydrogel/buffer interface, Eq. (I-26) is:

$$\left[N_I^{(e)}\right]^T\frac{\partial C_i^{(e)}}{\partial x}\Big|_{x_{k_I}}^{x_{k_I+1}}-\left[K_I^{(e)}\right]$$

(I-33)

where the characteristic matrix $\left[K_I^{(e)}\right]$, is:

$$\left[K_I^{(e)}\right] = \int_{x_{k_I}}^{x_{k_I+1}} \frac{\partial\left[N_I^{(e)}\right]^T}{\partial x}\frac{\partial C_i^{(e)}}{\partial x}\,dx$$

(I-34)

Following similar procedure for the hydrogel domain with $C_f = 0$ at the interface, the element characteristic matrix for the interface is:

$$\left[K_I^{(e)}\right] = \frac{1}{l_I^{(e)}}\begin{bmatrix}1 & -1\\ -1 & 1\end{bmatrix} + \frac{\mu_i F^2 z_i l_I^{(e)}}{2\varepsilon\varepsilon_0 D_i}\left\{\sum z_i C_i \begin{bmatrix}1 & -1\\ 1 & -1\end{bmatrix}\right\} - \frac{F^2 z_i l_I^{(e)}}{6\varepsilon\varepsilon_0 D_i}\sum z_i C_i \begin{bmatrix}2 & 1\\ 1 & 2\end{bmatrix}$$

(I-35)

Similarly, for an element within the buffer domain, the characteristic matrix is:

$$\left[K_B^{(e)}\right] = \frac{1}{l_B^{(e)}}\begin{bmatrix}1 & -1\\ -1 & 1\end{bmatrix} + \frac{\mu_i F^2 z_i l_B^{(e)}}{2\varepsilon\varepsilon_0 D_i}\left\{\sum z_i C_i \begin{bmatrix}1 & -1\\ 1 & -1\end{bmatrix}\right\} - \frac{F^2 z_i l_B^{(e)}}{6\varepsilon\varepsilon_0 D_i}\sum z_i C_i \begin{bmatrix}2 & 1\\ 1 & 2\end{bmatrix}$$

(I-36)

Accounting for the sharp concentration gradient of each species within the hydrogel/buffer interface will require that the left-hand side of Eq. (I-33) be evaluated for the element characteristic vector. Therefore, the LHS of Eq. (I-33) becomes:

$$\begin{aligned}\left[N_I^{(e)}\right]^T \frac{\partial C_i^{(e)}}{\partial x}\Big|_{x_{k_I}}^{x_{k_I+1}} &= \begin{Bmatrix}(x_{k+1}-x)/l_I^{(e)}\\ (x-x_k)/l_I^{(e)}\end{Bmatrix}\cdot \vec{C}_i^{(e)}\frac{d}{dx}\left[N^{(e)}\right]\\ &= \begin{Bmatrix}(x_{k+1}-x)/l_I^{(e)}\\ (x-x_k)/l_I^{(e)}\end{Bmatrix}\cdot\frac{1}{l_I^{(e)}}\begin{bmatrix}-1 & 1\end{bmatrix}\begin{Bmatrix}C_{i,k}^{(e)}\\ C_{i,k+1}^{(e)}\end{Bmatrix}\\ &= \left\{\begin{Bmatrix}(x_{k+1}-x)/l_I^{(e)}\\ (x-x_k)/l_I^{(e)}\end{Bmatrix}\cdot\frac{1}{l_I^{(e)}}\begin{bmatrix}-1 & 1\end{bmatrix}\begin{Bmatrix}C_{i,k}^{(e)}\\ C_{i,k+1}^{(e)}\end{Bmatrix}\right\}\Big|_{x_{k_I}}^{x_{k_I+1}}\end{aligned}$$

(I-37)

Normalizing the concentrations of all species, and introducing a Heaviside step function to smoothen the sharp concentration gradient in the interface transforms Eq. (I-37) to:

$$\left[N_I^{(e)}\right]^T \frac{\partial C_i^{(e)}}{\partial x}\Big|_{x_{k_I}}^{x_{k_I+1}} = \begin{Bmatrix}(x_{k+1}-x)/l_I^{(e)} \\ (x-x_k)/l_I^{(e)}\end{Bmatrix} \cdot \frac{1}{l_I^{(e)}} [-1 \quad 1] \begin{Bmatrix} \frac{1}{(1+e^{-x_k})} \\ \frac{1}{(1+e^{-x_{k+1}})}\end{Bmatrix} \Big|_{x_{k_I}}^{x_{k_I+1}} \cdot C_{io}$$

(I-38)

where C_{io}, is the reference concentration of species i.

Rewriting Eq. (I-7) as a system of algebraic equations gives the hydrogel/buffer system equation as:

$$\sum_{e=1}^{E} [K^e] \underline{C_i}^{(e)}(x) = \sum_{e=1}^{E} \vec{P}^{(e)}$$

(I-39)

where

$$[K^e] = \left[K_H^{(e)}\right] + \left[K_I^{(e)}\right] + \left[K_B^{(e)}\right];$$

$\underline{C_i}^{(e)}(x)$ is the element normalized concentration defined as:

$$\underline{C_i}^{(e)}(x) = \frac{C_i^{(e)}}{C_{io}}$$

(I-40)

$\vec{P}^{(e)}$ the element characteristic vector given by:

$$\vec{P}^{(e)} = \left\{ \begin{Bmatrix}(x_{k+1}-x)/l_I^{(e)} \\ (x-x_k)/l_I^{(e)}\end{Bmatrix} \cdot \frac{1}{l_I^{(e)}} [-1 \quad 1] \begin{Bmatrix} \frac{1}{(1+e^{-x_k})} \\ \frac{1}{(1+e^{-x_{k+1}})}\end{Bmatrix} \right\} \Big|_{x_{k_I}}^{x_{k_I+1}}$$

$$= -\frac{1}{l_I^{(e)}} \begin{Bmatrix} \frac{1}{(1+e^{-x_k})} - \frac{1}{(1+e^{-x_{k+1}})} \\ \frac{1}{(1+e^{-x_k})} - \frac{1}{(1+e^{-x_{k+1}})}\end{Bmatrix}$$

(I-41)

I.3 Mechanical Equation for the Deformation of the Hydrogel

The governing mechanical equation for the one-dimensional hydrogel deformation is:

$$(\lambda + 2\mu)\left[\frac{d^2u}{dX^2} + 3\frac{du}{dX}\left(\frac{d^2u}{dX^2}\right) + \frac{3}{2}\left(\frac{du}{dX}\right)^2\frac{d^2u}{dX^2}\right] - \frac{dP_{osmotic}}{dX} = 0 \tag{I-42}$$

where

$$P_{osmotic} = RT\sum(C_{k,gel} - C_{k,sol}) \tag{I-43}$$

The Lamé elastic constants are:

$$\lambda = \frac{\nu E}{(1+\upsilon)(1-2\upsilon)} \text{ and } \mu = \frac{E}{2(1+\upsilon))}$$

where E is the Modulus of elasticity and υ is the Poisson ratio.

Like Eqn. (I-5), the residue is:

$$R = \left((\lambda + 2\mu)\left[\frac{d^2u}{dX^2} + 3\frac{du}{dX}\left(\frac{d^2u}{dX^2}\right) + \frac{3}{2}\left(\frac{du}{dX}\right)^2\frac{d^2u}{dX^2}\right] - \frac{dP_{osmotic}}{dX}\right) \tag{I-44}$$

The discretized displacement of the hydrogel is:

$$u^{(e)}(x) = [N^{(e)}(x)]\vec{u}^{(e)}$$

1where the shape function $N^{(e)}$ had been defined earlier in Eqn. (I-9) as:

$$N^{(e)} = [N_k(x)\ \ N_{k+1}(x)]$$

and

$$N_k(x) = (x_{k+1} - x)/l^{(e)}$$

$$N_{k+1}(x) = (x - x_k)/l^{(e)}$$

Displacement across the whole hydrogel domain is obtained from the Galerkin formulation:

$$\sum_{e=1}^{E}\int_{x_i}^{x_j}\left[N^{(e)}\right]^T\left((\lambda + 2\mu)\left[\frac{d^2u^{(e)}}{dX^2} + 3\frac{du^{(e)}}{dX}\left(\frac{d^2u^{(e)}}{dX^2}\right) + \frac{3}{2}\left(\frac{du^{(e)}}{dX}\right)^2\frac{d^2u^{(e)}}{dX^2}\right] - \frac{dP_{osmotic}^{(e)}}{dX}\right)dX = 0 \tag{I-45}$$

Evaluating Eq.(I-45), for an element within the hydrogel domain gives:

$$\int_{x_k}^{x_{k+1}} \left[N^{(e)}\right]^T \left((\lambda + 2\mu) \left[\frac{d^2u^{(e)}}{dX^2} + 3\frac{du^{(e)}}{dX}\left(\frac{d^2u^{(e)}}{dX^2}\right) + \frac{3}{2}\left(\frac{du^{(e)}}{dX}\right)^2 \frac{d^2u^{(e)}}{dX^2} \right] - \frac{dP_{osmotic}^{(e)}}{dX} \right) dX$$

Examining the integral term by term gives:

$$k_1^{(e)} = (\lambda + 2\mu) \int_{X_k}^{X_{k+1}} \left[N^{(e)}\right]^T \frac{d^2u^{(e)}}{dX^2} dX \tag{I-46}$$

$$k_2^{(e)} = (\lambda + 2\mu) \int_{X_k}^{X_{k+1}} \left[N^{(e)}\right]^T . 3\frac{du^{(e)}}{dX}\left(\frac{d^2u^{(e)}}{dX^2}\right) dX \tag{I-47}$$

$$k_3^{(e)} = (\lambda + 2\mu) \int_{x_k}^{x_{k+1}} \left[N^{(e)}\right]^T . \frac{3}{2}\left(\frac{du^{(e)}}{dX}\right)^2 \frac{d^2u^{(e)}}{dX^2} dX \tag{I-48}$$

$$\vec{p}^{(e)} = (\lambda + 2\mu) \int_{x_k}^{x_{k+1}} \left[N^{(e)}\right]^T . - \frac{dP_{osmotic}^{(e)}}{dX} dX \tag{I-49}$$

Applying integration by parts to Eqn. (I-46) gives:

$$k_1^{(e)} = (\lambda + 2\mu) \left(\left[N^{(e)}\right]^T \frac{du^{(e)}}{dX} \Big|_{X_k}^{X_{k+1}} - \int_{X_k}^{X_{k+1}} \frac{d\left[N^{(e)}\right]^T}{dX} \frac{du^{(e)}}{dX} dX \right) \tag{I-50}$$

Integrating Eqn. (I-47) by parts gives Eqn. (I-52):

$$\int_{X_k}^{X_{k+1}} \left[N^{(e)}\right]^T . \frac{du^{(e)}}{dX}\left(\frac{d^2u^{(e)}}{dX^2}\right) dX$$

$$= \left[N^{(e)}\right]^T . \left(\frac{du^{(e)}}{dX}\right)^2 \Big|_{X_k}^{X_{k+1}}$$

$$- \int_{X_k}^{X_{k+1}} \frac{du^{(e)}}{dX}\left(\left[N^{(e)}\right]^T \frac{d^2u^{(e)}}{dX^2} + \frac{d\left[N^{(e)}\right]^T}{dX}\frac{du^{(e)}}{dX}\right)$$

$$= \left[N^{(e)}\right]^T . \left(\frac{du^{(e)}}{dX}\right)^2 \Big|_{X_k}^{X_{k+1}}$$

$$- \int_{X_k}^{X_{k+1}} \left[\left[N^{(e)}\right]^T \frac{du^{(e)}}{dX}\left(\frac{d^2u^{(e)}}{dX^2}\right) + \frac{d\left[N^{(e)}\right]^T}{dX}\left(\frac{du^{(e)}}{dX}\right)^2\right] dX$$

Expanding the above and collecting like terms give:

$$\int_{X_k}^{X_{k+1}} \left[N^{(e)}\right]^T . \frac{du^{(e)}}{dX}\left(\frac{d^2u^{(e)}}{dX^2}\right) dX$$

$$= \frac{1}{2}\left[N^{(e)}\right]^T . \left(\frac{du^{(e)}}{dX}\right)^2 \Big|_{X_k}^{X_{k+1}} - \frac{1}{2}\int_{X_k}^{X_{k+1}} \frac{d\left[N^{(e)}\right]^T}{dX}\left(\frac{du^{(e)}}{dX}\right)^2$$

(I-51)

Therefore, Eqn. (I-47) becomes:

$$k_2^{(e)} = (\lambda + 2\mu) \int_{X_k}^{X_{k+1}} \left[N^{(e)}\right]^T . 3\frac{du^{(e)}}{dX}\left(\frac{d^2u^{(e)}}{dX^2}\right) dX$$

$$= \frac{3}{2}(\lambda + 2\mu)\left[\left[N^{(e)}\right]^T . \left(\frac{du^{(e)}}{dX}\right)^2 \Big|_{X_k}^{X_{k+1}} - \int_{X_k}^{X_{k+1}} \frac{d\left[N^{(e)}\right]^T}{dX}\left(\frac{du^{(e)}}{dX}\right)^2\right]$$

(I-52)

In similar manner, Eq. (I-48) will result in Eqn. (I-53):

$$k_3^{(e)} = (\lambda + 2\mu)\int_{x_k}^{x_{k+1}} \left[N^{(e)}\right]^T . \frac{3}{2}\left(\frac{du^{(e)}}{dX}\right)^2 \frac{d^2u^{(e)}}{dX^2} dX$$

$$= \frac{3}{2}(\lambda + 2\mu)\left\{\left[N^{(e)}\right]^T . \left(\frac{du^{(e)}}{dX}\right)^3 \Big|_{X_k}^{X_{k+1}} - \int_{X_k}^{X_{k+1}} \frac{du^{(e)}}{dX}\left\{\left[N^{(e)}\right]^T 2\frac{du^{(e)}}{dX}\frac{d^2u^{(e)}}{dX^2} + \frac{d\left[N^{(e)}\right]^T}{dX}\left(\frac{du^{(e)}}{dX}\right)^2\right\}\right\}$$

$$k_3^{(e)} = \frac{1}{2}(\lambda + 2\mu)\left[\left[N^{(e)}\right]^T . \left(\frac{du^{(e)}}{dX}\right)^3 \Big|_{X_k}^{X_{k+1}} - \int_{X_k}^{X_{k+1}} \frac{d\left[N^{(e)}\right]^T}{dX}\left(\frac{du^{(e)}}{dX}\right)^3\right]$$

(I-53)

The fourth term in Eqn. (I-45b), which represents the element characteristic vector is:

$$\vec{p}^{(e)} = (\lambda + 2\mu)\int_{x_k}^{x_{k+1}} \left[N^{(e)}\right]^T . -\frac{dP_{osmotic}^{(e)}}{dX} dX$$

(I-54)

I.3.1 *Evaluation of the integrals*

Recall Eqn. (I-50),

$$k_1^{(e)} = (\lambda + 2\mu)\left(\left[N^{(e)}\right]^T \frac{du^{(e)}}{dX}\Big|_{X_k}^{X_{k+1}} - \int_{X_k}^{X_{k+1}} \frac{d\left[N^{(e)}\right]^T}{dX}\frac{du^{(e)}}{dX} dX\right)$$

The first term is assumed zero since the values of the derivative at the elemental nodes are unknown. The second term is given as:

$$k_1^{(e)} = (\lambda + 2\mu)\left(-\int_{X_k}^{X_{k+1}} \left(\frac{1}{l^{(e)}}\begin{Bmatrix}-1\\1\end{Bmatrix}\right)\frac{1}{l^{(e)}}\begin{bmatrix}-1 & 1\end{bmatrix}\begin{Bmatrix}u_k^{(e)}\\u_{k+1}^{(e)}\end{Bmatrix} dX\right)$$

$$k_1^{(e)} = (\lambda + 2\mu)\left\{\frac{1}{l^{(e)}} . \begin{bmatrix}1 & -1\\-1 & 1\end{bmatrix}\begin{bmatrix}u_k^{(e)}\\u_{k+1}^{(e)}\end{bmatrix}\right\}$$

(I-55)

From Eqn. (I-52),

$$k_2^{(e)} = \frac{3}{2}(\lambda + 2\mu)\left[\left[N^{(e)}\right]^T.\left(\frac{du^{(e)}}{dX}\right)^2\Big|_{X_k}^{X_{k+1}} - \int_{X_k}^{X_{k+1}} \frac{d\left[N^{(e)}\right]^T}{dX}\left(\frac{du^{(e)}}{dX}\right)^2\right]$$

Dropping the first term gives:

$$k_2^{(e)} = -\frac{3}{2}(\lambda + 2\mu)\left(\int_{X_k}^{X_{k+1}} \frac{d\left[N^{(e)}\right]^T}{dX}\left(\frac{du^{(e)}}{dX}\right)^2\right)$$

$$= -\frac{3}{2}(\lambda + 2\mu)\int_{X_k}^{X_{k+1}} \left(\frac{1}{l^{(e)}}\begin{Bmatrix}-1\\1\end{Bmatrix}\right)\left(\frac{1}{(l^{(e)})^2}[-1 \quad 1]\begin{bmatrix}-1\\1\end{bmatrix}\right)\begin{Bmatrix}u_k^{(e)}\\u_{k+1}^{(e)}\end{Bmatrix}dX$$

$$= -\frac{3}{(l^{(e)})^2}(\lambda + 2\mu)\begin{Bmatrix}-1\\1\end{Bmatrix}\begin{Bmatrix}u_k^{(e)}\\u_{k+1}^{(e)}\end{Bmatrix}$$

From Eqn. (I-53), dropping the first term gives:

$$k_3^{(e)} = -\frac{1}{2}(\lambda + 2\mu)\int_{X_k}^{X_{k+1}} \frac{d\left[N^{(e)}\right]^T}{dX}\left(\frac{du^{(e)}}{dX}\right)^3$$

$$= -\frac{1}{2}(\lambda + 2\mu)\int_{X_k}^{X_{k+1}} \left(\frac{1}{l^{(e)}}\begin{Bmatrix}-1\\1\end{Bmatrix}\right)\left(\frac{1}{(l^{(e)})^3}[-1 \quad 1]\begin{bmatrix}-1\\1\end{bmatrix}[-1 \quad 1]\right)\begin{Bmatrix}u_k^{(e)}\\u_{k+1}^{(e)}\end{Bmatrix}$$

$$k_3^{(e)} = \frac{(\lambda + 2\mu)}{(l^{(e)})^3}\left\{\begin{bmatrix}-1 & 1\\1 & -1\end{bmatrix}\begin{bmatrix}u_k^{(e)}\\u_{k+1}^{(e)}\end{bmatrix}\right\}$$

The displacement characteristic matrix becomes:

$$[K] = \left\{\frac{(\lambda + 2\mu)}{l^{(e)}}\begin{bmatrix}1 & -1\\-1 & 1\end{bmatrix} - \frac{3(\lambda + 2\mu)}{(l^{(e)})^2}\begin{Bmatrix}-1\\1\end{Bmatrix} + \frac{(\lambda + 2\mu)}{(l^{(e)})^3}\begin{bmatrix}-1 & 1\\1 & -1\end{bmatrix}\right\}\begin{Bmatrix}u_k^{(e)}\\u_{k+1}^{(e)}\end{Bmatrix} \tag{I-56}$$

For the displacement characteristic vector:

$$\vec{p}^{(e)} = (\lambda + 2\mu)\int_{x_k}^{x_{k+1}}\left[N^{(e)}\right]^T.-\frac{dP_{osmotic}^{(e)}}{dX}dX \tag{I-57}$$

I.4. Assemblage of System Equations

Assembling the element characteristic matrices and vectors results in the overall system equations:

$$[\underline{K}]\vec{C}_i = \underline{\vec{P}} \tag{I-58}$$

where

$$[\underline{K}] = \sum_{e=1}^{E} [K^{(e)}] \tag{I-59}$$

$$\underline{\vec{P}} = \sum_{e=1}^{E} [\vec{P}^{(e)}] \tag{I-60}$$

$[\underline{K}]$ and $\underline{\vec{P}}$ are obtained by placing the elements of the characteristic matrix $[K^{(e)}]$ and vector $[\vec{P}^{(e)}]$ in the location of the global characteristic matrix $[\underline{K}]$ and vector $\underline{\vec{P}}$ respectively, whose row and column of the unknown variables correspond to the those of the element in the matrix $[K^{(e)}]$ and vector $[\vec{P}^{(e)}]$. As *e* changes from 1 to *E*, assembling $[K^{(e+1)}]$ and $[\vec{P}^{(e+1)}]$ is done by adding to the existing values of matrix $[K^{(e)}]$ and vector $[\vec{P}^{(e)}]$ such that the global characteristic matrix and vector whose row and column degree of freedom correspond with the element of the matrix $[K^{(e)}]$ and vector $[\vec{P}^{(e)}]$. The overall assembled system characteristic matrix given in Table I.1, and characteristic vector in Table I.2.

Table I.1 Global Characteristic matrix of the Hydrogel /Solution System for a case of 13 nodal unknowns

Global dof	1	2	3	4	5	6	7	8	9	10	11	12	13
1	$K_{11}^{(1)}$	$K_{12}^{(1)}$	0	0	0	0	0	0	0	0	0	0	0
2	$K_{21}^{(1)}$	$K_{22}^{(1)}+K_{11}^{(2)}$	$K_{12}^{(2)}$	0	0	0	0	0	0	0	0	0	
3	0	$K_{21}^{(2)}$	$K_{22}^{(2)}+K_{11}^{(3)}$	$K_{12}^{(3)}$	0	0	0	0	0	0	0	0	0
4	0	0	$K_{21}^{(3)}$	$K_{22}^{(3)}+K_{11}^{(4)}$	$K_{12}^{(4)}$	0	0	0	0	0	0	0	0
5	0	0	0	$K_{21}^{(4)}$	$K_{22}^{(4)}+K_{11}^{(5)}$	$K_{12}^{(5)}$	0	0	0	0	0	0	0
6	0	0	0	0	$K_{21}^{(5)}$	$K_{22}^{(5)}+K_{11}^{(6)}$	$K_{12}^{(6)}$	0	0	0	0	0	0
7	0	0	0	0	0	$K_{21}^{(6)}$	$K_{22}^{(6)}+K_{11}^{(7)}$	$K_{12}^{(7)}$	0	0	0	0	0
8	0	0	0	0	0	0	$K_{21}^{(7)}$	$K_{22}^{(7)}+K_{11}^{(8)}$	$K_{12}^{(8)}$	0	0	0	0
9	0	0	0	0	0	0	0	$K_{21}^{(8)}$	$K_{22}^{(8)}+K_{11}^{(9)}$	$K_{12}^{(9)}$	0	0	0
10	0	0	0	0	0	0	0	0	$K_{21}^{(9)}$	$K_{22}^{(9)}+K_{11}^{(10)}$	$K_{12}^{(10)}$	0	0
11	0	0	0	0	0	0	0	0	0	$K_{21}^{(10)}$	$K_{22}^{(10)}+K_{11}^{(11)}$	$K_{12}^{(11)}$	0
12	0	0	0	0	0	0	0	0	0	0	$K_{21}^{(11)}$	$K_{22}^{(11)}+K_{11}^{(12)}$	$K_{12}^{(12)}$
13	0	0	0	0	0	0	0	0	0	0	0	$K_{21}^{(12)}$	$K_{22}^{(12)}$

Table I.2: Assembled system characteristic vector

Global dof	Characteristic vector
1	$P_1^{(1)}$
2	$P_2^{(1)} + P_1^{(2)}$
3	$P_2^{(2)} + P_1^{(3)}$
4	$P_2^{(3)} + P_1^{(4)}$
5	$P_2^{(4)} + P_1^{(5)}$
6	$P_2^{(5)} + P_1^{(6)}$
7	$P_2^{(6)} + P_1^{(7)}$
8	$P_2^{(7)} + P_1^{(8)}$
9	$P_2^{(8)} + P_1^{(9)}$
10	$P_2^{(9)} + P_1^{(10)}$
11	$P_2^{(10)} + P_1^{(11)}$
12	$P_2^{(11)} + P_1^{(12)}$
13	$P_2^{(12)}$

I.5. Boundary Condition

To solve the overall system equations for the entire domain, it is important to incorporate the boundary conditions else, the system characteristic matrix $[\underline{K}]$, will be singular and thus its inverse will not exist. There are many approaches to the inclusion of boundary conditions to the assembled characteristic matrix. However, the approach adopted in this study (explained in detail by Rao [220]) outlined below, was preferred since it retains the symmetry of the system equation and allows the characteristic matrix to be stored in band format.

Suppose C_{j1} is the prescribed value for the nodal unknown (e.g., concentration), C_j the procedure below followed to incorporate the boundary conditions.

Insert the prescribed value of C_j into the characteristic vector, such that $P_j = C_{j1}$

Modify the characteristic vector $\underline{\vec{P}}$ such that the other elements take the form:

$$P_{new} = P_1 - K_{ij}C_{j1}$$

Make the row and column of $[\underline{K}]$ associated with C_j all zero, except the diagonal elements, which should be unity; that is.

$$K_{ij} = 1$$

otherwise

$$K_{ij} = K_{ji} = 0$$

To incorporate the entire specified nodal unknowns (e.g., C_j for concentration, φ for potential and *u* for displacement), the steps above are repeated until all the boundary conditions are incorporated into the overall system characteristic matrix.

I. 6. Solution of the System Equation

Having incorporated the boundary conditions into the system of the governing differential equation (in its matrix form), the linear system of equations takes the tridiagonal and banded form:

$$\begin{bmatrix} a_1 & c_1 & & & & & & \\ b_1 & a_2 & c_2 & & & & & \\ & b_2 & a_3 & c_3 & & & & \\ & & b_3 & \ddots & \ddots & & & \\ & & & \ddots & a_i & c_i & & \\ & & & & b_i & \ddots & \ddots & \\ & & & & & \ddots & a_{n-1} & c_{n-1} \\ & & & & & & b_{n-1} & a_n \end{bmatrix} \begin{bmatrix} x_1 \\ x_2 \\ x_3 \\ \vdots \\ x_i \\ \vdots \\ x_{n-1} \\ x_n \end{bmatrix} = \begin{bmatrix} d_1 \\ d_2 \\ d_3 \\ \vdots \\ d_i \\ \vdots \\ d_{n-1} \\ d_n \end{bmatrix} \qquad (\mathrm{I}-61)$$

The system of equations can be solved using direct or iterative methods. Direct methods are methods that will yield the exact solution in a finite number of steps or operations in the absence of round-off and truncation errors. Whereas iterative methods are those that begin with an initial approximation or guess on a carefully chosen and well-suited algorithm to a successively better approximation [221]. For accuracy and ease of convergence with the use of digital computers, iterative method is advantageous. However, to describe the concept used in a clear manner, the direct method is chosen. Gaussian elimination and Choleski method are the two popular direct method employed for solving linear system of equations. However, since the characteristic matrix has banded structure, Gaussian Elimination, which handles banded matrix with ease, justifies the reason it was employed in the algorithm to solve the system of *n* linear equations in *n* unknowns. The steps in the algorithm are:

i. Subtract b_1/a_1 times row 1 from row 2, thus creating a zero element in the position of element b_1. This does not affect c_2 but changes the entries a_2 and d_2. That is:

$$\begin{cases} a_2 = a_2 - \left(\dfrac{b_1}{a_1}\right) c_1 \\ d_2 = b_2 - \left(\dfrac{b_1}{a_1}\right) d_1 \end{cases}$$

ii. Repeat the step (i) above using the new pivot row (i.e., the new row 2), to obtain the new a_i's and $d_i{}'$s.

$$\begin{cases} a_i = a_i - \left(\dfrac{b_{i-1}}{a_{i-1}}\right) c_{i-1} \\ d_2 = b_i - \left(\dfrac{b_{i-1}}{a_{i-1}}\right) d_{i-1} \end{cases}$$

After applying the forward elimination procedure above, the original system of equations eventually reduced to the form (different entries for the a_i's and d_i's but same as previous for the c_i's):

$$\begin{bmatrix} a_1 & c_1 & & & & & & \\ & a_2 & c_2 & & & & & \\ & & a_3 & c_3 & & & & \\ & & & \ddots & \ddots & & & \\ & & & & a_i & c_i & & \\ & & & & & \ddots & \ddots & \\ & & & & & & a_{n-1} & c_{n-1} \\ & & & & & & & a_n \end{bmatrix} \begin{bmatrix} x_1 \\ x_2 \\ x_3 \\ \vdots \\ x_i \\ \vdots \\ x_{n-1} \\ x_n \end{bmatrix} = \begin{bmatrix} d_1 \\ d_2 \\ d_3 \\ \vdots \\ d_i \\ \vdots \\ d_{n-1} \\ d_n \end{bmatrix} \qquad (\mathrm{I}-62)$$

iii. The unknowns $x_n, x_{n-1}, \dots, x_1$ obtained by using back substitution approach to solve Eqn. (I-62). That is:

$$\begin{cases} x_n = \frac{d_n}{a_n} \\ x_{n-1} = \frac{1}{a_{n-1}}\left(d_{n-1} - c_{n-1}x_n\right) \end{cases} \qquad (\mathrm{I}-63)$$

In general, for any unknown:

$$x_i = \frac{1}{a_i}\left(d_i - c_i x_{i+1}\right) \qquad (i = n-1, n-2, \dots, 1)$$

I.7 Summary of the Modelling Procedure

I.7.1 *Mathematical model*

The mathematical model that describes the hydrogel/solution interaction in response to pH changes in the environment are:

The steady state Nernst-Plank equation given as:

$$D_k \nabla^2 C_k + \mu_k z_k F \nabla C_k \nabla \varphi + \mu_k z_k F C_k \nabla^2 \varphi = 0 \qquad (k = 1,2,3, \dots N_{ion})$$

The Poisson equation given as:

$$\nabla^2 \varphi = -\frac{F}{\varepsilon \varepsilon_0} (\sum_{k=1}^{N} z_k c_k + z_f c_f)$$

The equilibrium mechanical/momentum equation given as follows:

$$\boldsymbol{\nabla_X} . [-\mathrm{J}\mathbf{F}^{-1} p_{osmotic} \mathbf{I} + \mathbf{FS}] = \mathbf{0}$$

In addition, the constitutive relations are:

The osmotic pressure $p_{osmotic}$ given as:

$$P_{osmotic} = RT \sum_{k=1}^{N} (c_k^h - c_k^s)$$

The fixed charge concentration c_f for an anionic hydrogel given as:

$$c_f = \frac{c_{mo}^s}{H} \frac{K_a}{(K_a + c_H)}$$

I.7.2 *Numerical model*

To develop a numerical model that approximates the behaviour of the continuum model outlined in Section I.4.1, the following steps were employed.

a. Discretization of the mathematical model into a global system of algebraic equation of the general form:

$$[K]\vec{C}_i = \vec{P}$$

where

$[K]$ is the system/global characteristic matrix formed from the assemblage of the element (local coordinate) characteristic matrices for:

i. **PNP equation**

$$[K^e] = \left[K_H^{(e)}\right] + \left[K_I^{(e)}\right] + \left[K_B^{(e)}\right]$$

where

$$\left[K_H^{(e)}\right] = \frac{1}{l_H^{(e)}}\begin{bmatrix} 1 & -1 \\ -1 & 1 \end{bmatrix} + \frac{\mu_i F^2 z_i l_H^{(e)}}{2\varepsilon\varepsilon_0 D_i}\left\{\left(\sum z_i C_i + z_f C_f\right)\begin{bmatrix} 1 & -1 \\ 1 & -1 \end{bmatrix}\right\} - \frac{F^2 z_i l_H^{(e)}}{6\varepsilon\varepsilon_0 D_i}\left(\sum z_i C_i + z_f C_f\right)\begin{bmatrix} 2 & 1 \\ 1 & 2 \end{bmatrix}$$

$$\left[K_I^{(e)}\right] = \frac{1}{l_I^{(e)}}\begin{bmatrix} 1 & -1 \\ -1 & 1 \end{bmatrix} + \frac{\mu_i F^2 z_i l_I^{(e)}}{2\varepsilon\varepsilon_0 D_i}\left\{\sum z_i C_i \begin{bmatrix} 1 & -1 \\ 1 & -1 \end{bmatrix}\right\} - \frac{F^2 z_i l_I^{(e)}}{6\varepsilon\varepsilon_0 D_i}\sum z_i C_i \begin{bmatrix} 2 & 1 \\ 1 & 2 \end{bmatrix}$$

$$\left[K_B^{(e)}\right] = \frac{1}{l_B^{(e)}}\begin{bmatrix} 1 & -1 \\ -1 & 1 \end{bmatrix} + \frac{\mu_i F^2 z_i l_B^{(e)}}{2\varepsilon\varepsilon_0 D_i}\left\{\sum z_i C_i \begin{bmatrix} 1 & -1 \\ 1 & -1 \end{bmatrix}\right\} - \frac{F^2 z_i l_B^{(e)}}{6\varepsilon\varepsilon_0 D_i}\sum z_i C_i \begin{bmatrix} 2 & 1 \\ 1 & 2 \end{bmatrix}$$

ii Mechanical equation

$$[K^e]_{Mech} = \left\{\frac{(\lambda + 2\mu)}{l^{(e)}}\begin{bmatrix} 1 & -1 \\ -1 & 1 \end{bmatrix} - \frac{3(\lambda + 2\mu)}{(l^{(e)})^2}\begin{Bmatrix} -1 \\ 1 \end{Bmatrix} + \frac{(\lambda + 2\mu)}{(l^{(e)})^3}\begin{bmatrix} -1 & 1 \\ 1 & -1 \end{bmatrix}\right\}\begin{Bmatrix} u_k^{(e)} \\ u_{k+1}^{(e)} \end{Bmatrix}$$

where

$\vec{P}$ is the system characteristic vectors derived from the assemblage of the element characteristic vectors for:

i. **PNP equation**

$$\vec{P}^{(e)} = \left\{\begin{Bmatrix} (x_{k+1} - x)/l_I^{(e)} \\ (x - x_k)/l_I^{(e)} \end{Bmatrix} \cdot \frac{1}{l_I^{(e)}}[-1 \quad 1]\begin{Bmatrix} \frac{1}{(1 + e^{-x_k})} \\ \frac{1}{(1 + e^{-x_{k+1}})} \end{Bmatrix}\right\}\Bigg|_{x_{k_I}}^{x_{k_I+1}}$$

$$= -\frac{1}{l_I^{(e)}}\begin{Bmatrix} \frac{1}{(1 + e^{-x_k})} - \frac{1}{(1 + e^{-x_{k+1}})} \\ \frac{1}{(1 + e^{-x_k})} - \frac{1}{(1 + e^{-x_{k+1}})} \end{Bmatrix}$$

ii. **Mechanical equation**

$$\vec{p}^{(e)} = \lambda + 2\mu \int_{x_k}^{x_{k+1}} \left[N^{(e)}\right]^T . - \frac{dP_{osmotic}^{(e)}}{dX} dX$$

b. Incorporation of the prescribed boundary conditions
c. Solving the linear system of equations
d. Plug the values of the concentrations at the interface into the osmotic pressure relation to calculate the osmotic pressure at the interface between the hydrogel and the buffer.
e. Use the osmotic pressure to couple the PNP equation with the mechanical equation to determine the deformation of the hydrogel as a function of changes in pH.

These steps elucidated in the flowchart of Figure I.1 as shown below.

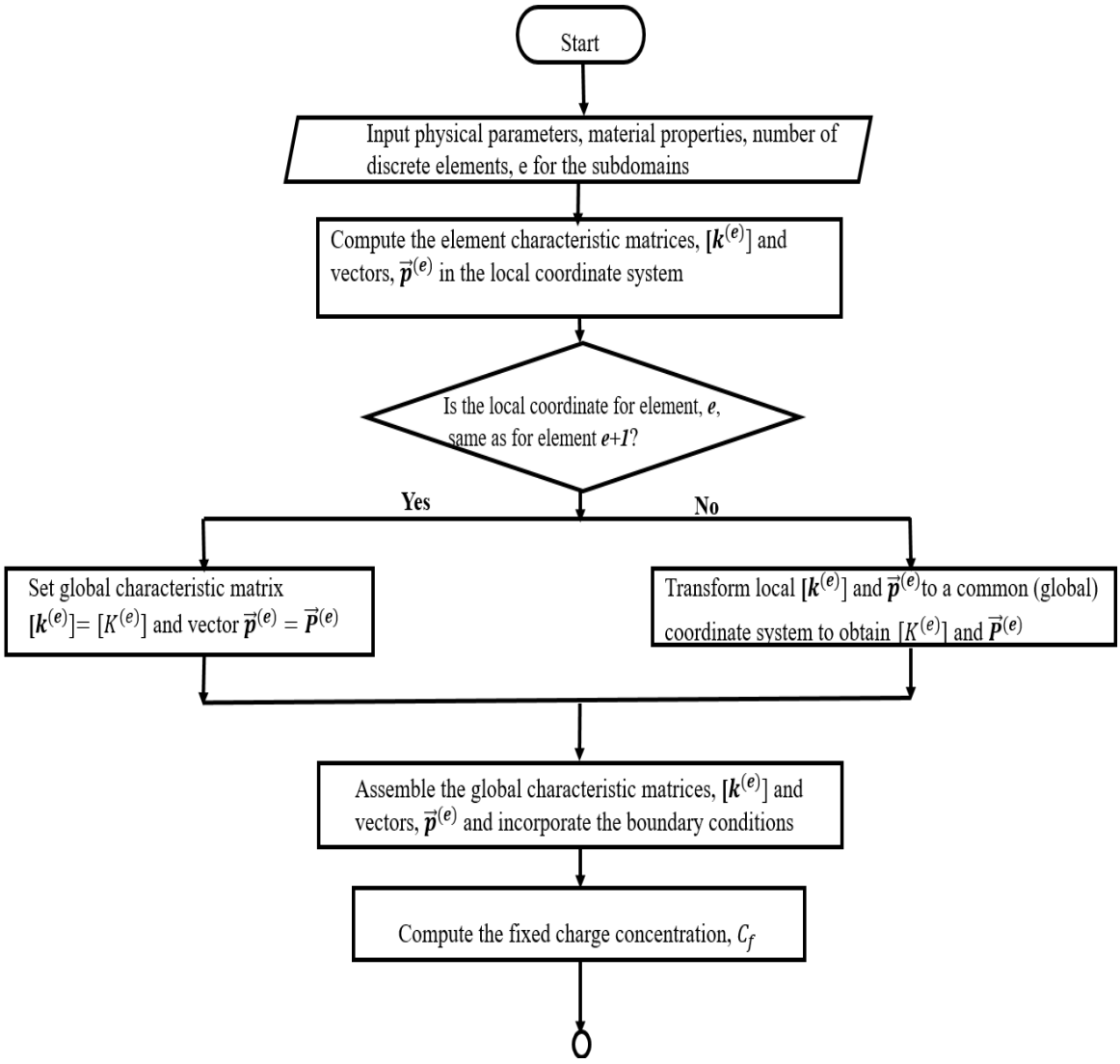

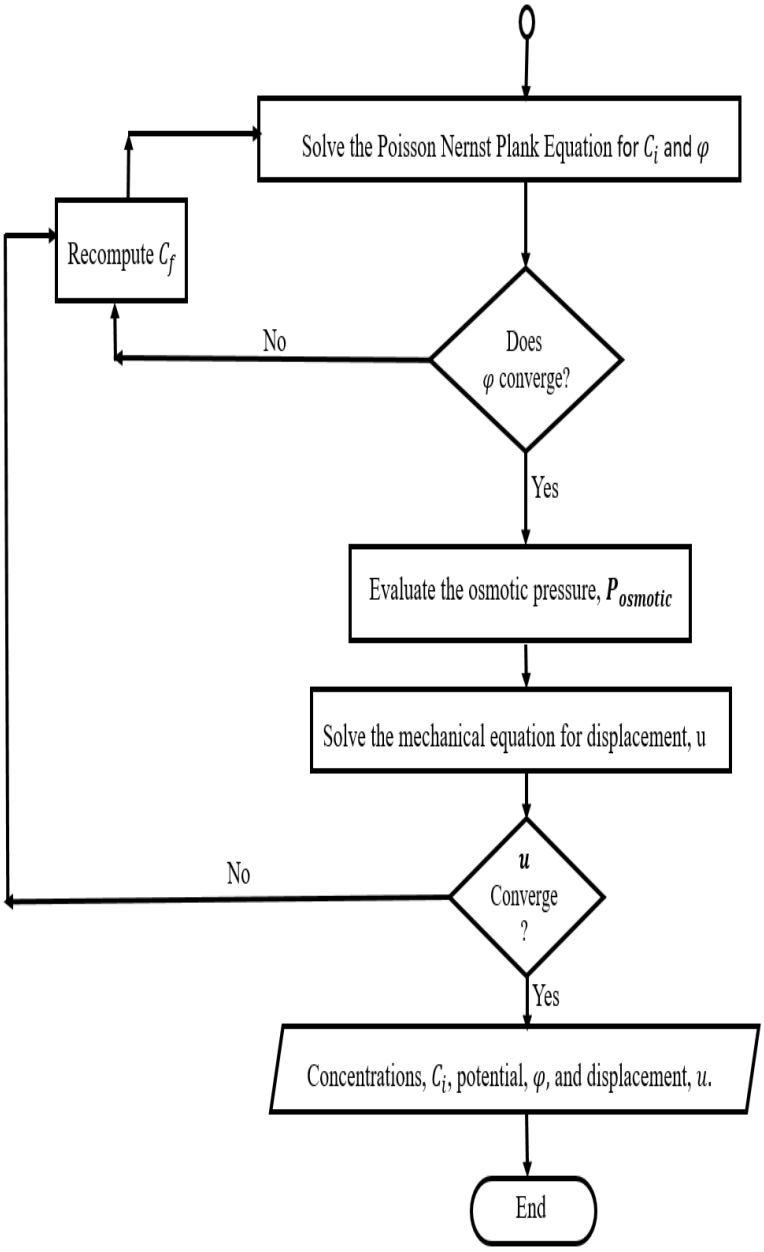

Figure I.1: Flowchart for Numerical modelling

APPENDIX II

NEWTON RAPHSON'S NUMERICAL SCHEME

Newton Raphson's method provides a good approximation for solving single variable nonlinear equation of the form:

$$f(x) = 0 \tag{II-1}$$

This numerical scheme consists of the following steps:

i. An initial guess of the solution to Eq. (II-1) is: x_0

ii. The step size, $h = -\frac{f(x)}{f'(x)}$

iii. The new or next point, $x_1 = x_0 + h$

⋮

iv. Other iteration points, $x_{n+1} = x_n - \frac{f(x_n)}{f'(x_n)}$ (II-2)

v. Stopping criteria is: $|x_{n+1} - x_n|/|x_n| < \varepsilon$ is reached (II-3)

Suppose the total osmotic pressure, μ due to mixing, elasticity, and ionic interaction is:

$$\mu = \mu_m + \mu_{el} + \mu_i \tag{II-4}$$

$$\mu_m = -\frac{N_A kT}{V_s}[In(1 - \nu_2) + \nu_2 + \chi(\nu_2)^2] \tag{II-5}$$

where $\nu_2 = {\nu_2}^0 {V_{eq}}^{-1}$

$$\mu_{el} = N_A v_0 kT\left(0.5{V_{eq}}^{-1} - {V_{eq}}^{-1/3}\right) \tag{II-6}$$

$$\mu_i = RTV_s\left(\frac{\alpha^2 c_f^2}{4I}\right) \tag{II-7}$$

Differentiating Eq. (II-4) w.r.t V_{eq} gives:

$$\frac{d\mu}{dV_{eq}} = \frac{d\mu_m}{dV_{eq}} + \frac{d\mu_{el}}{dV_{eq}} + \frac{d\mu_i}{dV_{eq}} \tag{II-8}$$

$$\frac{d\mu_m}{dV_{eq}} = \left(\frac{d\mu_m}{d\nu_2}\right).\left(\frac{d\nu_2}{dV_{eq}}\right) \tag{II-9}$$

$$\left(\frac{d\mu_m}{d\nu_2}\right) = -\frac{N_A kT}{V_s}\left[-\frac{1}{1-\nu_2} + 1 + 2\chi\nu_2\right] \tag{II-10}$$

$$\left(\frac{d\nu_2}{dV_{eq}}\right) = \frac{d}{dx}\left({\nu_2}^0 {V_{eq}}^{-1}\right) = -{\nu_2}^0 . {V_{eq}}^{-2} \tag{II-11}$$

Substituting Eq. (II-10) and (II-11) into Eq. (II-9) gives:

$$\frac{d\mu_m}{dV_{eq}} = \frac{N_A kT}{V_s}\left[1 + 2\chi\nu_2 - \frac{1}{1-\nu_2}\right].{\nu_2}^0.{V_{eq}}^{-2} \quad \text{(II-12)}$$

Therefore Eq. (II-9) becomes:

$$\frac{d\mu_m}{dV_{eq}} = \frac{N_A kT}{V_s}\left[1 + 2\chi\left(\frac{{\nu_2}^0}{V_{eq}}\right) - \frac{V_{eq}}{(V_{eq}-{\nu_2}^0)}\right] \quad \text{(II-13)}$$

From Eq. (II-6), the derivative is:

$$\frac{d\mu_{el}}{dV_{eq}} = \frac{d}{dV_{eq}}\left(N_A v_0 kT\left(0.5{V_{eq}}^{-1} - {V_{eq}}^{-1/3}\right)\right)$$

$$= N_A v_0 kT\left(-\frac{1}{2}{V_{eq}}^{-2} + \frac{1}{3}{V_{eq}}^{-4/3}\right) \quad \text{(II-14)}$$

Recall Eq. (II-7):

$$\mu_i = RTV_s\left(\frac{\alpha^2 c_f^2}{4I}\right)$$

where $c_f(V_{eq})$ is given as:

$$c_f = \frac{c_{mo}}{V_{eq}}\frac{C_{H^+}}{(K_a + C_{H^+})} \quad \text{(II-15)}$$

Differentiating Eq. (II-7) w.r.t to c_f gives:

$$\frac{d\mu_i}{dc_f} = 2\left(\frac{RTV_s\alpha^2}{4I}\right)c_f \quad \text{(II-16)}$$

Differentiating Eq. (II-15) w.r.t to V_{eq} gives:

$$\frac{dc_f}{dV_{eq}} = -\frac{c_{mo}C_{H^+}}{(K_a + C_{H^+})}{V_{eq}}^{-2} \quad \text{(II-17)}$$

Therefore

$$\frac{d\mu_i}{dV_{eq}} = \left(\frac{d\mu_i}{dc_f}\right).\left(\frac{dc_f}{dV_{eq}}\right)$$

$$= -2\left(\frac{RTV_s\alpha^2}{4I}\right)\frac{c_f^2}{V_{eq}} \quad \text{(II-18)}$$

Hence, the function and its derivative are Eq.(II-19) and (II-20):

$$f(V_{eq}) = -\frac{N_A kT}{V_s}[In(1-\nu_2) + \nu_2 + \chi(\nu_2)^2] + N_A v_0 kT(0.5{V_{eq}}^{-1} - {V_{eq}}^{-1/3}) + RTV_s\left(\frac{\alpha^2 c_f^2}{4I}\right) \quad \text{(II-19)}$$

$$f'(V_{eq}) = \frac{N_A kT}{V_s}\left[1 + 2\chi\left(\frac{{\nu_2}^0}{V_{eq}}\right) - \frac{V_{eq}}{\left(V_{eq} - {\nu_2}^0\right)}\right] + N_A \nu_0 kT\left(-\frac{1}{2}{V_{eq}}^{-2} + \frac{1}{3}{V_{eq}}^{-4/3}\right) - 2\left(\frac{RTV_s\alpha^2}{4I}\right)\frac{c_f^2}{V_{eq}}$$

(II-20)

Applying Newton Raphson's iteration scheme results in an equilibrium volume swelling ratio that makes the total osmotic pressure in the system zero. Thus, the equilibrium volume ratio is:

$${V_{eq}}_{n+1} = {V_{eq}}_n - \frac{f(V_{eq})}{f'(V_{eq})} \quad \text{(II-21)}$$

APPENDIX III

RESPONSE SURFACE DESIGN MATRIX

Std	Run	Factor 1 A:Cg wt.%	Factor 2 B:X -	Factor 3 C:I mM	Factor 4 D:pH -	Response V_{SR} -
21	1	0.4	0.34	450	7.4	0.380295
14	2	0.6	0.1	900	8.88	0.378759
7	3	0.2	0.58	900	5.92	2.16177
25	4	0.4	0.34	600	7.4	0.378772
17	5	0.3	0.34	600	7.4	0.38386
29	6	0.4	0.34	600	7.4	0.378772
30	7	0.4	0.34	600	7.4	0.378772
11	8	0.2	0.58	300	8.88	0.349358
1	9	0.2	0.1	300	5.92	2.75395
24	10	0.4	0.34	600	8.14	0.363853
27	11	0.4	0.34	600	7.4	0.378772
22	12	0.4	0.34	750	7.4	0.377507
5	13	0.2	0.1	900	5.92	2.17083
13	14	0.2	0.1	900	8.88	0.376784
16	15	0.6	0.58	900	8.88	0.349015
6	16	0.6	0.1	900	5.92	1.00249
20	17	0.4	0.46	600	7.4	0.371847
10	18	0.6	0.1	300	8.88	0.378759
8	19	0.6	0.58	900	5.92	0.988009
28	20	0.4	0.34	600	7.4	0.378772
23	21	0.4	0.34	600	6.66	0.719661
26	22	0.4	0.34	600	7.4	0.378772
12	23	0.6	0.58	300	8.88	0.349015
18	24	0.5	0.34	600	7.4	0.374452
4	25	0.6	0.58	300	5.92	1.20343
9	26	0.2	0.1	300	8.88	0.376784
15	27	0.2	0.58	900	8.88	0.349357
2	28	0.6	0.1	300	5.92	1.21646
19	29	0.4	0.22	600	7.4	0.385581
3	30	0.2	0.58	300	5.92	2.7458

With the design matrix above a regression model whose response surface in transformed variable state/scale is given as shown in Figures. A3a, A3b, and A3c.

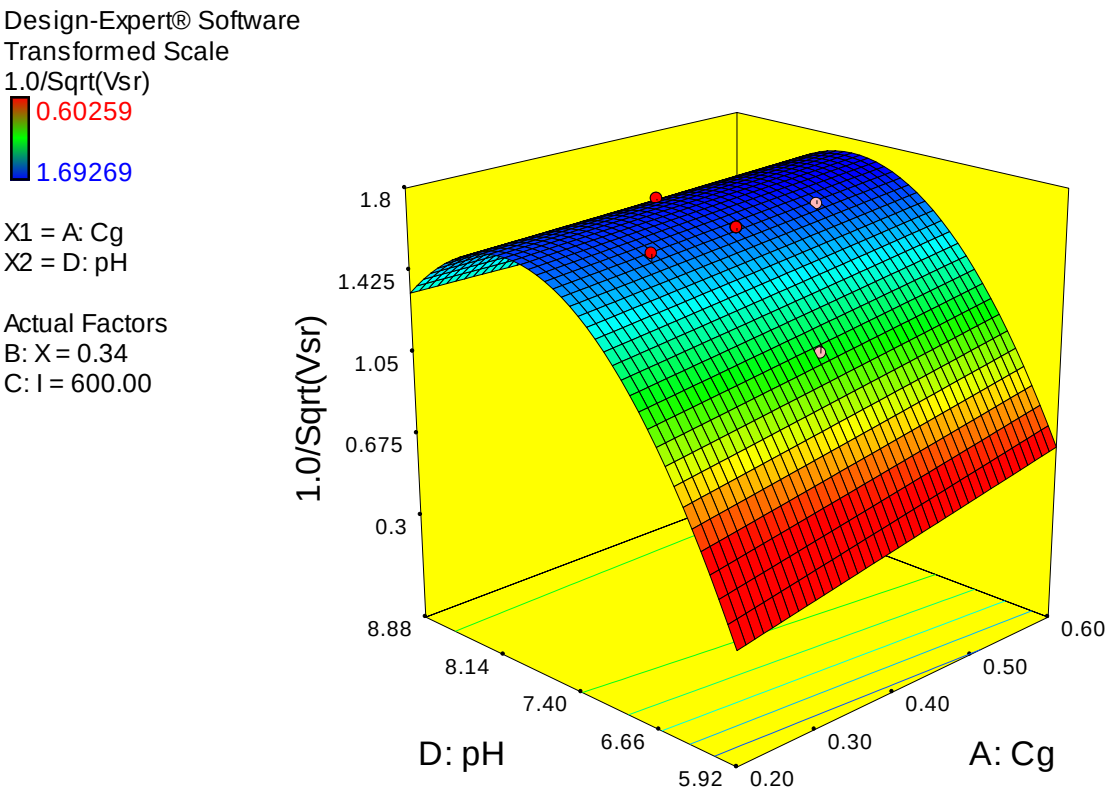

Figure A3a: Response surface (transformed scale) showing the influence of the pH and genipin concentration on the equilibrium swelling ratio.

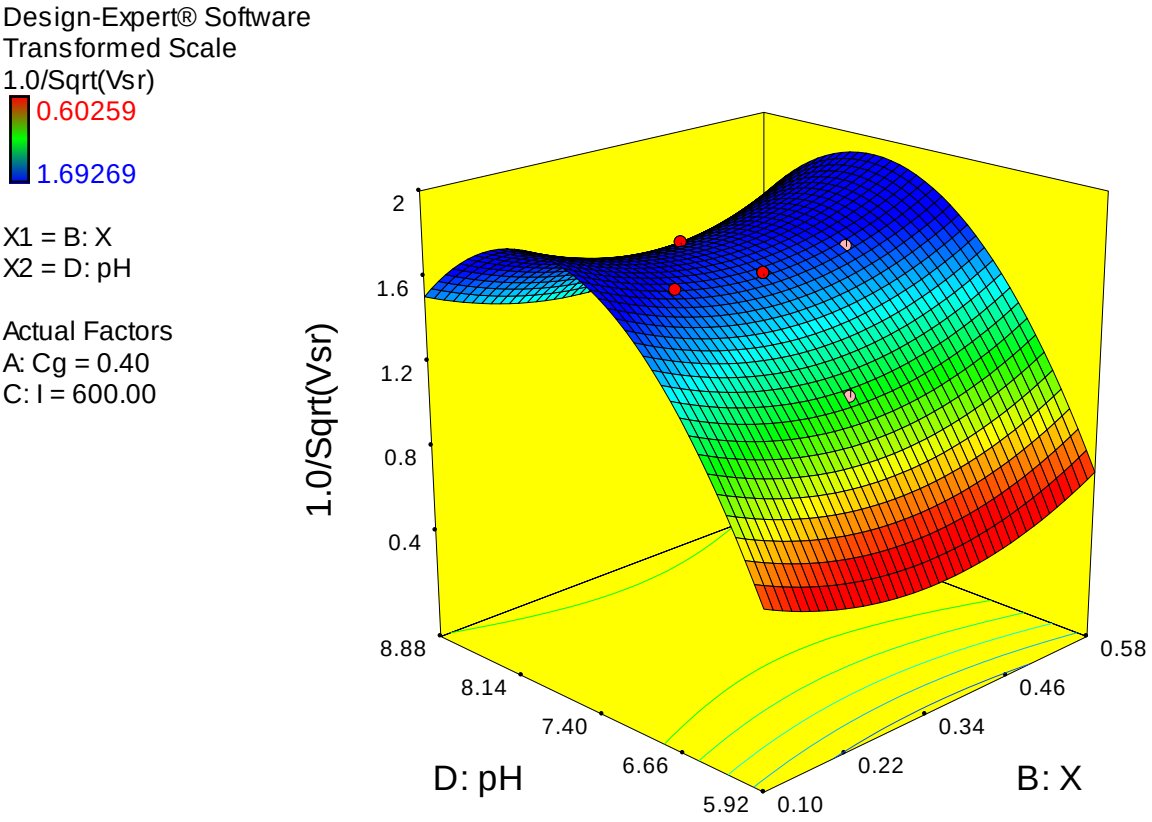

Figure A3b: Response surface (transformed scale) showing the influence of the pH and solvent interaction parameter on the equilibrium swelling ratio.

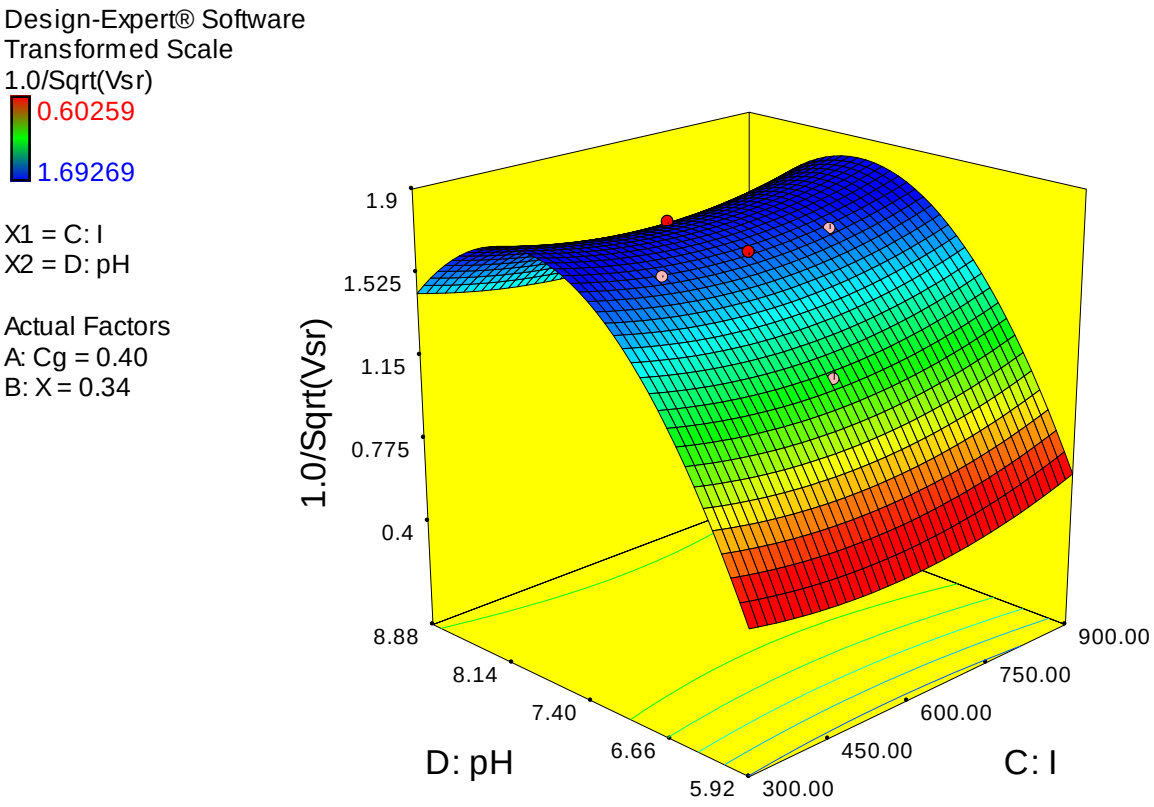

Figure A3c: Response surface (transformed scale) showing the influence of the pH and ionic strength of the swelling medium on the equilibrium swelling ratio.

APPENDIX IV

CONTINUUM APPROACH TO SWELLING KINETICS

The focus here is to determine how fast the crosslinked hydrogel swells or shrinks in the surrounding medium. To do this, the following assumptions were made:

i. The deformation or volume variation of the gel is a resultant effect of the chemo-electro-mechanical interactions taking place between the gel and its surroundings.
ii. The deformation (i.e., swelling/shrinking) process is based on the diffusion of the polymer network to the fluid phase, and not the diffusion of the surrounding fluid molecules to the gel phase.

With these assumptions, the gel can be viewed as a continuum, and the kinetics of deformation modelled using a black-box approach (i.e., ignoring the interplay of the chemical, electrical and mechanical fields). Thus, the equation of motion for an elemental volume (of the polymer network) moving in the fluid phase can be used to model the gel's deformation.

The equation of motion of a unit volume of a solid moving in a fluid is given as:

$$\rho \frac{\partial^2 \boldsymbol{u}}{\partial t^2} - \nabla . \tilde{\sigma} + f \frac{\partial \boldsymbol{u}}{\partial t} = 0 \qquad \text{(IV}-1\text{)}$$

where $\boldsymbol{u}$ is the displacement vector of a 3-dimensional body undergoing deformation, ρ is the density of the gel, f is the coefficient of friction between the polymer network and the fluid. The stress tensor, $\tilde{\sigma}$ whose component $\tilde{\sigma}_{ik}$, is the stress in the k-direction orthogonal to the *i*-direction, and given as:

$$\tilde{\sigma}_{ik} = \begin{pmatrix} \sigma_{11} & \sigma_{12} & \sigma_{13} \\ \sigma_{21} & \sigma_{22} & \sigma_{23} \\ \sigma_{31} & \sigma_{32} & \sigma_{33} \end{pmatrix} \qquad \text{(IV}-2\text{)}$$

Since volume variation of the gel is a slowly, gradual process, the first term in Eq. (IV−1) which represents the inertia (i.e., the product of the weight of the elemental volume of the solid and its acceleration) can be ignored. Thus, Eq. (IV−1) reduces to :

$$\nabla . \tilde{\sigma} = f \frac{\partial \boldsymbol{u}}{\partial t} \qquad \text{(IV}-3\text{)}$$

Eq. (IV−3) rewritten in terms of the stress components is given as:

$$\frac{\partial \boldsymbol{u}}{\partial t} = \frac{1}{f}\begin{pmatrix}\sigma_{11} & \sigma_{12} & \sigma_{13}\\ \sigma_{21} & \sigma_{22} & \sigma_{23}\\ \sigma_{31} & \sigma_{32} & \sigma_{33}\end{pmatrix}\begin{pmatrix}\frac{\partial}{\partial x}\\ \frac{\partial}{\partial y}\\ \frac{\partial}{\partial z}\end{pmatrix} = \frac{1}{f}\begin{pmatrix}\frac{\partial \sigma_{11}}{\partial x} + \frac{\partial \sigma_{12}}{\partial y} + \frac{\partial \sigma_{13}}{\partial z}\\ \frac{\partial \sigma_{21}}{\partial x} + \frac{\partial \sigma_{22}}{\partial y} + \frac{\partial \sigma_{23}}{\partial z}\\ \frac{\partial \sigma_{31}}{\partial x} + \frac{\partial \sigma_{32}}{\partial y} + \frac{\partial \sigma_{33}}{\partial z}\end{pmatrix} \quad \text{(IV−4)}$$

where the stress tensor ($\tilde{\sigma}$) is related to the displacement vector ($\boldsymbol{u}$), shear modulus (G), and the bulk modulus (K) in the following way:

$$\tilde{\sigma}_{ik} = (\underbrace{K\nabla.\boldsymbol{u}\delta_{ik}}_{\substack{stress\ due\\ to\\ volume\\ variation}} + \underbrace{2G(u_{ik} - \frac{1}{3}\nabla.\boldsymbol{u}\delta_{ik})}_{\substack{stress\ due\ to\\ shear\ deformation}} \quad \text{(IV−5)}$$

where;

$$u_{ik} = \left(\frac{\partial u_k}{\partial x_i} + \frac{\partial u_i}{\partial x_k}\right) \quad \text{(IV−6)}$$

Substituting Eq. (IV−6) into (IV−4) gives a more compact form of Eq. (IV−4) as:

$$\frac{\partial \boldsymbol{u}}{\partial t} = \frac{1}{f}\begin{pmatrix}(K + G/3)\frac{\partial}{\partial x}\nabla\boldsymbol{u} + G\Delta\boldsymbol{u}\\ (K + G/3)\frac{\partial}{\partial y}\nabla\boldsymbol{u} + G\Delta\boldsymbol{u}\\ (K + G/3)\frac{\partial}{\partial z}\nabla\boldsymbol{u} + G\Delta\boldsymbol{u}\end{pmatrix} \quad \text{(IV−7)}$$

For simplicity, assume the gel is spherical, so that the displacement vector takes the form:

$$\boldsymbol{u}(\boldsymbol{r}, t) = u(r, t).\hat{r} \quad \text{(IV−8)}$$

where $\hat{r}$ is the unit vector parallel to $\boldsymbol{r}$**.** Therefore, Eq. (IV−7)reduces to:

$$\frac{\partial u(r,t)}{\partial t} = \frac{1}{f}\left[(K + G/3)\frac{\partial}{\partial r}\nabla u(r, t) + G\nabla^2 u(r, t)\right].\hat{r} \quad \text{(IV−9)}$$

Note: In Eq. (IV−9) the operation $\Delta u = \nabla^2 u$

$$\frac{\partial u(r,t)}{\partial t} = \frac{1}{f}\left[(K + G/3)\frac{\partial}{\partial r}\nabla u(r, t) + G\frac{\partial}{\partial r}\nabla u(r, t)\right] \quad \text{(IV−10)}$$

$$\frac{\partial u(r,t)}{\partial t} = \left(\frac{K+\frac{4G}{3}}{f}\right)\frac{\partial}{\partial r}\nabla u(r, t) = D\frac{\partial}{\partial r}\nabla u(r, t) \quad \text{(IV−11)}$$

Applying ∇ for a 3D polar coordinate system, ignoring the partial derivative of the angle of rotation due to the sphere's symmetry, Eq. (IV−11) is rewritten as:

$$\frac{\partial u(r,t)}{\partial t} = D\frac{\partial}{\partial r}\left[\frac{1}{r^2}\frac{\partial}{\partial r}(r^2 u)\right] \qquad \text{(IV}-12\text{)}$$

where *D* is called the gel's collective diffusion coefficient.

Eq. (IV−12) which is called the "swelling equation" models the gel network diffusing into the solvent phase. Solving Eq. (IV−12), requires initial and boundary conditions.

D−1. Initial condition

D−1.1 *Strain*

Assume the gel swells from an initial radius, l_0 to a final equilibrium radius, l_∞. To define the strain, the deformed configuration (i.e., the equilibrium state) is considered as the reference condition since the initial state (i.e., the undeformed configuration) is not a stable initial condition. This implies that the pressure acting on the gel's surface compresses the radius of the gel from l_∞ to l_0 in the initial condition. Therefore, the strain of a point, which is at a distance *r* from the origin in the reference or equilibrium state is:

$$\frac{\partial u(r.0)}{\partial r} = \frac{(l_\infty - l_0)}{l_\infty} = \frac{\Delta l}{l_\infty} \qquad \text{(IV}-13\text{)}$$

Hence, the displacement of that point, *r*, from the origin, in the initial condition is:

$$u(r.0) = \frac{\Delta l}{l_\infty}.r \qquad \text{(IV}-14\text{)}$$

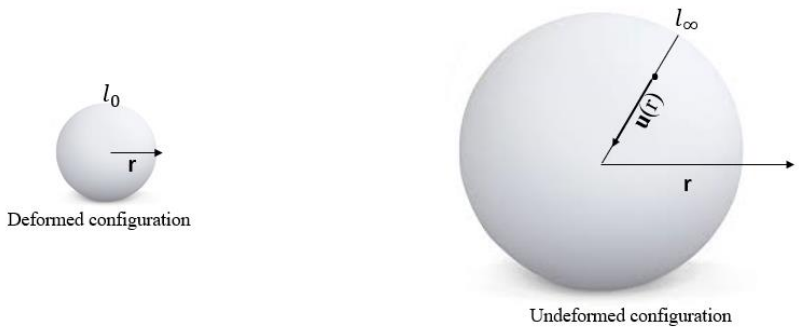

Figure A4a: The initial (left) and final/reference(right) states of the gel

D−1.2 ***Osmotic pressure***

The osmotic pressure, π_0, that results from the strain can be derived in the following way:

$$\pi_0 = M\frac{dV}{V} \tag{IV−15}$$

$$\pi_0 = M\frac{d(\frac{4}{3}\pi r^3)}{(\frac{4}{3}\pi r^3)} = 3M\frac{dr}{r} \tag{IV−16}$$

Substituting Eq. (IV−14) into (IV−16) gives:

$$\pi_0 = 3M\frac{\Delta l}{l_\infty} \tag{IV−17}$$

where *M* is the Young's modulus of the gel.

D−2. Boundary Conditions.

D−2.1 ***Initial state of the gel in solution***.

The stress acting on the surface of the gel in the initial state when the gel is immersed in the solvent is:

$$\sigma_r|_{r=l_0} = M\frac{\partial u(r.t)}{\partial r}\Big|_{r=l_0} = 0 \tag{IV−18}$$

The implication of Eq. (IV−18) is that, as the gel is immersed in the solvent, the osmotic pressure acting on the surface of the gel is zero.

D−2.2 ***Final swollen state of the gel***.

As the gel swells to equilibrium, the chain relaxation approaches completion, meaning the osmotic pressure approaches zero.

$$\sigma_r|_{r\to l_\infty} = M\frac{\partial u(r.t)}{\partial r}\Big|_{r\to l_\infty} \to 0 \tag{IV−19}$$

D−3. Solution

Solving Eq. (IV−12) analytically, incorporating the accompanying initial and boundary conditions gives [222]:

$$u(r.t) = \sum_n^\infty Q_n(r)\exp\left(-Dk_n^2 t\right) \quad \text{(IV−20)}$$

where Q_n and k_n are given as:

$$Q_n(r) = -6\frac{\Delta l}{l_\infty}\frac{(-1)^n}{k_n}\left[\frac{cosk_n r}{k_n r} - \frac{sink_n r}{(k_n r)^2}\right] \quad \text{(IV−21)}$$

$$k_n = \frac{n\pi}{l_\infty} \quad \text{(IV−22)}$$

To understand how the surface of the gel, $l(t)$, deforms with time. Let us relate the deformed configuration $l(t)$ to the reference configuration l_∞in the following way:

$$l(t) = l_\infty + u(l_\infty, t) \quad \text{(IV−23)}$$

The deformation of the surface of the gel, $u(l_\infty, t)$, can be determined from Eq. (IV−20):

$$u(l_\infty.t) = -6\Delta l\sum_n^\infty \frac{1}{l_\infty}\frac{(-1)^n}{\frac{n\pi}{l_\infty}}\left[\frac{cos\frac{n\pi}{l_\infty}l_\infty}{\frac{n\pi}{l_\infty}l_\infty} - \frac{sin\frac{n\pi}{l_\infty}l_\infty}{\left(\frac{n\pi}{l_\infty}l_\infty\right)^2}\right]\exp\left[-D\left(\frac{n\pi}{l_\infty}\right)^2 t\right]$$

$$u(l_\infty.t) = -6\Delta l\sum_n^\infty \frac{(-1)^n}{n\pi}\left[\frac{cosn\pi}{n\pi} - \frac{sinn\pi}{(n\pi)^2}\right]\exp\left\{-D\left(\frac{n\pi}{l_\infty}\right)^2 t\right\}$$

$$= -\Delta l\sum_n^\infty \frac{6}{(n\pi)^2}\exp\left\{-n^2 D\left(\frac{\pi}{l_\infty}\right)^2 t\right\}$$

$$u(l_\infty.t) = -\Delta l\sum_n^\infty \frac{6}{(n\pi)^2}\exp\left(-n^2\, t/\tau\right) \quad \text{(IV−24)}$$

where the time constant referred to as the longest relaxation time, τ is:

$$\tau = \frac{l_\infty^2}{\pi^2 D} \quad \text{(IV−25)}$$

Rewriting Eq. (IV−24) in normalized form gives:

$$\frac{u(l_\infty.t)}{\Delta l} = -\sum_n^\infty \frac{6}{(n\pi)^2} \exp\left(-n^2\, {}^t/_\tau\right) \qquad \text{(IV−26)}$$

The behaviour of the plot of displacement normalized with Δl , that is, $(u/\Delta l)$ against time normalized with the time-constant, (t/τ) for $n = 1$, gives approximately the change in volume of the spherical gel. That is, combining Eq. (IV−20) and (IV−26), for $n = 1$:

$$-\frac{u(l_\infty.t)}{\Delta l} = \frac{l_\infty - l(t)}{l_\infty - l_0} \cong \frac{6}{\pi^2} \exp\left(-\, {}^t/_\tau\right) \qquad \text{(IV−27)}$$

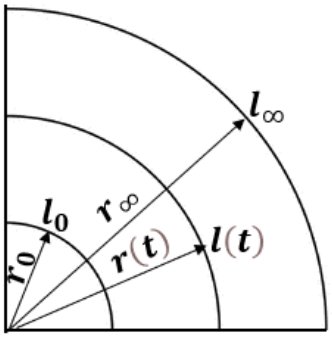

Figure A4b: The position of a particle on the surface of the gel in the initial (radius, r_0), at any time *t* (radius, $r\ (t)$), and the final/reference (radius, r_∞) states of the gel.

From Eq. (IV−27), we can estimate the volume or radius of the gel at any time, *r*(t) if the volume or radius of the gel at equilibrium swelling, r_∞ is known. Therefore:

$$r(t) \cong r_\infty - \left[\frac{6}{\pi^2} \exp\left(-\, {}^t/_\tau\right)\right](r_\infty - r_0) \qquad \text{(IV−28)}$$

where

$$\tau = \frac{r_\infty^2}{\pi^2 D} \qquad \text{(IV−29)}$$

From Eq. (IV−28) and (IV−29) it is clear that τ is directly proportional to r_∞^2, but inversely proportional to $\left(\frac{u(l_\infty.t)}{\Delta l}\right)$. Thus, it is established that the rate at which the gel swells or shrinks (or the dynamic swelling ratio) at a constant collective diffusion coefficient, *D*, depends on the size of the gel (that is, the rate of swelling decreases as the size of the gel increases).

Further, the time-evolutions of the volume or radius of the gel $r(t)$, by this approach, will require a knowledge of the size of the gel at equilibrium swelling state, r_∞. This can be obtained from equilibrium swelling experimental data.

D−4. Collective Diffusion Coefficient, D

To study the pH sensitivity of hydrogel, it is important we establish the relationship between the ionic strength (or pH of the surrounding medium) and the mechanical/elastic properties of hydrogel such as: the bulk modulus, *K*, and the shear modulus, *G*. In addition, another important relationship to be considered is the frictional coefficient, *f*, between the gel and the surrounding medium. All these parameters collectively characterize the diffusion coefficient, *D*, defined as:

$$D = \frac{K+\frac{4G}{3}}{f} \qquad \text{(IV−30)}$$

Where these parameters are difficult to measure, the collective diffusion coefficient can be measured using either dynamic light scattering (DLS) method [223] or by rheological techniques [224].

D−4.1 *Shear modulus, G*

One way to determine shear modulus of a polymer, theoretically, is to use the crosslink density, $\mu(\mathrm{m}^{-3})$ and number of network strands between each crosslink, $\nu(\mathrm{m}^{-3})$, through the following relation:

$$G = (\nu - \mu)kT \qquad \text{(IV−31)}$$

where $k = 1.3 \times 10^{-23}\, J/m^3$, is the Boltzmann constant, and *T* is the temperature.

Alternatively, the shear modulus, *G*, can be determined from known mechanical properties of the gel such as: Young's Modulus, *E* (which is a pH-dependent property of the deformed gel), and poison ratio υ_p, through the relation:

$$E = 2G(1 + \upsilon_p) \qquad \text{(IV}-32\text{)}$$

For Elastomers, $\upsilon_p \cong 0.5$, which implies that $E \cong 3G$.

Experimentally, G can be determined as a function of pH of the surrounding medium. Horkay *et al*. [225] observed an inverse relationship between shear modulus of crosslinked hydrogel (reported to increase from 29 ± 0.5 kPa to 32 ± 0.5 kPa) and the pH (reported to decrease correspondingly from 7.0 to 1.0) of the surrounding medium. Highlighting the importance of using pH-dependent shear modulus data for estimating the collective diffusion coefficient of pH responsive hydrogels.

Thus, shear modulus data for estimation of *D*, at different pH of the surrounding medium can be obtained from uniaxial compression measurement at a fixed pH value.

D−4.2 *Bulk Modulus, B*

Bulk modulus of the gel can be obtained from the correlation of Poisson ratio with Young modulus and bulk modulus given as:

$$E = 3B(1 - 2\upsilon_p) \qquad \text{(IV}-33\text{)}$$

D−4.3 *Frictional coefficient, f*

The Frictional coefficient, f of a crosslinked polymer molecule immersed in dilute solution as a function of the total concentration of the polymer takes the general form [226]:

$$\frac{f}{f_0} = 1 + k_s c + \cdots \qquad \text{(IV}-34\text{)}$$

where f_0 is the frictional coefficient at infinite dilution (i.e., the value of *f* in the limit of zero concentration), , and *c* is the total concentration of the crosslinked polymer. In addition, k_s and other coefficients of the higher powers of *c* are independent of the total polymer concentration (i.e., including both the main constituent and crosslinker).

For soft sphere, Pyun and Fixma [226] derived the frictional ratio as a function of polymer volume fraction before swelling as:

$$\frac{f}{f_0} = 1 + [7.16 - \kappa(A)]{\nu_2}^0 + \cdots \quad \text{(IV−35)}$$

where

$$\kappa(A) = 6.39/\sqrt{A + 2.6} \quad \text{(IV−36)}$$

where *A* is an adjustable parameter

By Stoke's law [226]

$$f_0 = 6\pi\eta r_0 \quad \text{(IV−37)}$$

where η is the dynamic viscosity of the surrounding fluid. Assume the surrounding fluid is water at 20℃, then the viscosity, $\eta = 0.001002\, kg/m.s$.

The polymer volume fraction (i.e., the total weight concentration) of the unswollen crosslinked hydrogel, ${\nu_2}^0$ at as prepared state is given as:

$${\nu_2}^0 = \left(\%c_c v_c + \%c_g v_g\right)/\left(\%c_c v_c + \%c_g v_g + \left(100 - \left(\%c_c + \%c_g\right)\right) v_w\right) \quad \text{(IV−38)}$$

Experimentally, the dependence of the frictional coefficient of poly(acrylamide) gel was studied by under conditions of constant molar concentration of the crosslinking agent at 1 mol%. The results showed that concentration of the gel depends on the frictional coefficient by a power law relation, given as:

$$f = C_f({\nu_2}^0)^{1.5} \quad \text{(IV−39)}$$

where C_f is a numerical constant.

Therefore, we can use either Eq. (IV−35), (IV−36), and (IV−37) or (IV−39) to estimate the value of frictional coefficient to be used in Eq. (IV−28) to predict the time-dependent swollen (or shrunk) volume of crosslinked hydrogel.